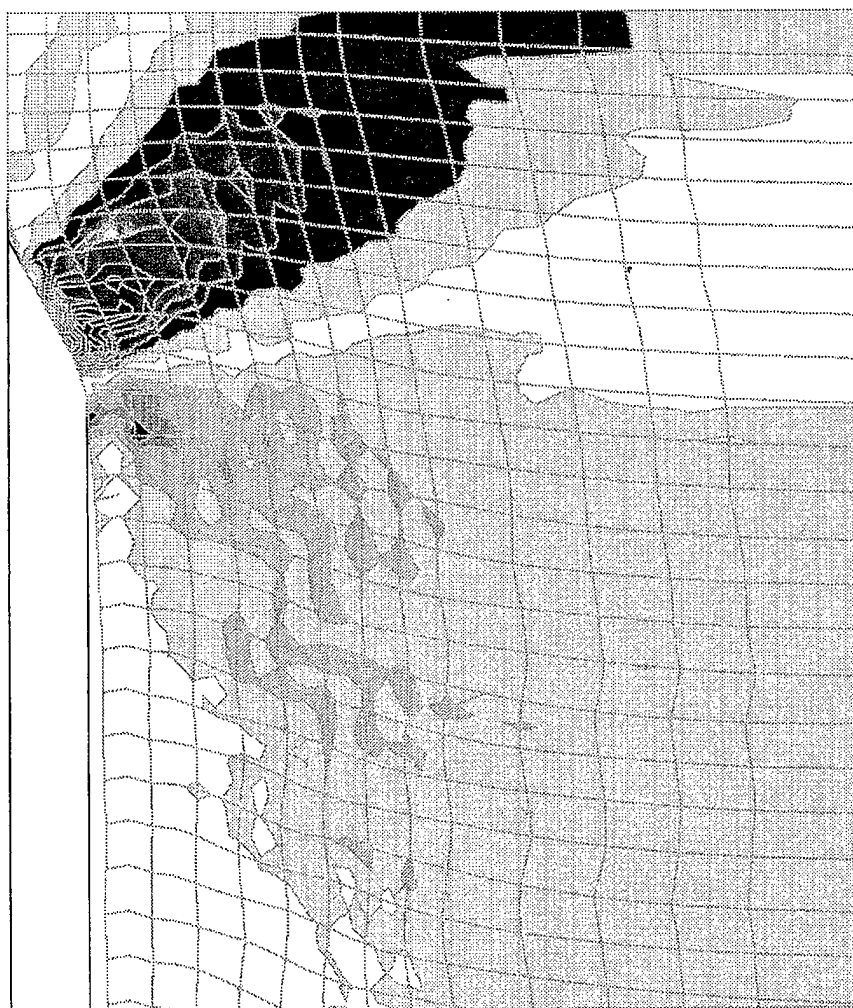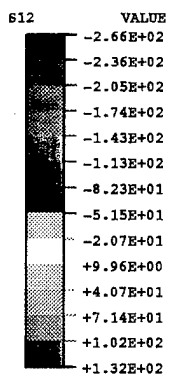NAVAL FACILITIES ENGINEERING SERVICE CENTER
Port Hueneme, California 93043-4370

TECHNICAL REPORT
TR-2081-SHR

NUMERICAL MODELING OF STEADY-STATE PLOW/SOIL INTERACTION

612	VALUE
	-2.66E+02
	-2.36E+02
	-2.05E+02
	-1.74E+02
	-1.43E+02
	-1.13E+02
	-8.23E+01
	-5.15E+01
	-2.07E+01
	+9.96E+00
	+4.07E+01
	+7.14E+01
	+1.02E+02
	+1.32E+02

by

Theodore A. Shugar, Ph.D.

August 1997

REPORT DOCUMENTATION PAGE

Form Approved
OMB No. 0704-018

1. AGENCY USE ONLY (Leave blank)	2. REPORT DATE August 1997	3. REPORT TYPE AND DATES COVERED Final; 1993-1995

4. TITLE AND SUBTITLE

Numerical Modeling of Steady-State Plow/Soil Interaction

5. FUNDING NUMBERS

6. AUTHOR(S)

Theodore A. Shugar, Ph.D.

7. PERFORMING ORGANIZATION NAME(S) AND ADDRESSE(S)

Naval Facilities Engineering Service Center
1100 23rd Avenue
Port Hueneme, CA 93043-4370

8. PERFORMING ORGANIZATION REPORT NUMBER

TR - 2081 - SHR

9. SPONSORING/MONITORING AGENCY NAME(S) AND ADDRESSES

10. SPONSORING/MONITORING AGENCY REPORT NUMBER

11. SUPPLEMENTARY NOTES

12a. DISTRIBUTION/AVAILABILITY STATEMENT

Approved for public release; distribution is unlimited.

12b. DISTRIBUTION CODE

13. ABSTRACT (Maximum 200 words)

A numerical model of steady-state plow/soil interaction in support of cable burial operations on the seafloor was developed. Coupled field equations for equilibrium of an elasto-plastic medium and pore water diffusion in the presence of rigid surfaces contacting and sliding through fully saturated soil were solved in two dimensions.

Time histories of unit plow forces contained distinct transient and steady-state phases reminiscent of total plow force histories recorded in the laboratory. The computed relationship between unit plow force and velocity was linear, although no critical velocity was evident in the results. Permanent soil deformation in the wake of the plow tip replicated observed behavior. Stress concentrations in the soil and contact forces distributed over the plow blade were consistent with patterns of severe wear on plow blades observed after usage in the field. Soil dilatation response was reasonable, and negative pore pressures were representative of measured response, although a modeling provision for pore water cavitation did not present itself.

Moreover, the model explains how the mean pressure stress builds forward of the plow tip strengthening the pressure sensitive soil through which it penetrates, and suggests why past field measurements of resistance exceeded predictions from conventional analysis procedures.

14. SUBJECT TERMS

Plow resistance, seafloor soil, cable burial, finiteelement modeling, soil/structure interaction, computational plasticity, effective stress, pore pressure.

15. NUMBER OF PAGES
180

16. PRICE CODE

17. SECURITY CLASSIFICATION OF REPORT	18. SECURITY CLASSIFICATION OF THIS PAGE	19. SECURITY CLASSIFICATION OF ABSTRACT	20. LIMITATION OF ABSTRACT
Unclassified	Unclassified	Unclassified	UL

EXECUTIVE SUMMARY

The development of a numerical model of steady-state plow/soil interaction in support of cable burial operations on the seafloor was addressed. It was guided by previous laboratory experiments showing a linear relationship between plow resistance and steady-state velocity up to a critical velocity in the range of 10 fps, beyond which resistance tended to remain constant. Further, the data showed that soil stress and pore water flow near the plow were three-dimensional quantities. Nonetheless, because of the unaffordable expense of full three-dimensional simulations, two-dimensional simulations were used to demonstrate behavior in a representative horizontal plane. Coupled field equations for equilibrium of an elasto-plastic medium and pore water diffusion were solved in the presence of rigid surfaces contacting and sliding through fully saturated soil. Commercial finite element technology imposed a multistep transient solution approach, and the representative software employed in the solution further imposed the usage of high order finite element formulations for soil. These restrictions contributed to a computationally intensive model, prohibiting a three-dimensional solution using available engineering workstation computers.

A summary was also provided of two alternative approaches: (1) a simplified semi-empirical model, and (2) a new single-step finite element demonstration model for solving the steady state problem directly. The former model included three-dimensional effects. The latter model exploited equivalency of time and spatial derivatives in the formulation of the problem. Both models were successful, but the latter demonstrated potential for ultimately achieving a rational numerical model in three dimensions.

The multistep transient solution considered a simplified two-dimensional plane strain formulation of a rigid thin-blade plow interacting with soil. Though inherently incapable of considering total plow resistance force, the model featured finite strains, a modified Drucker-Prager plasticity constitutive model, and large sliding along a frictional plow/soil interface. Special handling techniques enabled reasonable responses for variables and workable compute times.

Time histories of unit plow forces, in lieu of total plow forces, displayed distinct transient and steady-state phases reminiscent of total force histories recorded in the laboratory, and the computed relationship between unit plow force and velocity remained linear from zero to 13 fps, although no critical velocity was evident in the results. Permanent soil deformation in the wake of the plow replicated laboratory observation. Concentrations of effective stress and contact forces distributed over the plow blade were consistent with patterns of severe wear on plow blades observed in the field. Computed soil dilatation response was reasonable, and negative pore pressures were representative of measured response, although a provision for modeling cavitation in the pore fluid did not present itself. The model verified that only the tip of the thin-blade plow contacted the soil, it complemented available experimental data regarding lateral plow force, and it also evidenced expansive soil behavior as should be anticipated for dilatant seafloor soil . Moreover, the model explained how the mean pressure stress builds forward of the plow tip strengthening the pressure-sensitive soil through which it penetrates, and suggests why past field measurements of resistance exceeded predictions from conventional analysis procedures.

A parameter study further demonstrated the engineering utility of rational numerical plow/soil interaction models. The consequences of coulomb friction at the plow/soil interface were potentially significant for tow forces but not for lateral forces, and while the potential for blade sharpness to reduce tow force was also significant, sharper blades also reduce permanent soil displacement and the potential effectiveness of trench formation.

Commercial nonlinear finite element technology demonstrated substantial capability and surprising resilience in a highly specialized application to plow/soil interaction modeling. Future development of affordable three-dimensional numerical models should also consider special-purpose finite element software solutions based on a steady-state, single-step finite element method so that solutions can be realized for engineering design applications.

CONTENTS

CONTENTS

CONTENTS

1.0 INTRODUCTION

The problem addressed in this report is the interaction of a rigid thin-blade plow with dense 100 percent saturated sand as the plow is towed at a constant rate along the surface of the seafloor for the purpose of creating a trench. The important engineering information sought is the resisting force acting on the blade as it cuts through the soil. Plow resistance force or tow force and energy consumption measured in the field have reportedly far exceeded values predicted by conventional theories and by previous laboratory model tests. Reasons for the discrepancies include increase in soil strength related to plow velocity, and in laboratory investigations, inadequate preparation of soil test conditions which were not representative of fully saturated seafloor soils.

A substantial laboratory experimental program was developed at the Naval Facilities Engineering Service Center (NFESC) to resolve the laboratory issues. The laboratory apparatus for measuring resistance forces on scale models of thin blade plows is depicted in Figure 1-1. This sketch provides an overview of the physical problem with which the engineering investigation into the mechanics of plow/soil interaction is concerned. The portable soil test fixture shown in Figure 1-1a has a controlled hydraulic ram-cable linkage system which pulls with a force sufficient to maintain a preset constant velocity for the trolley and test article or thin blade plow. The instrument package measures the resistance force, F_R, as well as the moment of F_R. In addition to providing data at one atmosphere, the apparatus is also transportable for testing at various simulated ocean depths at distant hyperbaric chamber test sites.

The geometry of a typical thin blade plow is shown in Figure 1-1b. The main characteristics are the blade's thickness, length, depth, sweep angle, and tip included angle. For the plow shown these values are, respectively, 1/2 inch, 6.5 inches, 9-inch nominal, 90 and 60 degrees.

The experimental program has produced two main technical reports to date on test results with two types of fully saturated sand materials -- Cable et al. (1993) and Girard and Taylor (1994). Typical primary data obtained from these tests are shown in Figure 1-2a, for 6-inch-deep thin blade plow test articles having various thicknesses, and under various conditions of soil saturation (the full 100 percent saturation condition is of primary interest). In the range of test velocities up to about 8 fps, it is seen that the relationship between plow resistance and plow velocity is linear. The soil type was a medium dense grain-size sand in these data, i.e., a dense Yorba River sand. Similar results, in Figure 1-2b, for the 9-inch-deep thin blade plow shows the relationship to be linear up to 8 fps with a steeper slope. Beyond these so-called critical velocities, the behavior tends toward a constant resistance.

To help understand the controlling physics of this problem, the development of a numerical model of plow/soil interaction was authorized. How well commercial, general purpose finite element technology would perform in providing this capability was an immediate goal of the study. The aforementioned experimental program was instrumental in guiding the development.

Numerical modeling of the coupled equilibrium and porous media flow fields in the presence of rigid surfaces and sliding contact is a complex simulation problem. However, solutions are feasible although they generally cannot be rushed. It is mandatory to maintain

control of the development each step of the way by knowing the theoretical and numerical meaning of model data. In this way, a reliable and rational numerical model can provide new data and detailed insight describing the behavior of plow/soil interaction.

Development of a numerical model of plow/soil interaction using available commercial finite element technology was pursued. The approach taken includes modeling both nonlinear saturated soil material behavior and the mechanics of plow/soil interaction.

1.1 Objectives

The overall objective is to provide a numerical model for plow/soil interaction, and to:

1. Predict the resistance of a thin blade plow to steady-state motion through seafloor soil.

2. Provide an analysis tool for evaluating system parameters on a rational basis.

3. Assess the capability of commercial, general-purpose finite element computer programs to provide these capabilities.

1.2 Scope

ABAQUS/Standard, Version 5.3 (Hibbitt, Karlsson, and Sorensen, Inc., (HKS), 1993), was the computer program employed while conducting the study. This program is well-regarded for solving nonlinear problems in structural and solid mechanics and is very representative of commercial technology. With regard to geotechnical problems, it features special capabilities for effective stress analysis and three alternative plasticity-based soil models:

1. Modified Drucker-Prager Model

2. Modified Cap Model

3. Modified Cam-Clay Model

This program also has substantial interface modeling features including sliding and friction which are also applicable to geotechnical problems.

ABAQUS/Standard is an implicit finite element computer program suitable for quasi-static or dynamic problems. Like other commercial finite element programs, it has no capability for solving steady-state problems directly. That is, the user must simulate a steady-state problem using a multistep transient solution approach. The steady-state problem is viewed as a special case of the more general problem, requiring the solution of an initial transient phase preceding the solution of the steady-state phase.

Appendix A contains a discussion of some relevant technical issues and the consequences of project constraints which were prepared early on in this study.

Hydraulic winch system

Trolley with instrumentation package

Test article
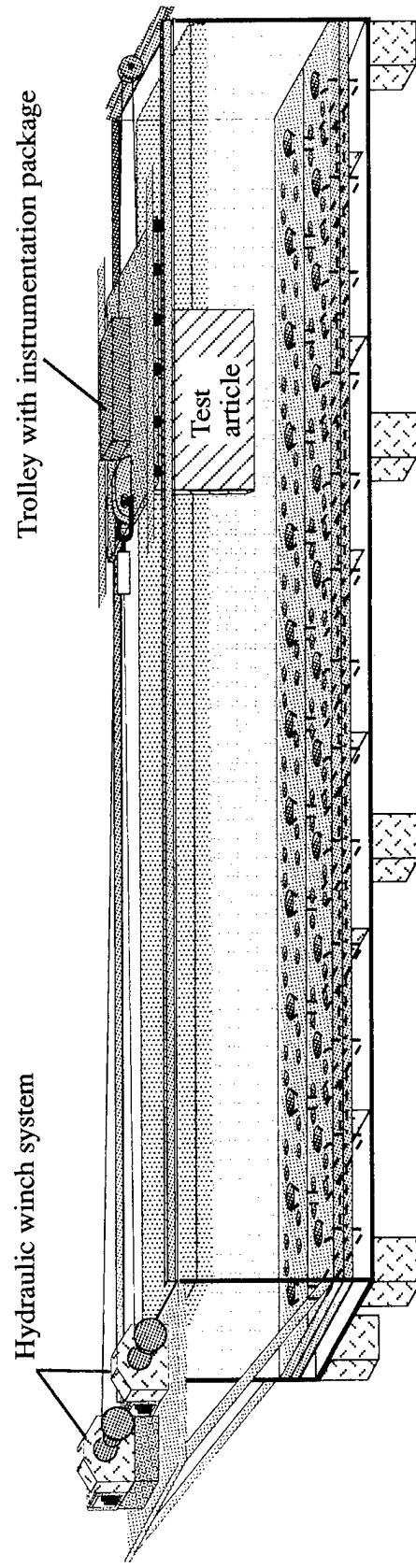
(a) Portable soil test fixture, test configuration.

Figure 1-1. Laboratory testing apparatus.

9.63"

A   A

6.50"

60°   0.50"

A-A

0.03" R

NOTES:
USE A36 PLATE
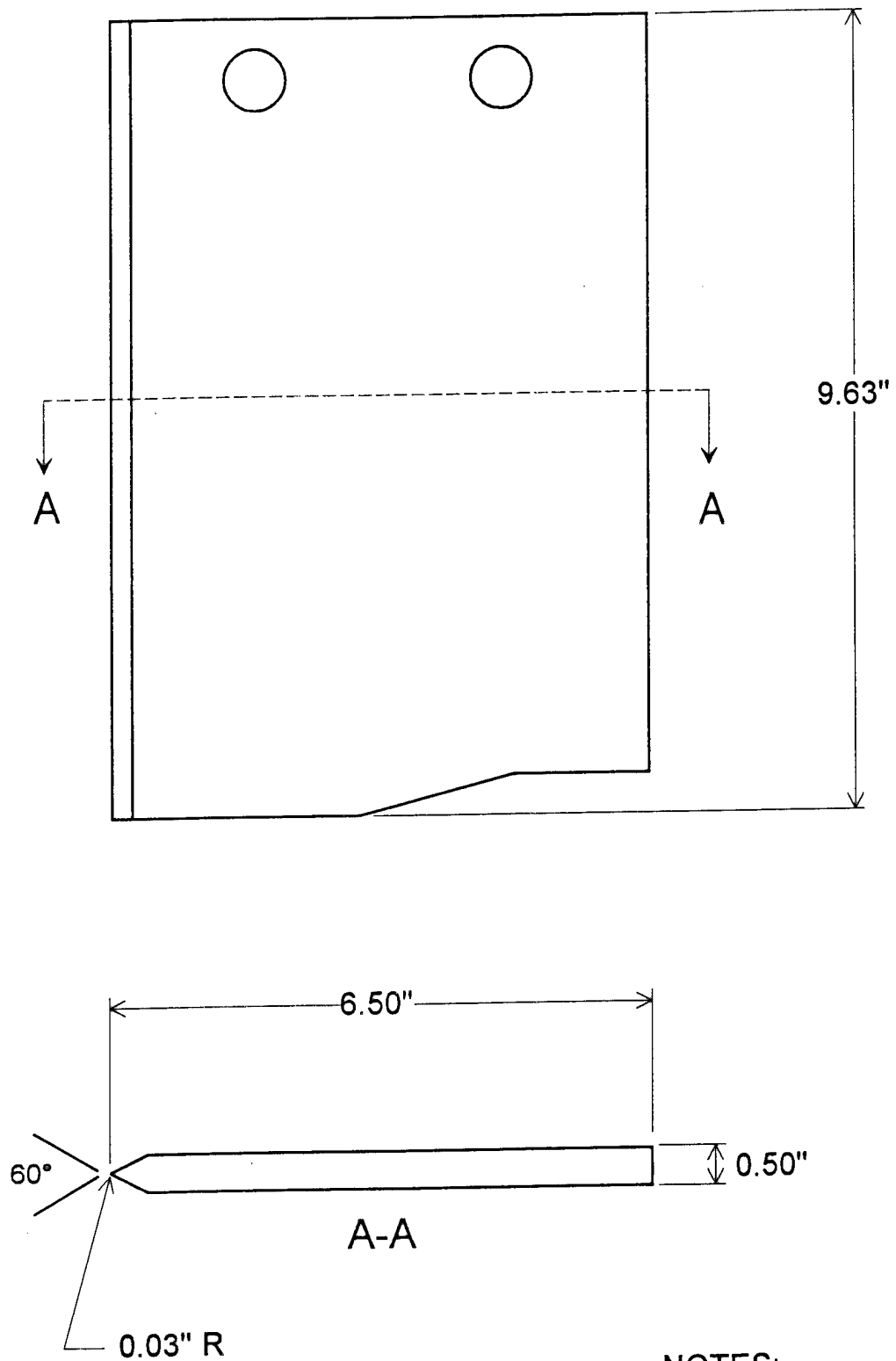
(b) Typical blade geometry.

Figure 1-1. Continued.

4
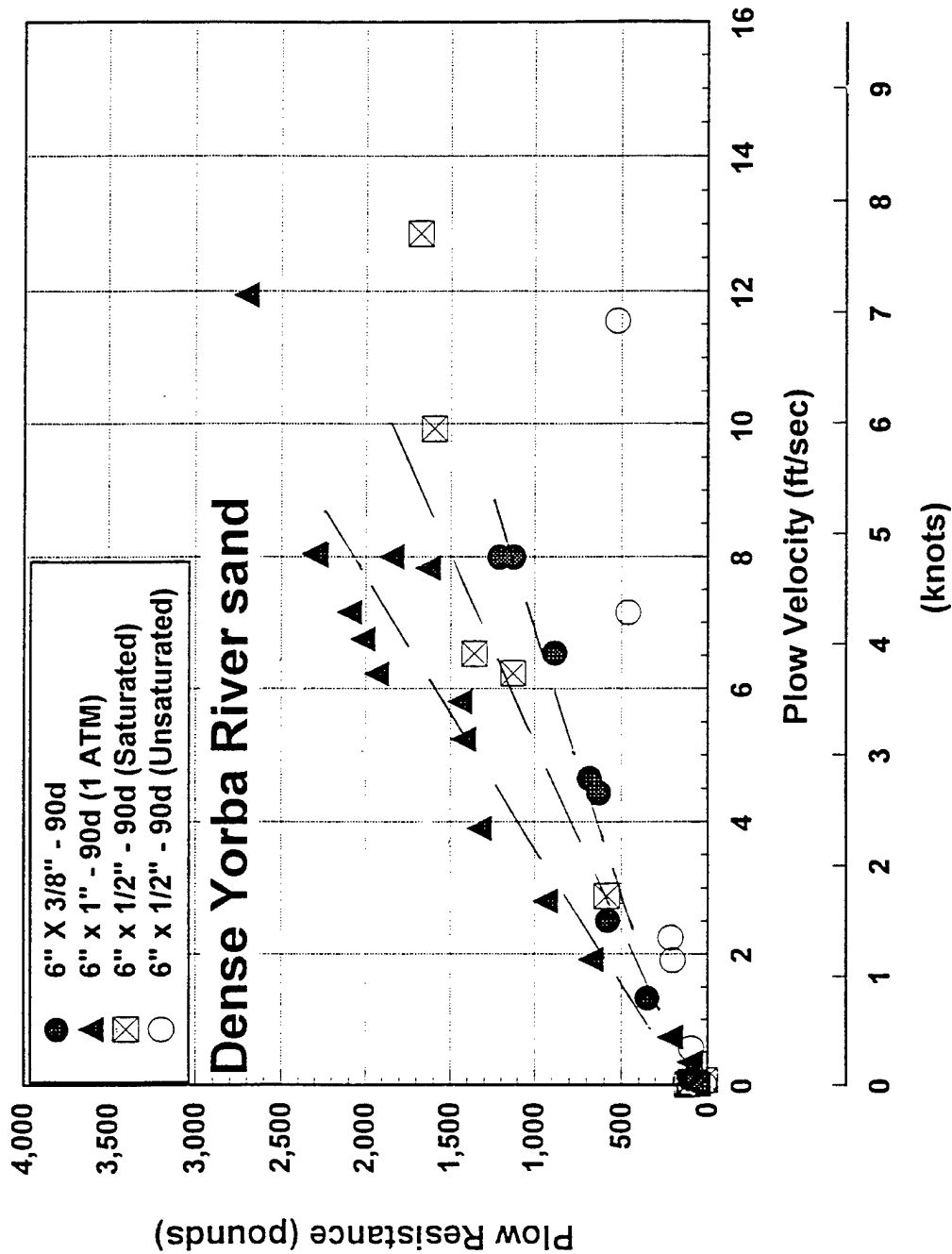
(a) Comparison of 6-inch blades.

Figure 1-2. Plow resistance vs. plow velocity.

Plow Resistance vs. Plow Velocity 9" Blade Comparison
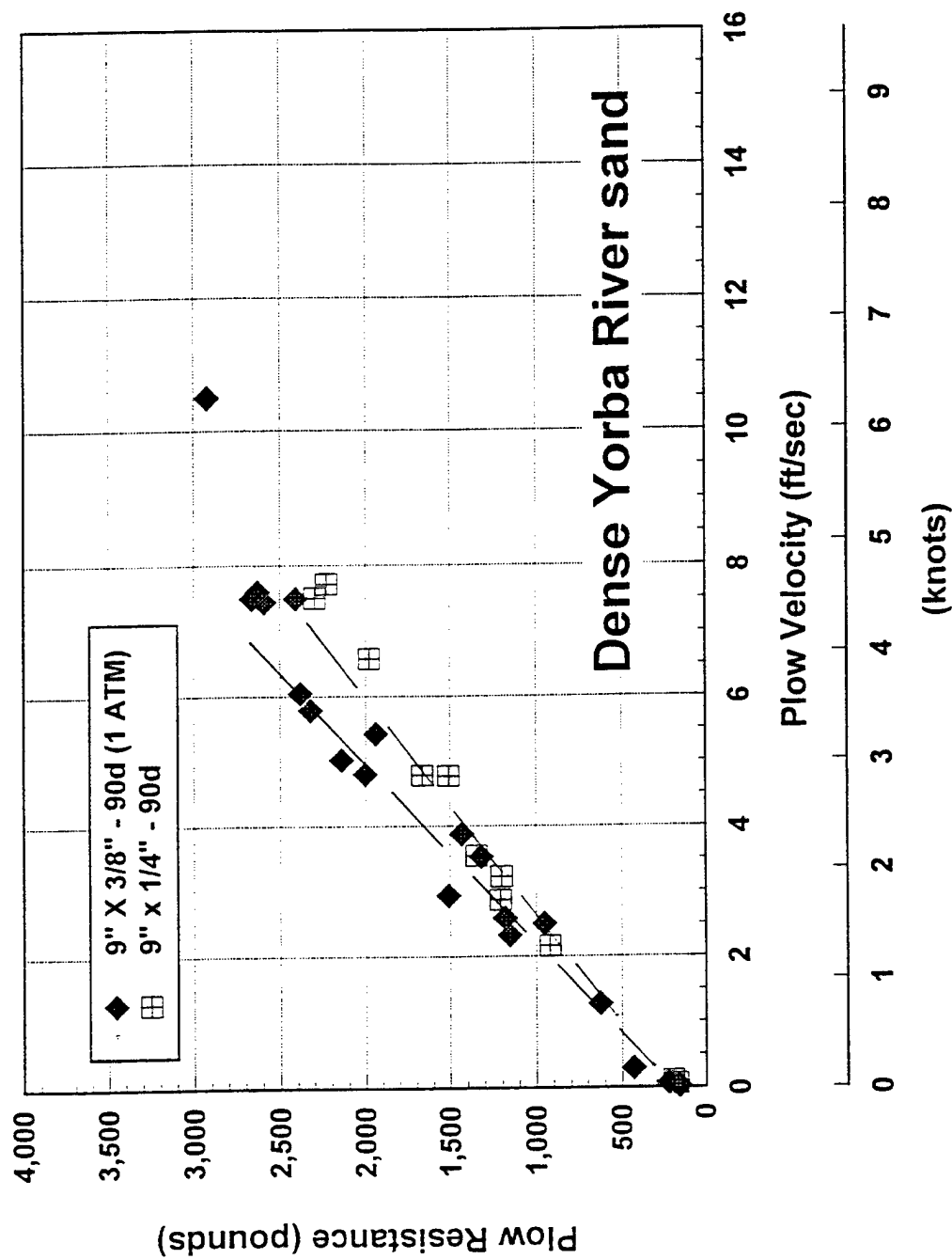
(b) Comparison of 9-inch blades.

Figure 1-2. Continued.

1.3 Apparent Technical Risk

No general purpose nonlinear finite element computer program is likely to have all the technical capabilities desired to solve a particularly complex problem. In most cases, solutions are coerced, at least to some degree, from the program selected. Often technical difficulty simply cannot be avoided because solution requirements simply exceed the resources of commercial state-of-the-art computational mechanics. Four areas of numerical modeling complexity encountered in the present treatment of coupled equilibrium/porous media flow problems are discussed in 1.3.1, 1.3.2, 1.3.3, and 1.3.4. They are generally related to the use of high order elements and constitutive models.

1.3.1 High Order Element Burden. Effective stress soil models are required so that pore water pressure effects may be included in the analysis. The effective stress principle in soil mechanics provides for this by conceptualizing the mechanical behavior of the soil skeleton in terms of an effective stress, while the overall equilibrium equations for the soil are formulated in terms of the total stress (algebraic sum of effective stress and pore pressure). In this way, pore pressure may be interpolated independently from displacements in a corresponding finite element spatial discretization of the problem. Most effective stress finite element formulations used throughout the industry work in this way (Zienkiewicz and Taylor, 1989) i.e., interpolation functions for the pore pressure field and the soil skeleton displacement field are different, whether the soil element is regarded as a high order or low order formulation.

Usage of a high order instead of a low order finite element formulation for analysis of coupled equilibrium/porous media flow was imposed by the software employed in this study. This lead to lengthy compute times and large input and output data files. Bearing in mind that both displacements and pore pressures are evaluated at corner nodes in this formulation, the two-dimensional version has four midside and four corner nodes and the three-dimensional version has twelve midside and eight corner nodes. Only displacements are evaluated at midside nodes. This is in comparison with four and eight corner nodes, respectively, for two- and three-dimensional elements of low order finite element formulations. Low order elements have no midside nodes, though there is one center node for evaluating pore pressure. Further, the high order two-dimensional element has 9 internal points (Gauss points) where stress and strain are evaluated, and also 4 points where velocity gradient is evaluated. The corresponding low order element has only 4 internal points for stress/strain evaluation and only a single point for evaluating velocity gradient. A low order soil element formulation would have been a welcome alternative in this study.

1.3.2 Clarity of Boundary Condition Specification. The element formulation for coupled equilibrium/porous media flow is necessarily a mixed finite element formulation; as indicated above, displacements and pore pressures are the primary variables and stress and velocity gradients are the secondary variables. This unavoidably complicates understanding and specification of boundary conditions for these variables, and it can be counter intuitive when compared to solving standard stress equilibrium problems which do not involve porous media flow.

1.3.3 Interface Modeling Complexity. The high order element and mixed element formulation further complicate interface modeling. This is a result of well-known anomalous behavior of nodal point reaction forces in high order elements. A simple three-dimensional example illustrates this point in Figure 1-3. Though the computed reaction forces are in equilibrium with the applied load, the corner node reactions are in fact in the wrong direction. This anomalous behavior can confuse an interface computational algorithm that imposes contact/release conditions on node points along the plow/soil interface during problem solution.

1.3.4 Accuracy of Constitutive Models. In a preceding project, advanced finite element technology was applied to a geotechnical problem involving penetration of rock anchors to help resolve discrepancies between field observation and analytical prediction (Hoge and Shugar, 1992). DYNA3D was employed in this study; and is an explicit finite element program particularly suitable for highly transient dynamic problems (Whirley and Hallquist, 1991). This investigation concluded that modeling nonlinear material behavior of rock was the primary challenge and that advanced constitutive models were required for rock. It is not unexpected that correctly modeling the nonlinear behavior of saturated seafloor soil is of key importance in the present study of plow/soil interaction. Thus, a requirement for more advanced soil models may well be anticipated in the long term for solution of this problem. The following discussion provides a short status report on what has been done at NFESC in this regard.

The Office of Naval Research (ONR) sponsored the development of modern, third-generation soil constitutive laws for use in numerical modeling of geotechnical systems which was conducted at NFESC, the University of California at Davis, and at Stanford University, all under the auspices of the NFESC's 6.1 project, Structural Modeling. Among the achievements in computational mechanics, this research resulted in a bounding surface plasticity constitutive model for clay soils which was validated in a fairly wide array of experiments (Dafalias and Herrmann, 1986; Herrmann, 1987). A fundamental experimental study on the behavior of sand was also completed (Kutter, Chen, and Shen, 1994). In this study, a large number of experimental validation tests on a medium to fine grain sand were conducted to provide an experimental data base for development and validation of a proposed bounding surface hypoplasticity model for sand (Wang, Dafalias, and Shen, 1990) and third-generation soil model development efforts conducted elsewhere. Initial attempts to validate the model with earthquake field test data were successful (Shen and Li, 1991). However, initial validation results were limited to one-dimensional soil-column models, and measured pore pressure data were below critical liquefaction levels and therefore insufficiently challenged the model. Further validation efforts involving laboratory data including geotechnical centrifuge experiments, were hampered by numerical inefficiency and also revealed shortcomings in the physical behavior of the proposed hypoplasticity model. For example, the hypoplasticity sand model assumed that the soil failure envelop for undrained conditions is the same as that for drained conditions, but laboratory data indicated otherwise. The experiments further showed that the shape of the phase transformation surface is different from the shape of the failure surface and suggested that the model should accommodate this difference as well.

These theoretical and numerical problems combine to place at risk successful validation of the hypoplasticity model for sand as currently proposed. Additional research on constitutive models for granular materials was recommended. The numerical problem is currently being addressed at U. C. Davis (Holland, 1996) and progress is being made by analyzing different

numerical integration algorithms for solving the so-called incremental rate equations (for evaluating effective stress at the Gauss points). These algorithms are central to efficient implementation of constitutive models in general. Residual basic research exists on these problems at this time, and no additional research is currently programmed to address either problem under ONR's basic research program. In spite of this, a recent National Science Foundation (NSF) sponsored study (Arulanandan and Scott, 1993) is encouraging, and has affirmed the potential of advanced constitutive models and their numerical implementation (for liquefaction problems) in geotechnical engineering.

ANOMALOUS BEHAVIOR OF HIGHER ORDER ELEMENTS

Pressure, P = 10 psi

Reaction Forces:

R_c = 0.833 lb

R_m = 3.333 lb

1" x 1" x 1" Cube

P

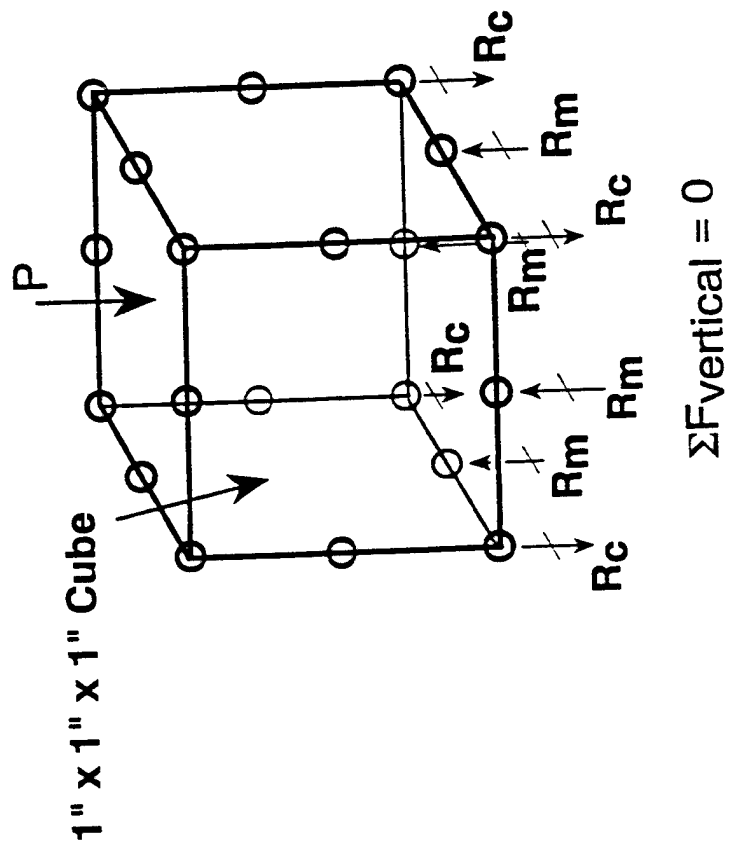R_c R_m R_c R_m R_c R_m R_c

$\Sigma F_{vertical} = 0$

Figure 1-3. Anomalous behavior of higher order elements.

2.0 ALTERNATIVE MODELS OF STEADY-STATE PLOW/SOIL INTERACTION

An analysis of the physical processes attending plow/soil interaction was an early imperative in support of the development of a numerical model. An engineering services contract was prepared for U.C. Davis. The statement of work is included as Appendix B and may be consulted for details.

In the sequel, two specialized approaches to plow/soil interaction modeling were developed at U.C. Davis which both complement and support the present modeling task employing commercial, general-purpose finite element technology. The contract was completed in the fall of 1994 and resulted in two published reports:

1. Kutter, B. L. and T. Voss (1995). "Analysis of data on plow resistance in dense, saturated cohesionless soil," CR 95.004-SHR, Naval Facilities Engineering Service Center, Port Hueneme, CA 93043-4328, February 1995.

2. Herrmann, L. R. and J. Mello (1994). "Investigation of an alternative finite element procedure: a one-step, steady-state analysis," CR 95.001-SHR, Naval Facilities Engineering Service Center, Port Hueneme, CA 93043-4328, December 1994.

These reports have been reviewed and a summary of their results and the plow/soil interaction models which they describe follows. The respective reports may be consulted for detailed accounts.

2.1 Approximate Analytical Model - A Semi-Empirical Approach (Kutter and Voss, 1995)

The dilatancy of dense sand can cause large negative pore pressures to develop during rapid plow penetration. Experimentally, this results in a nearly linear increase in the plow resistance with plow velocity up to a critical velocity at which cavitation of the pore fluid takes place. Dimensional analysis is useful for description of the relationship between plow resistance and velocity. The number of required parameters is reduced by the use of dimensionless variables. Critical state soil mechanics, bearing capacity theory, and Darcy's Law are used for guidance in the selection of alternative, physically-admissible, dimensionless groups of parameters. The experimental data base (Cable, et al., 1993; Girard and Taylor, 1994) provided a means to empirically evaluate an otherwise unknown function of dimensionless parameters that arose in the derivation of the admissible parameter groups. The result was a semi-empirical model which appears to correlate with experimental data, and which adequately describes the rate of change of plow resistance with velocity. In the empirical approach, all of the effects of assumptions, omitted parameters, etc., whether or not significant, are assumed to be lumped into the model error, -- the distance between the prediction and the data. Figure 2.1 schematically illustrates this error along with semi-empirical model parameters.

The semi-empirical plow/soil interaction model is based on existing bearing capacity equations used in geotechnical engineering of soil foundations (for example, see Wu, 1967). These equations are fundamentally based on Prandtl theory of slip lines formed in a rigid plastic material where bearing stresses are maximum and, which in the plow/soil model, emanate outward into the soil from the nose of the plow. The model does account for three-dimensional

11

flow and deformation of soil about the blade, as well as rake angle of the blade. However, the model omits parameters not included in the data base. For example, the model assumes that side friction on the blade is negligible compared to bearing resistance at the nose of the blade, and it has no parameter for blade tip included angle. Instead, it assumes a blunt tip thereby ignoring tip friction as well. Friction and blade sharpness are accounted for in the finite element numerical model approach.

The important properties of the soil which appear to govern the mechanics of plow/soil interaction are listed as follows, with friction angle and permeability being the two most important:

1. Friction angle, ϕ

2. Initial void ratio, e_0

3. Critical state void ratio, e_{crit}

4. Permeability, k

5. Vapor pressure of pore fluid, u_{cav}

6. Ambient pressure of pore fluid, u_0

The important geometric and kinematic parameters of the thin blade plow which govern its resistance to steady-state motion according to the present semi-empirical model were defined as follows (also refer to Figure 2-1).

1. Length, L

2. Thickness, B

3. Depth, H

4. Rake angle, θ

5. Velocity of penetration, v

A shear zone with its volume assumed to be proportional to the cross-sectional area of the blade is hypothesized. It comprises a region of uniform volumetric strain, ε_v ave, which approximates the volume of actual soil otherwise undergoing very nonuniform dilatation strain. This volume is determined empirically, through comparisons of the model with experimental data. It is also a function of initial and critical void ratios as discussed in the aforementioned (Kutter and Voss, 1995) report. Its purpose is to provide for the linear increase in plow resistance with velocity observed in the data.

A summary of the procedure for estimating plow resistance according to the proposed semi-empirical model follows:

1. Determine cavitation or vapor pressure of pore fluid, u_{cav}

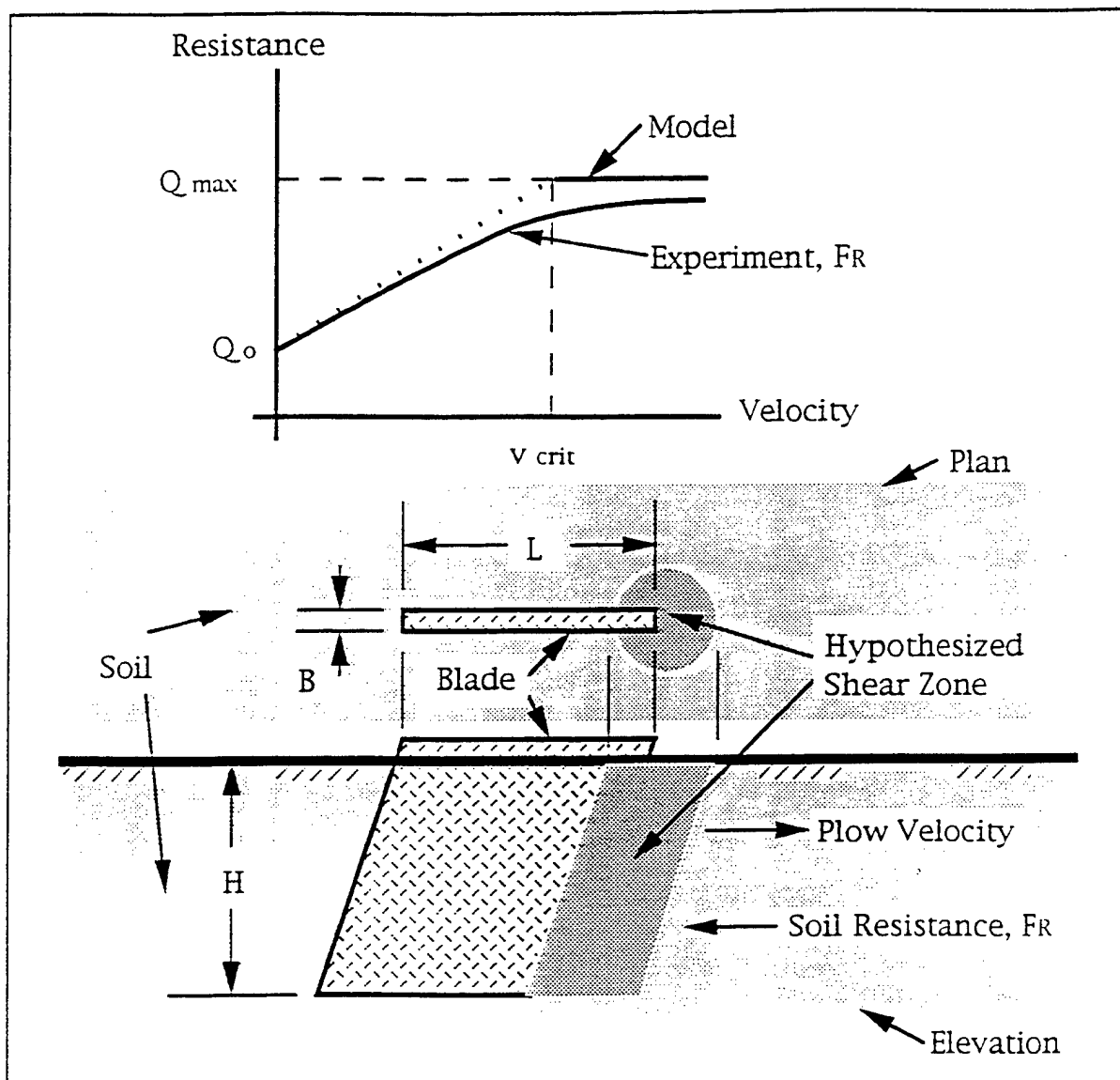2. Determine the maximum plow resistance by the smaller of either

12

Figure 2-1. Definition of variables for semi-empirical model of plow/soil interaction (Kutter and Voss, 1995).

$$Q_{max} = (u_0 - u_{cav}) N_q BH$$

or,

$$Q_{max} = c_u N_c BH.$$

where N_q (a function of friction angle - $\emptyset$) and N_c are conventional bearing capacity factors, respectively, for surcharge and for cohesion, and c_u is the undrained shear strength (Wu, 1967).

3. Estimate, or assume negligibly small, plow resistance at zero velocity, Q_0

4. Estimate rate of change of plow resistance with velocity, $\Delta Q/\Delta v$, using

$$\Delta Q/\Delta v = (\gamma_w N_q BH^2/k) * f_Q(\varepsilon_{v\ ave}, B/H, L/H, q)$$

where γ_w is the unit weight of water.

5. Estimate the critical velocity, i.e., velocity corresponding to maximum plow resistance using

$$v_{crit} = (Q_{max} - Q_0)/\Delta Q/\Delta v$$

Values for the unknown soil function f_Q were determined empirically using the experimental data base. They range between 0.0048 and 0.0122 for soil #1 (medium-dense sand) and between 0.0047 and 0.0071 for soil #2 (dense sand), depending on the geometry of the blade. This function also depends on three-dimensional aspects of soil deformation, and it may also be possible to evaluate it from the results of three-dimensional numerical models, as well as from experimental data.

It was concluded that the important soil mechanics features of plow/soil interaction are:

1. Resistance is predominately due to bearing on the leading edge of the plow.

2. Shear distortion of dense sand around the plow causes dilation, and the rate of dilation is a function of the rate of distortion, which is proportional to the velocity of plow penetration.

3. The tendency to dilate causes negative water pressures (relative to ambient water pressure) to develop in the shear zone.

4. Negative pressures draw water into the shear zone at a rate which is proportional to the change in pore pressure and the permeability of the soil. The flow of water into the shear zone permits dilation of particles to occur and relieves the negative pore pressure.

5. The negative pore pressures result in increased effective stresses in the region of the deformation of the soil.

6. Increased effective stress results in increased frictional resistance to plow penetration. Therefore, plow resistance increases as velocity of penetration increases.

7. The maximum magnitude of the negative pore pressure is limited by either:

    a. Cavitation of the pore fluid when the absolute pore pressure reaches the vapor pressure, or

    b. Achievement of a critical state condition in the shear zone. For a given value of void ratio, there is a critical value of the effective stress at which the soil may shear without further change in effective stress, pore pressure, or shear stress.

Recommendations were also given for additional material property testing and for additional laboratory plow/soil interaction testing.

2.2 Steady-State Finite Element Analysis Model - A Rational Model Approach (Herrmann and Mello, 1994)

A steady-state finite element analysis procedure that determines the stresses in the soil and the required driving force to pass a blade through soil at constant velocity has been developed. This type of analysis is shown to be a potentially attractive alternative to a multistep transient analysis (using a commercial finite element program) when the latter becomes computationally expensive. A steady-state analysis allows time-dependence to be expressed as space-dependence, and thus, a solution occurs in a single step. The feasibility of this type of analysis was demonstrated. It was determined that more investigation into soil failure conditions at the plow tip and an appropriate soil plasticity model for those conditions are required before a production three-dimensional single-step (or a multistep) computer program is developed.

A plane strain formulation for steady-state analysis of the plow soil/interaction problem is illustrated in Figures 2-2a and 2-2b. The region of soil which is depicted in plan is a horizontal plane which has unit thickness in the vertical direction. This formulation clearly ignores the proximity of the free surface. The dimensions in inches, and the size of the finite element model are indicated in Figure 2-2c, for a typical analysis with a steady-state velocity of five feet per second.

Results from the model predicted plow resistance to be a linear function of plow velocity as has been observed experimentally. Further, a rather dramatic dependence on plow shape, i.e., tip sharpness, and the apparent importance of including inertia forces were demonstrated as shown in Figure 2-2d. It is noted that soil inertia forces are explicitly neglected in the previous semi-empirical model for it has no mass density parameter. It was assumed that they were negligible.
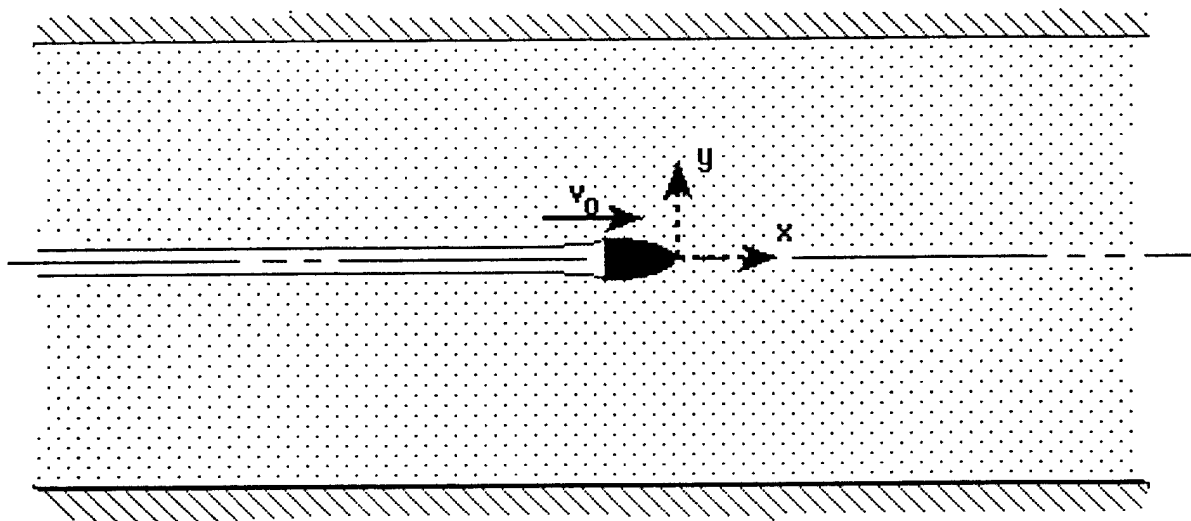
(a) Problem configuration.
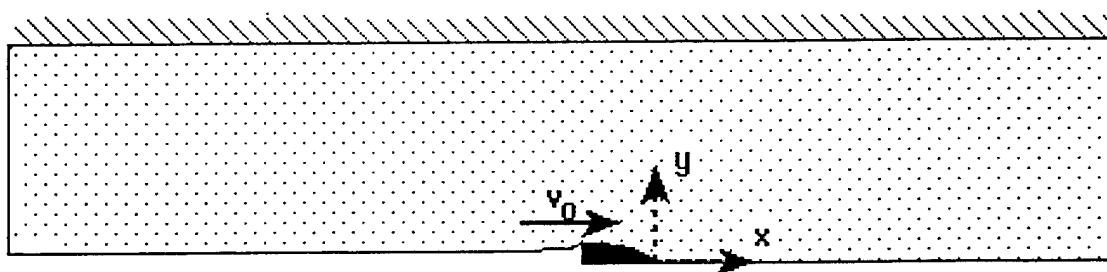
(b) Configuration for analysis.

Figure 2-2. Preliminary single-step steady-state finite element model of plow/soil interaction (Herrmann and Mello, 1994).
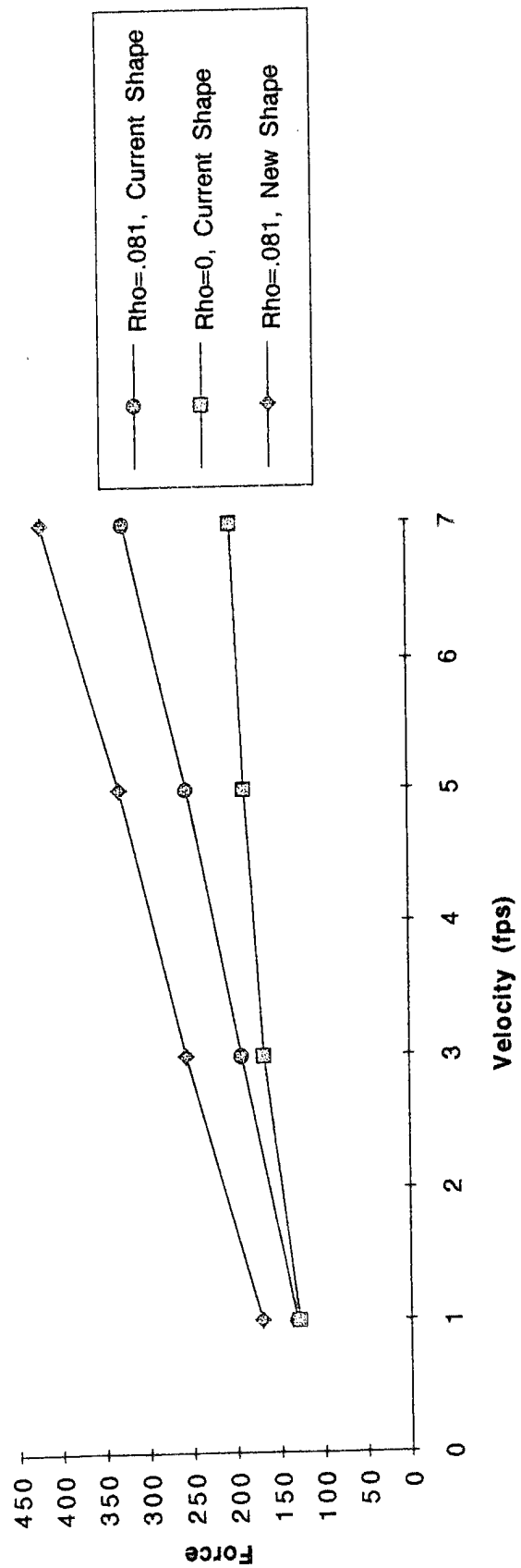
```
mesh limits:

xmin  -5.1500E+01
xmax   4.5000E+01
ymin   0.0000E+00
ymax   1.5000E+01
-----------------
status data:

nodes used  1440
elements    1357
```
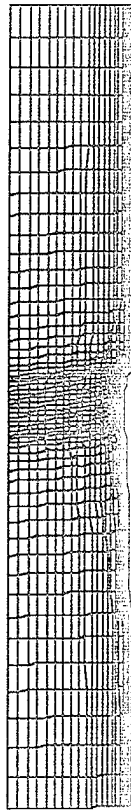
(c) Deformed mesh for plow problem, v_0 = 5 fps.

Figure 2-2. Continued.

(d) Dependence of plow force on plow velocity.

Figure 2-2. Continued.

In the deformed mesh shown, the blade is represented by a prescribed rigid surface which is "moving with steady-state velocity" along the centerline of the solution region, otherwise not visible (due to the expanded scale of the figure). A typical result for soil shear stress is shown in Figure 2-2e, where it is clear that the end boundaries of the model are sufficiently distant to have not affected the solution region near the plow. This isolation is more difficult to achieve with multistep transient numerical models because it results in greater computational effort.

A nearly incompressible, linear viscoelastic material model for soil was used in this demonstration. No soil inelasticity or pore water flow was considered in the formulation of the model and stresses are total stresses not effective stresses. However, substantial development of appropriate boundary conditions (including derivative boundary conditions and plow-soil interface modeling conditions, including friction) were completed to accommodate simulation of conditions imposed in the experimental test apparatus (Figure 1-1a).

Of primary significance was the inexpensive nature of the steady-state finite element analysis. The model consisted of 2,800 degrees of freedom and required only a matter of minutes to solve on an Intel 486-based personal computer. Only 5 to 10 iterations were required for convergence, and no time-stepping is required.

From this preliminary study several conclusions were drawn. Because of the very few iterations (with no time-stepping) required, it should be entirely feasible to perform a three-dimensional, steady-state, inelasticity study of the plow/soil interaction problem including parameter studies for different plow shapes and plowing velocities (implementation of inelastic behavior is ongoing at U. C. Davis). Thus, the single-step, steady-state analysis procedure offers a viable alternative to a multistep, transient analysis of the plow/soil interaction problem. However, because no suitable three-dimensional steady-state finite element program currently exists (so far as is known), it would seem that the best way toward a numerical solution is to use an available commercial program, to perform a multistep, transient analysis.

Two possible approaches to a three-dimensional nonlinear plow/soil interaction model based on a steady-state finite element algorithm were suggested along with a few tasks necessary to eliminate obvious deficiencies in the current software (also, see Appendix A for a related discussion involving contingency modeling plans).

1. The present two-dimensional code at U. C. Davis which has the single-step, steady-state algorithm can be extended by adding the following capabilities:

   a. Three-dimensional finite elements

   b. Effective stress and pore water flow formulation

   c. Nonlinear plasticity soil material models

2. NFESC's three-dimensional nonlinear finite element code Geneseos could be modified to include the following capabilities:

   a. Data structure change to accommodate the steady-state algorithm

   b. Merge existing effective stress soil model with new data structure

c. Interface element and slide lines

d. Large deformation

In either case, substantial software development is indicated. However, its cost can be reduced if it is designed and written in conjunction with universities.

Before any attempt is made to produce a steady-state finite element production program and analysis procedure, several items require further investigation. The failure condition in the soil at the tip of the plow, i.e., the state of the soil as it is cut by the plow tip to form a new surface, is not well understood and is an area that should receive further theoretical and experimental study. (This information is also required for a rigorous multistep, transient analysis of the plow problem.) The effect of using a realistic plasticity model for the soil on the rate of convergence of the iteration process in the single-step model must be studied. Finally, porous media flow must be coupled into the analysis.

Of these recommendations, only the computational plasticity issue is currently being addressed. Moreover, in this context, a finite element formulation for handling strain softening in the presence of inelastic behavior has been completed under Navy 6.1 funding support (Simo, 1994; Simo, Oliver and Armero, 1993). This work resulted in a new approach to the analysis and simulation of localization arising in inelastic solids that exhibit strain-softening response, and it has been extended to the finite deformation regime. The technique leads to the systematic construction of numerical models that completely eliminate the strong mesh dependence exhibited by conventional treatments of such problems. It has been recently extended to two-dimensional numerical simulations (Armero, 1995), and warrants further research in support of numerical models in soil mechanics and geotechnical engineering in general.

stress tau-xy

min -8.403E+01

max 3.036E+00

+1.4000E+01
+1.0000E+01
+6.0000E+00
+2.0000E+00
-2.0000E+00
-6.0000E+00
-1.0000E+01
-1.4000E+01
-1.8000E+01
-2.2000E+01
-2.6000E+01
-3.0000E+01
-3.4000E+01
-3.8000E+01
-4.2000E+01
-4.6000E+01
-5.0000E+01
-5.4000E+01
-5.8000E+01
-6.2000E+01
-6.6000E+01
-7.0000E+01
-7.4000E+01
-7.8000E+01
-8.2000E+01
-8.6000E+01
-9.0000E+01

(e) Contour plot of shear stress (τ_{xy}) in soil, $v_0 = 5$ fps

Figure 2-2. Continued.

3.0 MULTISTEP TRANSIENT NUMERICAL MODEL OF STEADY-STATE PLOW/SOIL INTERACTION

A description of the multistep plow/soil interaction numerical model developed in this study is provided in the following paragraphs. Since the problem is characterized by steady-state motion, the distinction is drawn between the previous single-step model approach proposed by Herrmann and Mello (1994) and the conventional multistep approach employed in the following development.

3.1 Finite Element Formulation for Porous Media

ABAQUS requires that a high order finite element be used for analysis of porous media. These elements are referred to as CPE8P and C3D20P, respectively, for two- and three-dimensional applications. The two-dimensional element is an 8-node bi-quadratic displacement and bi-linear pore pressure element, and the three-dimensional element is a 20-node tri-quadratic displacement, tri-linear pore pressure element. This compares with 4 and 8 nodes, respectively, for low order finite element formulations. Use of the high order elements requires managing larger data files due to the existence of midside nodes in addition to corner nodes. Although, high order elements are generally regarded as more efficient where the solution involves large gradients, in the context of large-scale computation, low order elements are generally favored for modeling simplicity.

The finite element formulation for porous media is a mixed formulation; displacements and pore pressures are primary variables, and stress and pore water velocity gradients are secondary (or conjugate) variables. Corresponding specification of boundary conditions for these primary and secondary variables can, at first, be counter intuitive. For example, on a symmetry plane, typically the displacement normal to the plane is constrained to zero. However, it would be incorrect to also constrain the pressure in this way, because this simultaneously implies that flow occurs through the plane in obvious violation of the flow boundary condition. Instead, the pressure variable is treated as a free variable to coerce a zero flow condition normal to a symmetrical boundary.

Moreover, higher order element formulations complicate specification of interface models involving contact forces. This is a result of well-known anomalous behavior of nodal point reaction forces in high order elements (Figure 1-3). Low order elements do not have this complication and tend to work more easily with interfaces.

3.2 Basic Plow/Soil Interaction Model Concepts

The design of a three-dimensional plow/soil interaction model has been considered. The basic model concept is highly constrained in that there are no known alternative approaches possible using ABAQUS/Standard. In discussions with technical support personnel at HKS, Inc., it was discovered that the program does not provide directly for contact problems in porous media that involve large amounts of sliding at an interface. However, its overall modeling capability is sufficiently robust that the following proposed approach is feasible in the case of either two- or three-dimensional modeling of the plow/soil interaction problem.

23

A sketch of the concept for the three-dimensional case is presented in Figure 3-1. The blade is modeled with rigid body elements. The soil is required to be modeled with high order, 20-node elements having the coupled equilibrium/porous media flow formulation (C3D20P). Between the blade and soil, two-dimensional interface elements are required to model the penetration process. However, the 20-node elements have the aforementioned anomalous behavior involving corner node forces. Corner node reaction forces are invariably incorrect in both magnitude and direction and these are the crucial contact forces that determine the resistance of the plow. Their usage in conjunction with contact algorithms can potentially cause havoc with solution convergence, and thus these elements are generally not recommended in contact problems (though an interface element is available for use with them in ABAQUS). However, by also specifying the multipoint constraint (MPC) feature of ABAQUS at the interface, the high order soil elements interpolate displacements linearly on the interface, as is if they were low order elements to begin with. The result is that only corner nodes are active, while midside nodes are suppressed, along with the interface.

By activating the MPC feature, corner node reaction forces can be expected to behave more smoothly. Four-node, vice eight-node, interface elements (IRS4) are then placed between the rigid plow elements and the deformable soil elements to maintain compatibility with the constrained 20-node soil elements. Subsequent specification of frictional behavior always complicates interface models, but it should not necessarily be more complicated because of this approach.

Development and validation of a three-dimensional plow/soil interaction model entails the generation of a finite element mesh, presumably in which the basic geometry and boundary conditions of the mesh would be selected to replicate the laboratory test apparatus (Figure 1-1a) as closely as possible. (ABAQUS PRE, an automatic pre-processor with a graphics user interface, is now available with Version 5.5 to assist in this future task). For the most part, a coarse mesh is anticipated. However, along the plow/soil interface a finer mesh is required to capture strong deformation gradients. This would be a critical consideration, as formidable compute times and data file sizes would have to be balanced with finite element mesh size and other modeling considerations to manage a three-dimensional, multistep transient analysis study.

3.3 Basic Two-Dimensional Model

As discussed for the single-step steady-state analysis demonstration, the multistep transient analysis also considered a plane strain formulation in the horizontal plane just beneath the surface of the soil. The assumption of a plane strain state of stress does not hold up well because the soil stress state is understood to be three-dimensional according to analysis of experimental data from laboratory studies (Cable et al., 1993, and Girard and Taylor, 1994). These data show that the stress distribution through the depth is not uniform. Further, this is not surprising given the proximity of a free-surface. Likewise, a plane stress assumption is also incorrect. ABAQUS supports the plane strain assumption with its CPE8P element, which is the porous media counterpart of the standard high order quadrilateral element for plane strain, the CPE8 element. However, there is no corresponding porous media element counterpart for the standard high order plane stress element, CPS8. Therefore a plane strain formulation, as depicted in Figure 3-2, was pursued to demonstrate the numerical model approach to plow/soil interaction.

SKETCH OF 3-D PLOW/SOIL INTERACTION MODEL

C3D2OP

MPC

MPC

MPC

IRS4

SYMMETRY PLANE
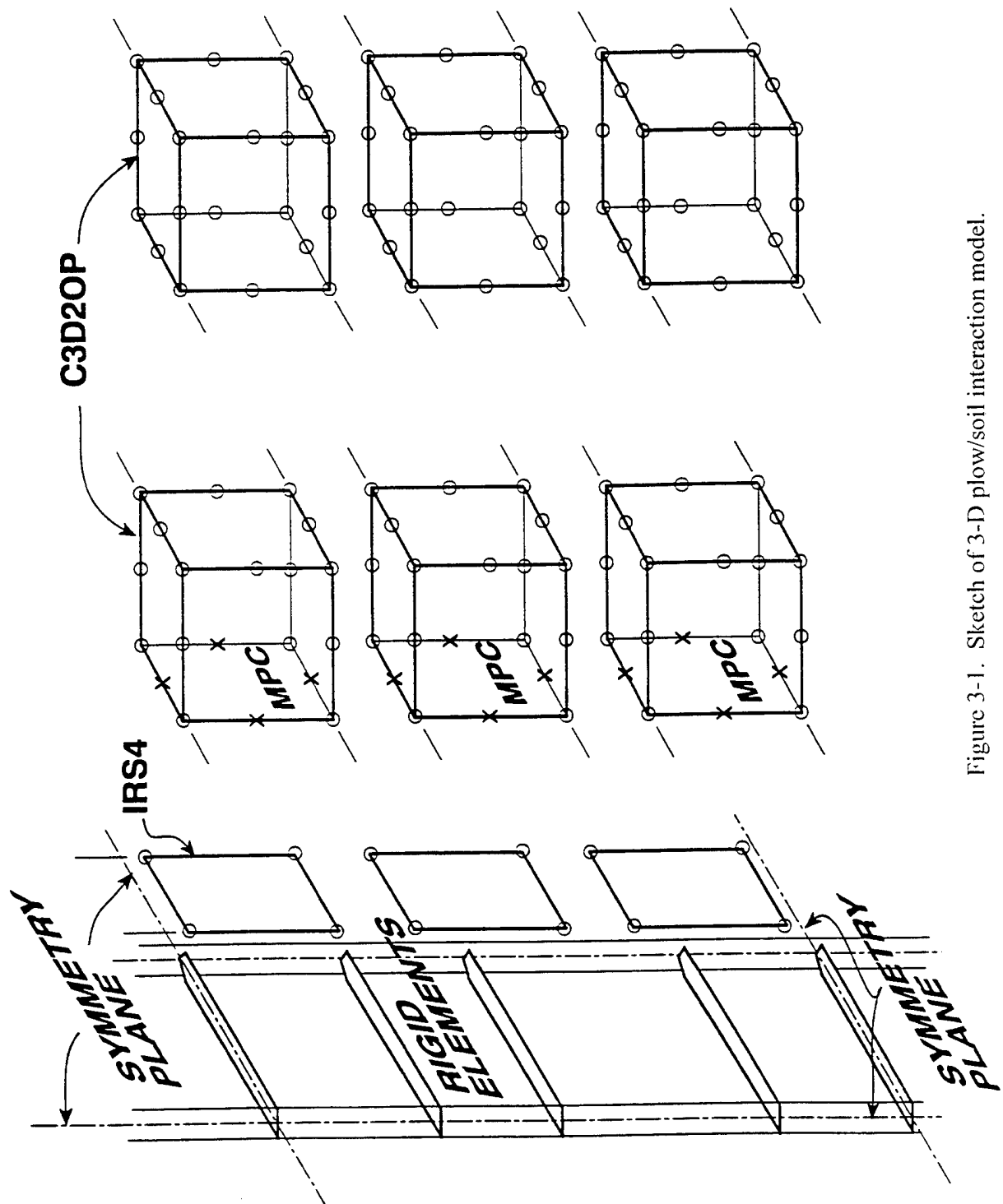
RIGID ELEMENTS

SYMMETRY PLANE

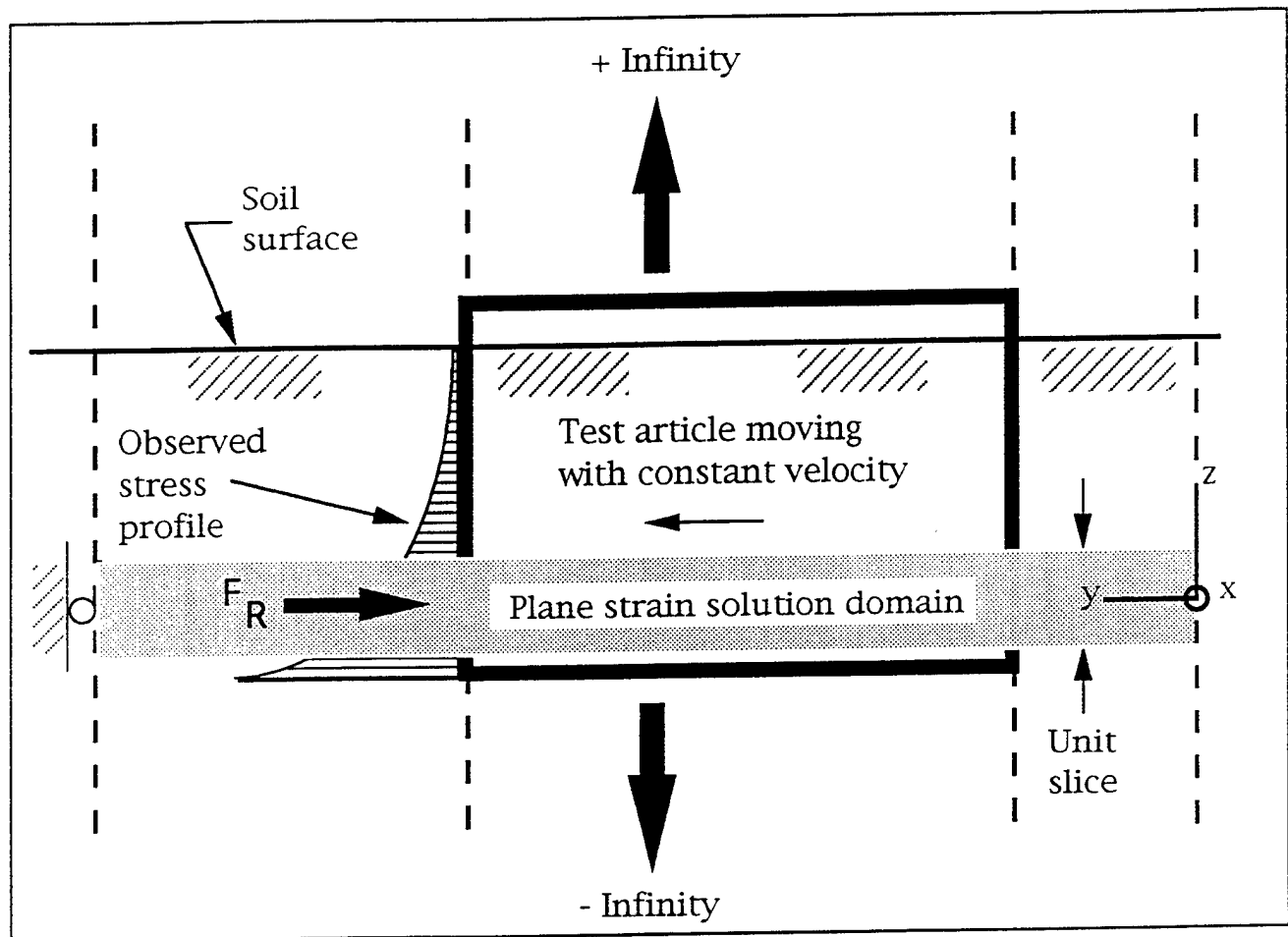Figure 3-1. Sketch of 3-D plow/soil interaction model.

Figure 3-2. Plane strain formulation of plow/soil interaction.

The actual soil resistance force F_R has been observed to act well below the center of the test article (plow blade) in the laboratory data, so it follows that the shape of the actual stress profile would be roughly linear or quadratic (as shown) with depth from the free surface. The plane strain formulation ignores this observed profile in favor of a uniform stress profile (not shown) extending to + and - infinity in the z-direction. The corresponding plane strain solution domain consists of a unit slice of this system, as shown, with the coordinate system and a reaction boundary support located at the ends. The direct strain component in the z-direction is zero in the solution domain.

This two-dimensional analysis was justified on a preliminary basis due to the anticipated numerical modeling complexity of the plow/soil interaction problem. For example, it would be necessary to model soil plasticity behavior, pore water flow, large deformations, large strain, steady-state motion of rigid surfaces involving substantial penetration of a rigid blade, and a frictional contact interface with surrounding soil. Dealing with this complexity is best accomplished deliberately with a series of two-dimensional models before attempting a three-dimensional numerical model of plow/soil interaction. Once these issues are resolved it is presumed that an extension to three-dimensions would be at least conceptually straightforward, considerations of large compute times aside.

Test conditions in the experimental apparatus (Figure 1-1a) guided the overall development of the numerical model so that despite the crude nature of a plane strain formulation of this problem, some comparison of calculated and measured response would be qualitatively feasible.

The corresponding plane strain finite element model is shown in plan in Figure 3-3. One plane of symmetry is exploited as indicated by the symmetry line. The origin of the global coordinate system is placed at the lower left-hand corner of the soil region, with the x-y-z reference axes labeled 1-2-3, respectively. The soil region shown is a 6- by 12-inch rectangular region, and the blade is 6.5 inches long with a 1/4-inch half-width, simulating a 1/2-inch thick blade. The plane strain model has unit thickness. The finite element mesh is finely graded along the intended path of travel to capture expected high gradients of effective stress, strain, pore pressure, and flow response in the region of the blade tip during penetration. The CPE8P porous media elements are high order, two-dimensional quadrilateral elements, and in combination with this mesh, should provide sufficient resolution of the computed response of the soil. To minimize computation time, prescribed element aspect ratios deteriorate with distance from the centerline and primary solution region. The motion of the blade is steady-state, allowing the blade to penetrate the soil to a distance of 9.6 inches where the simulation is terminated. This distance is sufficient for steady-state conditions in the soil response to evolve while providing for complete penetration of the 6.5-inch long blade. It is probably insufficient to effectively isolate the solution domain from the effects of artificial boundaries.

The primary nodal variables are denoted U1, U2, and p; they are, respectively, the x- and y-displacements at (both corner and midside) node points, and the pore pressure at corner node points. The boundary conditions at the left edge of the model impose symmetry conditions on these variables. The U1 component must remain nonnegative to satisfy this condition and the U2 component must remain free. That is, soil must be allowed to displace in all directions except through the symmetry line. Perhaps not so obvious is that pore pressure, p, must also remain free

(i.e., undetermined) so that its conjugate, flow velocity, will be correspondingly constrained to zero in the direction normal to the symmetry line.

All ABAQUS contact elements are referred to loosely as "interface" elements. These elements are intended for rigid-to-deformable body contact in two- and three-dimensions. The specific rigid surface contact element used in the plow/soil interaction model is the IRS21. This one-dimensional element has two nodes at either end and two Gauss points coincident with the nodes. It allows large relative motion to occur between contacting bodies, and the rigid surface element output data are contact pressures (a positive quantity reported at the nodes). Rigid surface contact elements also have a geometry specification option for defining the shape of a rigid body which corresponds to the contact element. These shapes have a single node located at the center of the body which is known as a rigid body reference node. Since rigid bodies may also have motion, the motion of this node must also be appropriately constrained. The IRS21 contact elements are located on the surface of the deformable body which is to come into contact with the specified rigid body.

To implement the inequality constraint $U1 \geq 0$ and to provide for large sliding motion to occur along the symmetry line, this line is regarded as rigid surface along which the plow, also regarded as rigid, slides. A series of IRS21 contact elements are therefore specified along the symmetry line, each of which corresponds to a rigid body reference node at the center of the specified rigid surface (extending from $y = -1$ to $y = 13$ inches). Since this rigid surface must remain fixed, its reference node is completely restrained. The rigid surface has the effect of a wall through which soil elements may not penetrate as they are deformed in advance of the approaching plow.

Once the plow has arrived and displaces soil away from the wall, large relative motions and contact conditions must also be provided for at the interface between soil and the plow. To this end, a second series of IRS21 contact elements are specified along the symmetry line, one for each of the 75 soil elements. Unlike the first series, which are linked to the rigid wall surface, this series is linked to the rigid body reference node at the center of a prescribed rigid surface having the shape of the half plow blade, as shown. This rigid body reference node is completely restrained except for translation along the centerline. In this direction, the plow's reference node is constrained to move at a steady-state velocity. The corresponding reaction forces of interest which are reported at this node are the drawbar, or tow force, and the lateral force (RF1 and RF2, respectively) necessary to coerce the prescribed steady-state velocity for the plow through the soil.

Specification of the interface behavior for the plow/soil interaction model was involved. (Version 5.4 ABAQUS/Standard is reported to be substantially improved in this regard). This behavior, however, may be thought of simply as a parting of the two prescribed layers of IRS21 contact elements which are initially co-linear along the symmetry line, and which are later separated by the advancing plow. One layer sticks to the wall and the other is pried away and becomes sandwiched between the plow blade and the soil while the blade passes by.

Two alternative failure modes for the soil are supported by these interface models along the centerline. They are indicated in Figure 3-4, and are termed a displacement failure mode and a tearing failure mode. In either case the plow must slide along the centerline and the soil must slide over the blade. The difference is in the conditions under which the soil separates from the centerline ahead of the plow tip.
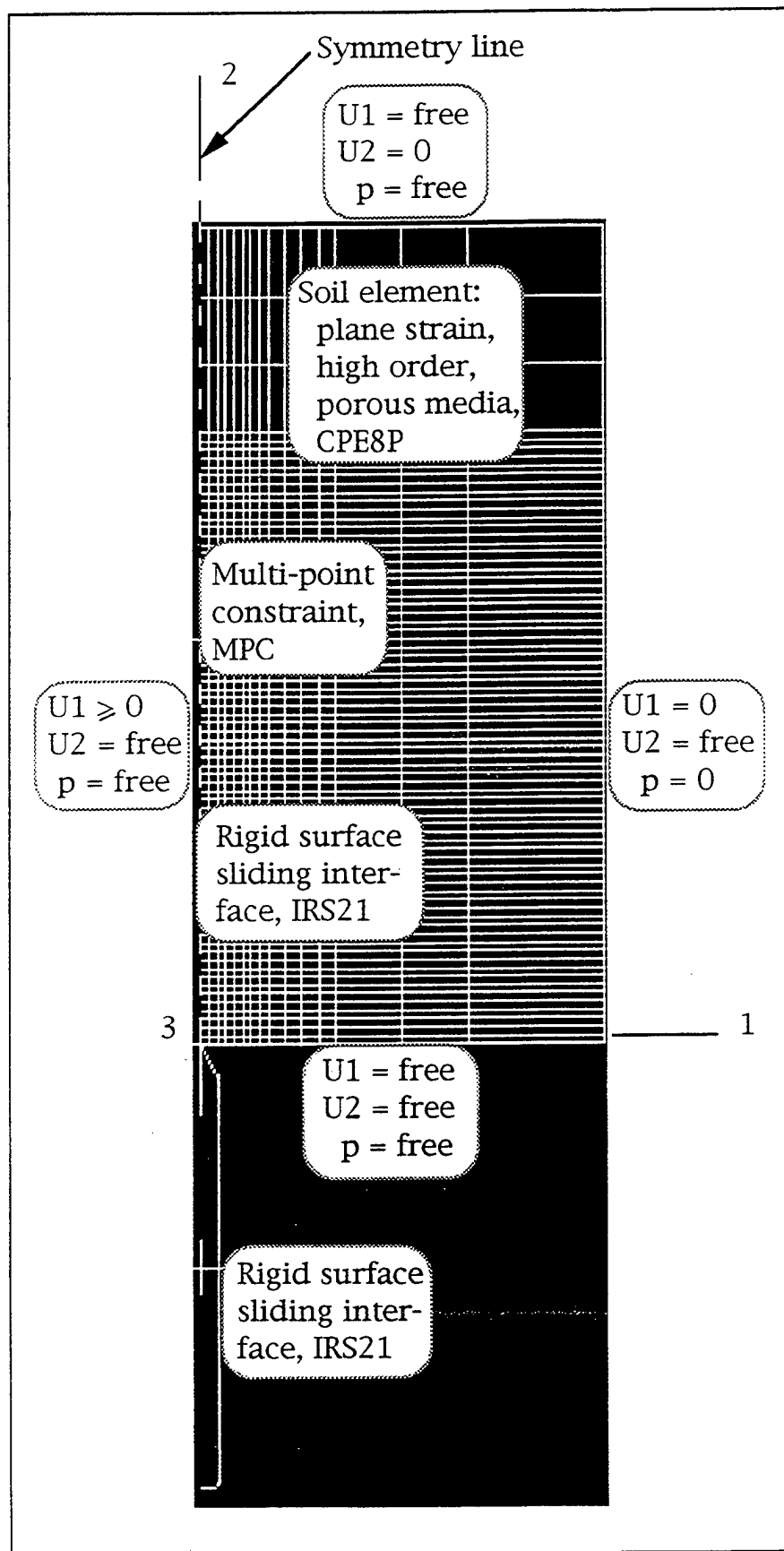
Figure 3-3. Two-dimensional plane strain finite element model of plow/soil interaction.
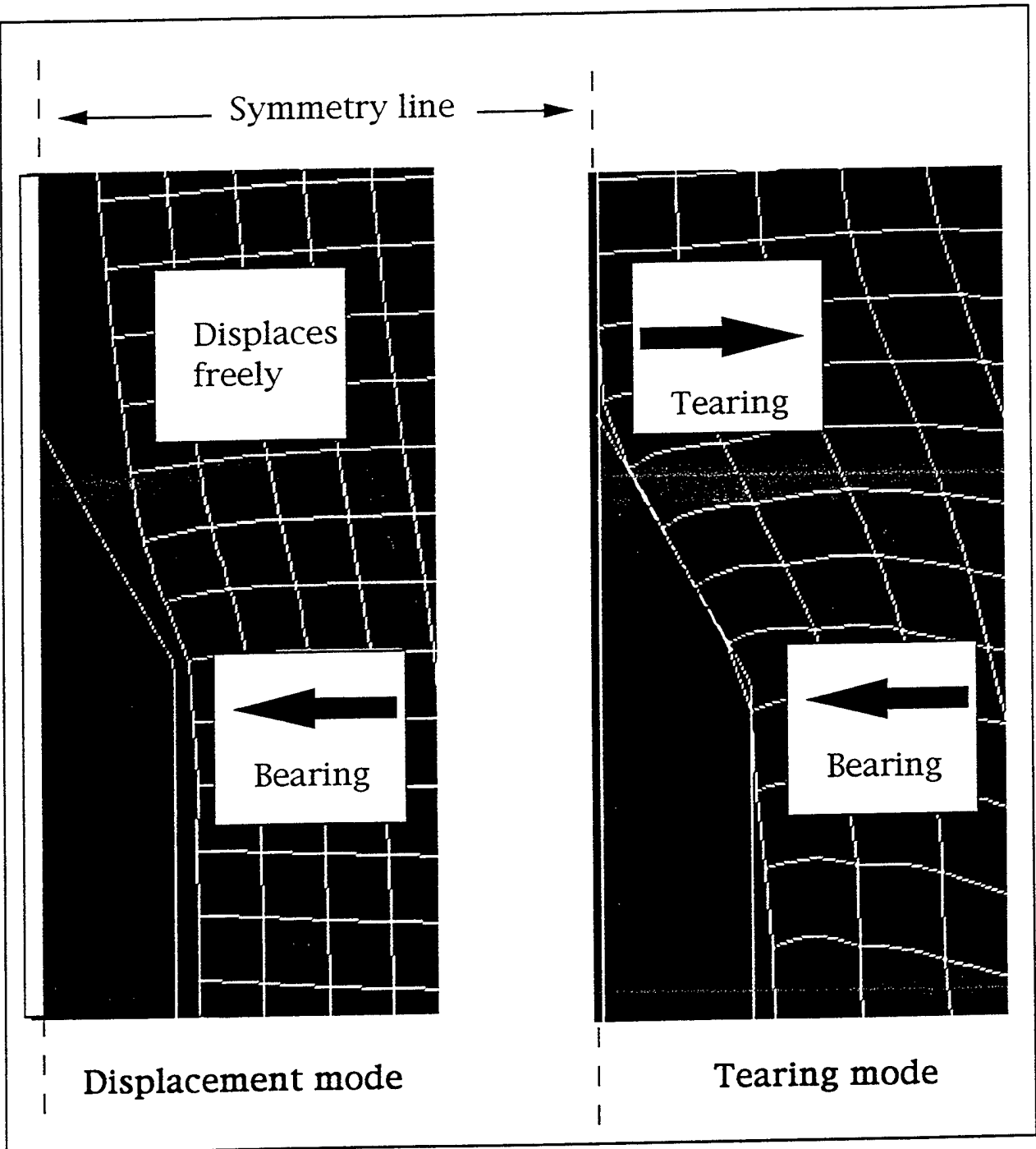
Figure 3-4. Alternative failure modes.

Along the upper boundary of the plow/soil interaction model, the U2 displacement component is constrained to zero to provide a reaction to the plow draw bar force, and simulate rather coarsely the distant rigid end of the experimental apparatus, which is a long narrow box filled with soil (Figure 1-1a).

ABAQUS has no cavitation pressure cutoff capability, and drainage paths in the z-direction cannot exist in the two-dimensional model so negative pore pressures tend to large values as the soil dilates. This can lead to incorrect prediction of negative pore pressure beyond the cavitation pressure associated with the test apparatus (about -14.5 psi). To mitigate this difficulty, the pressure variable, p, is constrained to zero along the edge line (x = 6 inches) allowing flow normal to this boundary as if the side wall was porous. The prescribed displacement boundary conditions along this edge are designed to simulate a rigid side wall, i.e., U1 is zero and U2 is free.

Soil displacement at the lower edge of the model (y = 0) is unconstrained to allow soil displaced by embedment of the rigid blade to escape confinement. Upon constraining this displacement, it was found that penetration of the blade was prevented due to nearly incompressible behavior in the soil. Also, soil in the experimental test apparatus is displaced vertically by the blade rather easily due to the presence of the free surface, and this unconstrained boundary at the lower edge partially compensates for the model having no such free surface.

3.4 Analysis with Preliminary Two-Dimensional Numerical Models

The aforementioned features of the plow/soil interaction model were not all implemented at once. Two preliminary models were developed and studied from which these features evolved.

3.4.1 Two-Dimensional Elastic Analysis Model.

A preliminary two-dimensional elastic analysis initially demonstrated that penetration of the blade into the soil could indeed be simulated in a satisfactory manner. A multistep, steady-state transient analysis using eight-node quadrilateral elements (CPE8; or dry soil elements) for the soil was conducted for this demonstration. Linear elastic properties prescribed for the soil were Young's modulus equal to 6,000 psi and Poisson ratio equal to 0.2.

This demonstration incorporated most of the aforementioned interface and rigid surface modeling techniques necessary to simulate large sliding, and constituted a reasonable beginning for the plow/soil interaction model. A one-dimensional high order rigid surface contact element (IRS22) designed to work directly with the two-dimensional high order element was used. The multipoint constraint condition was not specified for the soil nodes along the centerline in this initial demonstration. Constant velocity (1 ft/s and 8 ft/s) penetration was prescribed for the blade, and it was successfully advanced along the sliding surface into the soil under quasi-static conditions.

Run times for this preliminary model were from 3-1/2 to 4-1/2 hours on a Sparc 2 Workstation. This may seem long for a linear elastic characterization of the soil, but interface elements are essentially nonlinear, and therefore the analysis is nonlinear. During a computer run, many iterations of the contact algorithm were required to resolve inconsistencies between both gaps/over-closures and forces at the interfaces. Furthermore, nonlinear geometric behavior was specified to provide for large displacements in the soil near the plow blade.

31

A dynamic analysis of the plow/soil interaction model could not be performed, since no inertia is included in the ABAQUS formulation for transient, coupled soil-structure interaction analysis. Inclusion of inertia forces in the soil is crucial for earthquake problems, for example, but was generally considered unimportant to the present problem which was otherwise regarded as a low velocity penetration problem. The kinetic energy transferred from the blade to the soil correspondingly was assumed to be negligible. Kutter and Voss (1995) seem to agree with this assumption, at least for smaller velocities, while Herrmann and Mello (1994) indicate that soil inertia forces may be important. Nonetheless, quasi-static procedures were employed to start the plow from rest and carry it through the soil in this initial two-dimensional elastic plow/soil interaction model.

3.4.2 Two-Dimensional Elastic-Plastic Analysis Model. In this analysis, the added complexity of material nonlinearity was introduced into the plow/soil interaction model. The soil was modeled as an elastic-plastic solid. This preliminary model was also prompted by solution convergence difficulty with a Drucker-Prager model specification for dry soil, i.e., a total stress version of the plow/soil interaction model, which was the next model studied after the elastic analysis described above. (The Drucker-Prager model was eventually made to work (see Section 3.5.1)). As before, the elastic properties were Young's modulus equal to 6,000 psi and Poisson ratio equal to 0.2. The yield strength was set to 30 psi, and strain hardening was defined by specifying an ultimate strength of either 800 or 900 psi at various yield strains, beyond which the material model behaves perfectly plastic. The yield strength of 30 psi was representative of the failure stress for a dense sand. Four different strain-hardening curves were tested, only one of which led to a converged solution, as indicated in Figure 3-5. Convergence of the plasticity algorithm was often prevented by too much deformation in the soil near the shoulder of the plow tip. Successful run times typically required about seven hours for the two-dimensional elastic-plastic plow/soil interaction model.

3.5 Drucker-Prager Material Model Calibration

This task involved studying the response of the Drucker-Prager plasticity material model under various conditions with a simple finite element model of a triaxial test specimen. These conditions included use of this model with dry soil and with pore water under both drained and undrained conditions, and with both associative and nonassociative flow laws. Elastic behavior is also modeled by a linear elasticity model (*ELASTIC) for greater efficiency compared to the optional porous elasticity model (*POROUS ELASTIC). Although the latter might be more appropriate, most of the strain in the neighborhood of the plow was plastic strain. These options and those which are discussed below for controlling the elastic-plastic behavior of the soil model are prescribed under the *MATERIAL command in ABAQUS (see Appendix C).

The material model study of a triaxial specimen was carried out in three dimensions. The same finite element formulation used in the two-dimensional plow/soil interaction model was also used in this three-dimensional model of the triaxial specimen. Success was based on how well the measured response of triaxial soil samples was replicated using the Drucker-Prager soil material model in conjunction with the three-dimensional model of triaxial test specimens. Reasonable agreement with measured response constituted calibration of the Drucker-Prager model. A graph of triaxial test data showing deviator stress versus axial strain was used to

partially calibrate the Drucker-Prager model directly. Consequently, the calibrated model reproduces this data accurately, within an arbitrary number of piecewise linear segments.

3.5.1 Modified Drucker-Prager Material Model.

A Modified Drucker-Prager material model was used to simulate soil in the plow/soil interaction study. The variables and features of this model are indicated in Figure 3-6. It is specifically more suited to analysis involving monotonic loading, such as for limit load analysis of a soil foundation. It assumes that a purely elastic response regime exists within the yield surface, shown in Figure 3-6a in principal stress space, beyond which some of the material deformation is not recoverable and can be idealized as being plastic. Yield behavior depends on hydrostatic pressure, so that the material becomes stronger with hydrostatic confinement stress as shown. However, since the yield surface is not closed, this model cannot predict compaction well in consolidation type problems. To do this the modified Cap model in ABAQUS would be required. The Modified Drucker-Prager model also provides for isotropic strain hardening and strain softening of the material. The input data is described in Table 3-1.

Inelastic behavior is generally accompanied by plastic volume change for sand. Either an associative or a nonassociative plastic strain flow rule is allowed, according to whether the angle of dilatancy, Ψ, equals or is less than the friction angle, β. As indicated in Figure 3-6b, in the plane of deviatoric stress, q, and mean pressure stress, p, (i.e., the meridional plane) in the former case, the direction of an increment of plastic strain, $d\varepsilon^{pl}$, is taken to be normal to the yield surface and consequently no volume change takes place during material loading. In the latter case, the loading direction has a component parallel to the yield surface which indicates the amount of plastic volume change. For sands in general, the experimental and analytical evidence is clear that Ψ is less than β. Thus, a nonassociative flow rule was specified exclusively throughout this material study, and for the plow/soil interaction model.

3.5.2 Calibration of Stress-Strain Behavior.

The calibration method used for drained conditions is illustrated in Figure 3-7. A physical triaxial soil sample has a cylindrical shape. The method of loading and the flow of pore water during consolidation in this case are indicated in Figure 3-7a. The stress state and response of the sample is generally regarded as homogeneous until localized failure of the sample occurs. That is, the soil state is assumed the same throughout the sample during any instant of loading up to localized failure. To model the triaxial sample, a 2 by 2 by 2 cube of soil at the center of the triaxial specimen, as shown in Figure 3-7b, is considered to be a representative sample of the specimen undergoing uniform behavior. A finite element model of this cube is employed rather than of the entire cylindrical sample. Exploiting three planes of symmetry, the analysis is accomplished with a single, unit cube, finite element as shown in Figure 3-7c. Thus, the material model study is carried out in an expedient way which is reasonably accurate for calibration, and which is also representative of the finite element formulation which is to be employed in the plow/soil interaction model.

The model is executed in two successive load phases. The first is a geostatic phase whereby initial effective stresses, pore pressures, and confinement stresses are prescribed and allowed to gradually seek equilibrium. The second phase simulates the triaxial test and prescribes a uniform displacement to the top surface, compressing the model to 20 percent axial strain, as shown in Figure 3-8; deformation of the unit cube is indicated in Figure 3-8a, and the

33

corresponding pore pressure distribution on the surface is indicated in Figure 3-8b. As indicated in (Figure 3-7c), node 1 at the origin is completely restrained, and also the path of fluid flow is along the major diagonal from node 209 to node 1. In these data the volume increase due to imposed deviatoric stress and dilation, and the negative pore pressure contours and pore pressure gradients on the cube surface are consistent with flow towards the origin.

Stress-strain triaxial test data for soil #1 from Cable et al. (1993), are plotted in Figure 3-9. Experimental strain-hardening behavior is indicated in the graph of deviator stress versus axial strain in Figure 3-9a. The corresponding model result is shown (solid line), where it is seen that the measured behavior was replicated by the calibrated model. Both strain hardening and softening are clearly required in the Drucker-Prager model if it is to replicate the measured triaxial test behavior. By contrast, a simplified (elastic-perfectly plastic material) version of the Drucker-Prager model can capture the residual stress behavior, but not the hardening and softening behavior.

The accompanying volume change in the measured triaxial data is only calibrated well for strains up to a certain level, after which the model over predicts volume change. Volume change is simulated by specification of a nonassociative flow model. The calibrated value for the dilation angle, $\Psi = 21.5$ degrees, was obtained through a trial and error process. The model begins to over predict volume expansion of the triaxial test specimen for axial strains larger than about 11 to 15 percent, as shown in Figure 3-9b.

The strength of the material is prescribed by a fixed value for friction angle, which was determined from experimental data to be $\beta = 46.2$ degrees. It was prescribed, along with the dilation angle, using the *DRUCKER PRAGER option which describes the yield surface for the elastic-plastic model. That these values are not allowed to vary with material state, introduces error and accounts for the discrepancy in modeling volume expansion.

Likewise, the amount of isotropic strain hardening and softening in the Modified Drucker-Prager model is not allowed to vary with the material state, and otherwise artificially controlled by specifying a value for the cohesion parameter, d (Figure 3-6b). The input data for hardening and softening behavior is listed in Table 3-1, and graphed in Figure 3-10. These data are the plastic part of the triaxial data (Figure 3-9a).
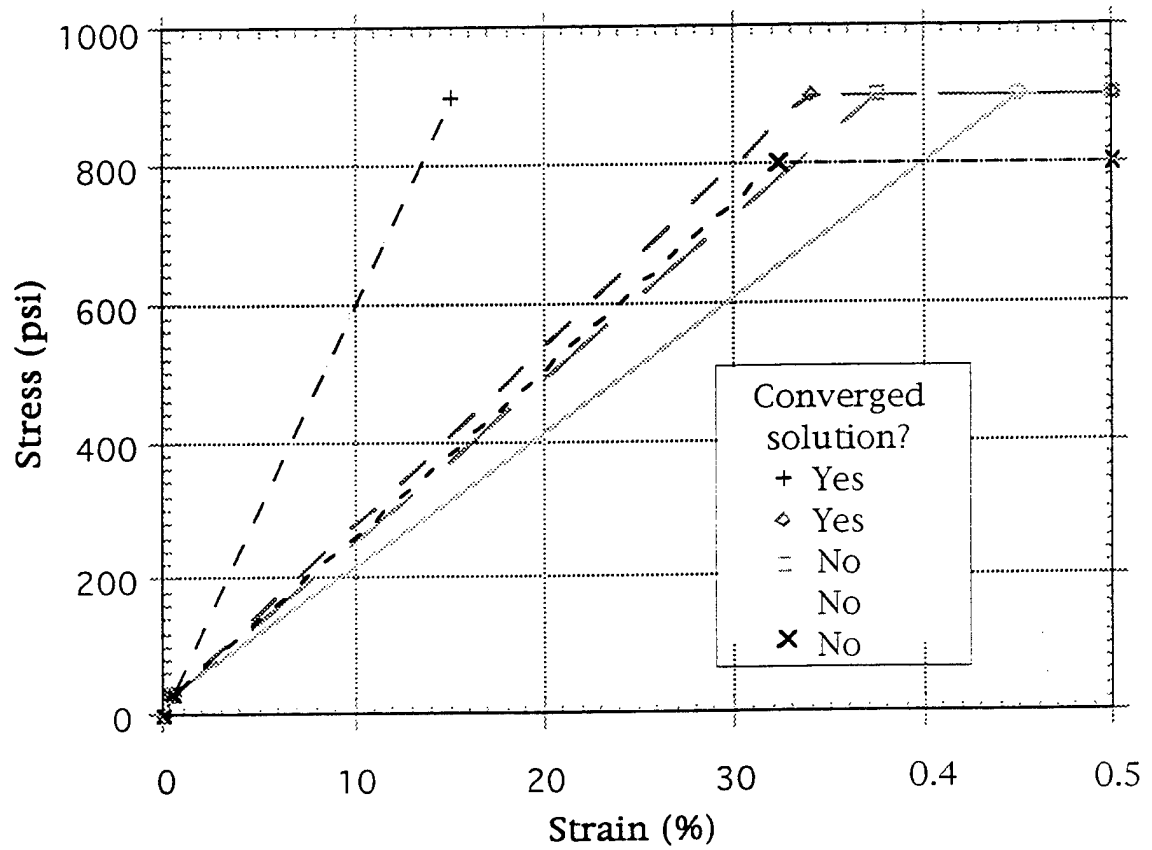
34

Figure 3-5. Elastic-plastic soil models for 2-D plane strain plow/soil interaction model.
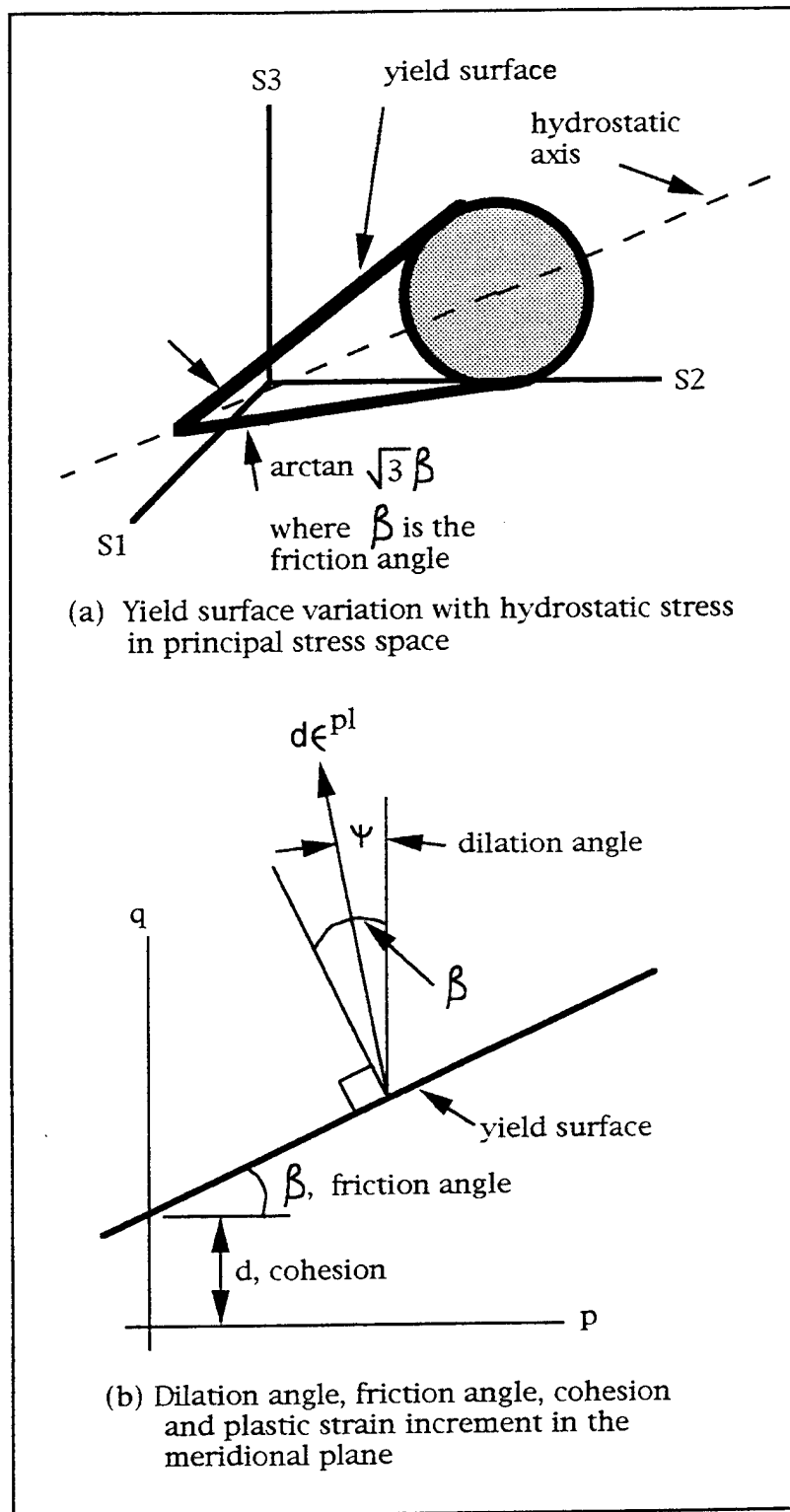
(a) Yield surface variation with hydrostatic stress in principal stress space

(b) Dilation angle, friction angle, cohesion and plastic strain increment in the meridional plane

Figure 3-6. Modified Drucker-Prager plasticity model.

Controlled consolidation displacement

Permeable loading platen at both ends; p = 0

Vertical pore water entrainment path

Soil sample

Impermeable membrane

(a) Triaxial Test System

(b) Sample of Material at Center of Triaxial Specimen

Displacement and pore pressure symmetry conditions imposed on 3 coordinate planes

Node # 209
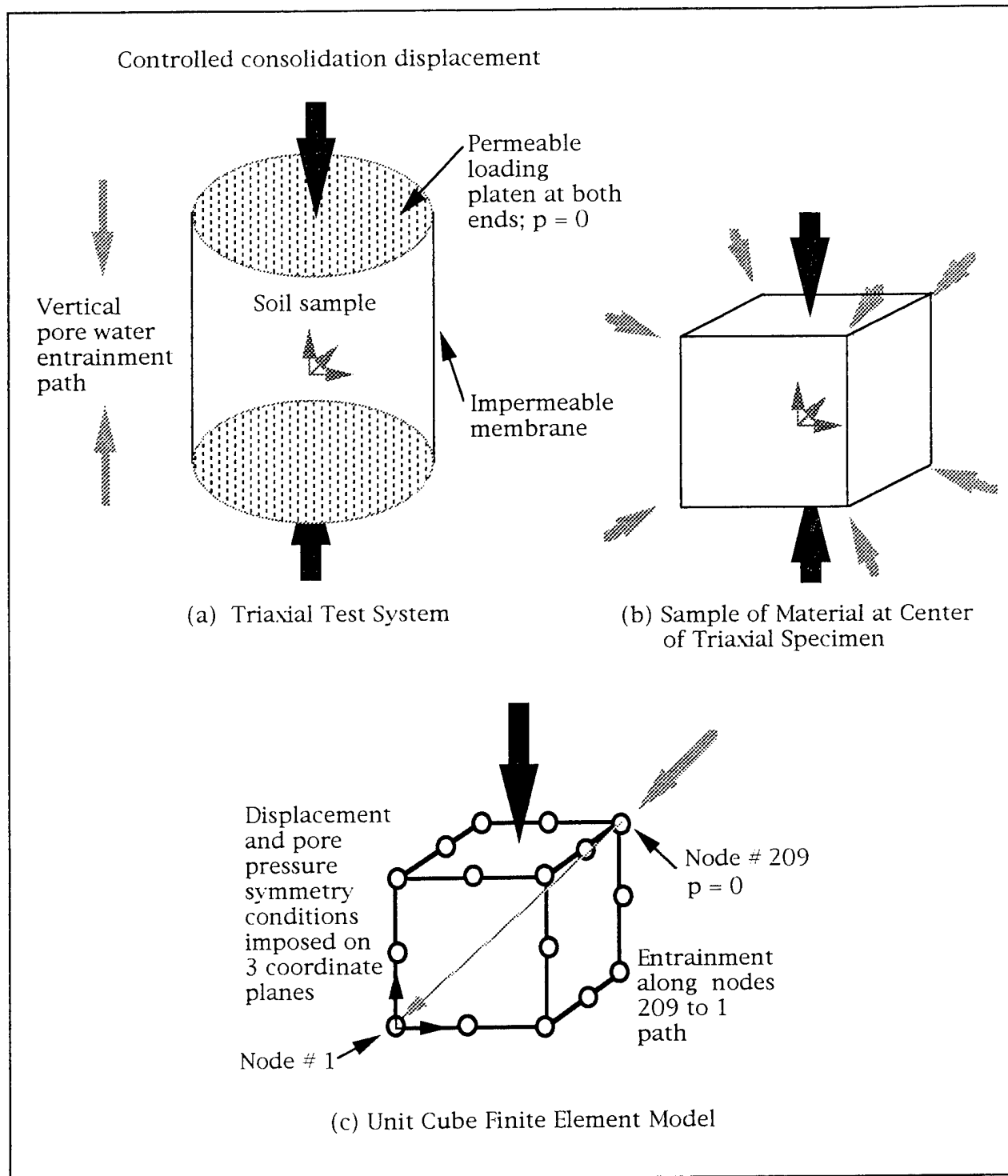p = 0

Entrainment along nodes 209 to 1 path

Node # 1

(c) Unit Cube Finite Element Model

Figure 3.7. Drained triaxial test simulation approach for calibration of Drucker-Prager material model.

ORIGINAL MESH   DISPLACED MESH
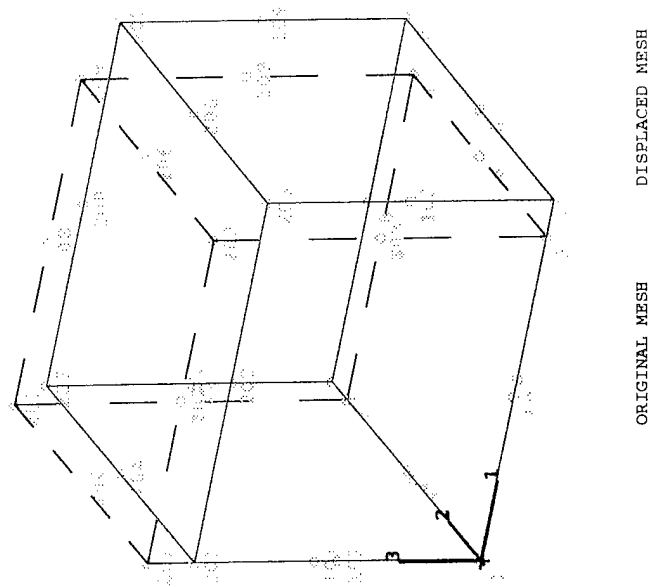
(a) Deformation of Drucker-Prager cube.

Figure 3-8. Triaxial test numerical model results.

POR

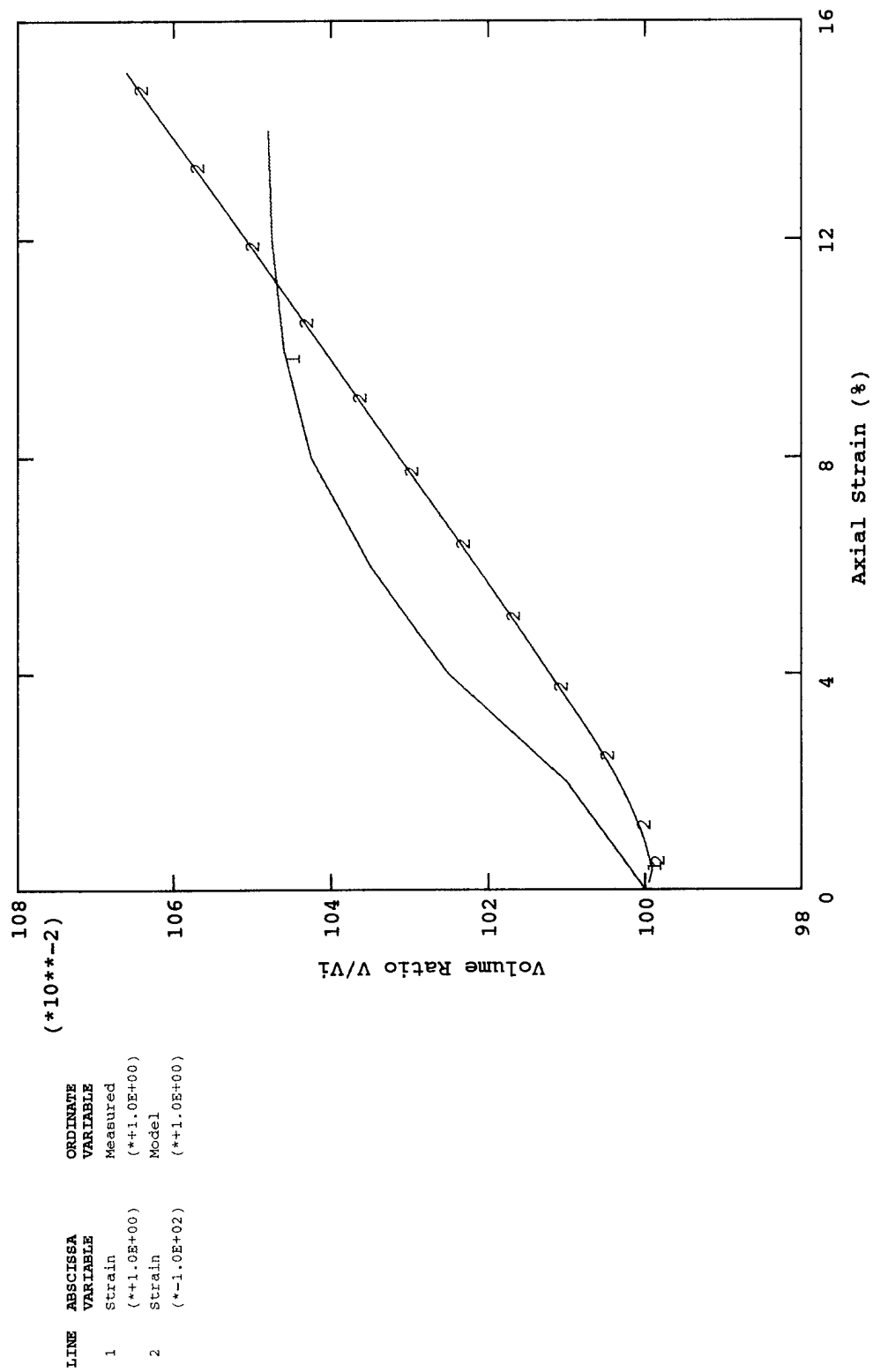| VALUE |
|---|
| -1.88E-03 |
| -1.74E-03 |
| -1.59E-03 |
| -1.45E-03 |
| -1.30E-03 |
| -1.16E-03 |
| -1.01E-03 |
| -8.70E-04 |
| -7.25E-04 |
| -5.80E-04 |
| -4.35E-04 |
| -2.90E-04 |
| -1.45E-04 |
| +0.00E-00 |
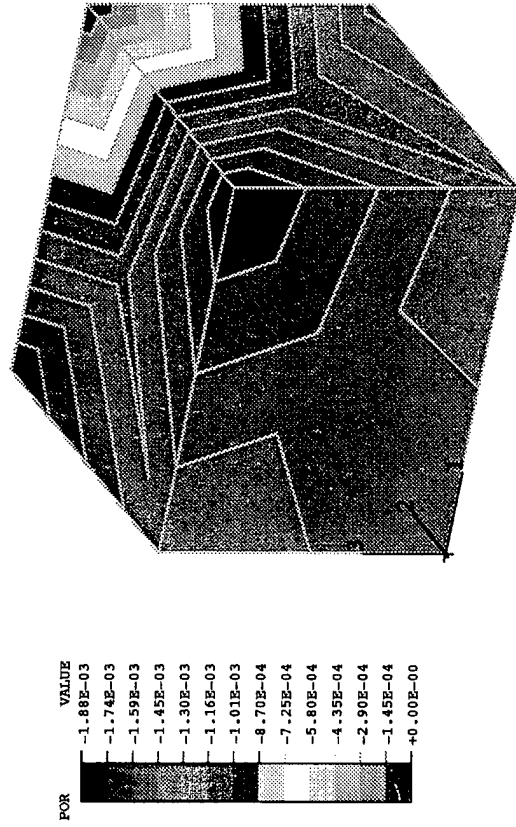
(b) Pore pressure distribution on surface of cube.
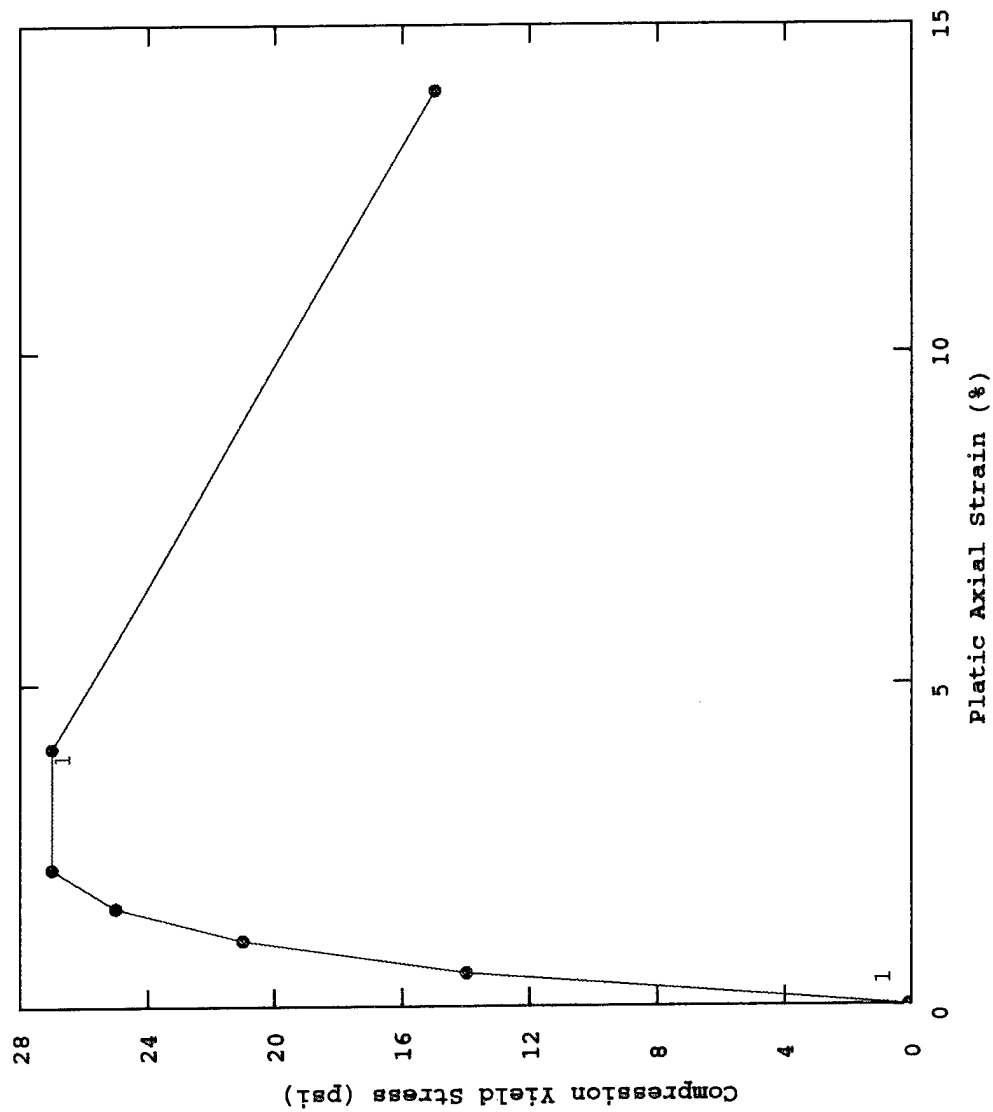
Figure 3-8. Continued.
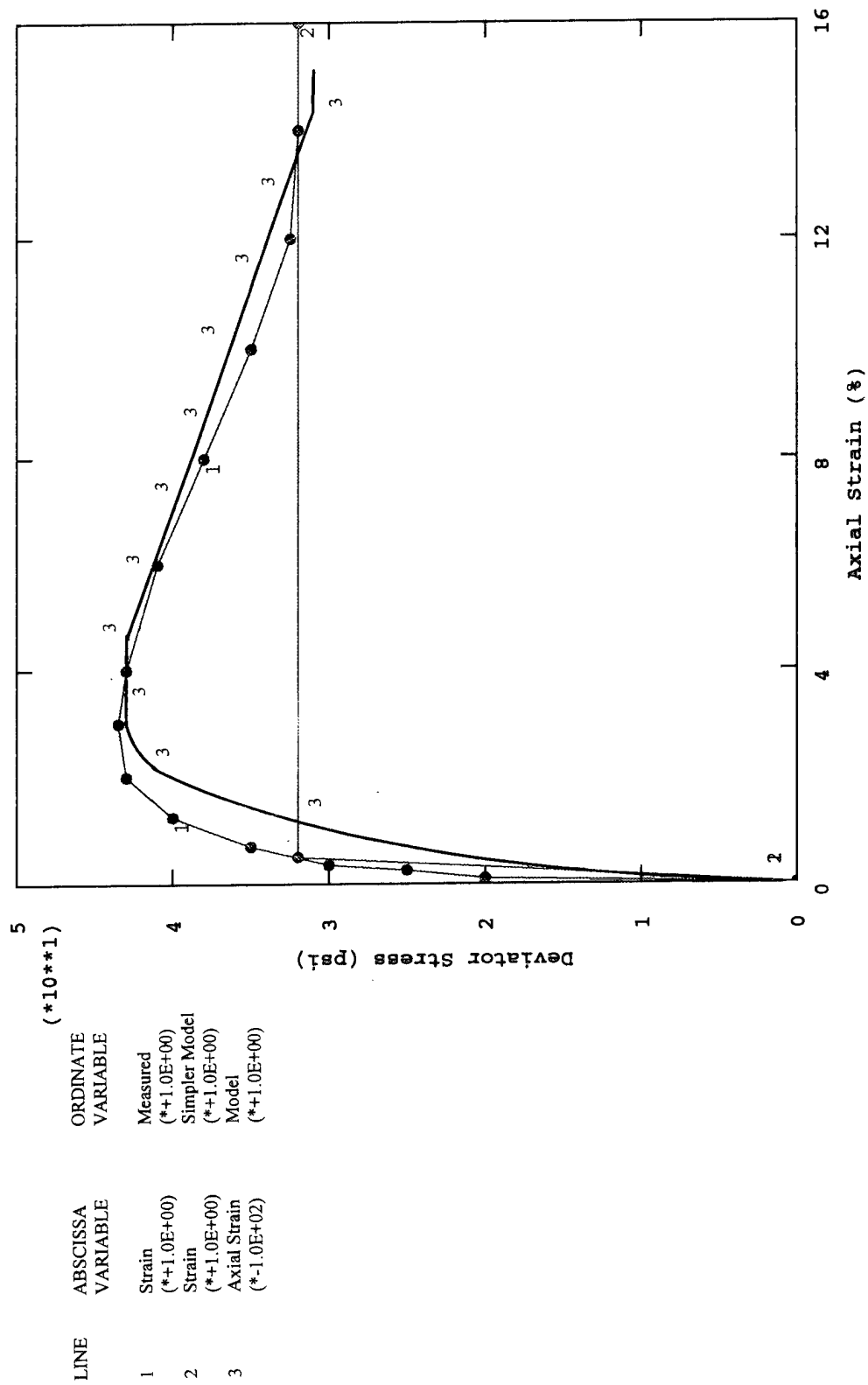
(a) Calibrated deviation stress behavior.

Figure 3-9. Stress-strain behavior in triaxial specimen.

(b) Calibrated volumetric behavior.

Figure 3-9. Continued.

Figure 3-10. Yield stress versus plastic axial strain in compression.

Table 3-1. Input Table for Calibrating Strain Hardening/Softening
Behavior in Drucker-Prager Model

Deviator Stress (psi)	Plastic Component of Axial Strain (in.)
0.1	0.0
14.0	0.005
21.0	0.010
25.0	0.015
27.0	0.021
27.0	0.040
15.0	0.140

3.6 Two-Dimensional Effective Stress Model with Special Handling Features

The plow/soil interaction model is based on a nonlinear quasi-static coupled deformation/flow analysis. A multistep, steady-state transient analysis solution is employed using a simplified version of the aforementioned Modified Drucker-Prager effective stress soil model.

A description of four potential modeling deficiencies in the problem of plow/soil interaction follows:

1. Inertia forces are neglected in the formulation for dynamic soil-structure interaction. It is not clear that these forces are significant in the present problem, but there is no way to know without this capability.

2. Cavitation in the fluid phase cannot be simulated. This was initially thought to have been an insignificant limitation because the experimental data showed evidence of pore pressure values near, but below, cavitation. However, negative (or tensile) pore pressures greater than the cavitation pressure were predicted by the model and there was no satisfactory way of preventing these high negative pore pressures.

3. Problem solution time is very large. This makes it difficult to anticipate investigation of model parameters, although some parametric studies were nonetheless pursued. The required CPE8P soil element is a high order element and a major reason for large solution time. The two-dimensional model required about one week to run, and a three-dimensional model would be prohibitive on the Sparc 2 workstation. A three-dimensional model would most certainly require substantial super computer access time. In a typical computer run, hundreds of gap over-closures and openings occur at interfaces, causing the system to cut back on the increment size and to try again until the impenetrability constraints have been satisfied within a prescribed tolerance. Occasionally, negative eigen values are computed and the system warns of numerical instability, but the system generally does recover.

43

4. The Modified Drucker-Prager soil material model is overly sensitive to tensile values of mean pressure which inevitably develop in small isolated regions near the tip and wake of the blade. Consequent numerical problems would cause the simulation to crash. To overcome this, the calibrated hardening/softening behavior in the material model had to be discarded in favor of a simplified elastic-perfectly plastic behavior (Figure 3-9a). This allowed a closed form algorithm extant for automatic calculation of a material stiffness to be invoked to avoid numerical problems and allow the simulation to continue. As stated, this simplified model does replicate residual stress behavior, and further strains should be large at the interface of the blade, where the material is expected to be in a failure state. Unfortunately, this could not be shown by calculation since the plow/soil interaction model could not be made to work unless the Modified Drucker-Prager material model was first simplified as discussed.

3.6.1 Simplified Drucker-Prager Soil Model.

The plow/soil interaction model worked satisfactorily with an elastic soil model. Further, the Drucker-Prager constitutive model was satisfactorily calibrated using a single three-dimensional finite element having the same basic formulation as the two-dimensional finite element employed in the plow/soil interaction model (Figure 3-3). The elastic model study and the material model calibration are recommended preliminary steps in the development of a complex model for plow/soil interaction. There was a reasonable expectation that the basic plow/soil interaction model in combination with the calibrated Modified Drucker-Prager soil model would then also work smoothly enough from the beginning. Unfortunately, this was not true, due to a numerical problem associated with a singularity in the yield surface of the Drucker-Prager model which did not manifest itself during the rather extensive calibration study.

The source of the singularity can be seen in Figure 3-6a, for example, where at the vertex of the yield surface in the tension region, the gradient of the yield surface is undefined. When the mean stress at any point in the soil becomes tensile (negative) conditions are created such that the rate equations in the formulation of the Drucker-Prager model will not converge to a solution. A tensile stress state, as represented by a stress point on the tensile part of the yield surface, will generally tend to gravitate towards this vertex. Since the formulated rate equations include terms involving the gradient of the surface, which at the vertex is undefined, the solution for the stress state in the soil will not converge. This often happens, for example, in the analysis of soils with large angles of friction (46.2 degrees in the present study) and causes these stress-point integration algorithms to become numerically unstable.

ABAQUS signals plasticity algorithm warnings during the computation in these instances, and nonconvergence was experienced in some cases even for very small or initial penetration of the plow tip, and even for very small time-step sizes of order 10^{-12}. Very isolated and very minor tensile values were invariably noted in contour plots of mean stress just ahead of the plow tip, and also sometimes in the wake of the plow blade. They were otherwise dominated by compression throughout the soil region. Nonetheless, these insignificant tensile stresses were apparently the source of the difficulty.

Several unsuccessful attempts were made to eliminate the possibility of tensile stress by precompressing the soil region using a combination of prescribed boundary conditions for stress and displacement. However, the difficulty could not be eliminated, and it was concluded that,

because of the singularity problem associated with usage of the Drucker-Prager material model, the distributed version of ABAQUS, Version 5.3, was not capable of executing the plow/soil interaction model without substantially simplifying the calibrated Drucker-Prager material model.

A development version of ABAQUS, Version 5.4, (for which a special UMAT routine (a user-provided FORTRAN subroutine for a material model) for the Drucker-Prager model has been written at HKS (West), Inc.) proved successful in executing the plow/soil interaction model. The UMAT routine included an artificial stiffness to stabilized numerical difficulty. Unfortunately, it was found that the output data files from Version 5.4 could not be post-processed by the distributed Version 5.3 of POST, the ABAQUS post-processor, so that no data from the successful simulation was available. Further, this unreleased version of ABAQUS was generally unavailable outside HKS, Inc., at the time.

The course pursued was to simplify the Drucker-Prager model so that the troublesome stress-point algorithm would be avoided in the calculation of stress at the Gauss integration points within each element. This would allow Version 5.3 to be used successfully, but at the expense of the Drucker-Prager model calibration effort which replicated the hardening and softening behavior evident in the laboratory triaxial test data for the sand material.

A software fix for the vertex problem in the Drucker-Prager model exists in Version 5.3, but only if the model is simplified by eliminating the strain hardening and softening parts of the stress-strain behavior in favor of a simpler elastic-perfectly plastic model of stress-strain behavior (Figure 3-9a). With this simplification, a closed form analytical formulation is substituted for the more complicated numerical stress-point algorithm when computing stress at Gauss points. Clearly, this action is driven by convenience and is somewhat arbitrary but it obviates numerical convergence difficulties with the material model. Further, an argument can be made that the residual stress in the triaxial behavior of the sand material, i.e., the stress corresponding to very large strain, is the important part of the material behavior in the present study. This is because the material next to the plow is obviously subjected to very large strain, and thus levels of bearing stress on the plow are likely to be representative of residual stress levels.

In spite of this simplification, the friction angle which accounts for soil strength and the angle of dilation which accounts for volume expansion of the Drucker-Prager material, both of which derive from experimental observation, remain intact and valid for the material model used in all subsequent simulations of the plow/soil model. Further, though the solid phase characterization has been simplified, recall that the plow/soil interaction model also accounts for the fluid phase of the soil and remains an effective stress model.

The aforementioned Drucker-Prager vertex singularity problem has been recognized in the literature by Abbo and Sloan (1993). Their solution is to approximate the classical Drucker-Prager yield surface with a smooth hyperbola that is continuous and differentiable for all states of stress on the yield surface including tensile states. The hyperbola can be fitted to the Mohr-Coulomb surface (straight part of the Drucker-Prager surface) with two parameters. The hyperbolic approximation everywhere approaches the classic Drucker-Prager yield surface from the inside, and so the approximation of soil strength is conservative with this method. An approximate Drucker-Prager model based upon this comparatively simple fix would be highly desirable as an option to the existing Modified Drucker-Prager material model, since no compromise would be necessary regarding calibration of observed strain hardening and softening

45

behavior in sands. (Such a fix has been announced by HKS, Inc. for ABAQUS/Standard, Version 5.5.)

3.6.2 Tearing the Soil in Advance of the Plow.

The failure mode of the soil directly in front of the plow tip is an important modeling consideration. Two failure modes were investigated in this study; a displacement mode, and a tearing mode (Figure 3-4). The displacement failure mode is comparatively easy to simulate and was implemented first. This mode assumes that the resistance to the plow through the soil is due to displacement of the soil to the side, and that in the direction perpendicular to the centerline, the x-direction, only compression stress can be sustained at the centerline. It is implemented via a unilateral contact condition in the x-direction at the centerline, allowing centerline nodes to freely displace in the positive x-direction while preventing displacement in the negative x-direction, in advance of the plow tip (Figure 3-3). This is implemented with an *INTERFACE command operating on a set of (specially created) centerline elements establishing them as contact elements, and with a *RIGID SURFACE option establishing a rigid surface at the centerline with which the contact elements are to interact.

It was found that the resulting wedging action of the plow tip reduces the critical surface over which the soil is in contact with the blade bevel to about 25 percent of the total surface. In the absence of friction, plow resistance is due exclusively to bearing stress on this surface. Consequently, prediction of this resistance was very low, and the addition of side friction between the soil and blade would be the only way to correct this deficiency associated with the displacement failure mode. Further, a corresponding prediction of a very distinct gap in the soil well ahead of the plow tip contradicts experimental observation. Consequently, this failure mode was rejected, even though it was not apparent at the time how the alternative tearing mode would be modeled.

The tearing failure mode assumes that the plow tip is the main source of resistance, or conversely, that side friction is a minor factor, and that to advance, the plow must fail the soil by tearing it away from the centerline. This tearing failure mode is also known in the study of fracture mechanics of brittle materials as a mode-I failure. Fortunately, ABAQUS provides crack propagation simulation features which support fracture mechanics studies, and moreover, these features are also available in conjunction with the present plow/soil interaction model. However, this additional complexity also proved to degrade the performance or run-time of the model.

Adding the *BOND SURFACE sub-option to the *INTERFACE modeling option, the prescribed unilateral contact surface along the centerline will then also provide for initially bonded nodes. These nodes may also debond, as prescribed by a further specification of a subsequent *DEBOND load history option. This latter option defines a linear rate at which the stress carried by the bonded interface is diminished as a function of time after the interface begins to debond. Its sub-option, *CRACK GROWTH, is used to specify a linear crack growth rate beginning at a fixed reference node, CRACKREF. Hence, a constant crack tip velocity, V_c, with which the interface debonds beginning at the reference node is specified. The prescribed velocity should be only slightly greater than the prescribed velocity of the plow, V, so that the plow does not overtake the crack tip, and the interface does not debond too far in advance of the plow, forming a large gap as described for the displacement failure mode.

The x-direction force at a bonded node prior to separation, F_0, is reduced linearly to zero over an interval of time, $\pm t_0$, centered at the time the crack arrives at the node. The time tolerance t_0 is user-prescribed. In this study, it is set to the time that it takes the plow to travel half an element length, Δy, along the centerline. Thus, the nodal point bond force, F_b, reduces to zero in an interval $2t_0$ centered about the time the crack arrives, as shown in Figure 3-11. Values for these parameters are presented in Table 3-2, with the crack tip velocity which is selected to be less than 0.1 percent higher than the prescribed plow velocity, V.

Table 3-2. Tearing Failure Mode Modeling Parameters

V		Δy	t_0	V_c
(fps)	(in./sec)	(in.)	(ms)	(in./sec)
1	12	0.125	5.208	12.01
3	36	0.125	1.740	36.03
5	60	0.125	1.040	60.05
6	72	0.125	0.868	72.06
8	96	0.125	0.651	96.08
10	120	0.125	0.521	120.10
13	156	0.125	0.401	156.13

Though V_c is only slightly greater than V, the crack will gradually pull away from the plow tip according to this tearing failure model. This in turn causes the loaded bearing area of the plow tip to diminish slightly with time, so that the steady-state resistance will correspondingly diminish slightly with time. Nonetheless, the tear failure model accounts for substantially larger (~2.5 times larger) predictions for plow resistance force than the displacement failure model, primarily because it coerces a larger soil-bearing area at the plow tip. Since the Drucker-Prager model is pressure-dependent, and the tearing failure model also tends to produce higher mean pressure stress at the plow tip (and greater negative pore pressure as well) the material through which the plow moves is correspondingly stronger. This also accounts for higher predictions of resistance.

Despite this very positive additional feature of the plow/soil interaction model, additional research is required to establish the actual failure characteristics of the soil at the plow tip, and then to model the actual failure mode.

3.6.3 Modeling Drainage Paths in Two Dimensions.
Plow resistance which was dependent on plow velocity, as observed experimentally, was not achieved with the plow/soil interaction model as described above. Further, the continuity equation, which governs the pore fluid phase, and which the model obeys, would indicate that velocity dependence should be a characteristic of the solution. For velocities below the critical velocity, resistance should be a function of the rate at which pore fluid flows in the neighborhood of the advancing plow tip.

The influence of the continuity equation is felt only when the fluid is given a chance to flow. If the plow is moving so fast through the soil that the pore fluid, as modeled, had insufficient time to flow, then the soil, in effect, behaves as an incompressible medium. This

47

appears to be the condition in the soil when plow velocity exceeds the critical velocity. Under this condition, the theoretical result is that resistance would be independent of plow velocity. This type of behavior characterized the results with the initial plow/soil interaction model described above. A further indication of this was that initial predictions of maximum (negative) pore pressures were two orders of magnitude larger than experimentally observed values (recall that ABAQUS has no cavitation cutoff mechanism). Moreover, the location of the maximum negative pressure was invariably aft of the plow tip and acting on the side of the blade, rather than at the plow tip where it had been observed experimentally in the laboratory apparatus (see discussion in Kutter and Voss, 1994). To remedy this, attention was focused on compensating for the three-dimensional drainage paths which characterize the actual or physical model (Figure 1-1).

There are two differences in the drainage path characteristics between the numerical model and the physical model.

1. The plane strain numerical model drainage paths are two-dimensional, whereas in the physical model the drainage paths are three-dimensional and have been estimated at 3 to 6 inches in length.

2. The numerical model is confined and has no free surface, while actual flow in the neighborhood of the plow tip occurs in the presence of a free surface.

To account for these differences, two adjustments were made to the plow/soil interaction model. The first was discussed above in connection with Figure 3-3, namely, specification of a zero pore pressure boundary condition along the boundary line, $y = 6$ inches. This improved control of the large negative pore pressures, but it is not sufficient by itself. The second adjustment was based on examination of some experimental soil consolidation results by Gibson et al. (1967). In this work, consolidation tests were run in both two- and three-dimensional soil media, and consolidation was observed to occur approximately 100 times more quickly for the three-dimensional medium. To replicate this difference in the plow/soil interaction model, values for soil permeability were increased two orders of magnitude beyond experimentally observed values for the soil in the physical model.

The actual coefficient of permeability k for the soil was empirically determined to be a function of void ratio cubed (True, 1994),

$$k = 0.087 \, e^3 \, (in/sec)$$

as shown in Figure 3-12 for the anticipated range of void ratio. The prescribed value of permeability for the plow/soil interaction model was given by this relation, times a factor of 100, to account for drainage path differences in two- and three-dimensional soil consolidation media according to the aforementioned experimental result.

Results from the model subsequent to this change were immediately recognizable and positive. The maximum predicted (negative) pore pressures dropped by two orders of magnitude to levels representative of the laboratory test apparatus, and the maximum pore pressure

48

distribution enveloped the plow tip, consistent with observed pore pressure distribution in the physical model.

3.6.4 Solution Control Parameters. A summary of the features and size of the numerical plow/soil interaction model is given in Table 3-3. In addition to the usage of a Drucker-Prager material model, geometric and material nonlinearity, coupled deformation/porous flow behavior, and interface nonlinear behavior, the model has 8,787 unknowns (nodal displacements and pore pressures). With this complexity, solution convergence problems may well be anticipated. It is then useful to relax certain solution control parameters. ABAQUS provides for this with a *CONTROL command. Further, default tolerance values are considered overly tight, and often engineering accuracy can be retained after these tolerances are relaxed to foster improved performance. In the present study it was necessary to use non-default values of residual and correction quantities for both the solid and fluid phases.

The default and non-default solution control parameters which were used are given in Table 3-4. Default values for residual force and displacement correction, 5.0E-03 and 0.01, respectively, have been overridden to promote solution convergence in the solid phase. The largest residual nodal point force in any solution increment must be no larger than 0.01 or 1 percent of the largest increment in nodal point force. Further, the ratio of largest solution correction (for nodal displacement) to largest solution increment (for nodal displacement) must be less than 0.5. Otherwise, convergence is not achieved for the increment and further iteration occurs. All other solution control parameters were assigned default values.
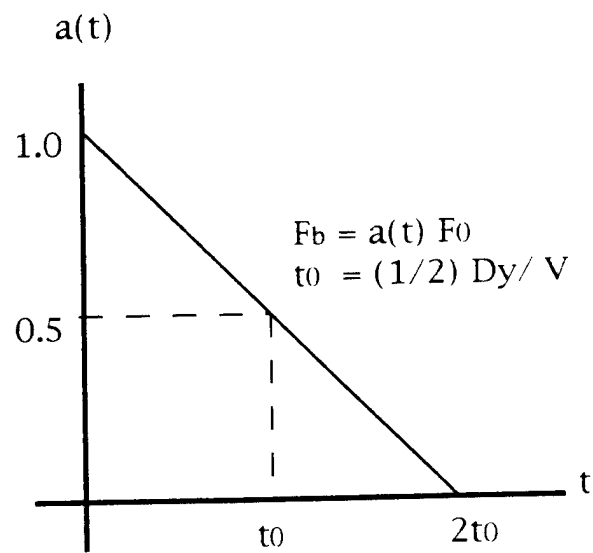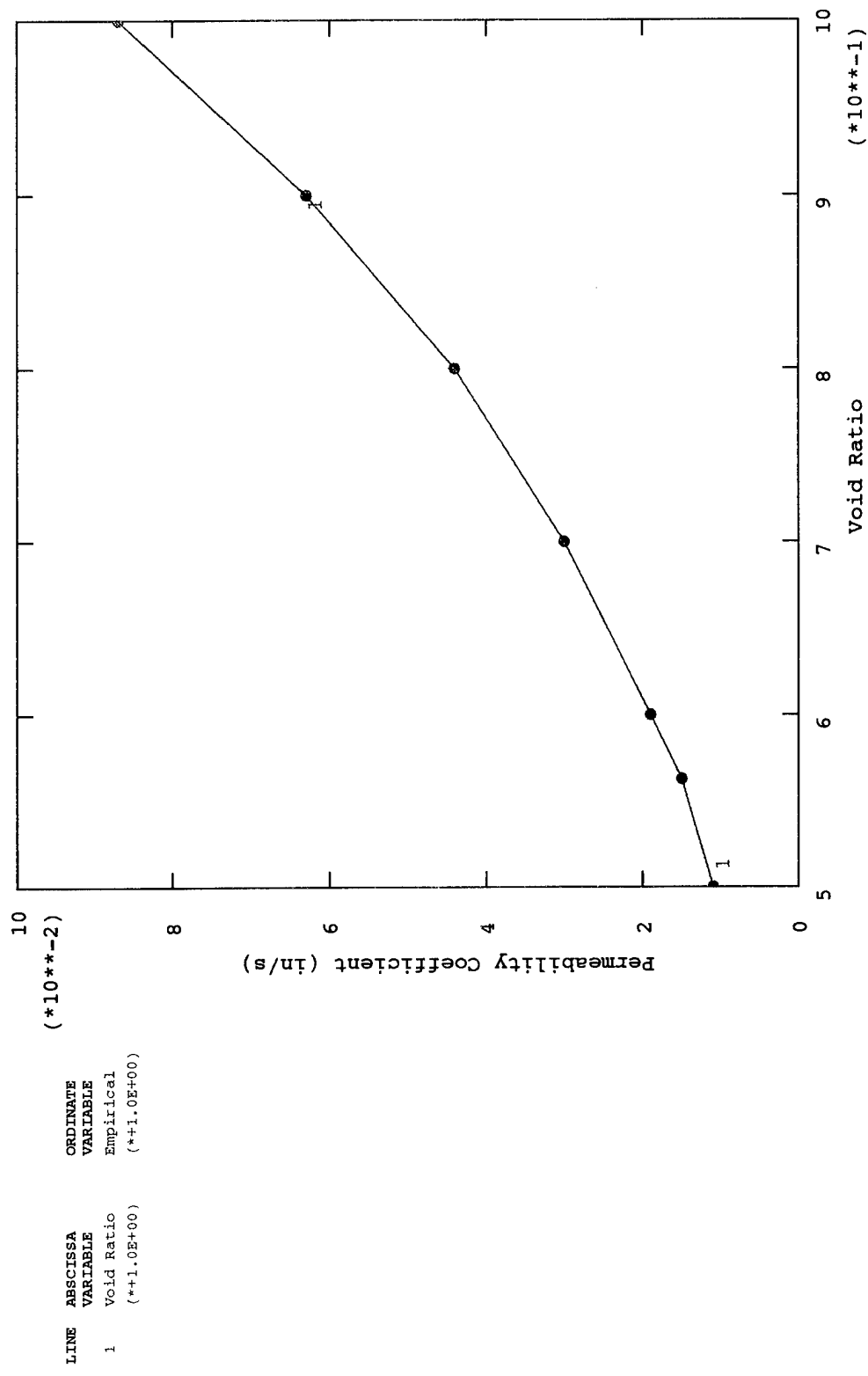
Figure 3-11. Centerline nodal point debond force.

Figure 3-12. Permeability variation with void ratio.

Table 3-3. Summary of Finite Element Features for 2-D Plow/Soil Interaction Model

Type of soil element	8-node plane strain quadrilateral element w/bi-quadratic displacement and bilinear pore pressure interpolation.
No. of soil elements	1,274
No. of nodal points	3,935
No. of rigid surfaces	2; Rigid wall centerline and rigid blade.
No. of propagating cracks	1; Constant velocity crack forming at centerline ahead of plow tip with linearly debonding nodal force.
Type of contact element	2-node planar element w/linear interpolation.
No. of contact elements	149; 74 on wall centerline and 75 on soil centerline.
Type of multipoint constraint	Lagrange multiplier; linear interpolation of soil element midside node displacement along centerline.
No. of multipoint constraints	75
Pore pressure boundary constraints	Pore pressure constrained to zero at 151 centerline nodes, and at 151 edge nodes (line, x = 6 inches).
Displacement boundary constraints	Normal displacement constrained to zero at center-line, and along edge lines x = 6 inches and y = 12 inches.
No. of degrees of freedom (DOF)	8,787 (including Lagrange Multipliers)
Maximum DOF wavefront estimate	107 (optimized; RMS estimate, 104)

Table 3-4. Default and Non-Default Convergence Parameter Settings for Plow/Soil Interaction Numerical Model

Parameter	Value
Convergence Tolerance Parameters for Force	
Criterion for residual force for a nonlinear problem[a]	1.000e-02
Criterion for displacement correction in a nonlinear problem[a]	5.000e-01
Initial value of time average force	1.000e-02
Alternate crit. for residual force for a nonlinear problem	2.000e-02
Criterion for zero force relative to time average force	1.000e-05
Convergence Tolerance Parameters for Volume Flux	
Criterion for residual vol. flux for a nonlinear problem[a]	5.000e-03
Criterion for p.press. correction in a nonlinear problem[a]	1.000e-02
Initial value of time average volume flux	1.000e-02
Alternate crit. for residual vol. flux for a nonlinear prob.	2.000e-02
Criterion for zero vol. flux relative to time avrg. vol. flux	1.000e-05

[a] Indicates use of non-default convergence tolerance parameter selected with a *CONTROLS command (e.g., *CONTROLS, PARAMETERS=FIELD, FIELD=DISPLACEMENT with the following data card; 0.01, 0.5).

4.0 COMPUTATIONAL RESULTS OF PLOW/SOIL INTERACTION MODEL

To gain an understanding of the multistep numerical model of plow/soil interaction, typical quasi-static results are presented and discussed in some detail. Results are presented primarily in graphical form using color to promote their interpretation. These results include unit plow resistance forces and deformation, stress and pore pressure in the surrounding soil during both transient and steady-state motion conditions. Time histories and spatially contoured distributions are presented for most response variables. In the former case, data are reported for a series of node points and elements along the centerline or path of travel for the plow. In the latter case, data are reported for both the solid and fluid phases of soil surrounding the tip of the plow. These data are reported from high order interpolated elements for the solid phase, and from low order interpolated elements for the pore fluid phase. They typify the solution detail of which the finite element method is capable for complex nonlinear problems. The engineering parameter studies derived from the model and reported in Section 5.0 are based on these data.

4.1 Model Displacements

It is useful to first study the soil displacement of the plow/soil interaction model to become familiar with its behavior. Also, soil deformation is directly related to how a trench is formed, which is of practical interest. In Figure 4-1, the displacement of the plow blade (6.5 inches in length) and the surrounding soil are shown when the plow has penetrated into the soil. Corresponding response time histories of resisting force verify that the plow is moving under steady-state conditions when having penetrated this distance. The characteristics of soil deformation shown are typical of the plow/soil interaction model, irrespective of the steady-state plow velocity. The bevel of the plow tip bears directly against the soil pushing it aside as the plow blade progresses. The deformation in the soil medium is maximum in the region of the plow tip. Soon after the shoulder of the plow tip moves past, the soil separates from the plow blade. Soil along the plow blade tends to shear in the direction of travel. Due to local plastic deformation of the soil, interface separation occurs and appears to increase with distance along the blade to a maximum at the aft end. A distinct wake is formed aft of the plow which is also in qualitative agreement with experimental observation. Rebound is evident in the wake indicating elastic deformation in the soil mass as well. Aft of the plow, a substantial amount of extruded soil material is shown which is actually flowing opposite to the plow in the present plow/soil interaction model. This material is escaping the confinement of the model's rigid boundaries and is displaced by the penetrating plow blade. It is an artifact of the model.

A section of the model along the path of travel is presented in Figure 4-2 to show the location of nodes and elements where response time histories are sampled to support discussion of response of the system. Data are sampled at the node points and the elements shown which are located directly on or adjacent to the centerline of the path of the plow. It will be useful to refer to these locations when studying strain, stress and pore pressure results. Up to 1,000 implicit solution time increments are often required to complete a typical analysis. Data is written to output files every 10 increments, so time-history graphs are often constructed with up to 100 data points.

In the following discussion, the plow is moving at a steady-state velocity of 5 fps, the blade (full) width is 0.5 inches, the blade length is 6.5 inches, the included angle of the beveled

53

tip is 60 degrees (Figure 1-1b), and the plow/soil interface is frictionless. Depth and sweep angle of the blade leading edge are not parameters of this plane strain plow/soil interaction model, and are therefore absent from the discussion. The depth is assumed to be unity and the sweep angle is assumed to be 90 degrees.

In summary, the computed soil displacements evidence the basic behavior of the plow/soil interaction model. The important displacements are confined to the plow tip region. Essentially, only the plow tip is in contact with the soil, and the response of the model is otherwise independent of the length of the plow blade. Specific features of model displacements are:

- Maximum localized deformation occurs in the region of the plow tip.

- Separation occurs at a point just aft the shoulder of the plow tip, and increases with distance along the plow blade.

- Soil is sheared in the direction of motion and contains both elastic and plastic deformation.

- A permanent wake is formed behind the plow.

4.2 Plow Forces

Since the plow/soil interaction model is not three-dimensional, the total steady-state towing resistance cannot be computed directly and would have to be estimated. The estimation method is crude and includes the computed force history per unit depth given by model, a reasonable interpolation of bearing stress through the depth of the soil, and experimental observation of the tow force. These considerations are discussed along with the computed contact stress distribution on the plow blade.

4.2.1 Unit Tow Force History. Time histories of the two rectangular components of force-per-unit depth acting on the plow are shown in Figure 4-3. The computed time history of the force-per-unit depth required to tow the (half) blade through the soil at 5 fps is shown in Figure 4-3a. (Its magnitude can be corrected for the full blade thickness by multiplying by two.) Because the two-dimensional plow/soil interaction model has unit thickness in the depth direction, the tow force is a force per-unit-depth having dimensions, lb/in. It is the integral of in-line bearing stress (total stress) over the projected edge of the blade. In these data the initial or transient phase of the tow force is clearly evident and shows a slight overshoot involving initial penetration of the plow blade, after which a steady-state force condition occurs. The oscillations in the data are generally due to numerical noise relating to the numerical algorithms for handling interface contact and nonlinear material behavior. (They are not unlike the noise oscillations seen in typical graphs of measured force time histories in the laboratory.) The steady-state magnitude of the unit tow force can be obtained by merely averaging these data near the end of the range shown when the entire blade length is sufficiently embedded (Figure 4-1).
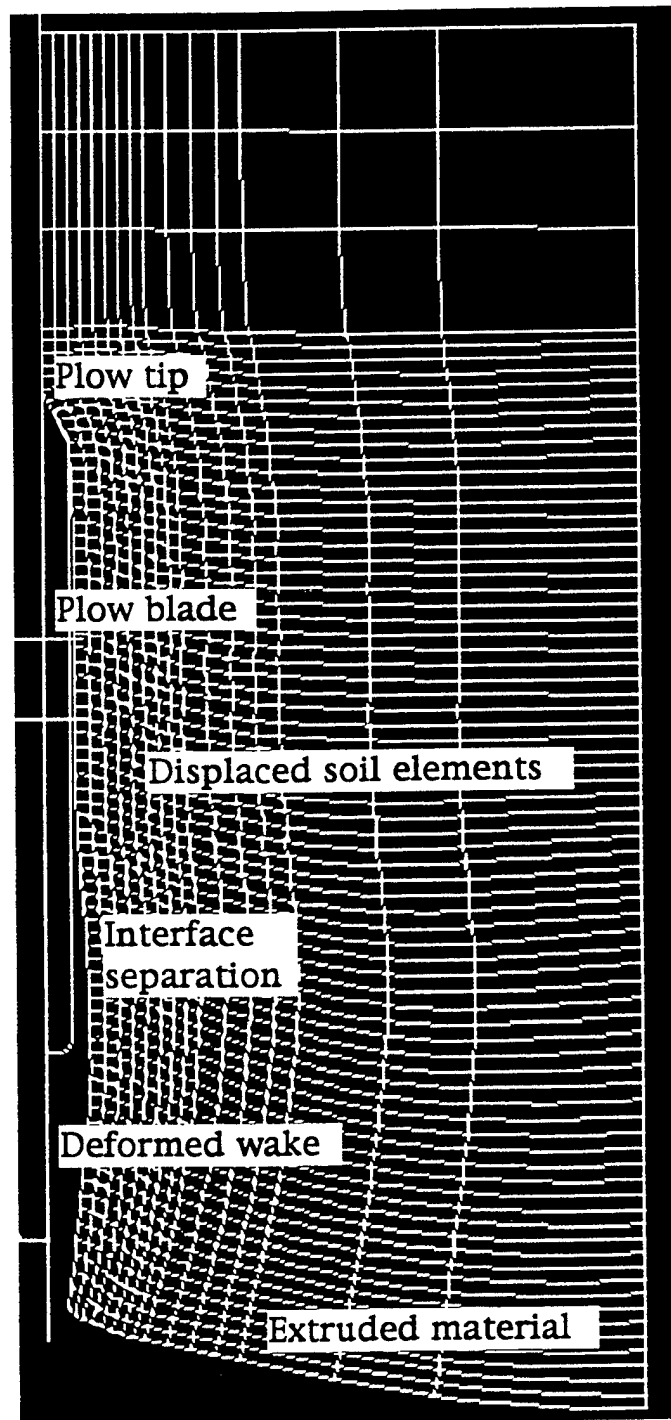
54

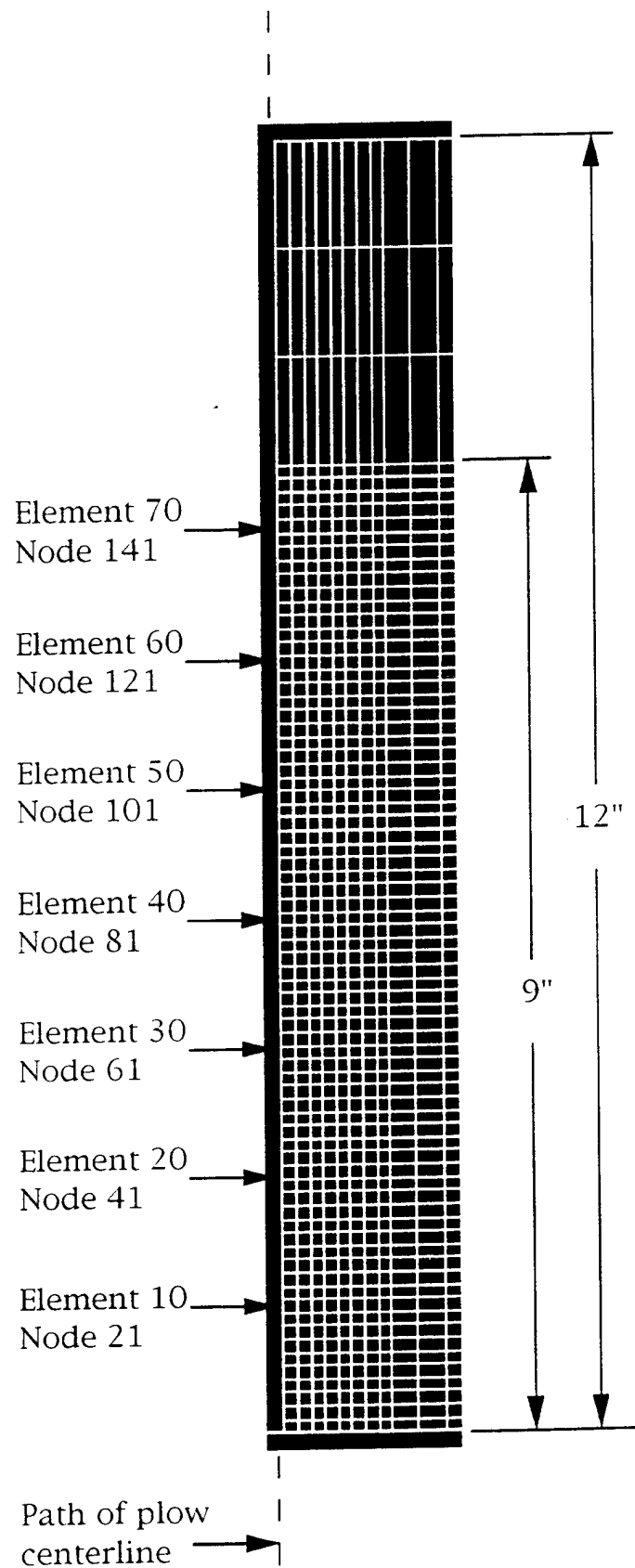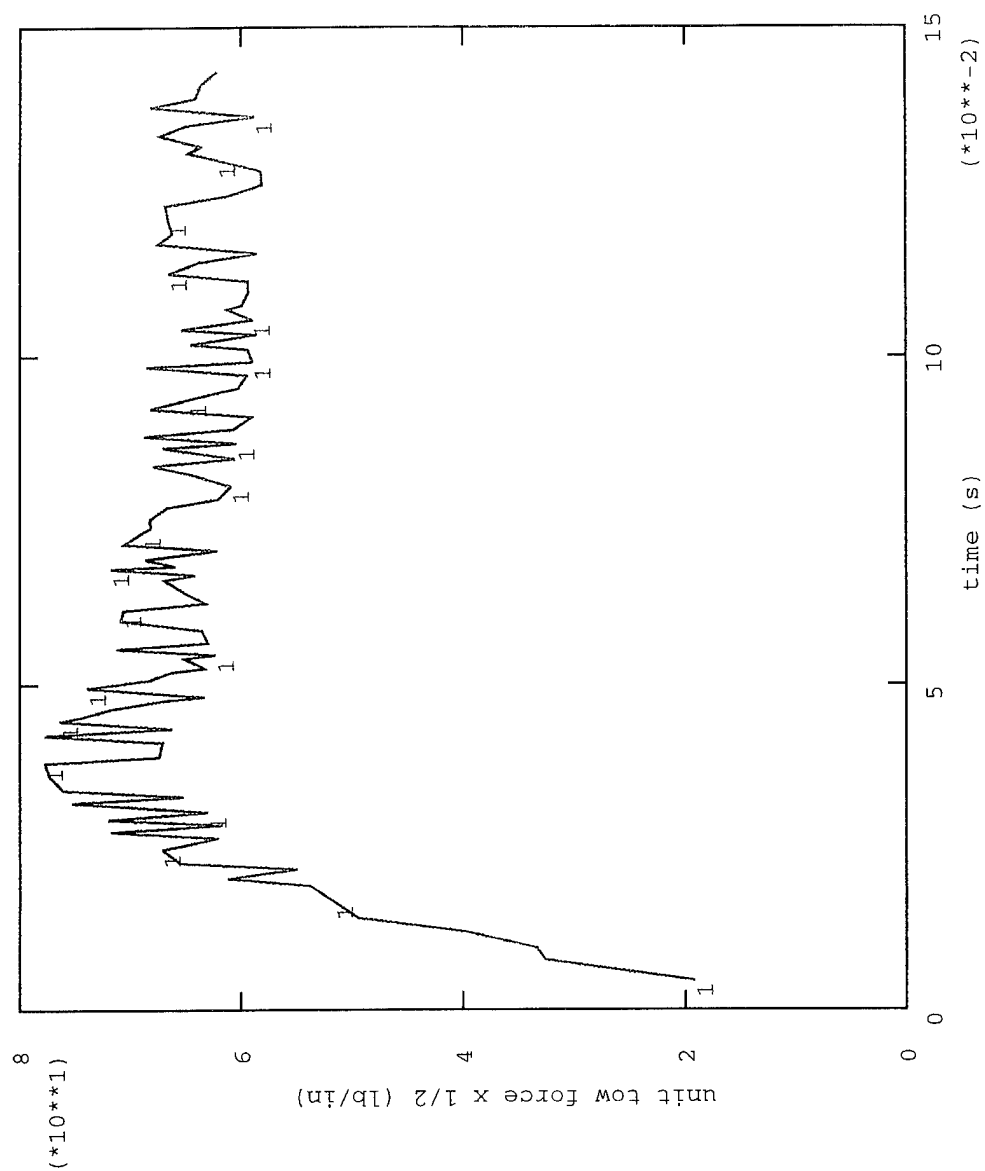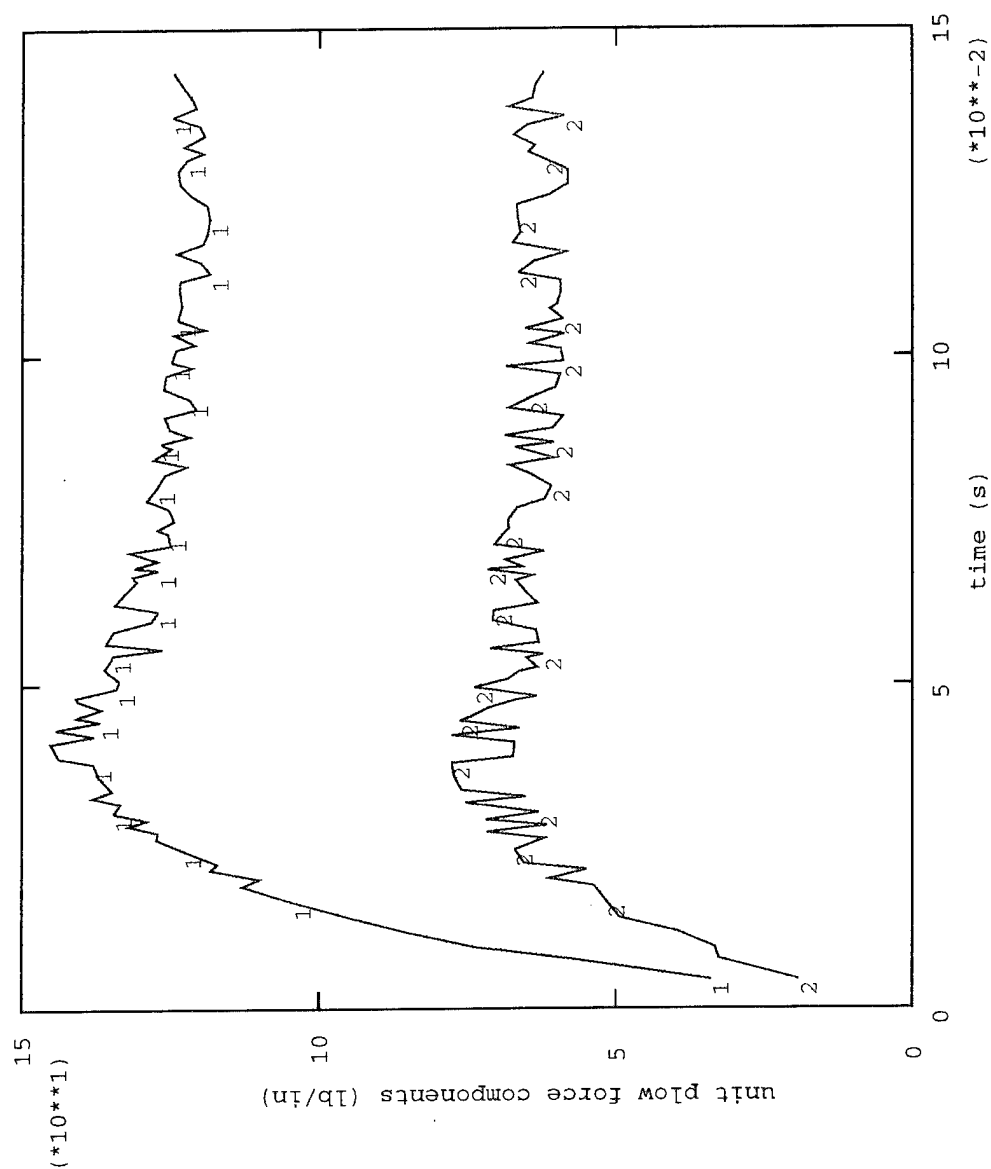Figure 4-1. Displacement of plow and surrounding soil elements.

55

Figure 4-2. Location of sampled response nodes and elements along path of plow.

(a) Plow tow (half) force per unit depth of blade.

Figure 4-3. Unit plow force component histories at 5 fps steady-state plow velocity.

(b) Lateral and tow (half) force components per unit depth of blade.

Figure 4-3. Continued.

4.2.2 Unit Lateral Plow Force History. In addition to the tow force or in-line component, the plow/soil interaction model computes the unit lateral or side component of force on the plow which acts perpendicularly to the blade (tending to pinch the blade) as shown in Figure 4-3b. This component is the integral of total soil stress over the area of the leading edge of the blade up to the point of interface separation (Figure 4-1). Graphed against the half-tow force component, the lateral force is approximately twice as large, which makes the lateral and the tow force components about equal. Both components clearly evidence steady-state conditions. Depending on blade roughness and interface conditions, the lateral component could lead to significant side friction force. For the frictionless blade condition, this component has no role in the estimate of resistance force. Instrumentation in the laboratory apparatus cannot measure the lateral component; it can only measure the unbalanced force in the lateral direction.

4.2.3 Unit and Total Plow Resistance. A total resistance force for the plow, F, can be crudely estimated in conjunction with the steady-state unit tow force component computed by the plow/soil interaction model (Figure 4-3), herein denoted f_{ss}. However, the main points of this exercise are to emphasize that the two-dimensional plow/soil interaction model cannot predict total resistance force, and to reinforce the meaning of the quantity, unit plow force. Two assumptions are necessary, as depicted in Figure 4-4:

1. The plow/soil interaction model is assumed to pertain to a two-dimensional region of soil at an arbitrary depth, H', between the surface of the soil bed and the bottom of the plow at depth H. The value of H' may be determined or calibrated in conjunction with measured data for total resistance force, F_R, so as to achieve agreement between measured and estimated resistance force.

2. The distribution of bearing or resistance force with depth along the leading edge of the plow cannot be predicted by a two-dimensional plow/soil interaction model, and must be assumed. Experimental evidence from the laboratory apparatus suggests that the total resistance force acts below the center of the plow, and erosion/wear of the leading edge of blades tested in the field shows an increase with depth along the leading edge. Thus, for convenience, a linear distribution of bearing force with depth may be assumed.

In the present case of a frictionless 1/2-inch blade with depth H = 6 inches (Figure 1-1b) and moving at 5 fps through a 100 percent saturated sand, the computed unit steady-state tow force f_{ss} is approximately 126 lb/in. (Figure 4-3a), and the measured total resistance force from the laboratory apparatus, F_R, is approximately 950 pounds (Figure 1-2a). The corresponding calculated value of H' would therefore be about 2.4 inches, using the formulas in Figure 4-4. This value can then be considered a constant, and knowing f_{ss} from the model, a total resistance force F can then be estimated, albeit very crudely.

4.2.4 Lateral Contact Force Distribution. Lateral contact force is a force-per-unit length along the plow/soil interface, and it is based on total soil stress. The lateral contact force distribution over the plow blade is graphed in Figure 4-5. These data are reported by the contact elements located at the plow/soil interface. The lateral force-per-unit depth acting on the plow, which is independently reported by the rigid plow blade element (Figure 4-3b), is the integral over the contact zone of the contact force distribution shown. Profiles of both the deformed soil and rigid blade surfaces are also shown. Axes with tick marks have their origins along the deformed soil interface. This interface is coincident with the rigid plow blade for only a short distance near the plow tip where contact exists. The contact force is zero along the interface aft of the blade shoulder (and forward of the blade tip) and non-zero near the tip of the plow. The peak lateral contact force occurs at the shoulder of the blade tip. Magnitudes shown are indicative of steady-state conditions, but they are greater under transient or startup conditions, just as plow forces are greater under transient conditions (Figure 4-3).

4.2.5 Summary of Model Plow Forces. Though it can be measured adequately in the laboratory apparatus, it is not possible with a two-dimensional plane strain model of plow/soil interaction to directly predict the total resistance force acting on the plow. However, plow forces per unit depth, or unit plow forces, can be predicted which contribute to the understanding of plow/soil interaction, as follows:

- It is more accurate to speak in terms of plow tip forces, rather than plow forces, for all mechanical interaction with the soil corresponds to the plow tip.

- With the plow undergoing constant velocity motion, time histories of plow tip forces exhibit two phases of response, initial startup transient forces as the blade enters the soil, and subsequent steady-state forces after the blade is fully embedded. The peak transient force overshoots the steady-state force, and the model predicts their relative magnitudes.

- The two rectangular components of plow tip force are predicted; i.e., the in-line or tow force component and the lateral or side force component. The model predicts their relative difference, whereas the lateral force component cannot be measured in the current laboratory apparatus.

- Lateral contact forces along the bevel of the plow tip vary approximately linearly from the tip to a maximum value at the shoulder.
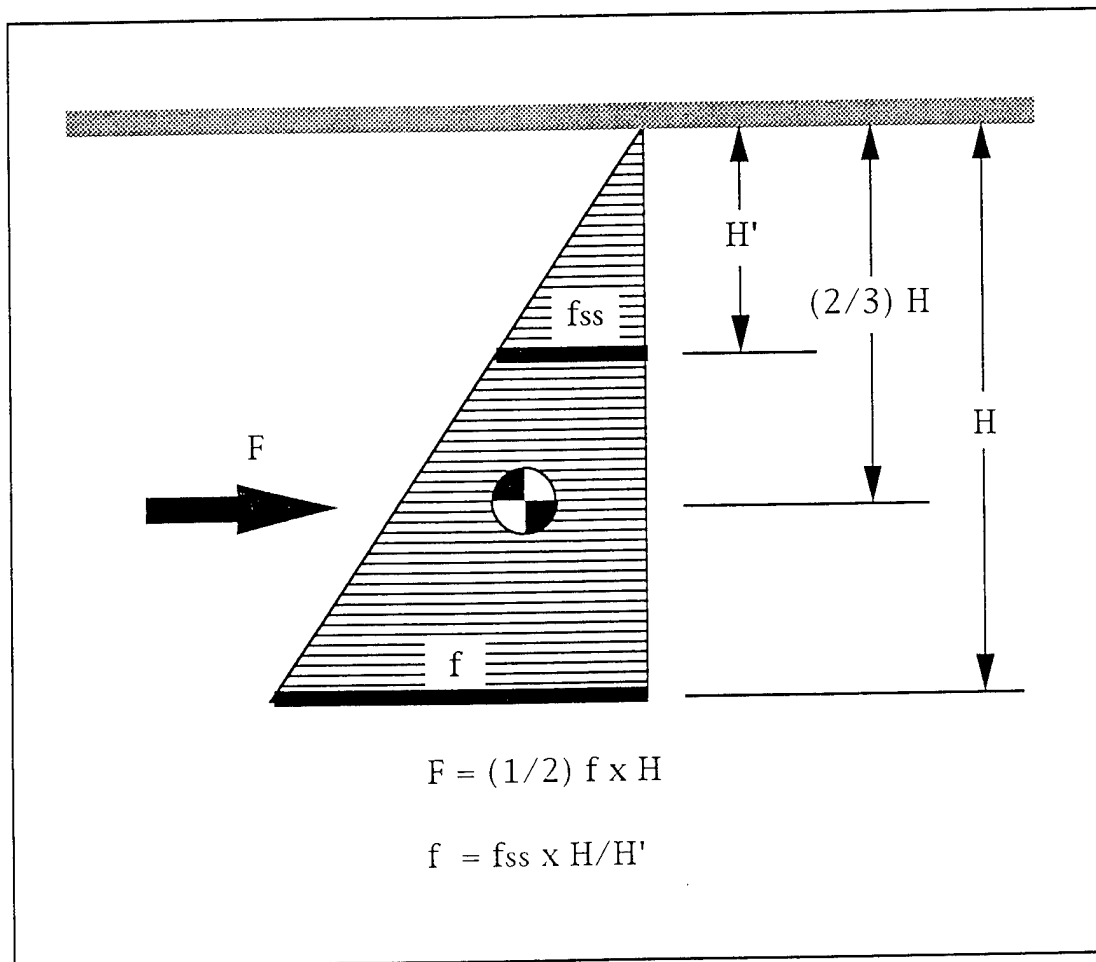
$$F = (1/2) \ f \ x \ H$$

$$f = f_{ss} \ x \ H/H'$$

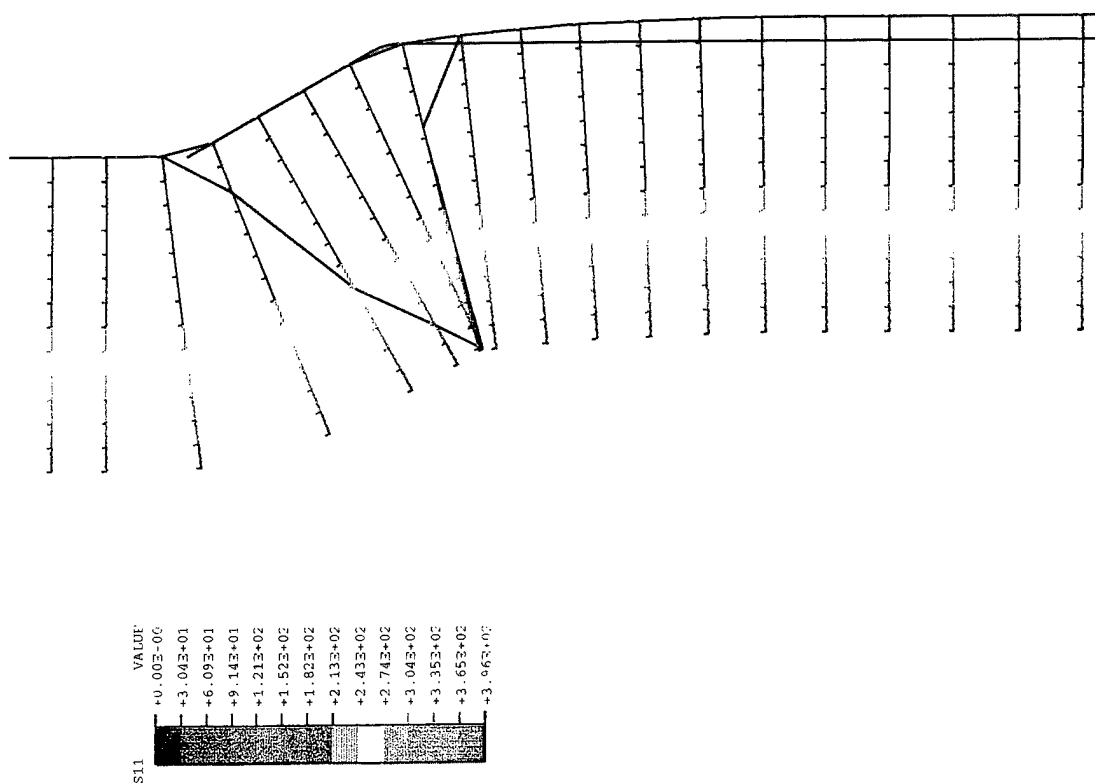Figure 4-4. Method for extrapolating to total resistance force on plow.

61

Figure 4.5. Distribution of lateral interface contact force on plow at 5 fps steady-state plow velocity.

4.3 Deformation in the Soil

The plasticity constitutive model (Section 3.5) employed for modeling the soil is an important aspect of the plow/soil interaction model. Investigating the computed deformation in the soil is also important because, among other things, the soil is a dilatant material, and the soil model should evidence this characteristic. To analyze the computed volume increase that occurs as the soil is sheared, response of the direct or normal strain component must be discussed. For completeness, the shear strains are also included in the discussion. In classic plasticity theory, strain is resolved into an elastic and a plastic component. The following data will show that, near the plow/soil interface, the plastic strain component dominates the elastic strain component for both the direct and shear components.

Strains are element data and the data presented are computed at the centroid of each element. In the former, the data are taken from the selected centerline elements (Figure 4-2), and in the latter, the strain fields shown are enlarged views of a region near the plow tip when the plow is at a position undergoing steady-state motion (Figure 4-1). Regarding the strain field contour data, it is important to point out that the post-processor algorithm averages the element centroid values at adjacent node points before constructing the contour plots.

4.3.1 Direct Strain. The two non-zero components of direct strain, E11 and E22, are presented in Figure 4-6, and each of these strain components is the sum of an elastic and a plastic part. The third component, E33, is constrained to zero under the assumption of a plane strain model. The total strain and plastic strain response are presented; elastic strain can be inferred as their difference.

Time histories for E11, the lateral component of total strain, along the centerline (CL) or path of the plow, are shown in Figure 4-6a. This strain component is apparently tensile along the centerline. The history traces are characterized by a peak response which occurs during arrival and departure of the plow tip, and thereafter subside to a steady residual tensile strain response which is a substantial fraction of the peak response. The residual strain characterizes the total lateral strain component in the soil at the free edge of the groove or wake produced by the plow tip. The spatial distribution of this strain under steady-state conditions, shown in Figure 4-6b, indicates that actual peak strains occur just off the interface and adjacent to the plow tip rather than on the interface. Residual strain extends to a distance of about two blade thickness to the side of the groove, beyond which it quickly dissipates.
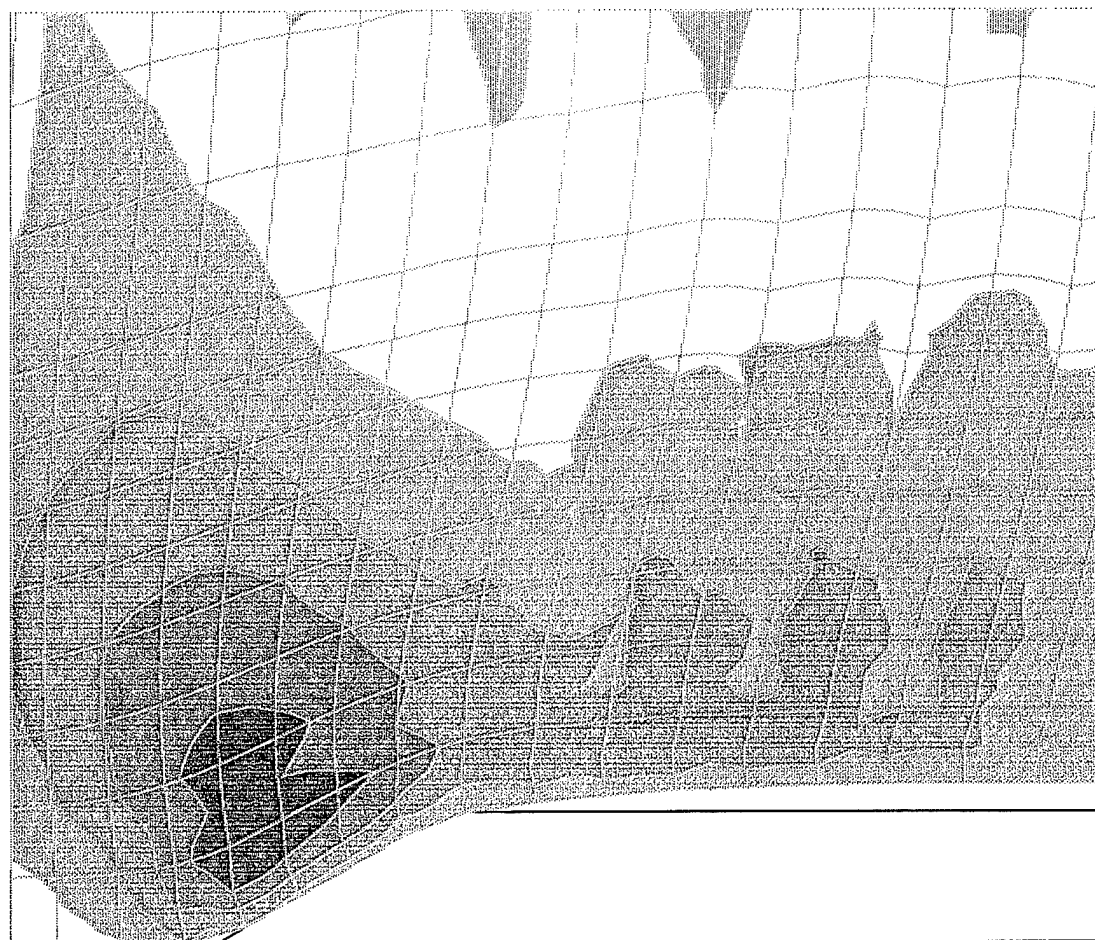
Time histories for PE11, the plastic part of the lateral strain component along the centerline, are shown in Figure 4-6c. Compared to the total strain (Figure 4-6a), the plastic strain is nearly equal in the residual portion of the response. Thus, the residual elastic strain is minute in these data, as would be expected since the soil has unloaded. The spatial distribution of PE11 which is shown in Figure 4-6d is also very much like that for E11 (Figure 4-6b). Most of the total strain component E11 is plastic strain and, therefore, there should be little rebound in the soil at the edge or lip of the soil groove after the blade shoulder passes.

Time histories for E22, the component of total strain in the direction of the plow motion along the centerline or path of the plow, are shown in Figure 4-6e. The history traces are characterized by a transient compressive strain response which occurs during arrival and departure of the plow tip, and thereafter reverses to a steady residual tensile strain response which is comparable in magnitude to the transient response.
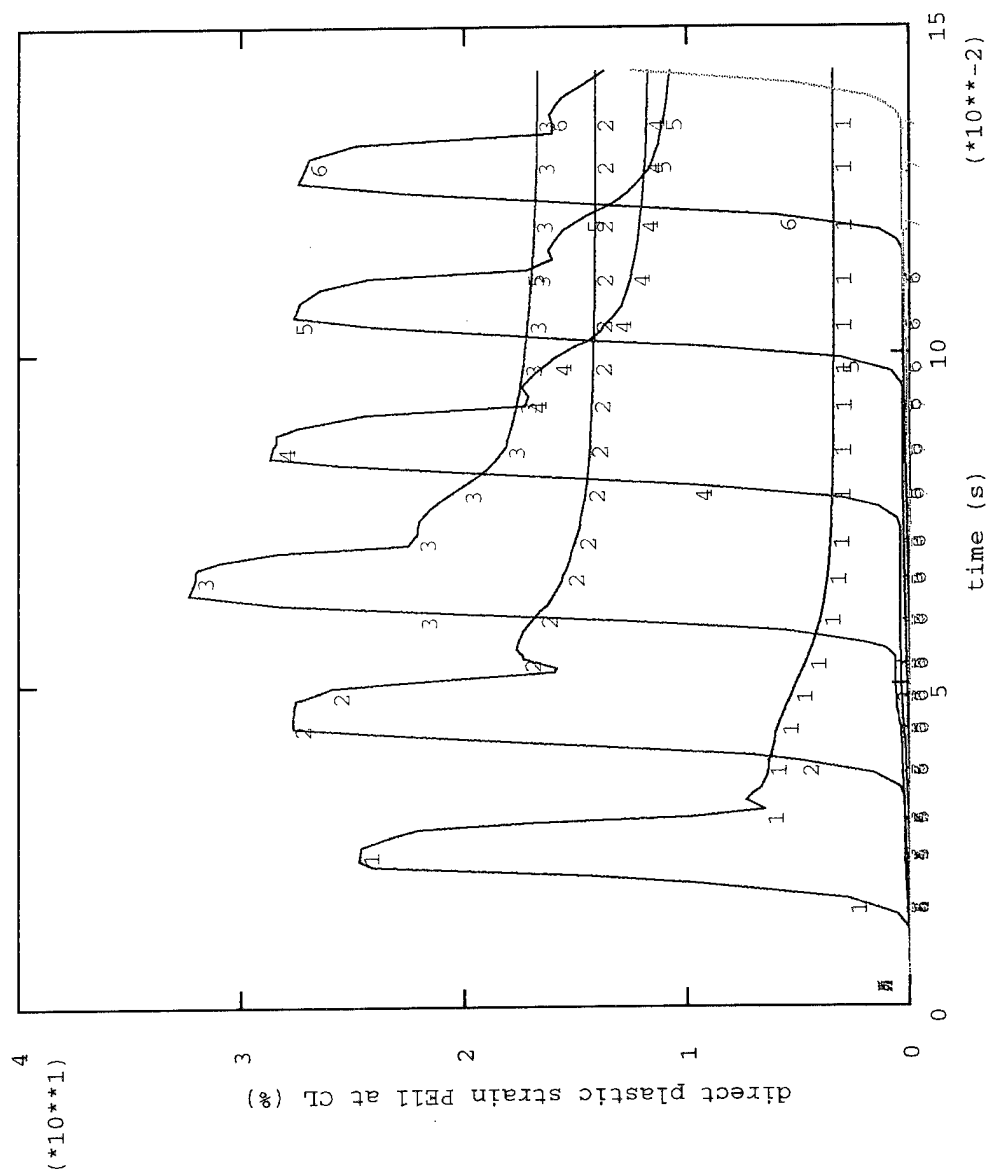
63
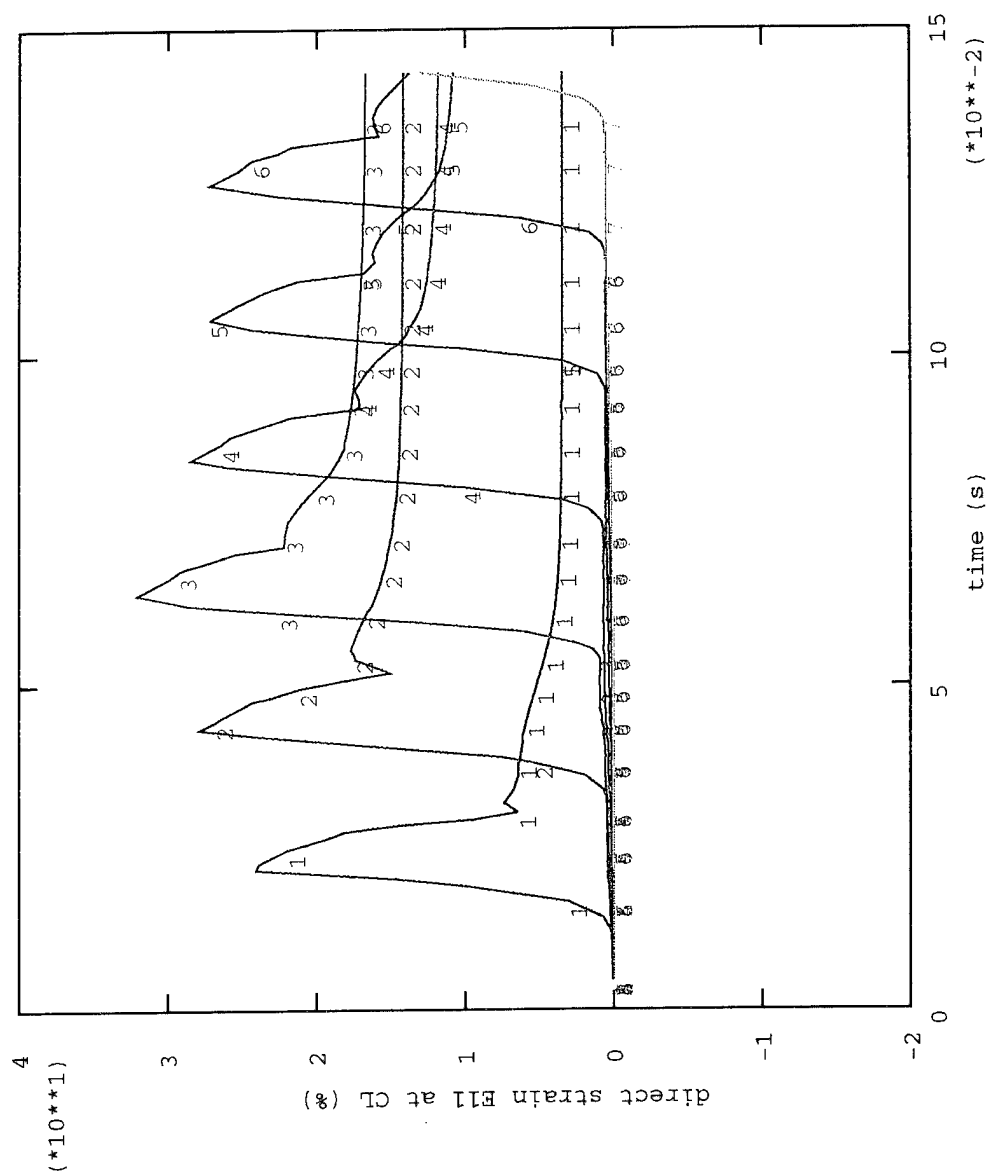
(a) Total strain E11 histories at sampled response points along path of plow.

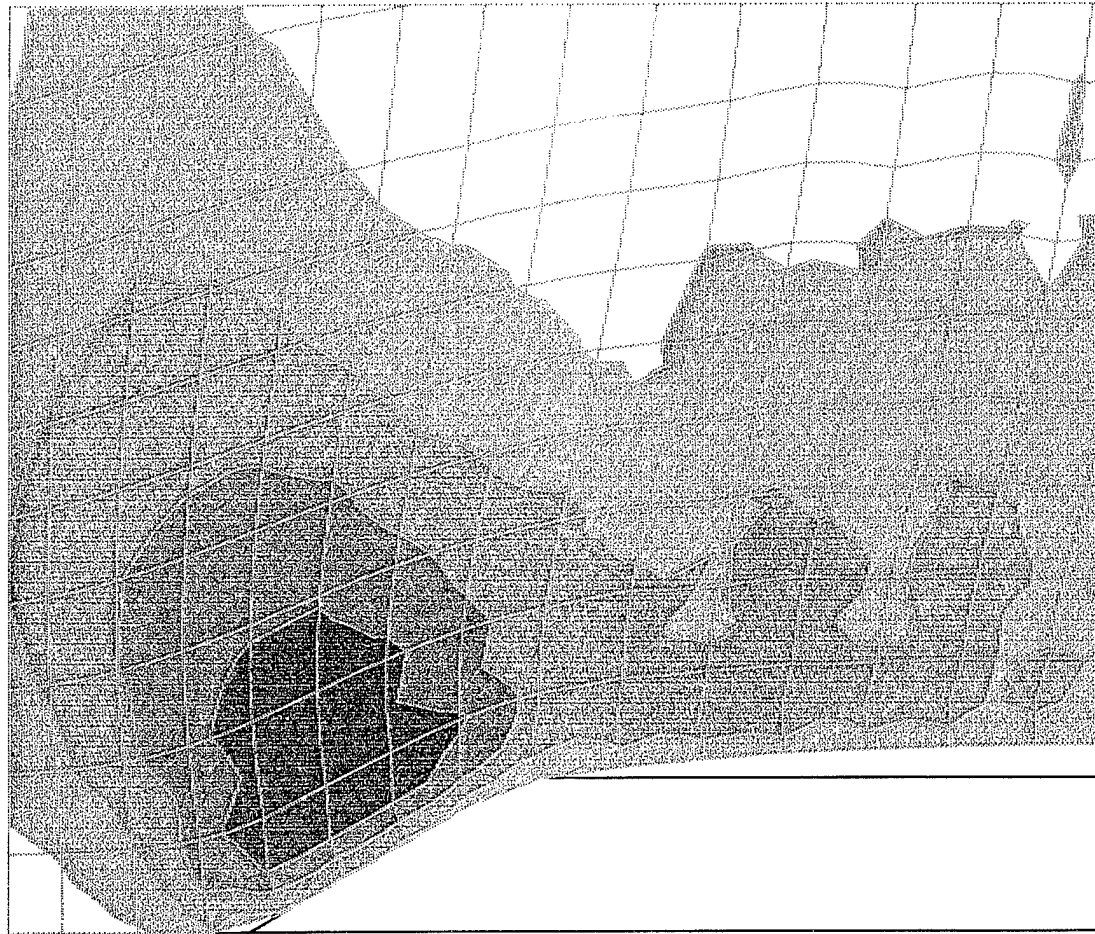Figure 4-6. Direct strain components in soil at 5 fps steady-state plow velocity.

(b) Total strain E11 distribution near plow tip.

Figure 4-6. Continued.

E11 VALUE
- -5.81E-01
- -5.11E-01
- -4.41E-01
- -3.71E-01
- -3.01E-01
- -2.31E-01
- -1.61E-01
- -9.10E-02
- -2.10E-02
- +4.89E-02
- +1.18E-01
- +1.89E-01
- +2.59E-01
- +3.29E-01

(c) Plastic strain PE11 histories at sampled response points along path of plow.

Figure 4-6. Continued.

(d) Plastic strain PE11 distribution near plow tip.

Figure 4-6. Continued.

Both direct strain components at the edge of the groove are tensile in the residual response and, therefore, the material has dilated due to the shearing action of the plow. This would be consistent with a dilatant soil. The spatial distribution of E22 under steady-state conditions, shown in Figure 4-6f, indicates that actual maximum values occur just off the interface adjacent to the plow tip rather than on the interface, similar to E11. Residual strain E22 is slightly larger than E11 along the groove. However, maximum transient values for E11 are larger than for E22. Except for the plastic region near the plow tip and also along the groove, both direct strain components are negligible in the surrounding soil..

Time histories for PE22, the in-line component of plastic strain along the centerline, are shown in Figure 4-6g. When compared to the total strain E22 (Figure 4-6e), the plastic component is also compressive, behaves in nearly the same manner, and also accounts for most of the total strain. The spatial distribution of PE22 which is shown in Figure 4-6h is also very much like that for E22 (Figure 4-6f). Most of both residual direct strain components E11 and E22 are plastic along the interface.

4.3.2 Volume Change. Volume change in the material is reported in terms of time histories of element volume for the selected elements, as shown in Figure 4-7. Each of these elements are 0.125 inches square in the undeformed configuration, with a constant unit depth. Therefore, their initial or undeformed volume is 0.0156 inches cubed. Element volume increases with arrival of the plow blade. During arrival and departure of the plow tip, there is a distinct initial peak increase with a small rebound, and then, as the blade shoulder slides by shearing the soil, the element volume rises to a maximum residual level. In these data, the residual volume expansion is about 31 percent and is due to plastic tensile strain.

Alternatively, if element volume is denoted as EVOL, then the change in element volume, ΔEVOL, equals the algebraic sum of the direct strains E11 and E22. For the residual response, this sum is about 27 percent (Figures 4-6a and 4-6e). The average strain is therefore reasonably within the calibration range for the dilation angle (Figure 3.9b) of the Drucker-Prager model.

4.3.3 Shear Strain. Time histories of the shear strain, E12, along the centerline, shown in Figure 4-8(a), exhibit a reversal response during arrival and departure of the plow tip, first positive and then negative. Due to symmetry, the shear strain must remain zero at the centerline until the plow tip arrives and cleaves the soil, and then the response includes a precipitous reversal of shear strain. The residual response subsequent to passing of the blade shoulder is negative and nearly equal to the peak negative response. The spatial distribution of the steady response of E12 is shown in Figure 4-8b. Shear strain is evident in the distortion of the element grid lines shown which otherwise intersect at right angles in the undeformed state. The actual peak or maximum response occurs well off the interface, perhaps two blade widths away, in the region of the plow tip. It is also opposite in sign to the shear strain which is located in an apparent thin interface boundary layer of soil adjacent to the plow blade.
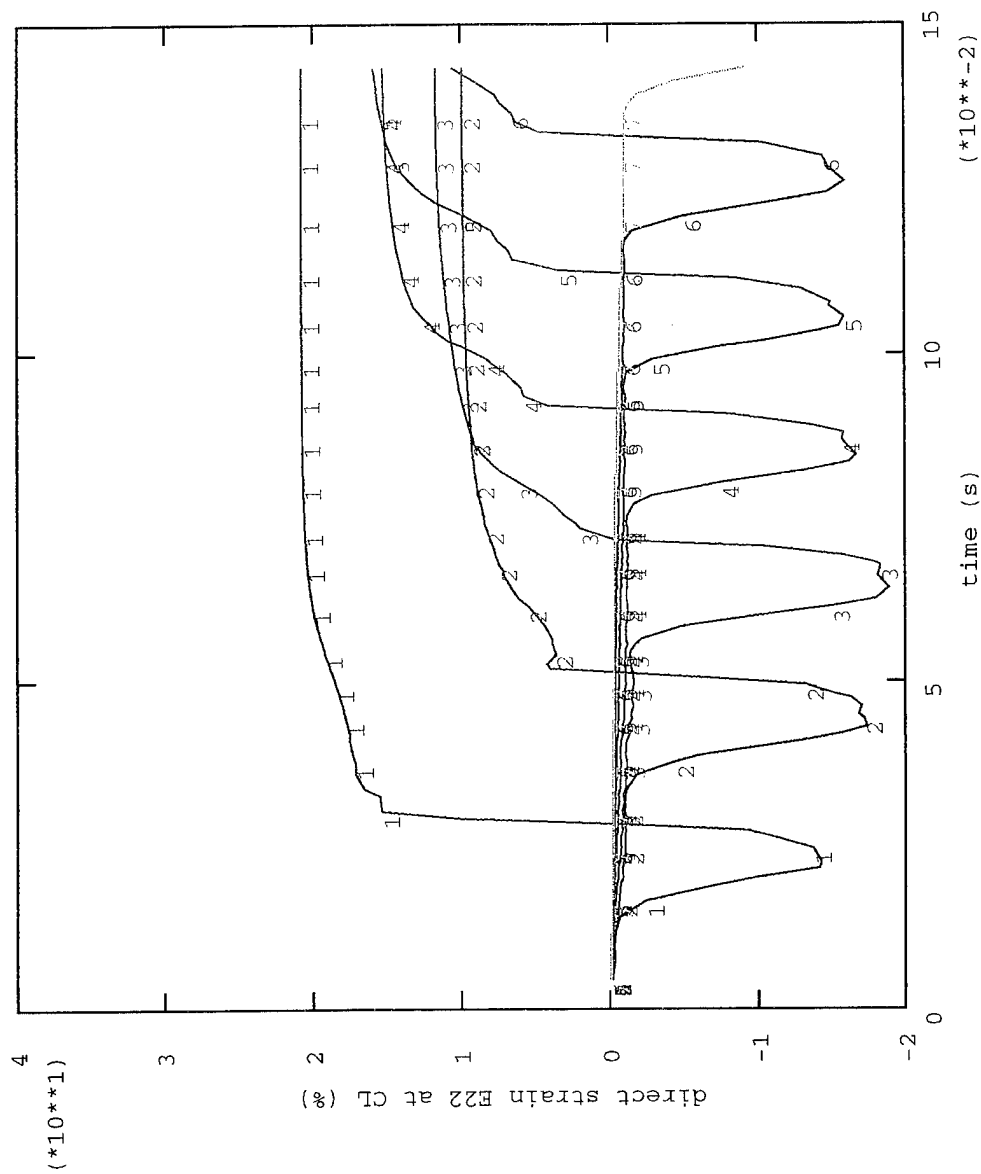
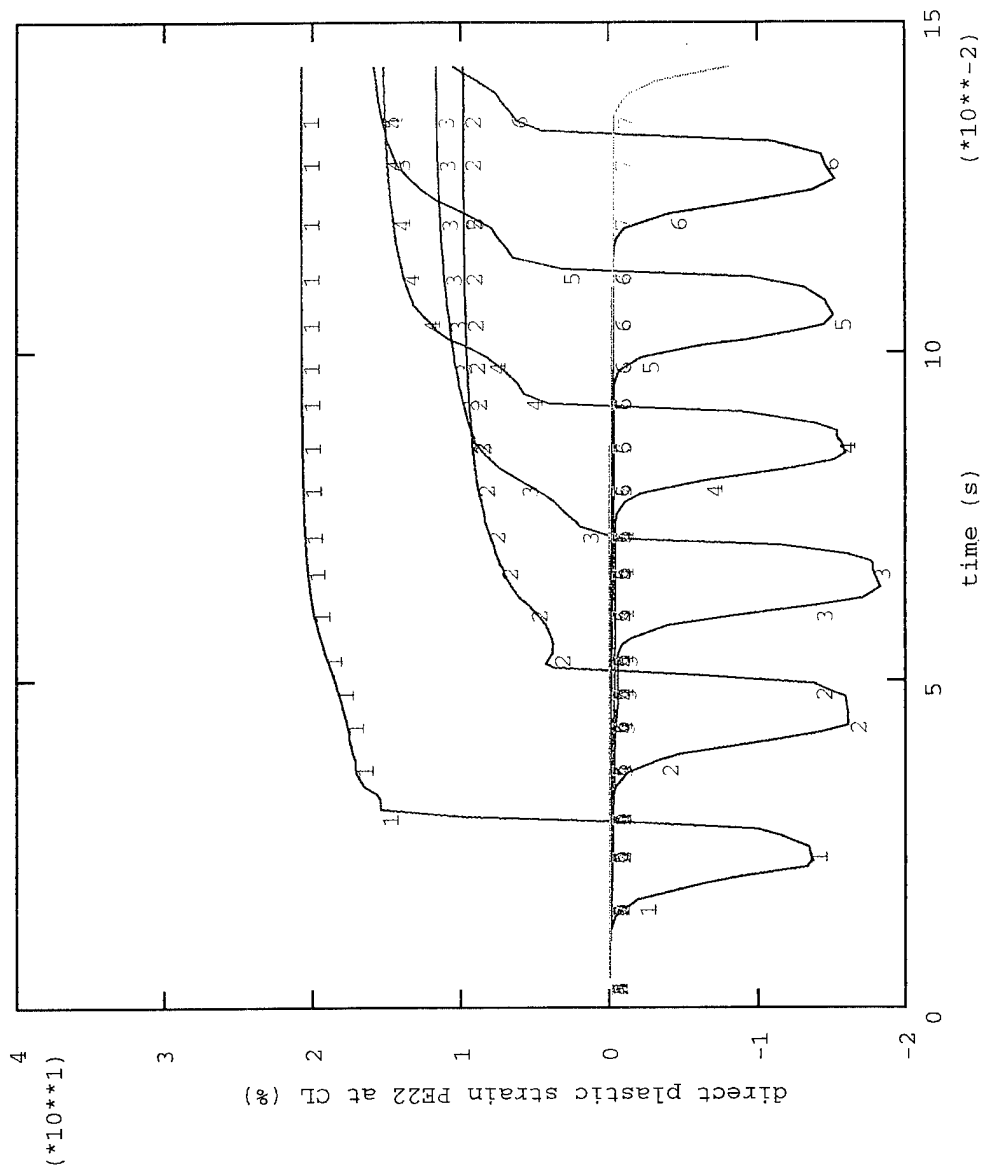(e) Total strain E22 histories at sampled response points along path of plow.

Figure 4-6. Continued.

69
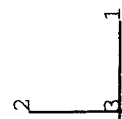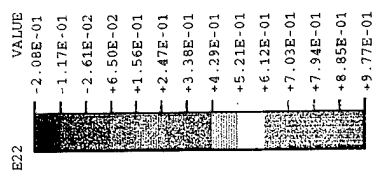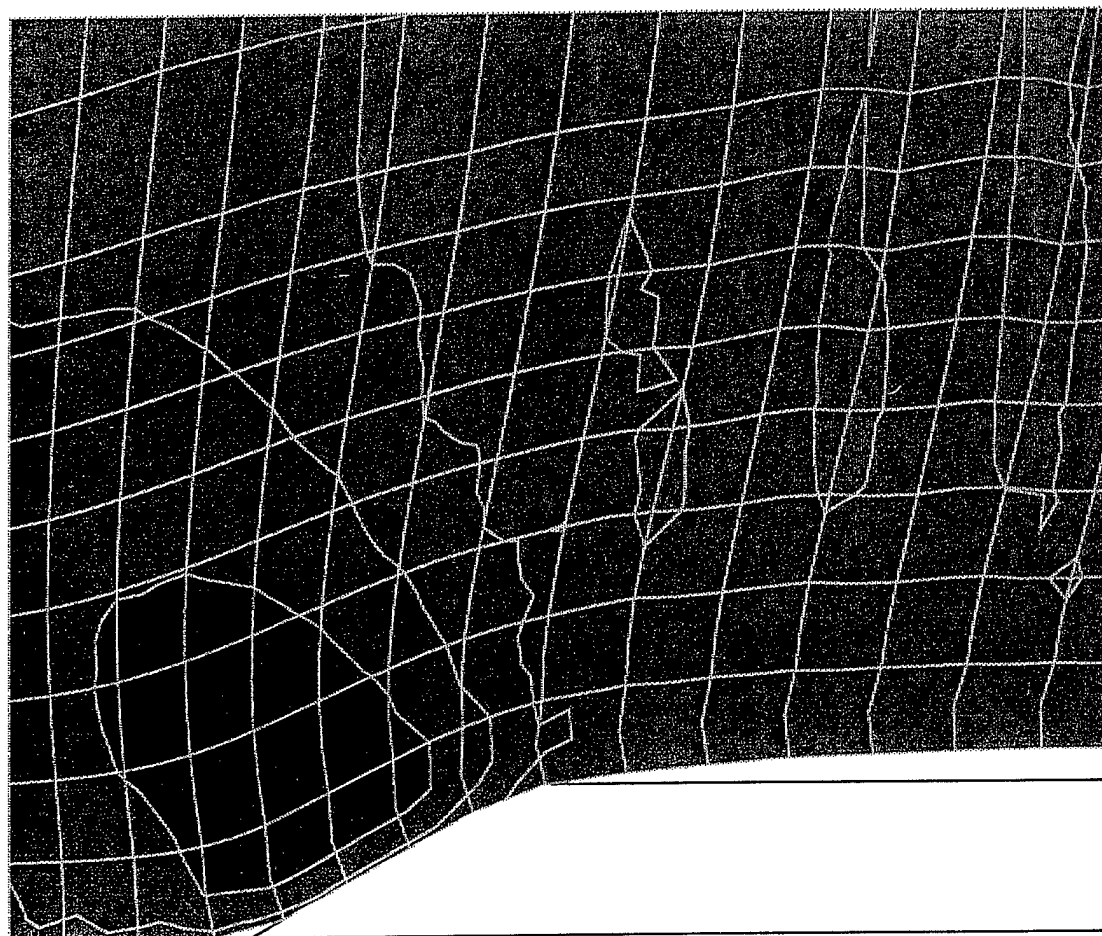
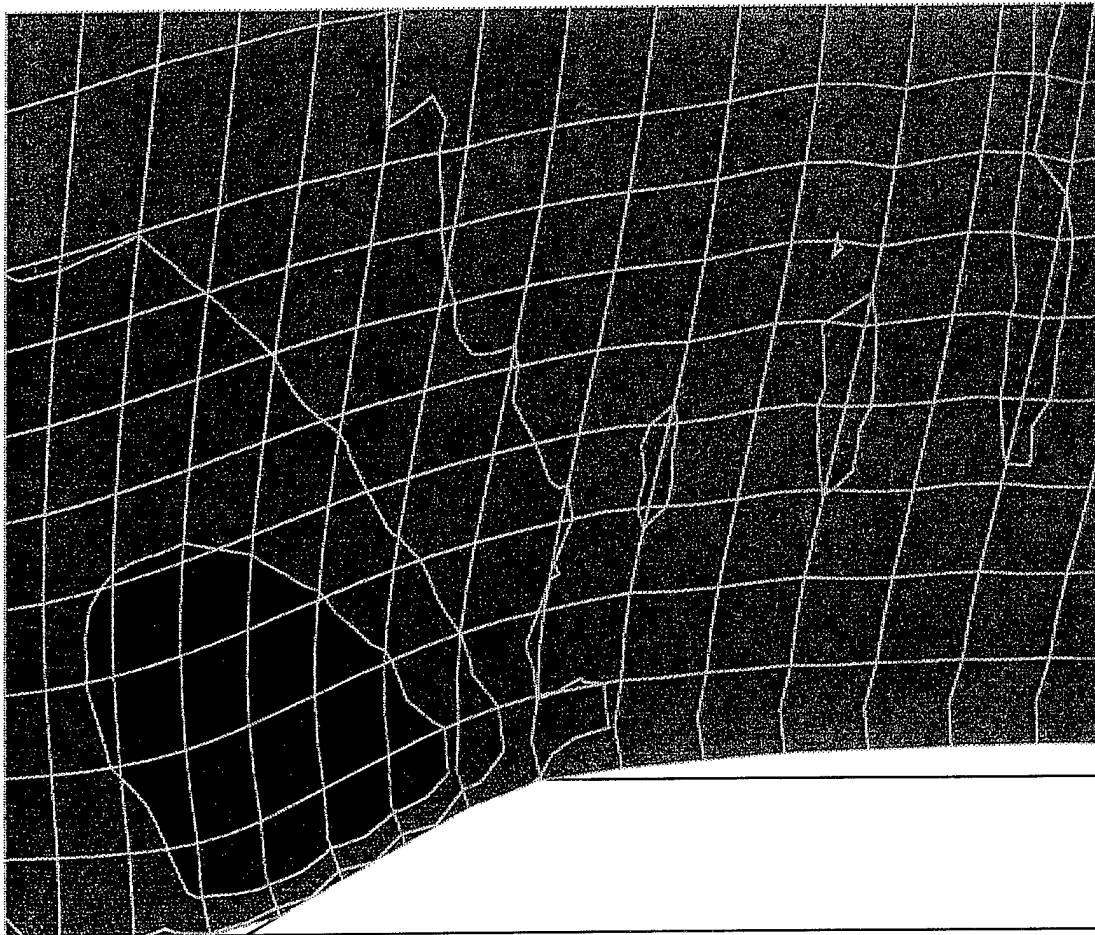(f) Total strain E22 distribution near plow tip.
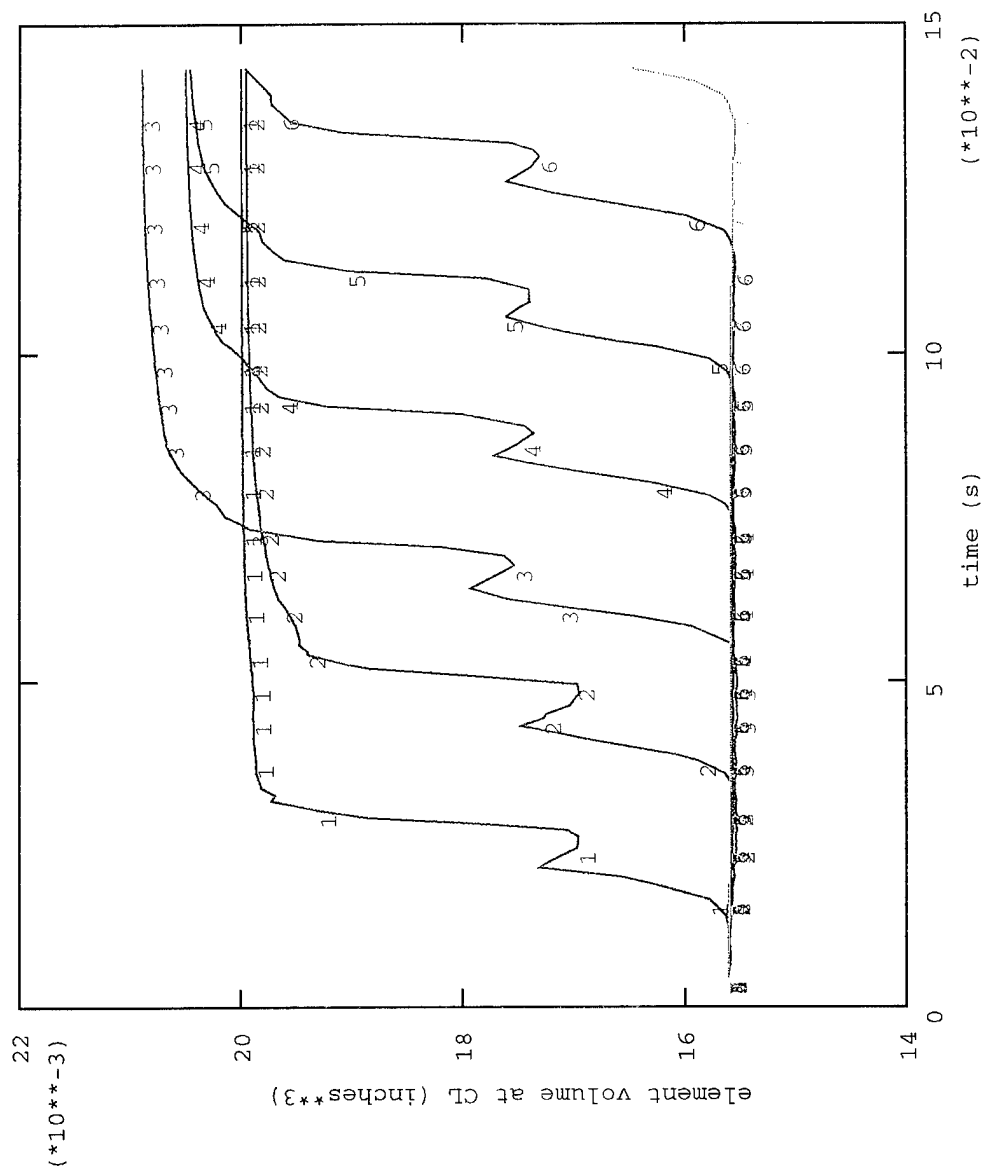
Figure 4-6. Continued.

(g) Plastic strain PE22 histories at sampled response points along path of plow.
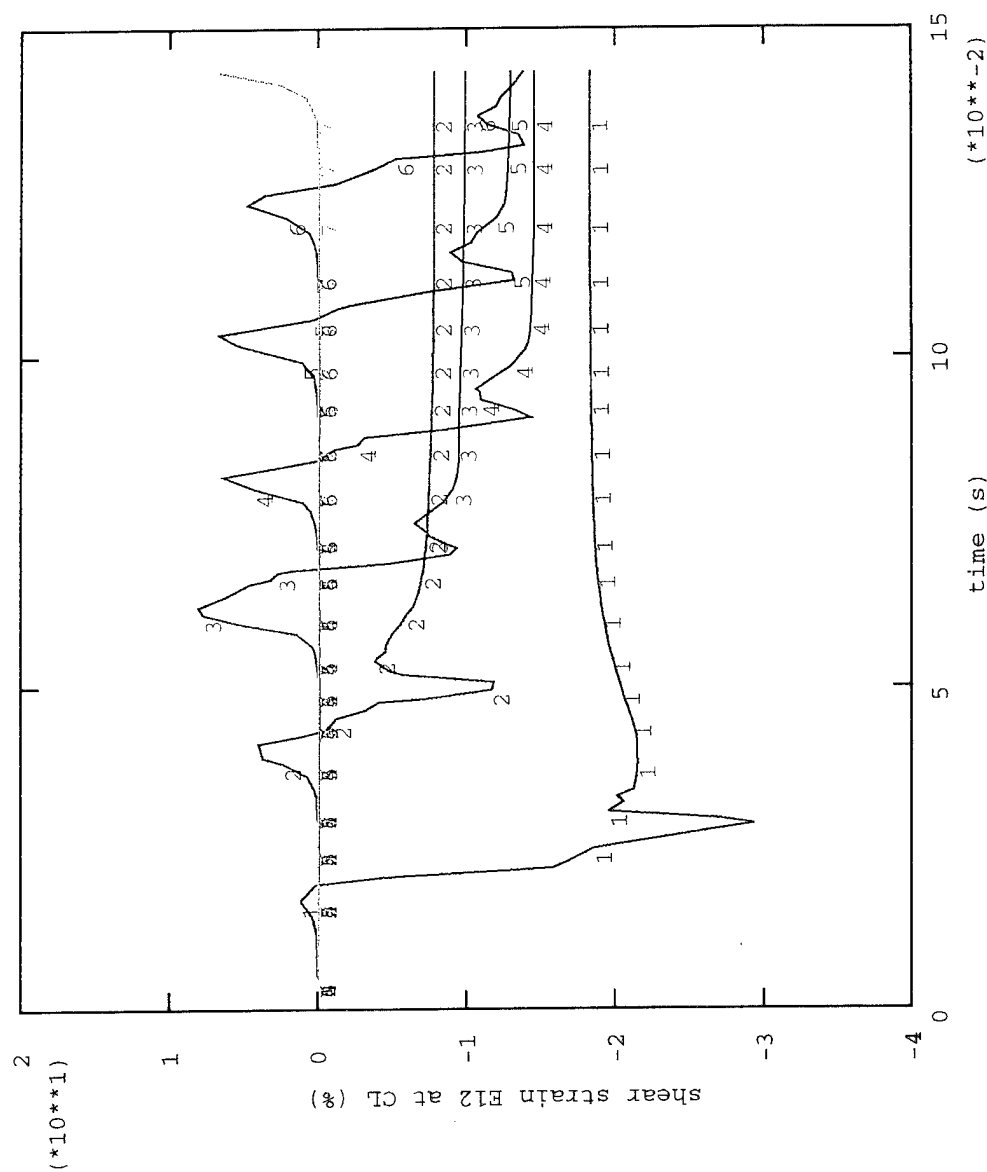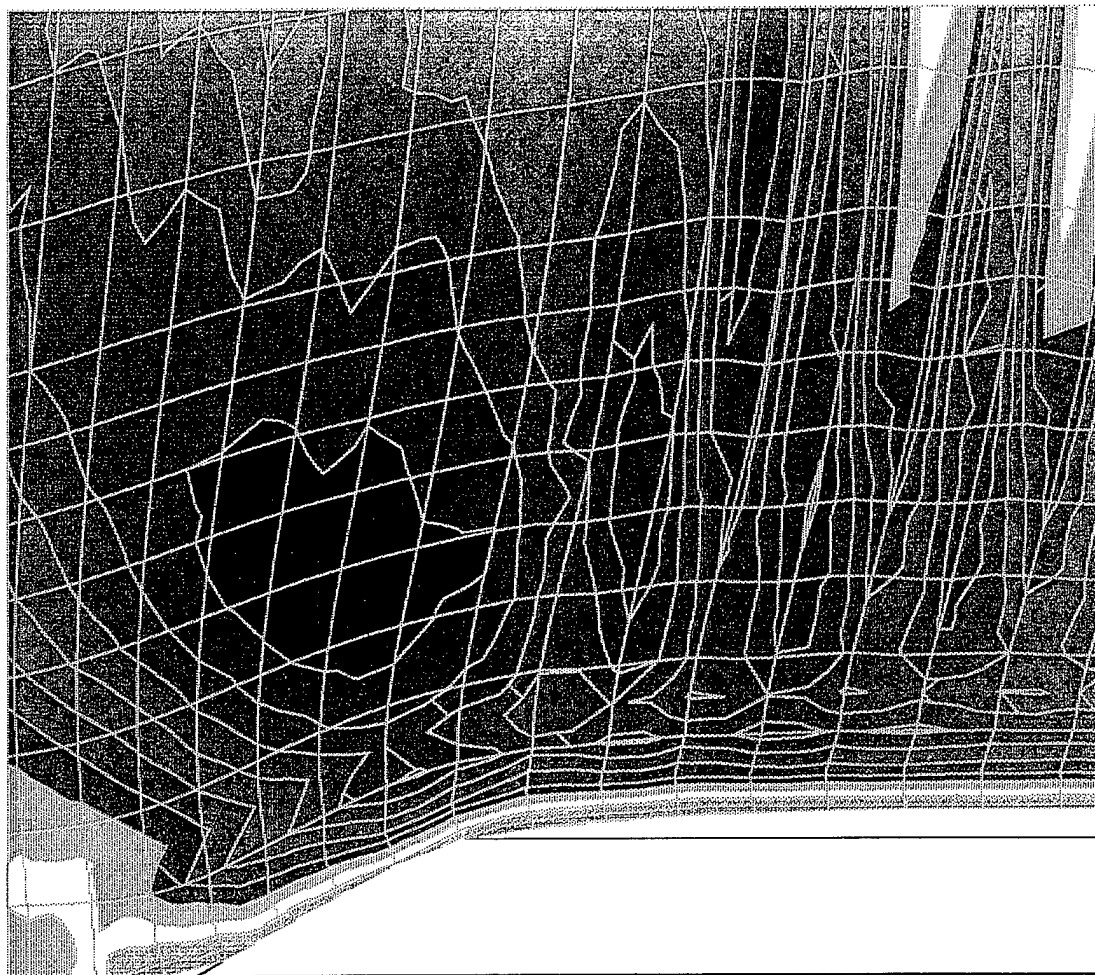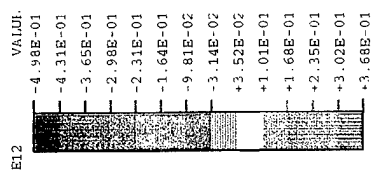
Figure 4-6. Continued.

71

PE22   VALUE
        -1.93E-01
        -1.03E-01
        -1.33E-02
        +7.69E-02
        +1.67E-01
        +2.57E-01
        +3.47E-01
        +4.37E-01
        +5.28E-01
        +6.18E-01
        +7.08E-01
        +7.98E-01
        +8.89E-01
        +9.79E-01

(h) Plastic strain PE22 distribution near plow tip.

Figure 4-6. Continued.

Figure 4-7. Element volume change histories at 5 fps steady-state plow velocity.

73

(a) Total shear strain E12 histories at sampled response points along path of plow.

Figure 4-8.   Shear strain in soil at 5 fps steady-state plow velocity.

(b) Total shear strain E12 distribution near plow tip.

Figure 4-8. Continued.

The plastic component of shear strain, PE12, is nearly identical to the total shear strain as shown in Figures 4-8c and d. Thus, the elastic shear strain component is essentially zero in these data. Plastic strain completely characterizes the response of the soil, within one or two blade widths from the blade. Plastic shear strain, PE12, dominates residual strain in the wake or groove material, while direct plastic strain dominates in the region nearest the plow tip.

4.3.4 Summary of Model Strains in the Soil. Results for model strain reveal a residual, plastic strain response for the soil bordering the wake formed behind the plow. Time histories show that soil develops peak strain upon arrival of the blade shoulder, and retains a sizable percentage as residual strain after it passes. The rise and fall in strain is precipitous. Primary soil strain response is confined to one or two blade widths from the plow, and strain gradients are large. Specific results are:

- The lateral direct strain component remains tensile, while the in-line direct strain component is compressive forward of the plow tip, and reverses to a tensile residual response aft the plow tip. Shear strain also reverses as the plow tip passes, and also retains a residual response.

- Both direct strain components retain a significant tensile residual response in the wake, which demonstrates the model correctly replicates volumetric expansion behavior in a dilatant soil subjected to the shearing action of the plow.

4.4 Effective Stress in the Soil

Direct effective stress in the soil is the algebraic sum of the total direct stress and the pore pressure, while effective and total shear stresses are identical quantities. Under plane strain conditions there are four non-zero effective stress components, S11, S22, S33, and S12 which define the state of stress in the soil skeleton at any point. The first three are direct stress components and the fourth is the shear stress component. S11 and S22 are bearing stresses, but only the S22 component contributes directly to plow resistance force since friction is neglected in the present analysis. The S33 component arises primarily because of the constraint on deformation inherent in the otherwise artificial plane strain conditions.
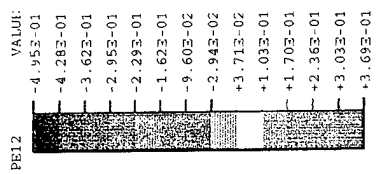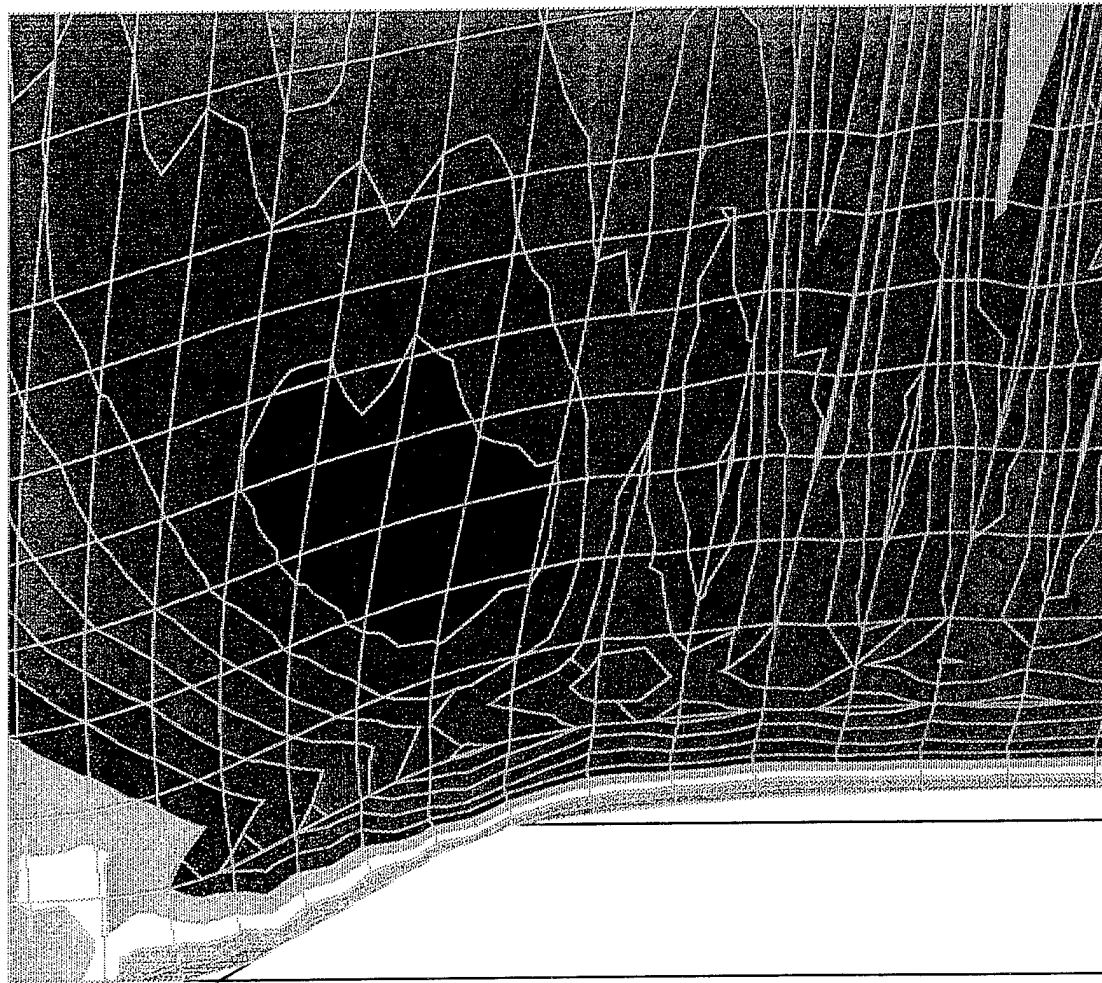
Two derived stresses or equivalent stresses are also reported. Both are invariant quantities. The Mises equivalent stress is a measure of deviatoric (distortion) behavior in the soil skeleton. The equivalent pressure stress, is indicative of the dilatation behavior in the soil skeleton. In this study, it is defined as the negative of mean effective stress or hydrostatic stress.

Like strains, stresses are element data, and the data presented are computed at the centroid of an element, whether they are graphs of time-histories of stress or contour plots of spatial distributions of stress. In the former, the data are reported at selected centerline elements (Figure 4-2) and in the latter, the stress fields shown are enlarged views of a region near the plow tip when the plow is in steady-state motion (at nearly the position shown in Figure 4-1). In the stress contour data, the post-processor algorithm averages the computed element centroid values at each adjacent node point before constructing the contours.
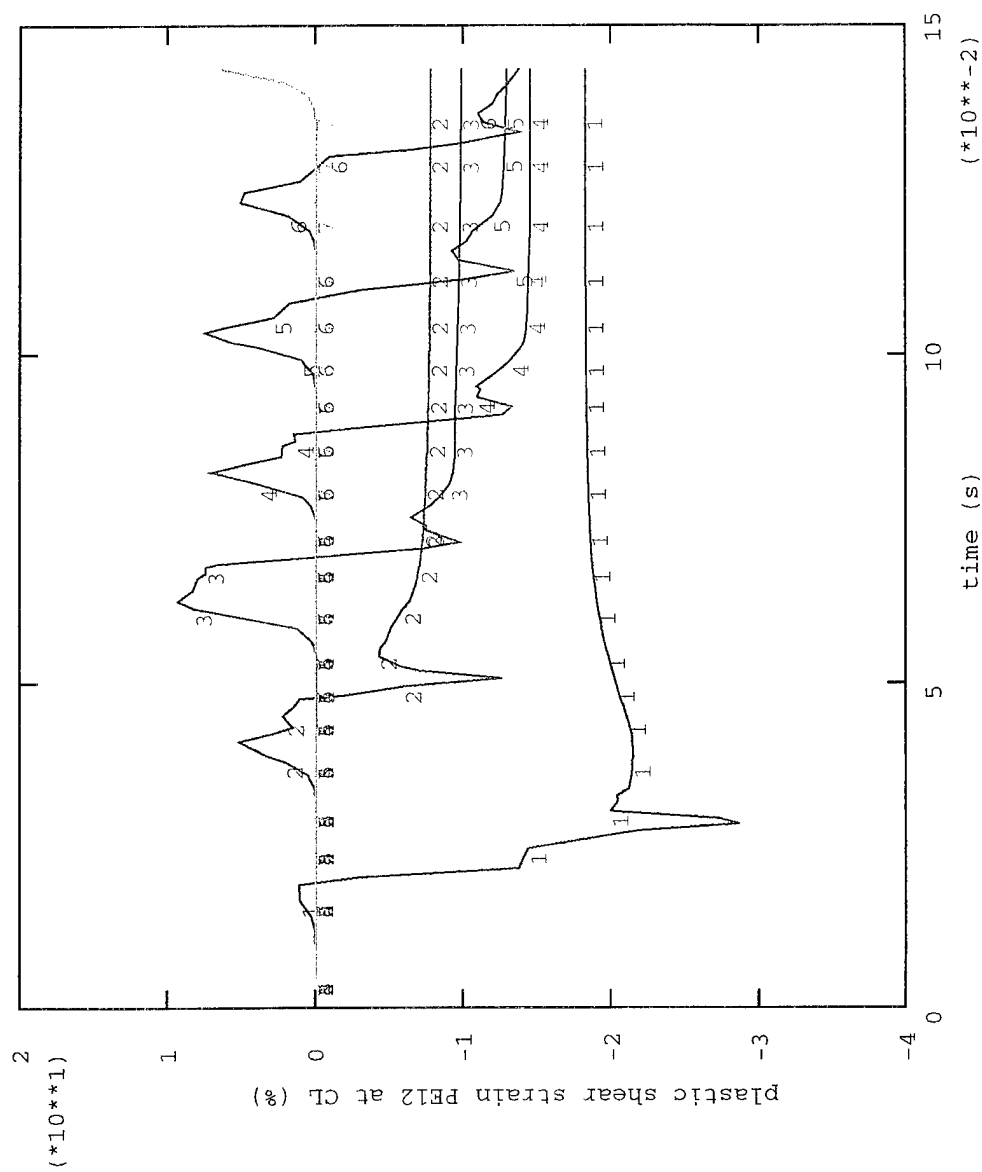
(c) Plastic shear strain PE12 histories at sampled response points along path of plow.

Figure 4-8. Continued.

PE12   VALUE
        -4.95E-01
        -4.28E-01
        -3.62E-01
        -2.95E-01
        -2.29E-01
        -1.62E-01
        -9.60E-02
        -2.94E-02
        +3.71E-02
        +1.03E-01
        +1.70E-01
        +2.36E-01
        +3.03E-01
        +3.69E-01

(d) Plastic shear strain PE12 distribution near plow tip.

Figure 4-8. Continued.

The important peak or maximum response in stress history data is associated with arrival and departure of the blade shoulder as for the corresponding strain data. Residual stress in the wake of the plow, unlike residual strain, is invariably zero.

4.4.1 Direct Stress. The results for direct stress components S11 and S22 are shown in Figure 4-9. The lateral component S11 is compressive along the centerline or path of travel of the plow blade according to the time histories shown in Figure 4-9a. These graphs rise and fall exactly according to the arrival and departure of the tip of the plow blade. Steady-state behavior is evident from these data at all centerline elements beyond element 40. Their spatial distribution in Figure 4-9b also includes a graph of S11 along the centerline which is essentially a normal section through the contour map along the interface. This graph includes a line drawn through the grid axes just above their midpoint that indicates the zero-stress datum. The graph shows that S11 is maximum at the shoulder of the blade and tapers linearly towards zero at the tip of the blade, and that it is zero forward of the tip along the centerline and also aft of the point of interface separation. These data are directly related to the aforementioned contact force (Figure 4-5) where the approximately linear variation over the bevel of the blade tip is perhaps seen more clearly. This lateral stress component could be important to both the resistance force of the plow and wear of the blade shoulder, depending on the coefficient of friction (assumed zero here) between the plow and the soil (See Section 5.2).

The in-line component S22 contributes directly to the unit resistance force. Time history graphs are shown in Figure 4-9c. They show that steady-state behavior is achieved at all centerline elements beyond element 50. These graphs show a gradual increase in S22 before the blade tip arrives, unlike the more precipitous graph for S11. When the blade tip does arrive and depart the corresponding increase and decrease in S22 are also precipitous. The peak magnitude of S22 is noticeably smaller than for S11. These data (S11 and S22) also show that the peak startup or transient stresses are substantially higher than the maximum steady-state stresses. In Figure 4-9(d) the spatial distribution of S22 shows only a minor concentration at the shoulder of the blade, i.e., a more uniform distribution along the bevel. Overall, the maximum value for S22 is located on the bevel surface, and is somewhat smaller than the maximum value for S11. The predicted unit plow force (Figure 4-3) is also very sensitive to the surface area over which S22 is distributed. This bearing area is slightly truncated near the tip of the plow in the present plow/soil interaction model due to the assumed mode of failure of the soil at the tip. Consequently, the unit resistance force may tend to be under-predicted.

Time histories for S33 are presented in Figure 4-9e. Steady-state behavior is achieved at all centerline elements beyond element 40. The gradual rise in stress level while the plow tip is approaching is similar to S22; both S22 and S33 sense the approaching plow tip, where S11 does not. Peak values of the S33 history graphs are intermediate between S11 and S22 peak values. Without the artificial deformation constraint imposed by plane strain conditions, S33 would likely be the smallest of the three direct stress components due to the proximity of a free surface at the soil bed. In Figure 4-9e, large gradients of S33 emanate from the blade surface similar to S11 and S22. The average of these three direct stress components determines the strength of the soil in the pressure-dependent Drucker-Prager soil model. If S33 and hence the soil strength are over-predicted, the unit resistance force may tend to be over-predicted, countering the under-predicting effect of reduced bearing area.
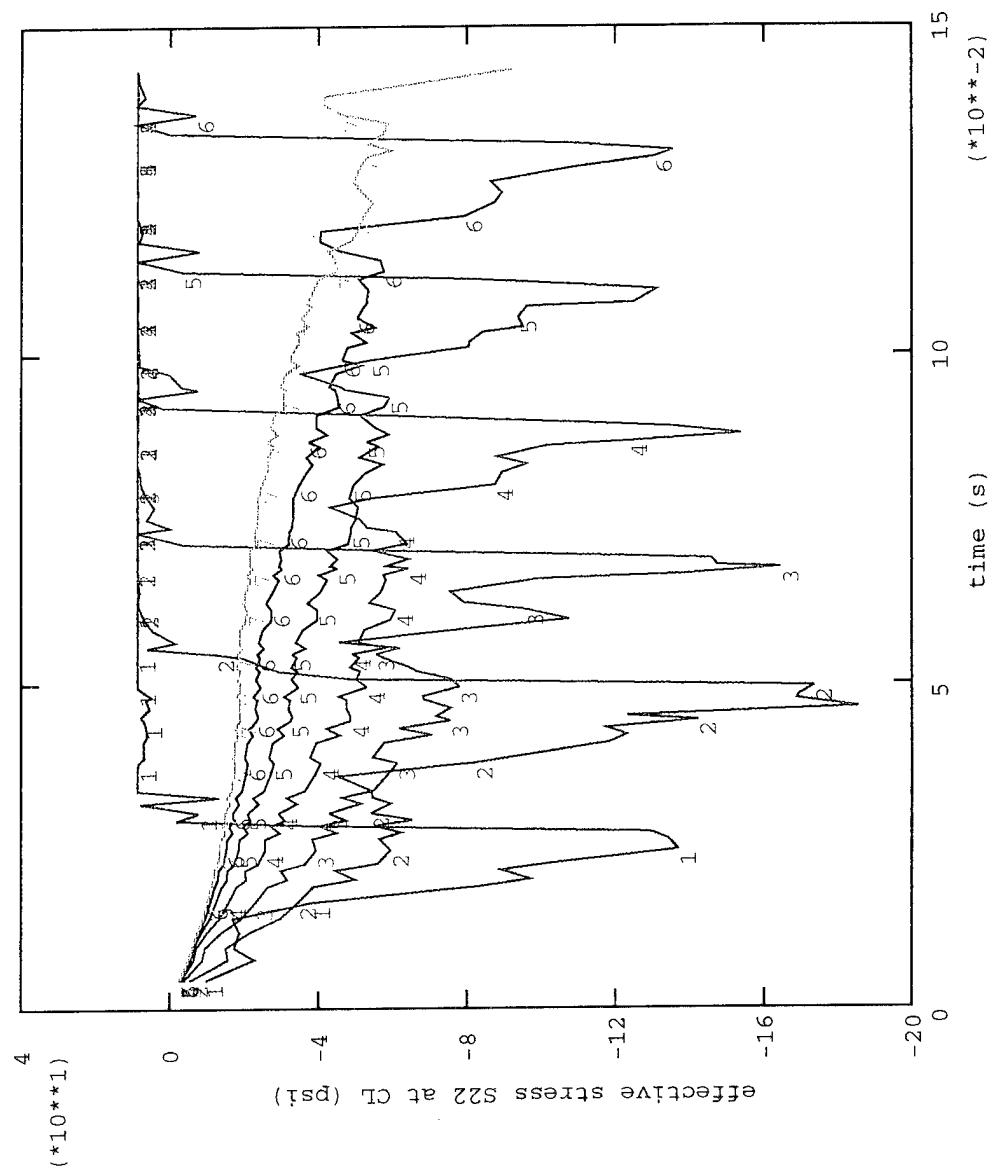
79
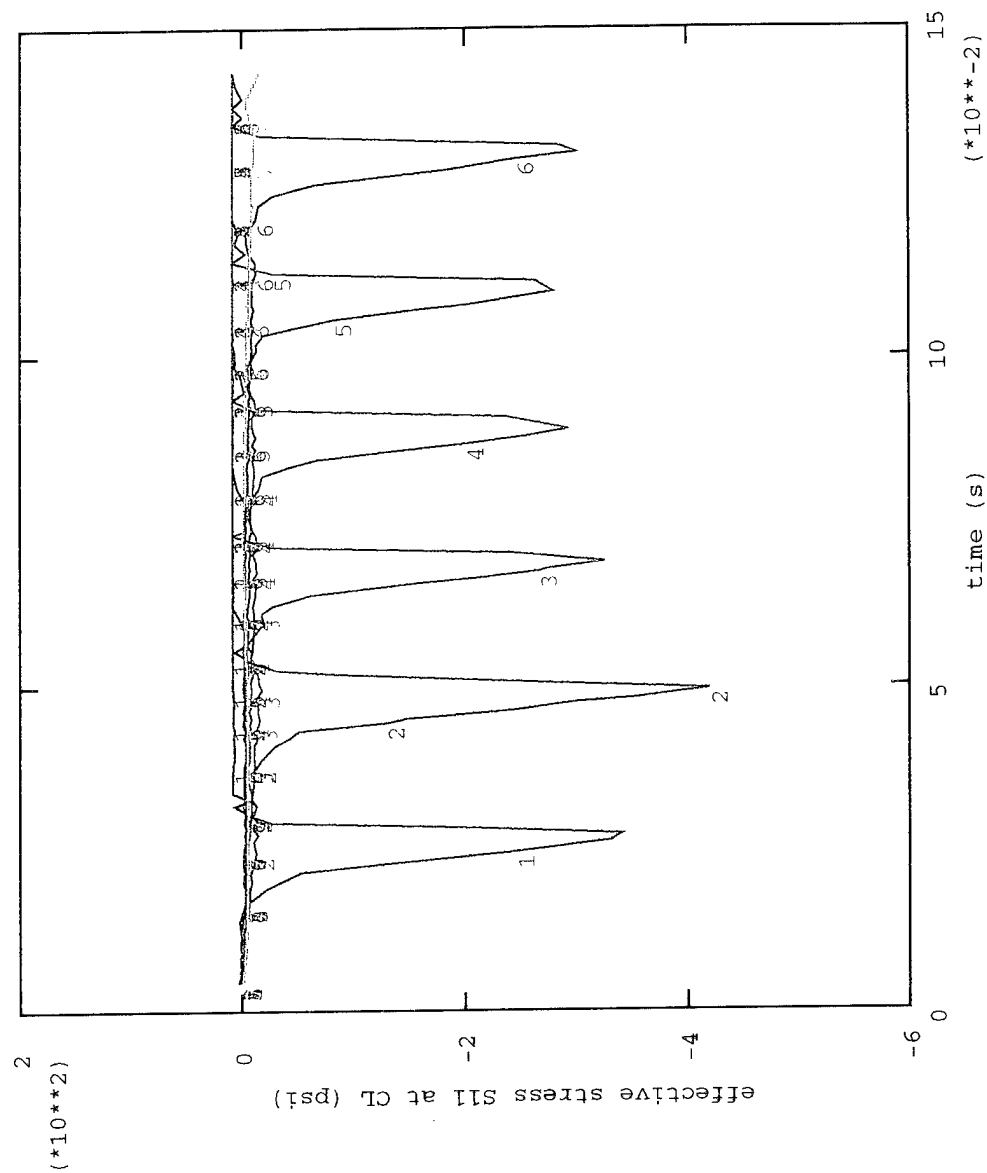
(a) Effective stress S11 histories at sample response points along path of plow.

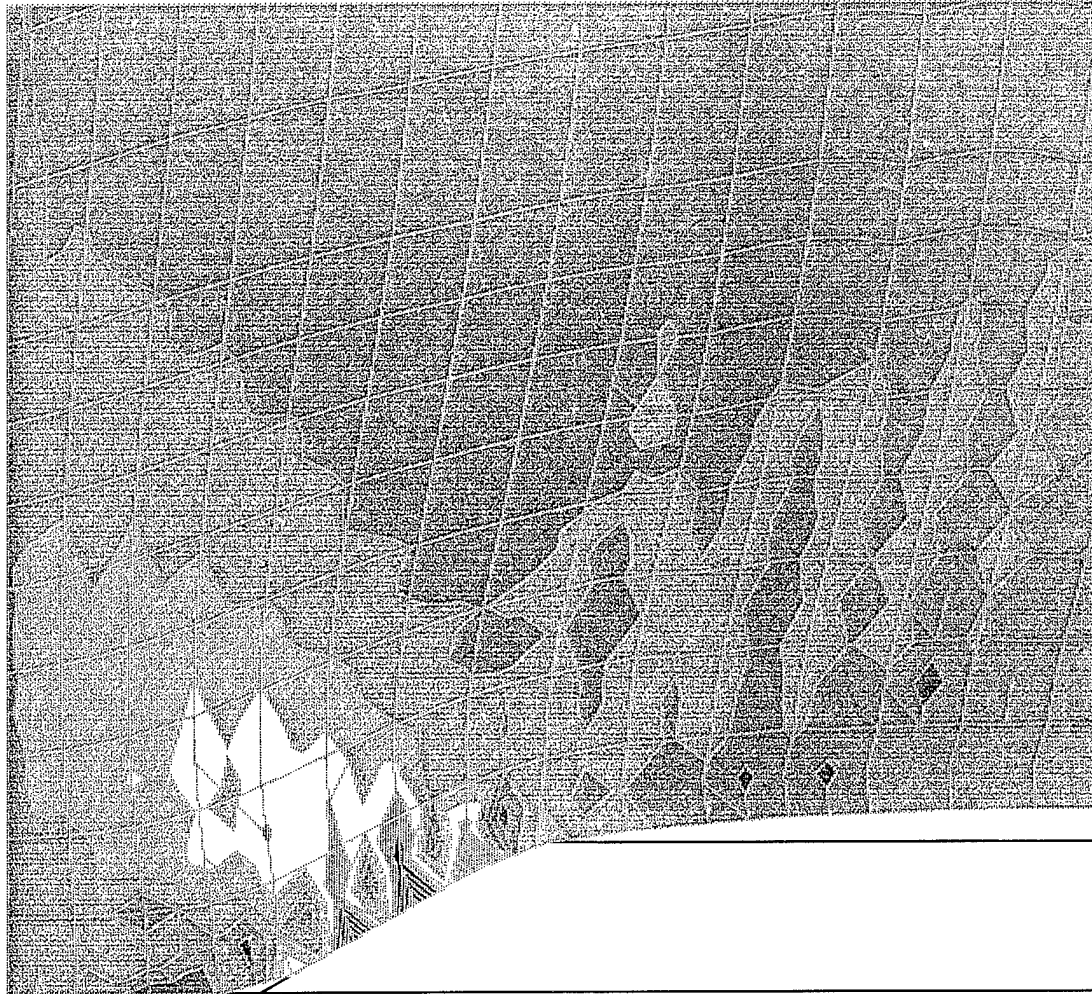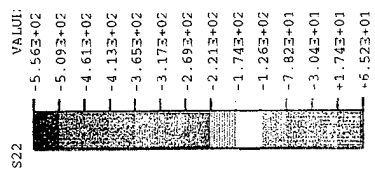Figure 4-9. Direct effective stress components in soil at 5 fps steady-state plow velocity.
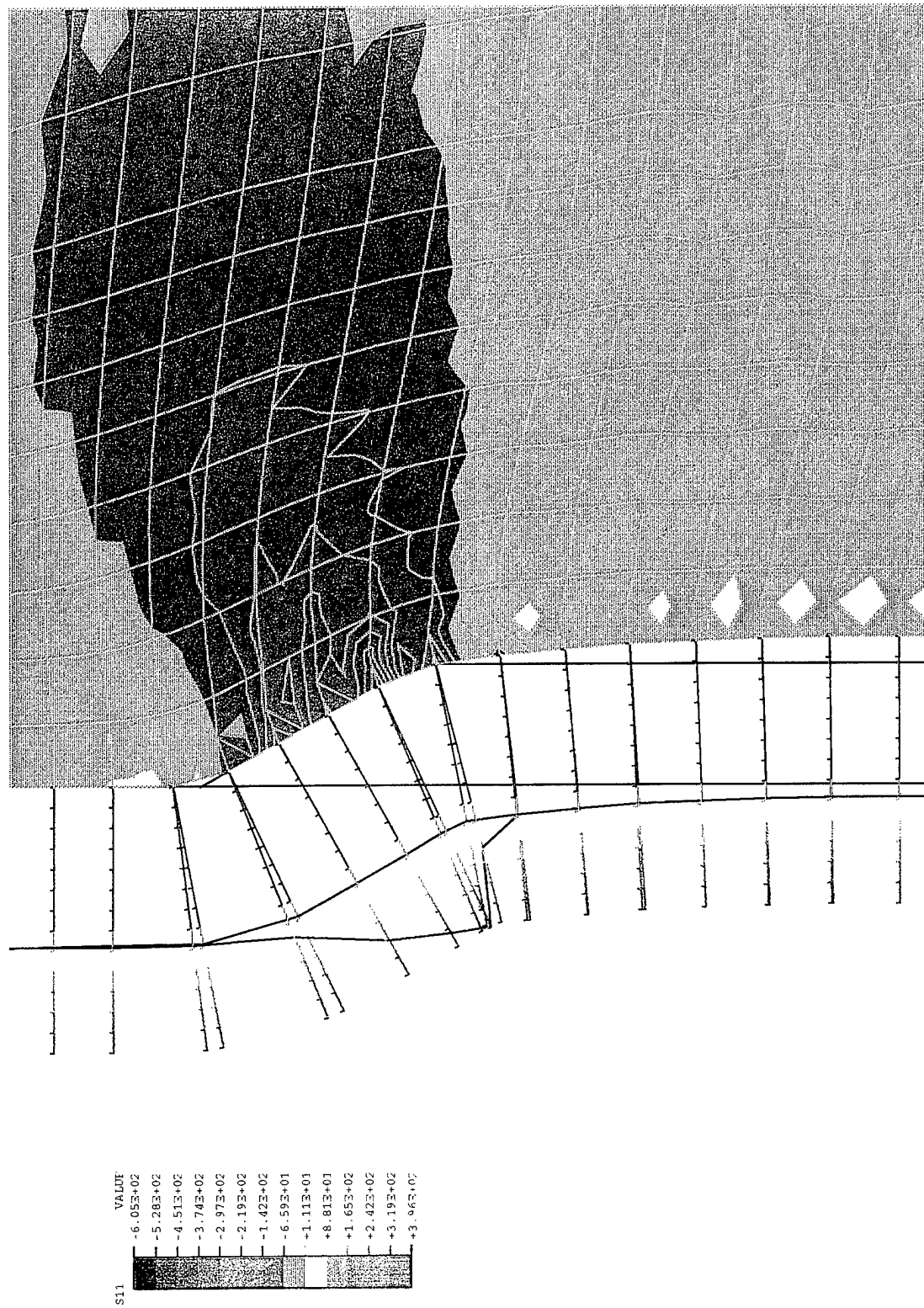
(b) Effective stress S11 distribution near plow tip.

Figure 4-9 Continued.

(c) Effective stress S22 histories at sampled response points along path of plow.

Figure 4-9 Continued.

82

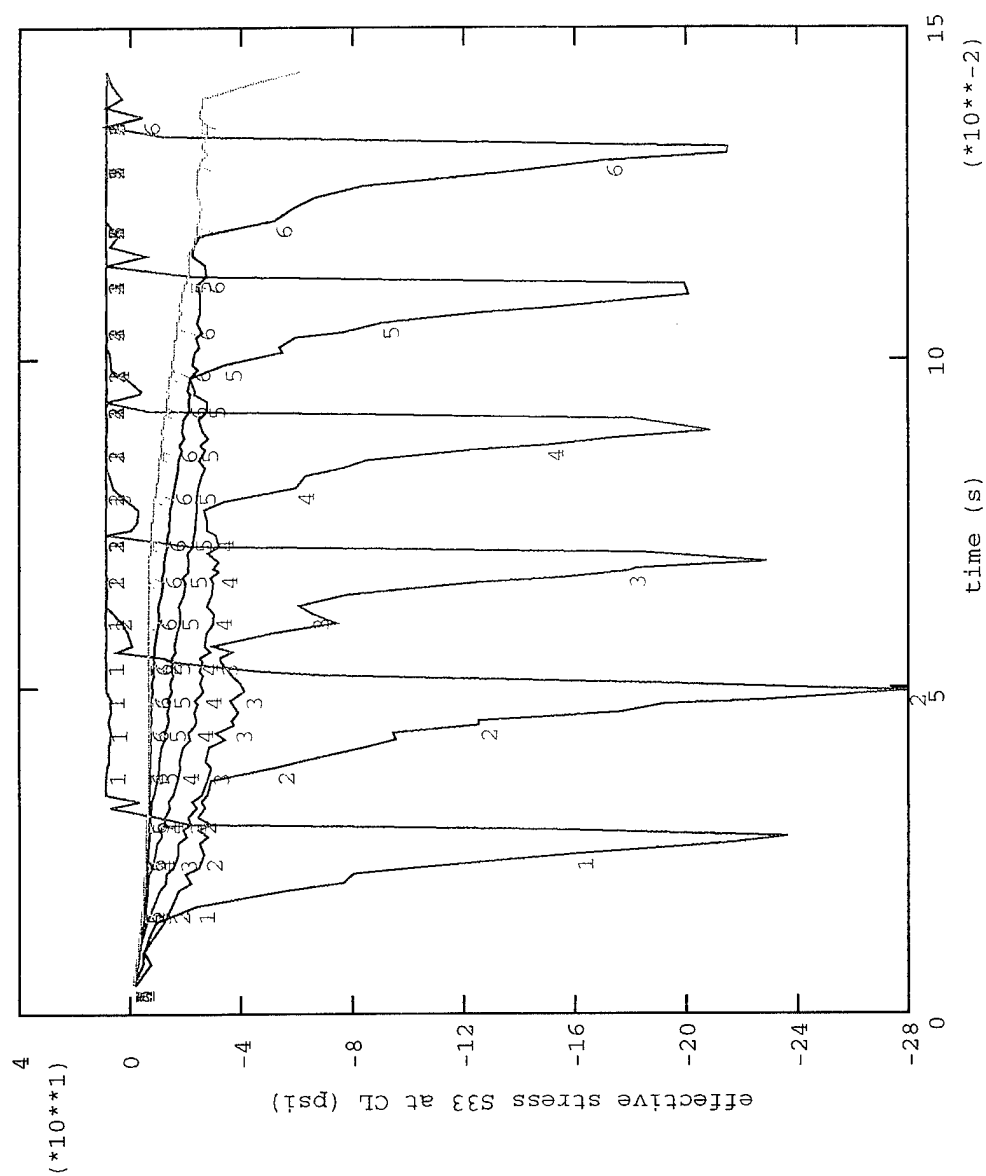(d) Effective stress S22 distribution near plow tip.

Figure 4-9 Continued.

4.4.2 Shear Stress. Shear stresses S12 are shown in Figure 4-10. Time histories rise and fall very precipitously at the centroids of centerline elements as shown in Figure 4-10a. They are nearly flat zero due to the imposed symmetry boundary condition along the centerline until the arrival of the blade tip. A slight reversal in sign is apparent before and after arrival, consistent with the reversal noted in shear strain (Figure 4-8a). Steady-state behavior is evident at all centerline elements beyond element 40. Peak values in shear stresses are substantially smaller than peak direct stress magnitudes. Contours of shear stress are shown in Figure 4-10b. Unlike direct stress, the actual maximum shear stress tends not to be on the interface, but just off the surface of the bevel of the plow tip. Shear stress is zero, as expected, on the free surface formed aft the point of interface separation.

4.4.3 Mises Equivalent Stress. Maximum distortion stress is perhaps better represented by the Mises stress shown in Figure 4-11, an invariant measure of deviatoric stress behavior in the soil. Stress histories, shown in Figure 4-11a, substantially exceed those for shear stress component S12 (Figure 4-10a). Further, they sense the approaching blade with a gradual increase in value; thereafter a precipitous rise and fall attends actual arrival and departure of the plow tip. Contour data, Figure 4-11b, shows the maximum MISES stress component at a location just off the blade surface, though it also appears to be related to the shoulder of the blade.

4.4.4 Equivalent Pressure Stress. The equivalent pressure stress, denoted PRESS, is presented in Figure 4-12. PRESS is defined as the negative of the mean effective stress in these data, so it can be easily interpreted as the latter quantity where convenient. PRESS is an invariant stress measure related to the dilatation in the soil, and the strength of the soil is linearly related to PRESS according to the pressure-dependent Drucker-Prager soil model. Time history graphs of PRESS are shown in Figure 4-12a. The dilatant material expands due to shearing by the plow as has been noted in the discussion of soil strain (Figure 4-6). The mechanical response of the partially confined soil to this volume expansion is a state of compression in the mean effective stress, as the plow tip arrives and departs. The pressure-dependent strength of the soil at a point in the path of the plow along the centerline correspondingly rises and decays with the arrival and departure of the plow tip. However, when observed from a point on the steadily moving plow tip, the plow will appear continuously confronted with soil at an elevated strength. Figure 4-12b shows steady-state contour values of PRESS. They can be interpreted as contours proportional to soil strength, and show soil with the maximum strength bearing on the surface of the plow tip, resisting its motion.

Also, while the time histories of PRESS and MISES are apparently very similar in shape and magnitude, the spatial distributions of PRESS and MISES differ somewhat. The former is similar to S11, S22, and S33, all of which are maximum on the surface of the bevel of the plow tip, while the latter is maximum just off this surface.

(e) Effective stress S33 histories at sampled response points along path of plow.
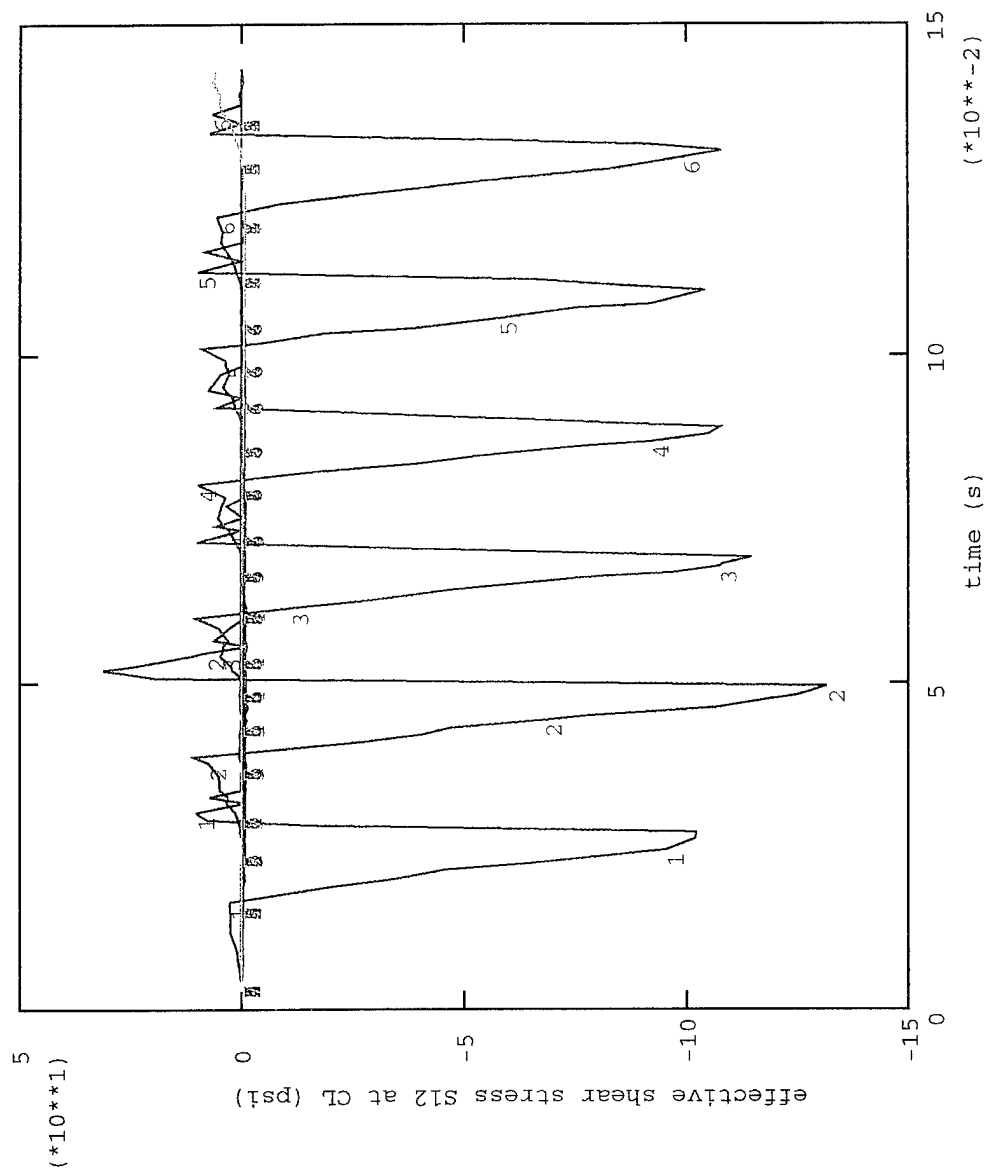
Figure 4-9 Continued.
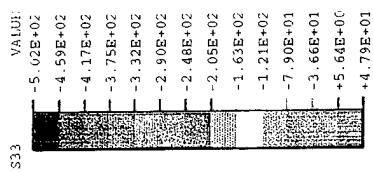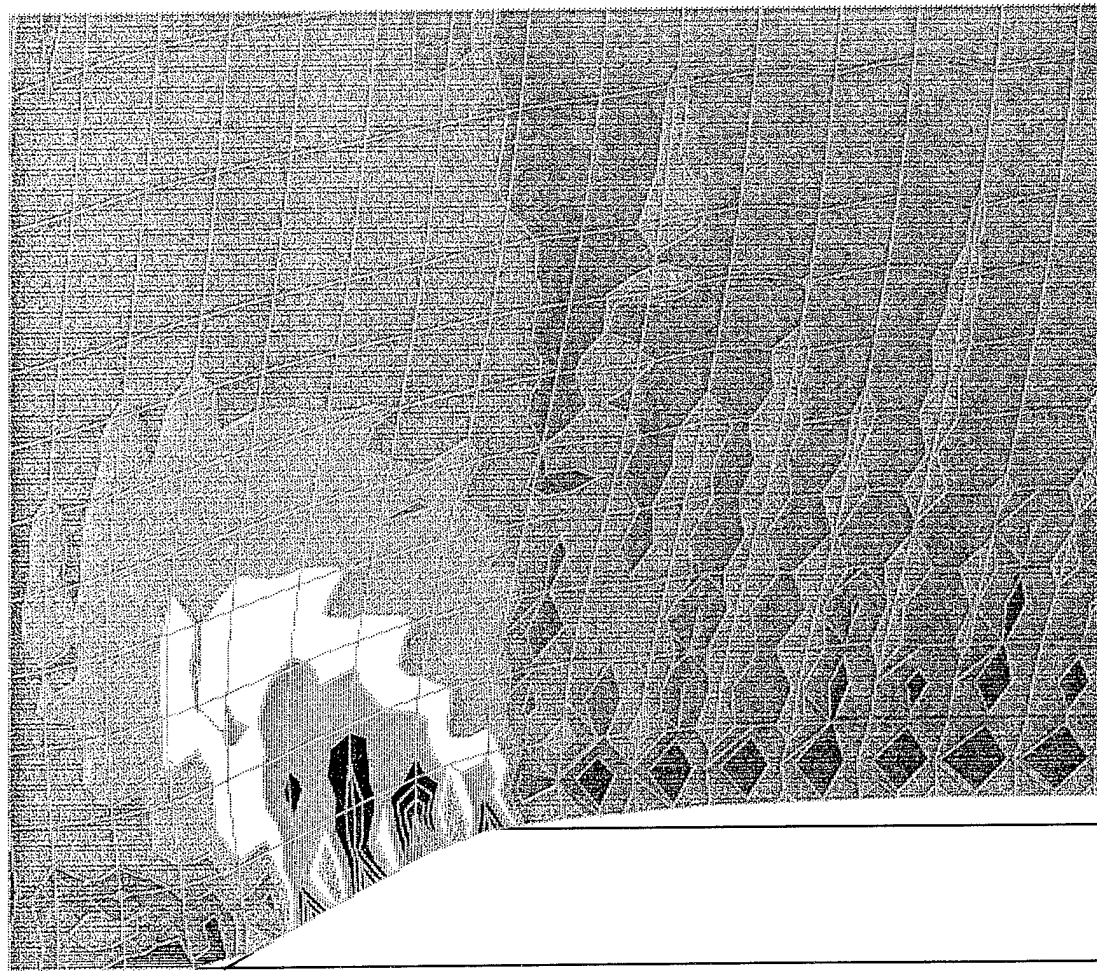
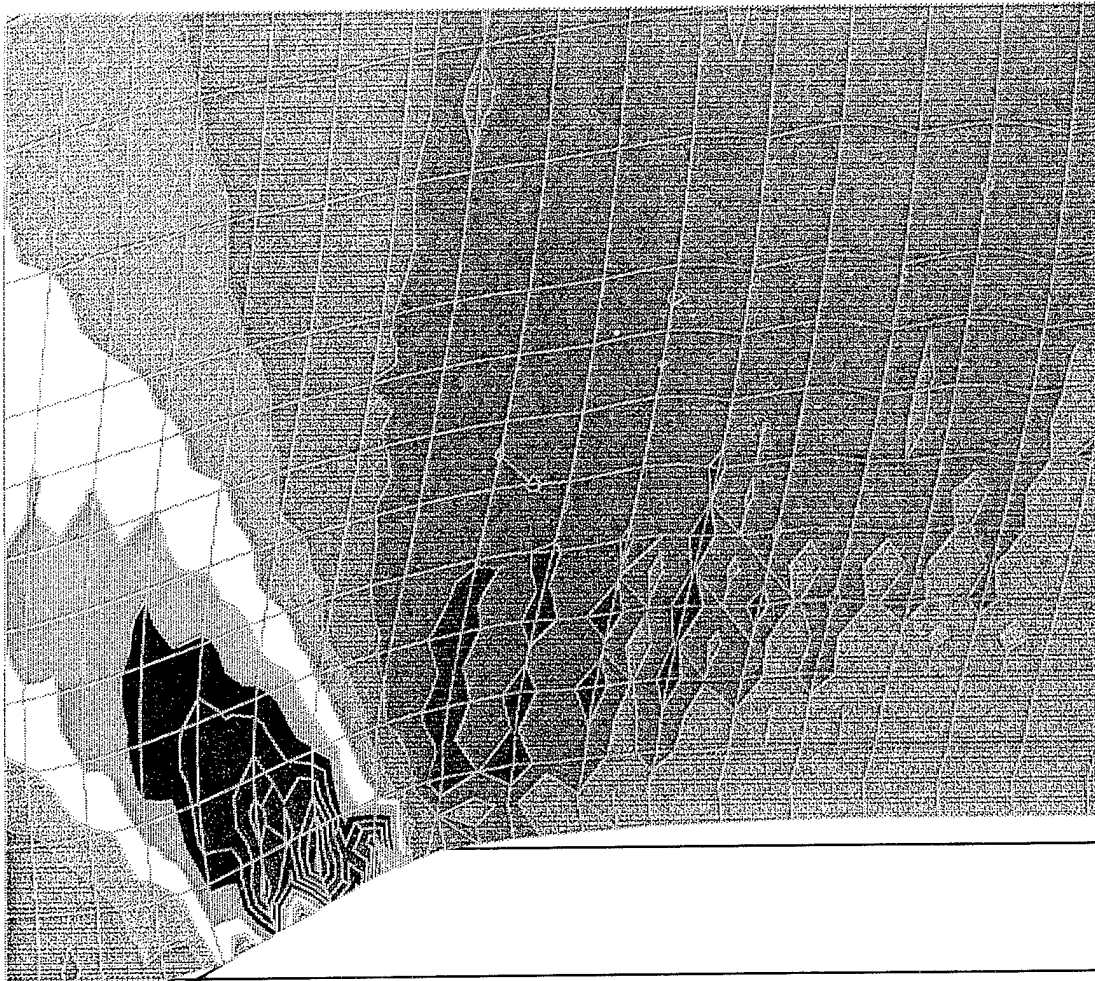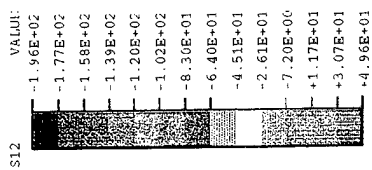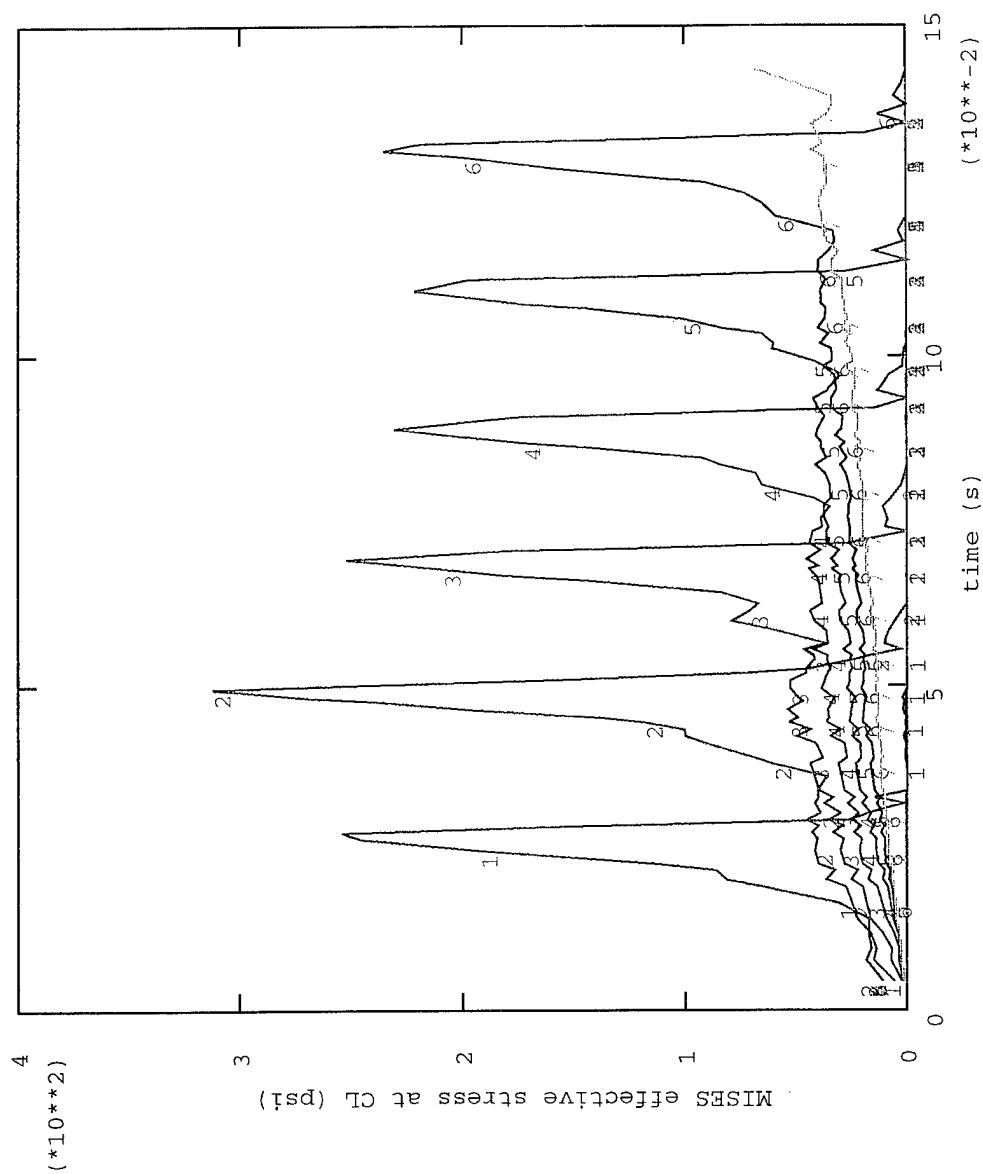(f) Effective stress S33 distribution near plow tip.

Figure 4-9 Continued.

(a) Effective shear stress S12 histories at sampled response points along path of plow.

Figure 4-10. Effective shear stress in soil at 5 fps steady-state plow velocity.

87

(b) Effective stress S12 distribution near plow tip.
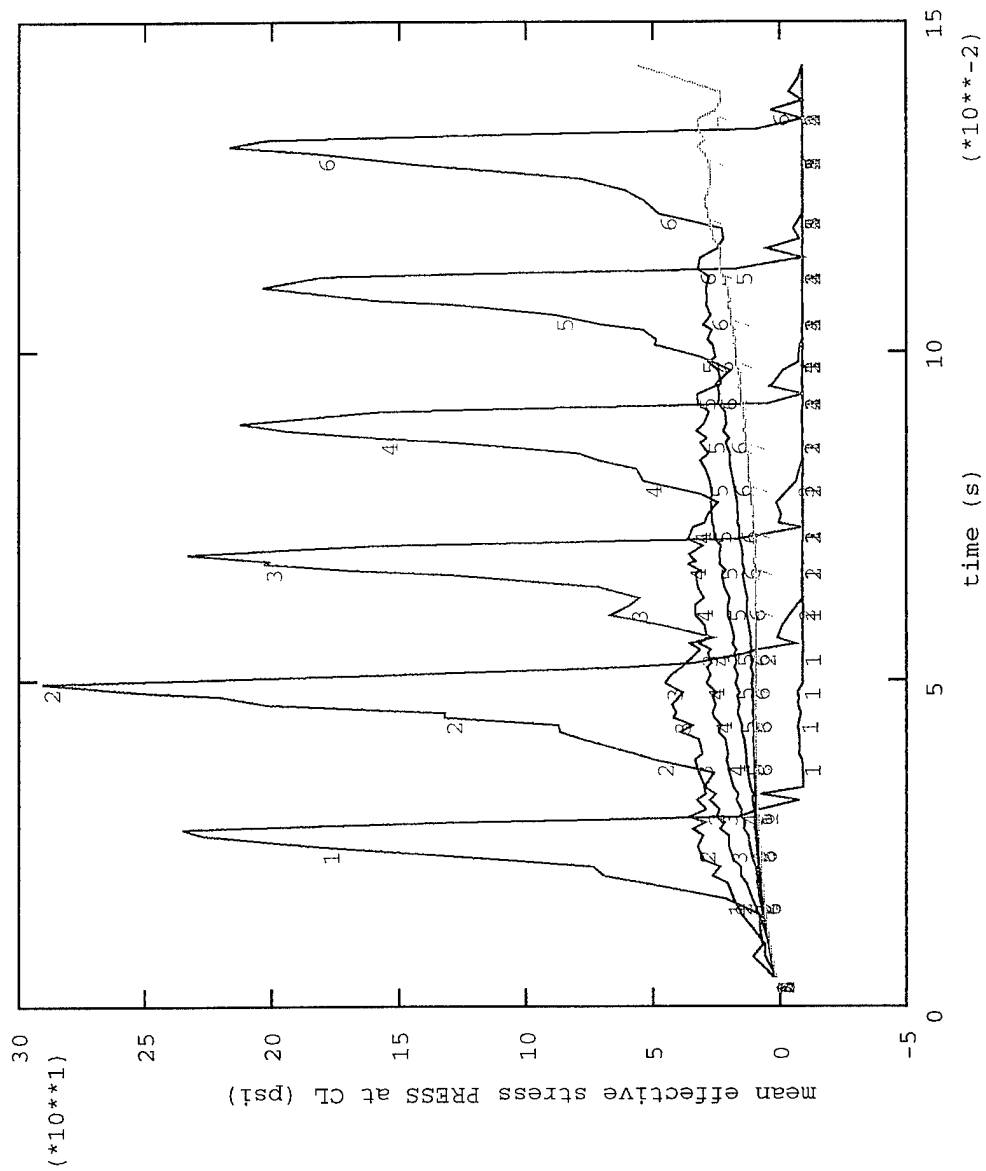
Figure 4-10 Continued.

88

(a) Mises effective stress histories at sampled response points along path of plow.

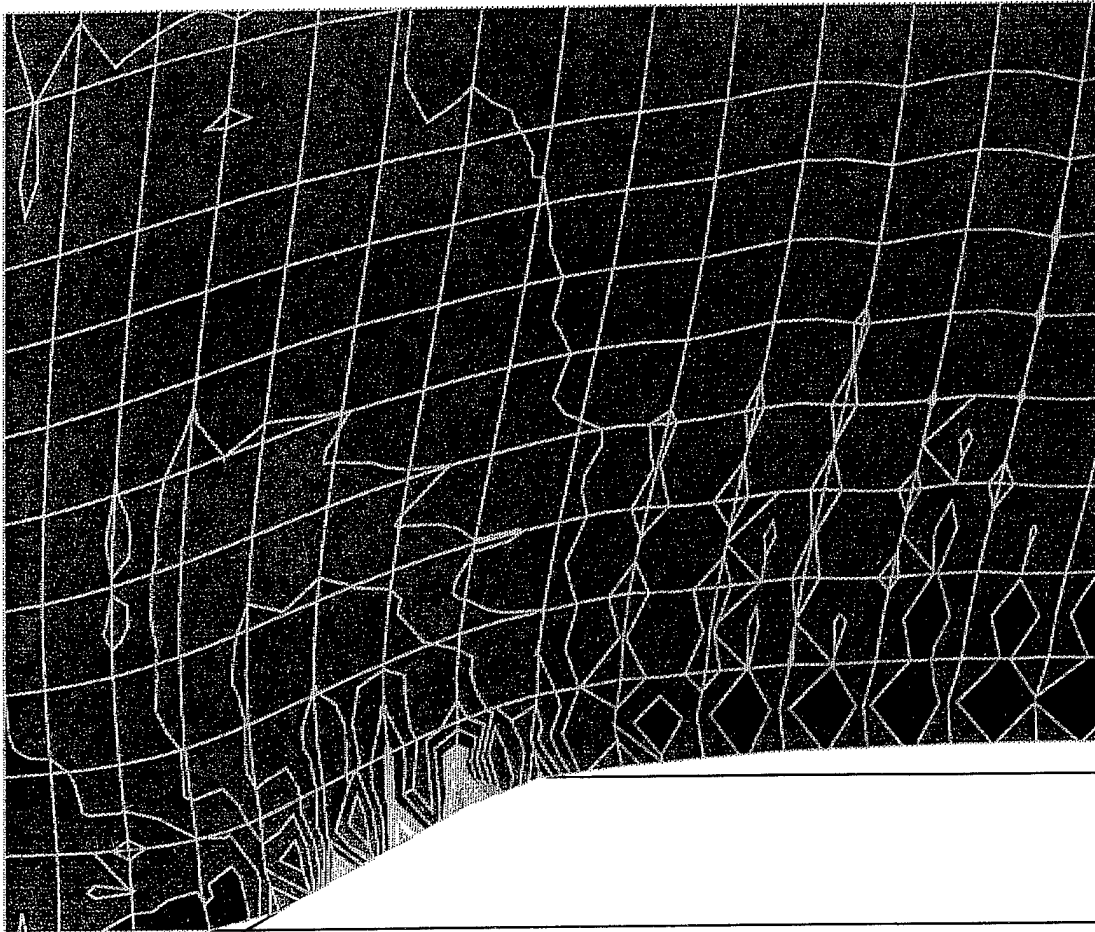Figure 4-11. Mises effective stress in soil at 5 fps steady-state plow velocity.

(b) Mises effective stress distribution near plow tip.

Figure 4-11 Continued.

(a) Mean effective stress histories at sampled response points along path of plow.

Figure 4-12. Mean effective stress in soil at 5 fps steady-state plow velocity.

91

(b) Mean effective stress distribution near plow tip.

Figure 4-12 Continued.

Soil dilatancy can now be revisited. If element volume is denoted as EVOL, then the change in element volume is ΔEVOL and is defined as the algebraic sum of the direct strains, E11 and E22. Thus ΔEVOL has an elastic and a plastic component. The latter component is the algebraic sum of PE11 and PE22, and the former component is the mean effective stress divided by the elastic bulk modulus K (5,000 psi in the present case). Thus,

$$
\begin{aligned}
\Delta\text{EVOL} &= \text{E11} + \text{E22} \\
&= (\text{E11}^{\text{el}} + \text{E22}^{\text{el}}) + (\text{E11}^{\text{pl}} + \text{E22}^{\text{pl}}) \\
&= (-\text{PRESS/K}) + (\text{PE11} + \text{PE22})
\end{aligned}
$$

The volumetric expansion of the soil can be determined with this expression. For example, where the residual value of PRESS is zero, the elastic part of the residual volumetric expansion is zero. The residual expansion of the material in the wake is therefore the sum of residual plastic strain components PE11 and PE22 (Figures 4-6c and h). In this case, the maximum residual volumetric expansion equals 27 percent, as before.

4.4.5 Summary of Model Stresses in the Soil. The mechanical response of the soil skeleton is characterized by effective stresses. Like the strain response, the effective stress response is primarily confined to one or two blade widths from the plow tip, and stress gradients are very large. Effective stress components rise and fall precipitously during arrival and departure of the plow tip, as do their corresponding strain components. However, unlike strains, stresses return to zero as the soil is unloaded and there is no residual stress response. Although plow tip forces are based on total stress, the distribution of effective stress over the plow tip is consistent with these forces. The assumed failure mechanism for cleaving the soil at the plow tip causes a small reduction in the area of contact at the tip of the plow which is countered by an over-prediction of soil strength. Further features of the computed stress response in the plow/soil interaction model are:

- The location of the maximum distortion stress corresponds to the shoulder of the plow tip.

- The distribution of the lateral stress component over the bevel of the plow tip is approximately linear, varying from zero at the tip to a maximum at the shoulder. This result is consistent with wear patterns observed on steel blades employed continuously in the field which show maximum wear on the shoulder of the plow tip.

- The distribution of the in-line component of stress over the bevel of the plow tip is more uniform, although slightly truncated at the tip.

- Soil strength is proportional to mean pressure stress according to the Drucker-Prager soil model employed. Contours of pressure stress demonstrate how the plow tip, to progress forward, must continuously overcome soil at maximum strength conditions.

93

4.5 Pore Pressure in the Soil

Whereas effective stress reflects the behavior of the soil skeleton or solid phase of the soil, pore pressure reflects the behavior of the fluid phase of the soil. It is denoted by the variable POR. Unlike effective stress, pore pressure is computed and reported at the node points; no averaging or interpolation occurs in post processing of these data.

In Figure 4-13, a negative or reduced pore pressure field is shown which results when a dilatant soil is subjected to the shearing action of the plow. This response evidences the coupling that exists between the fluid and solid phases of the soil. The maximum negative pore pressure coincides with the plow tip where maximum volumetric expansion occurs.

The pore pressure field is more diffuse in time and space than the effective stress field. While the absence of large gradients facilitates accurate modeling of the pore pressure field with low order finite elements, its diffuse nature makes it more difficult to simulate without contaminating the solution in the region of interest near the plow tip due to effects from the artificial, finite boundaries of the model. Nonetheless, there are several similarities in the responses of computed pore pressure and measured pore pressure (with the laboratory apparatus, Figure 1-1).

In Figure 4-13a, time histories of pore pressures are presented at seven uniformly spaced nodes along the centerline (Figure 4-2). Pore pressure change is clearly sensed well in advance of the plow, a response also observed experimentally. There is a substantial overshoot in peak pore pressure as the plow begins to penetrate into the soil during the startup transient phase of the motion. According to these data, pore pressure response becomes steady-state when the plow has penetrated to node 101 and beyond in the plow/soil interaction model. The peak steady-state pore pressures shown are representative of measurements taken near (but not on) the centerline in the laboratory apparatus for the particular plow configuration and plow velocity corresponding to this simulation. In Figure 4-13b, the maximum negative pore pressure or trough, envelops the tip of the plow blade. The trough is roughly circular in shape and surrounds the leading edge of the blade, both of which are observations made for measured pore pressure distribution in the laboratory apparatus. Also, refer to Kutter and Voss (1994) where similar pore pressure contours were reconstructed from measured data.

The reduced view in Figure 4-13c shows the diffuse nature of pore pressure over the entire field of the plow/soil interaction model. The graph of pore pressure distribution along the path of the plow shows the peak response at the plow tip, and the gradual decay forward and aft of the plow tip. Pore pressure gradients are relatively small in comparison to gradients of effective stress and strain in the soil skeleton. However, where the pore pressure does not approach zero at a boundary of the plow/soil interaction model (except at the centerline), the pore fluid region may be considered artificially truncated, and the response may not be an accurate representation of pore pressure in that region.
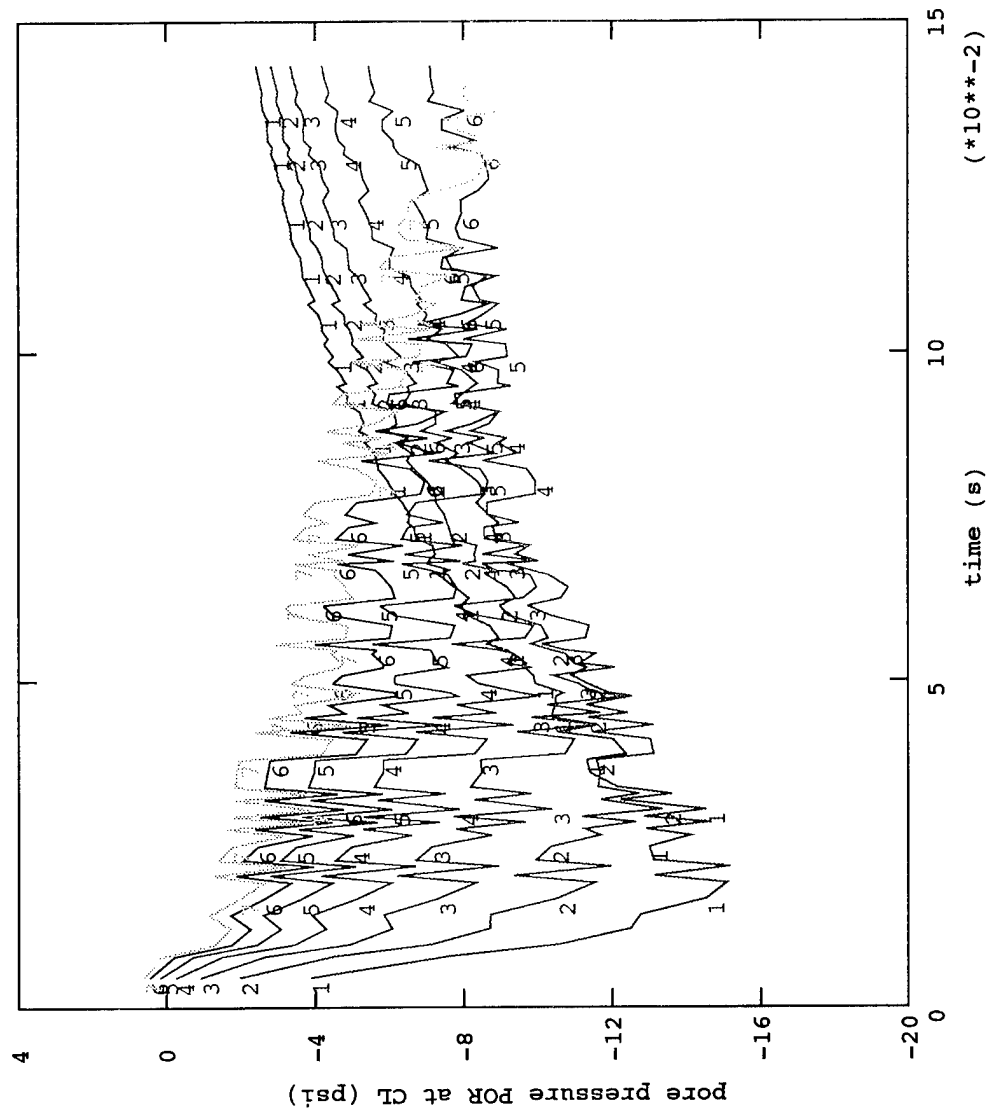
(a) Pore pressure histories at sampled response points along path of plow.

Figure 4-13. Pore pressure in soil at 5 fps steady-state plow velocity.
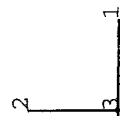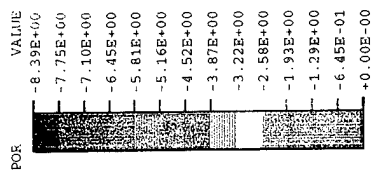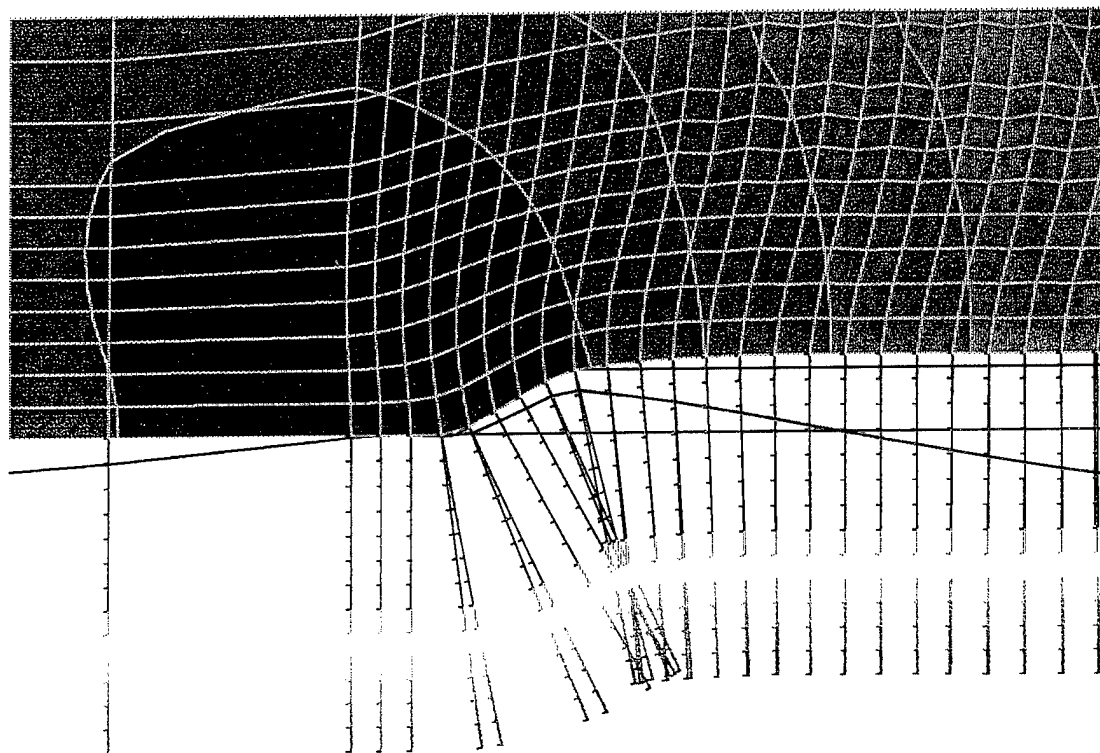
(b) Pore pressure distribution near plow tip.

Figure 4-13 Continued.
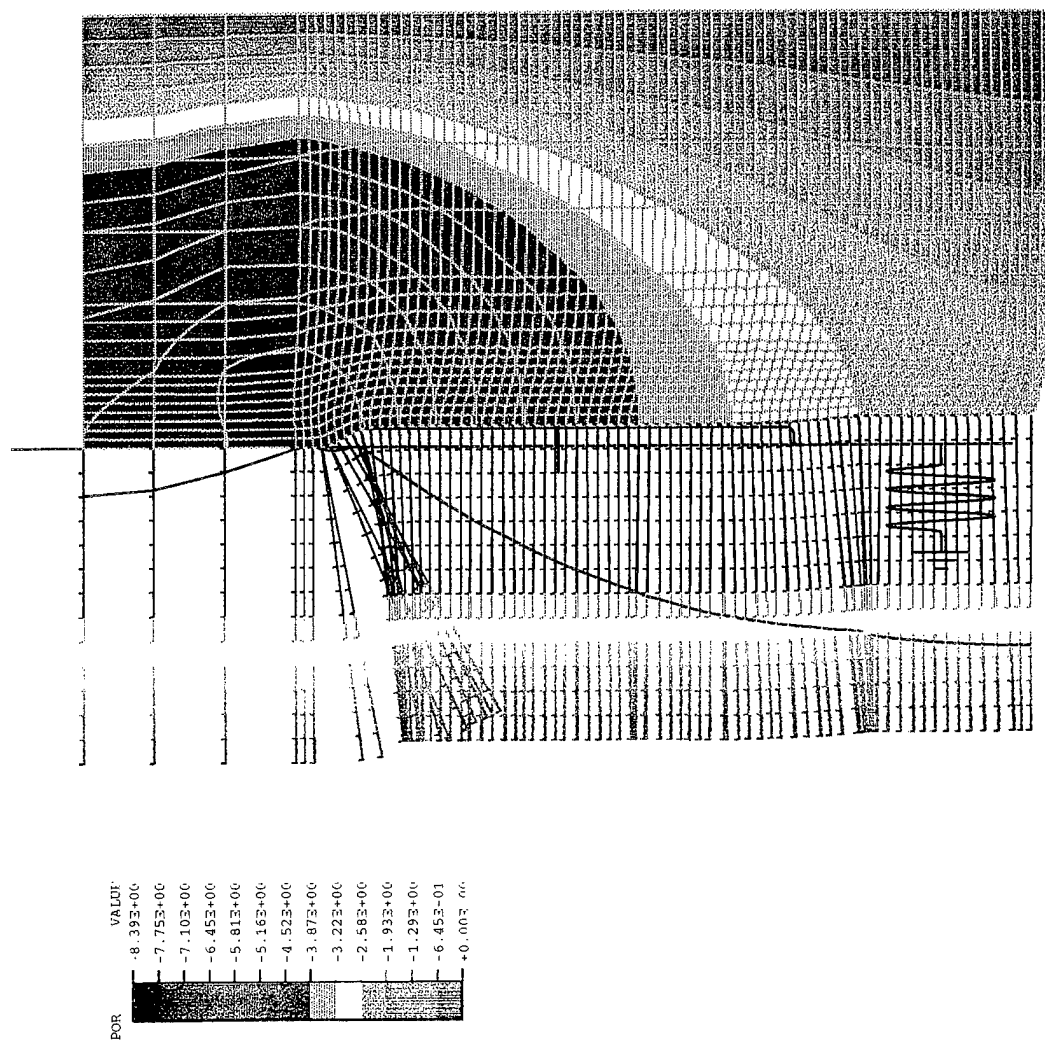
(c) Pore pressure field for plow/soil interaction model.

Figure 4-13 Continued.

In summary, the pore pressure field computed by the plow/soil interaction model is very diffuse as contrasted with the effective stress field computed by the model which is characterized by large gradients.

- The pore pressure field computed by the plow/soil interaction model is everywhere negative, behavior which is expected of a dilatant soil subjected to shear stress.

- Pore pressure magnitudes are representative of measured pore pressures in the laboratory apparatus. In comparison to maximum effective stresses, the maximum pore pressures are small, explaining why at high stress locations the total and effective stress responses appear equal.

- The roughly circular trough in the contour map of computed pore pressure envelops the plow tip. It corresponds to the area of maximum volumetric expansion, and the location of maximum negative pore pressure measured in the laboratory apparatus.

5.0 PARAMETER STUDY

This parameter study demonstrates the kind of engineering data that can be derived from a rational numerical model of plow/soil interaction. The parameters chosen relate to properties of the plow; they are the plow velocity, the coefficient of friction between the blade and soil, and the shape of the blade as represented by the included angle of the blade tip. Baseline conditions or standard blade properties were selected as follows: 10 fps, no blade or interface friction, and a 1/2-inch-thick blade with a 60-degree blade tip included angle (Figure 1-1b). The effect that velocity, friction and shape parameters have on plow forces, and on soil stress and pore pressure along the path of travel are studied.

The effect of velocity on tow force can be studied more accurately by experiment in the portable test apparatus (Figure 1-1a) since the present two-dimensional numerical model predicts only unit tow force, not total force. Therefore, no attempt is made to directly compare experimental and numerical data, although frequently experimental observations and model predictions are qualitatively compared in the discussion. Conversely, the effect of parameters like blade friction and blade shape can perhaps be studied more easily with the numerical model. These parameters have not been studied experimentally in the portable test apparatus to date. The study demonstrates how the numerical model can complement experimental approaches to gain understanding of plow/soil interaction.

5.1 Effect of Plow Velocity on Performance and Soil Response

The steady-state velocities listed in Table 3-2 are used to study the effect of plow velocity. The plow/soil interaction model was run for each of these velocities until the plow achieved steady-state conditions and traveled approximately the same embedment distance (Figure 4-1). A frictionless blade was assumed and the standard 1/2-inch-thick blade with a 60-degree blade tip angle was assumed.

5.1.1 Plow Forces. Histories of tow and lateral force components acting on the plow are shown in Figure 5-1 for the case of 10 fps steady-state velocity. These are forces per unit depth of the plow blade, or unit plow force components. The steady-state forces for each component are obtained graphically by averaging the steady portion of the history data shown. The lower curve is the tow force component for half the blade thickness, so the tow force on the full 1/2-inch-thick blade is twice the steady-state value shown in the graph. This clearly makes it approximately equal to the lateral component shown in the upper graph.

The linear relationship that these plow force components apparently have with steady-state plow velocity, over the range of velocities studied, is shown in Figure 5-2. This is in agreement with experimental observation. However, there is little evidence of a critical velocity in these data such as has been observed experimentally (Figure 1-2), and as proposed by the semi-empirical model (Figure 2-1). This is perhaps related to the numerical model's inability to allow softening in the Drucker-Prager model of the solid phase, or to allow a cavitation pressure cutoff in modeling the fluid phase. On closer inspection, a quadratic least squares curve fit to the tow force data is perceptively better than a linear curve fit indicating only a very slight tendency toward critical velocity behavior.
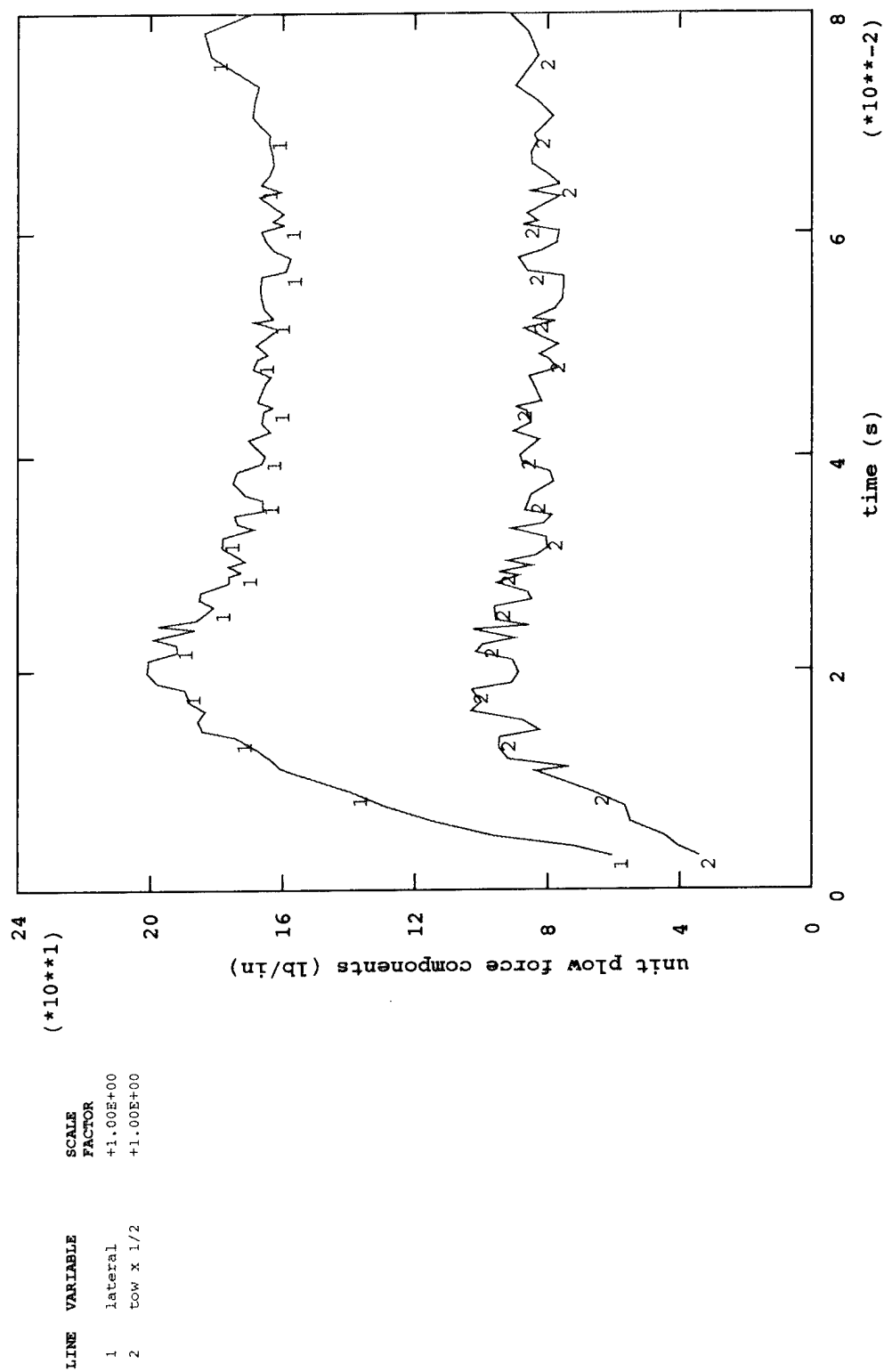
Figure 5-1. Unit plow force histories at 10 fps steady-state plow velocity.
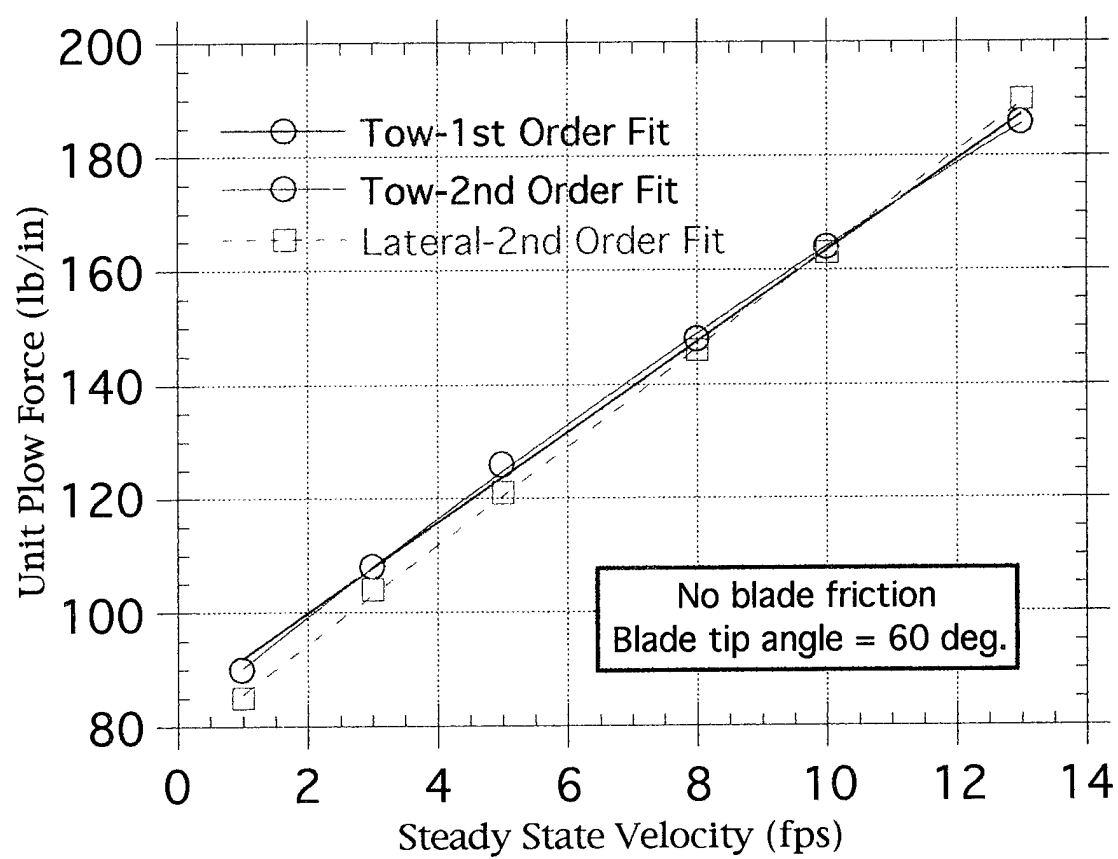
Figure 5-2. Effect of velocity on steady-state plow forces.

A static tow force, i.e., the tow force at zero velocity, can be estimated from this graph using the method of Section 4.2.3. The static tow force is typically non-zero, as shown in the experimental data (Figure 1-1b). However, comparison between computed unit plow forces and measured total plow forces can be misleading for the two-dimensional plane strain model cannot predict total force.

The apparent equality between the unit tow and lateral force components occurs for the entire range of velocities studied for the case of the standard frictionless blade. There is no apparent reason why this should be so, but it is a useful rule of thumb since lateral force has not been measured.

Unit plow force is an integral of contact force distribution over the tip of the plow blade, as shown for the 10 fps case in Figure 5-3. Contact forces are forces per unit length (lb/in.) along the plow/soil interface. Typically, the predicted profile of the lateral contact force along the interface varies nearly linearly from zero forward of the tip of the blade, to a maximum at the shoulder of the blade, and then rapidly to zero just aft of the shoulder where interface separation begins. The maximum contact force would be expected to increase linearly with plow velocity.

5.1.2 Behavior of Principal Stresses in the Soil.

Total stresses in the soil which act at the plow/soil interface account for the aforementioned contact forces and the overall resistance the plow experiences during penetration. Total stress is the algebraic sum of the effective stress and pore pressure in the soil, but the former is generally much larger than the latter. A reasonably complete picture of resistance is therefore provided by the distribution of principal (effective) stresses near the plow tip.

Contours of maximum and minimum principal stresses in the soil near the tip of the plow are presented in Figure 5-4 for the case of the standard frictionless plow blade moving at 10 fps (intermediate principal stress is omitted). The maximum shear stress is also indirectly included in these data, and is obtained as one-half the difference between the minimum (SP1, lowest negative or compression stress) and maximum (SP3, highest negative or compression stress) principal stresses presented in Figures 5-4a and b, respectively. The greatest stress acts directly on the shoulder of the blade where field observation correspondingly reveals most of the wear.

Variation of principal stresses with steady-state velocity is illustrated in Figure 5-5. Data plotted are the extreme contour values (Figure 5-4) for each velocity. A least squares 2nd order polynomial curve fit to these data is clearly superior to a linear curve fit. Principal stresses therefore appear to be approaching a lower bound or saturation level. Also, the minimum and maximum curves draw closer (by about 37 percent in this case) over the range of velocities studied. Half their difference, at a particular velocity, is an upper bound on the maximum shear stress that exists near the plow tip at that velocity. Accordingly, the maximum shear stress decreases, and the two principal stress components increase (negatively) toward a bound, with increasing steady-state plow velocity.

5.1.3 Pore Pressure Behavior.

Due to the shearing action of the plow tip, the dilatant soil expands as the plow approaches, and because of the plasticity in this deformation, element volumes in the path of the plow (along the centerline, CL, of the model) increase permanently to the residual levels shown in Figure 5-6, for the standard frictionless blade moving at 10 fps. Pore water migration into the void is thereby initiated according to soil permeability, a prescribed function of void ratio (Figure 3-12). The corresponding pore pressure histories are shown in

102

Figure 5-7a. Data sampled at node points above node 61 (Figure 4-2), vary similarly and verify that steady-state behavior exists in the fluid phase of the plow/soil interaction model. Pore pressures are everywhere negative, and the minimum steady-state pore pressure can be determined from these data. The minimum pressure or trough in pore pressure at the plow tip created by shearing of the dilatant soil is evident in Figure 5-7b. The algebraic sum of this negative pressure and the effective stress (compressive, Figure 5-4a) near the tip, i.e., the total stress, constitutes the source of resistance to plow penetration. According to these results, the minimum pore pressure engulfing the blade tip an order of magnitude smaller than the principal stress at the shoulder of the blade tip.

The variation of minimum pore pressure at the blade tip with steady-state velocity is shown to be linear in Figure 5-8. The minimum pore pressure decreases without bound because the plow/soil interaction model does not include any provision for cavitation in the pore fluid.

5.2 Effect of Plow Friction on Performance and Soil Response

The smoothness/roughness condition of the plow blade is undoubtedly an important parameter as it relates to performance, effectiveness, and operational cost of trenching operations. It can be represented by a kinetic coefficient of friction at the plow/soil interface in conjunction with the standard Coulomb friction model in the plow/soil interaction model. The aforementioned parametric results (Figures 5-1 through 5-8) pertain to a frictionless interface between the plow and soil. In this parameter study the coefficient of friction between the blade and soil was varied to determine its effect on plow forces and on behavior of the soil. The effect of small amounts of friction, i.e., 5 and 10 percent, are studied with the standard blade moving at 10 fps steady-state velocity. The perfectly smooth case (zero percent) is considered the baseline case.

5.2.1 Plow Forces. Unit plow force histories including the effect of friction are presented in Figure 5-9. Predictably, both components of plow force have increased compared to the baseline case (Figure 5-1), and both components increase with the value of the coefficient of friction as seen by comparing the graphs of Figures 5-9a and b which show the results for 5 and 10 percent friction, respectively. When friction is present, the lateral force is somewhat less than the tow force, and the aforementioned equality between lateral and tow force components apparently pertains only to the case of a frictionless interface (i.e., the lower curves have drawn closer to the upper curves as friction is increased, and when multiplied by two to correct for a half-blade thickness, they exceed the magnitudes of the upper curves).

This is seen more clearly in Figure 5-10, where the tow and lateral force components are shown to vary with the coefficient of friction due to the Coulomb friction sliding interface model. The normalized values shown are obtained by dividing the two steady-state plow force components by their respective baseline values, which were essentially equal. The tow force component increases linearly and more rapidly with blade friction than the lateral force component. Indeed, the plow/soil interaction model predicts that the tow force increases 35 percent for a coefficient of friction of 10 percent between the blade and soil, for the case of the standard blade moving with 10 fps steady-state velocity. The lateral force increases less than linearly towards an apparent bound of only 4 percent.
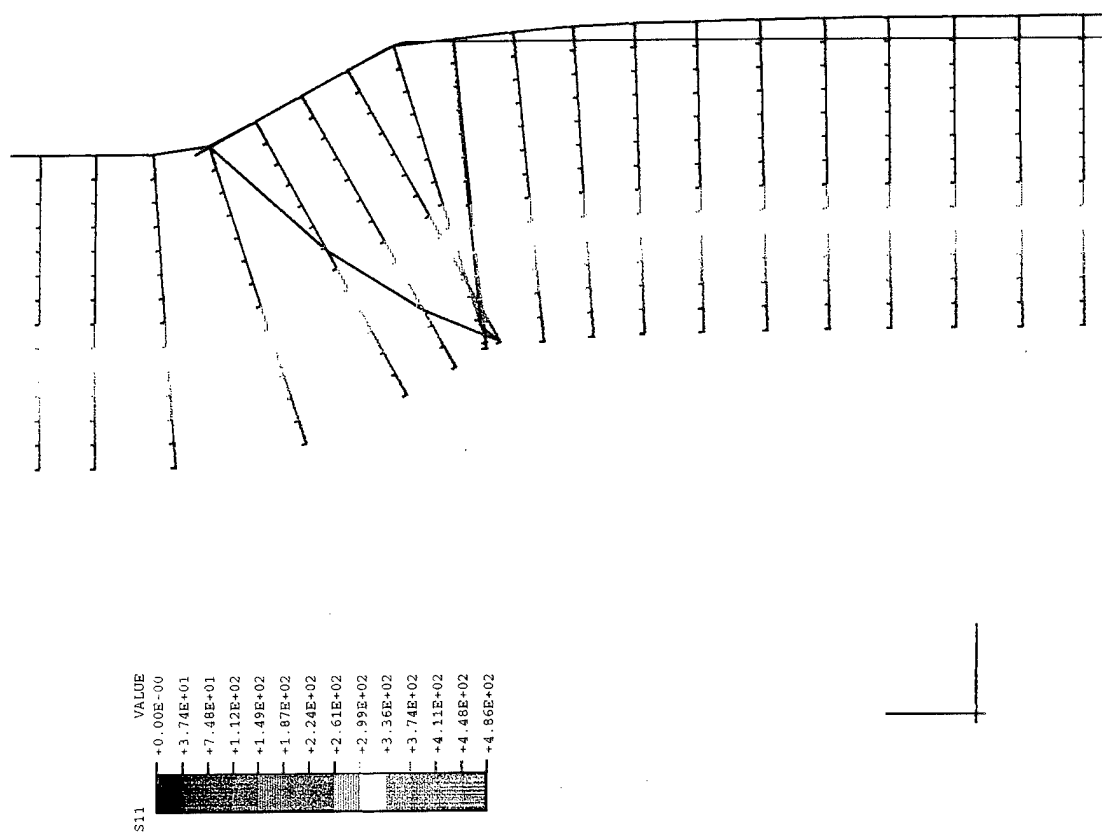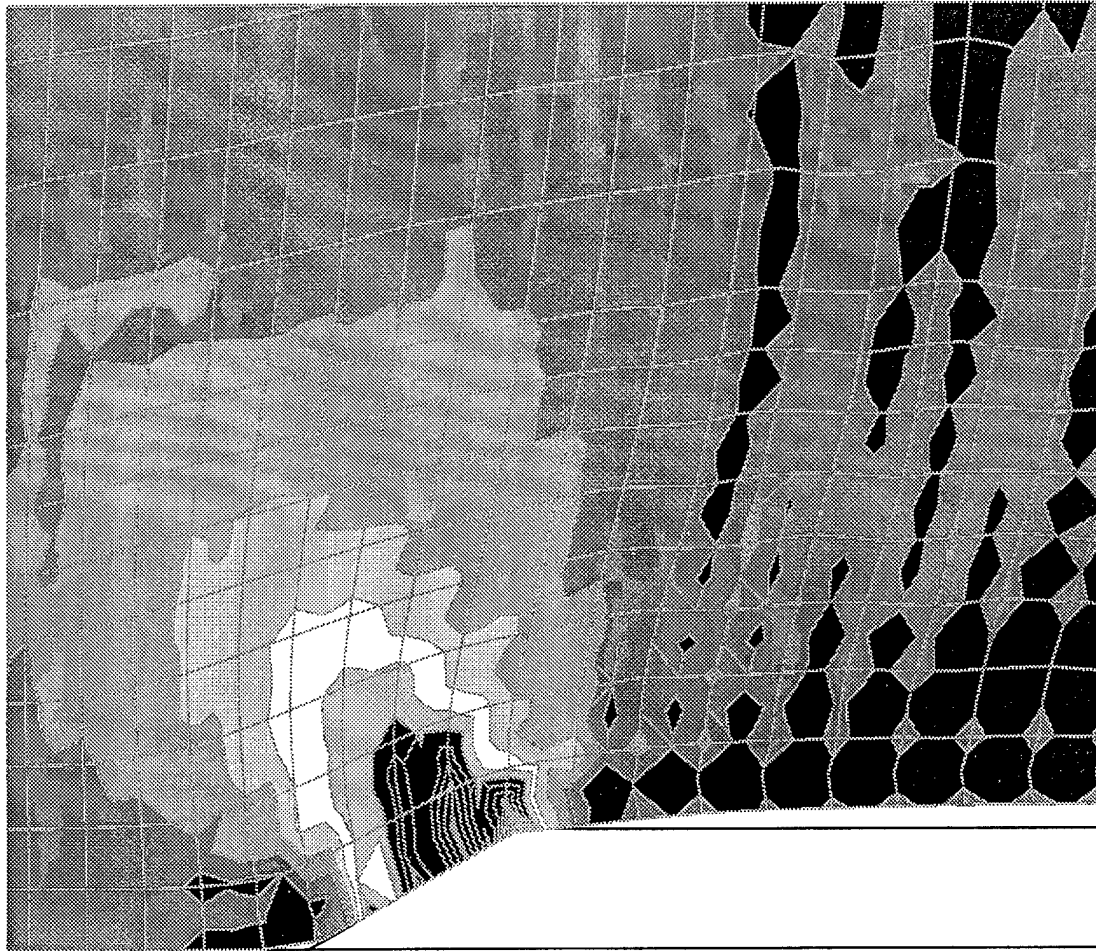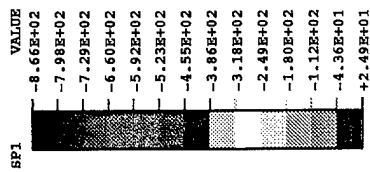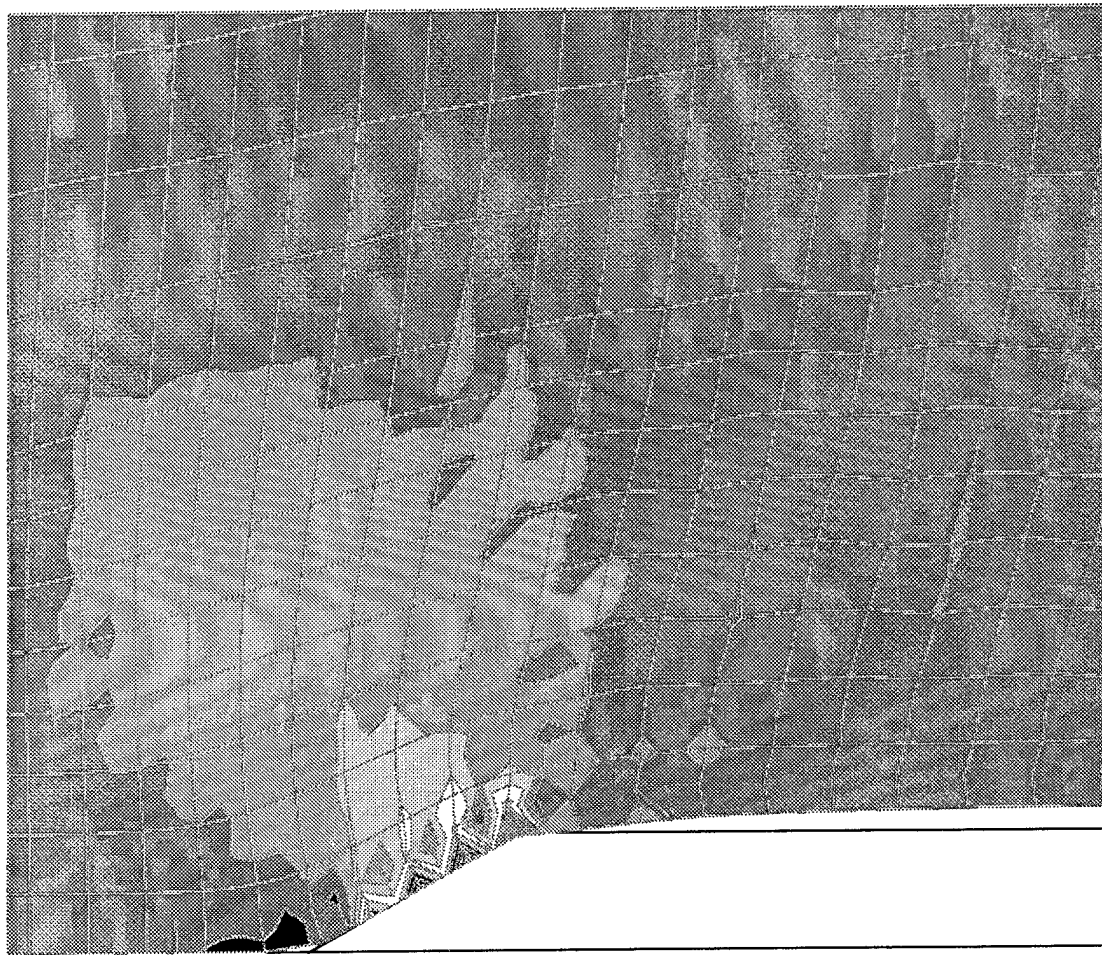
Figure 5-3. Distribution of lateral interface contact force on plow at 10 fps.

S11	VALUE
	+0.00E-00
	+3.74E+01
	+7.48E+01
	+1.12E+02
	+1.49E+02
	+1.87E+02
	+2.24E+02
	+2.61E+02
	+2.99E+02
	+3.36E+02
	+3.74E+02
	+4.11E+02
	+4.48E+02
	+4.86E+02

(a) Minimum principal stress SP1 distribution near plow tip.

Figure 5-4. Principal stress components in soil at 10 fps steady-state plow velocity.
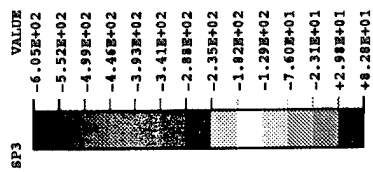
(b) Maximum principal stress SP3 distribution near plow tip.
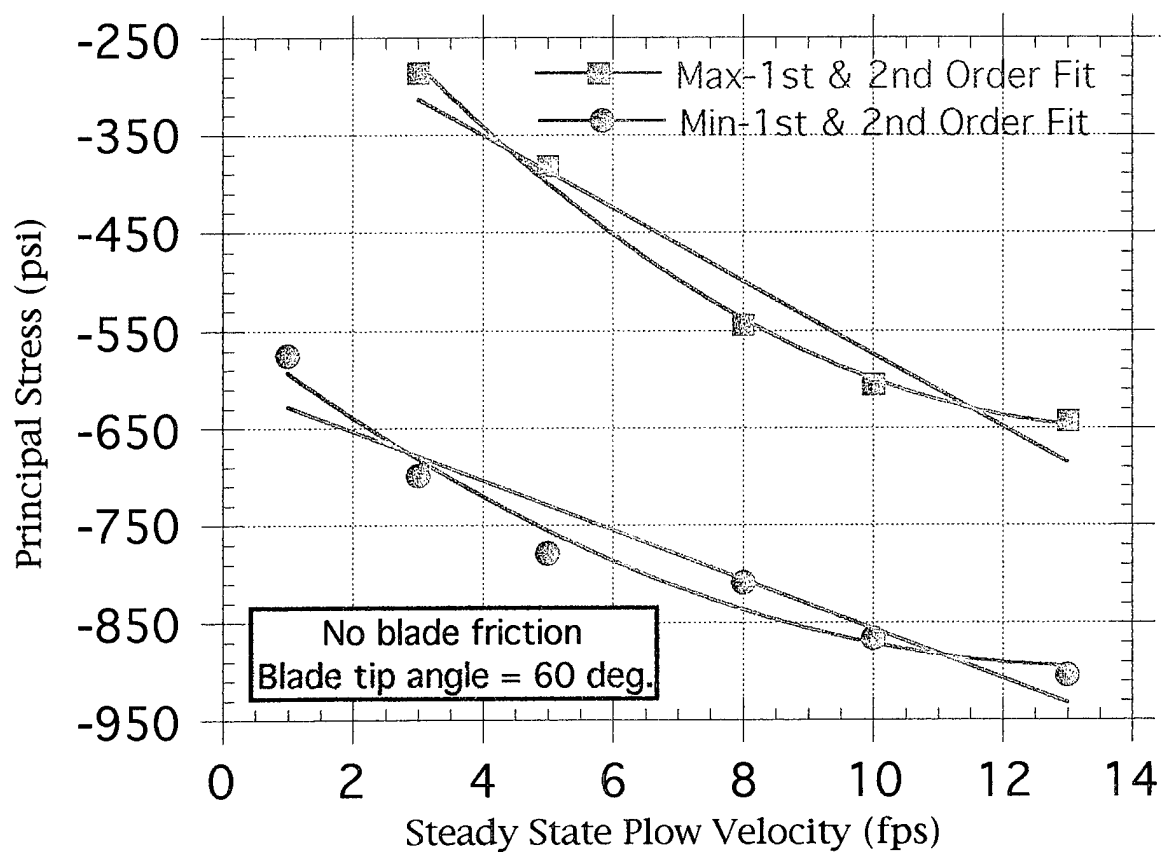
Figure 5-4 Continued.

Figure 5-5. Effect of plow velocity on principal stresses in soil.
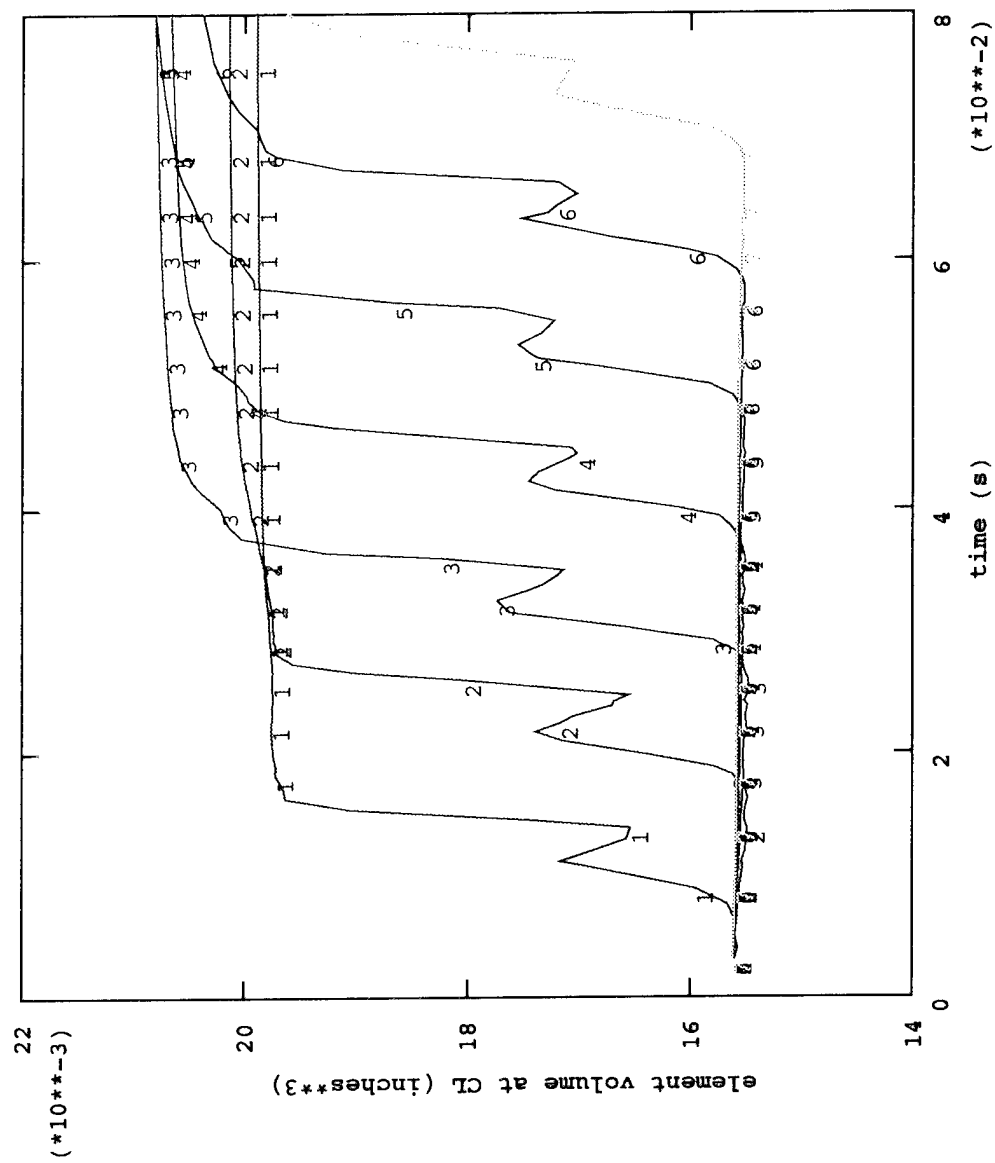
Figure 5-6. Element volume change histories at 10 fps steady-state plow velocity.
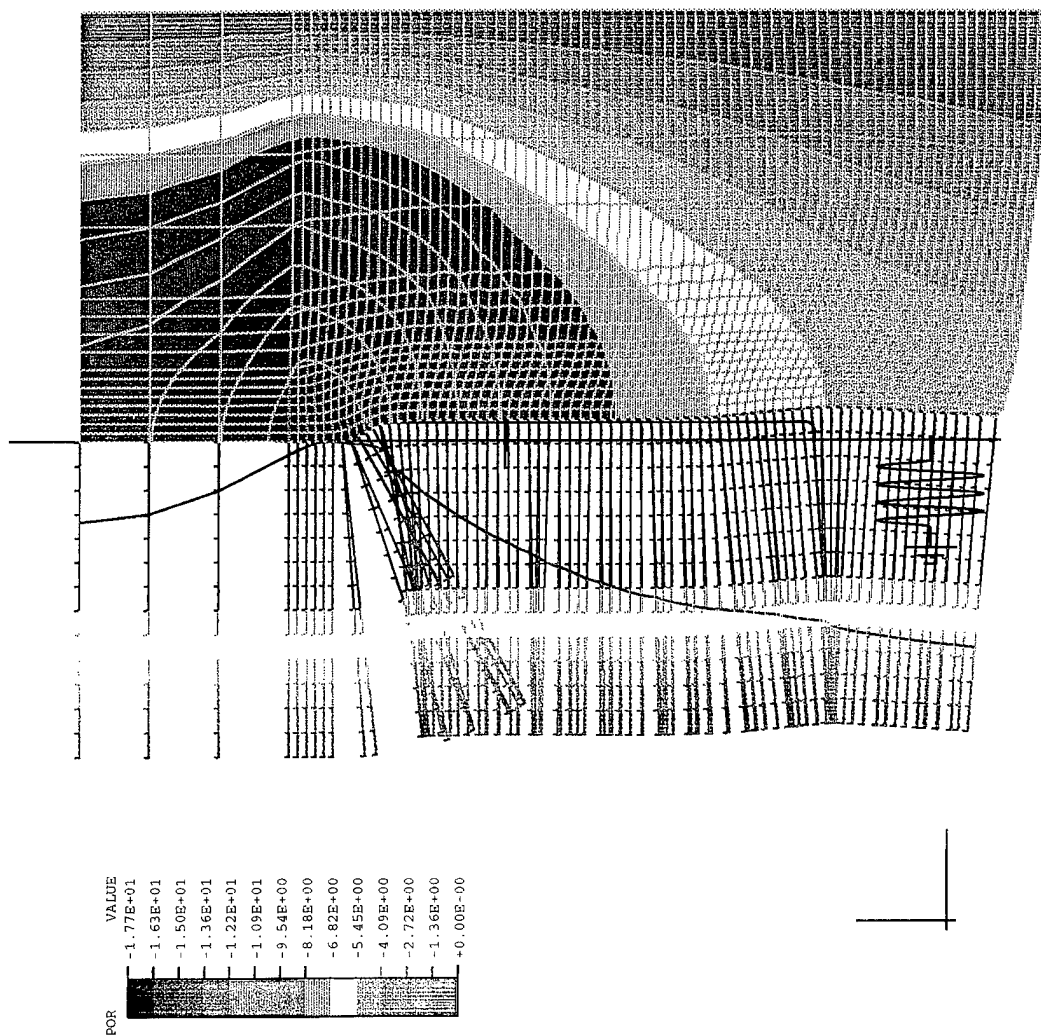
(a) Pore pressure histories at sampled response points along path of plow.

Figure 5-7. Pore pressure in soil for 10 fps steady-state plow velocity.

109
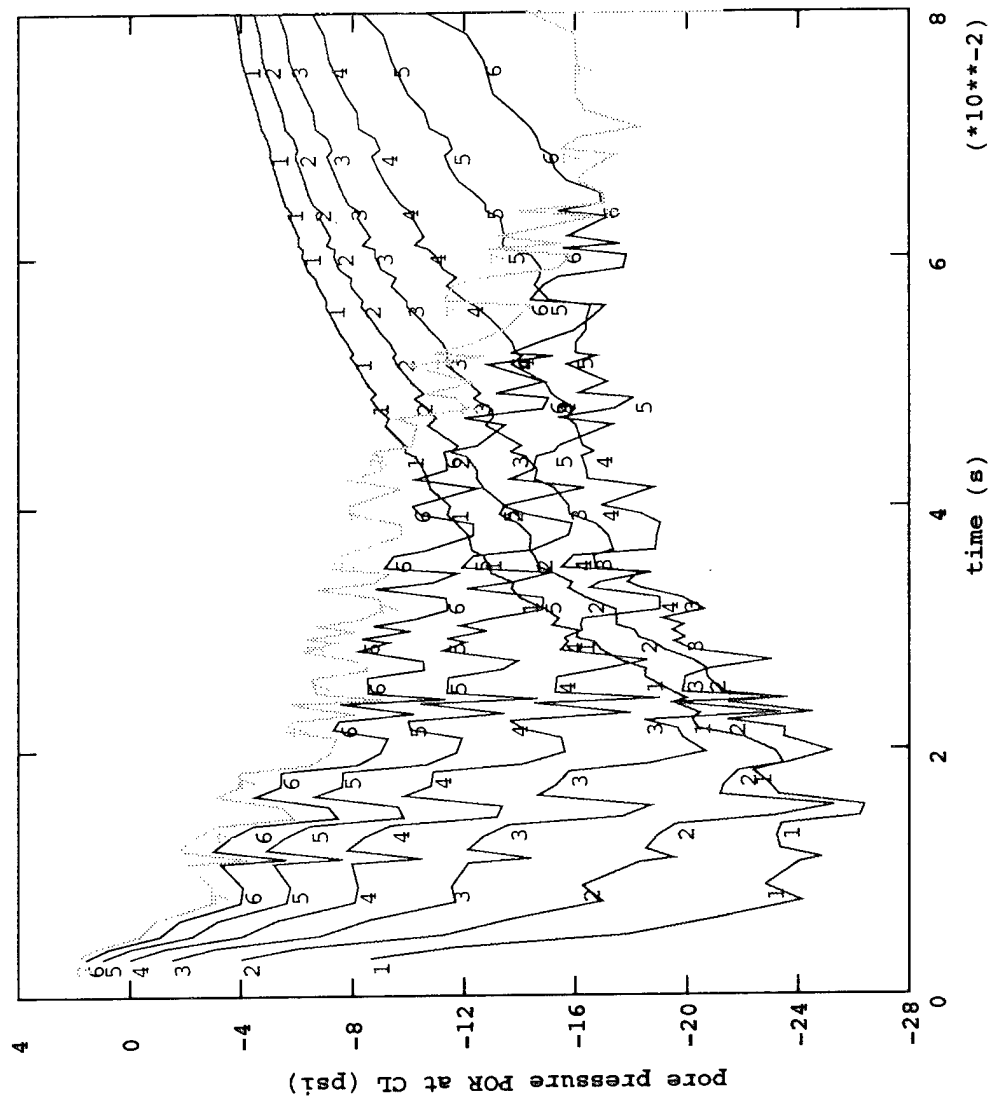
(b) Pore pressure distribution in soil surrounding plow.

Figure 5-7 Continued.

Figure 5-8. Effect of plow velocity on minimum pore pressures.

111

(a) Lateral and tow (half) force components per unit depth of blade with 5 percent friction.

Figure 5-9. Unit plow force histories at 10 fps steady-state plow velocity with friction.

(b) Lateral and tow (half) force components per unit depth of blade with 10 percent friction.

Figure 5-9 Continued.

Figure 5-10. Effect of friction on steady-state plow forces.

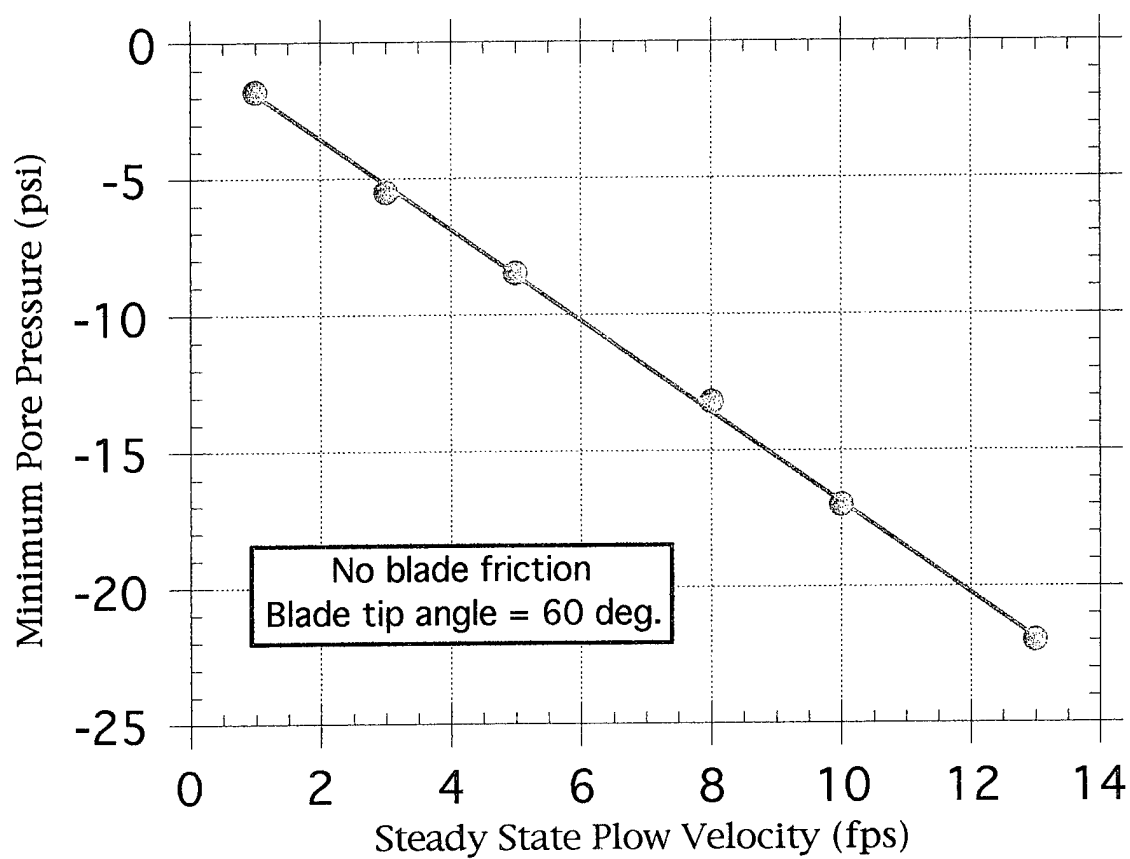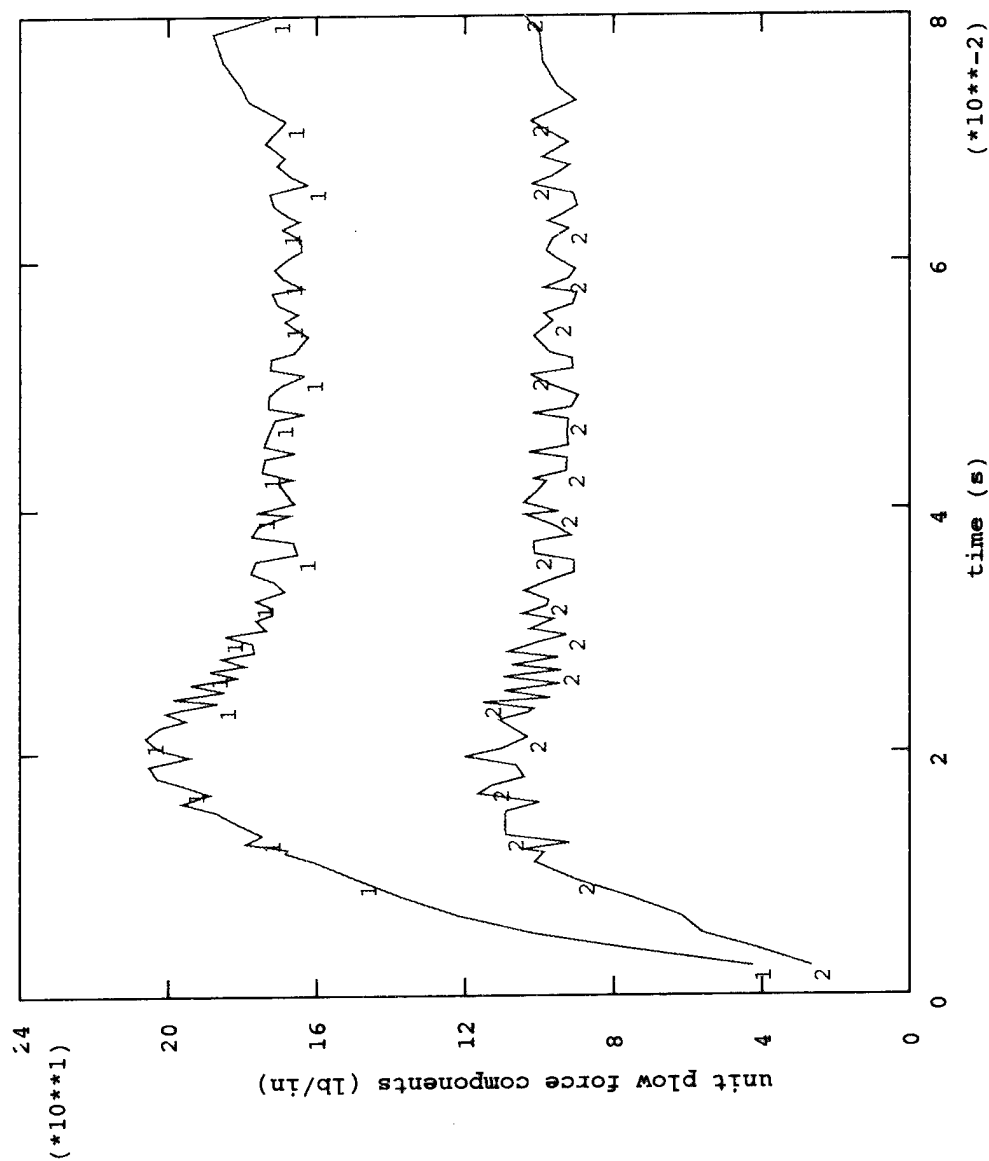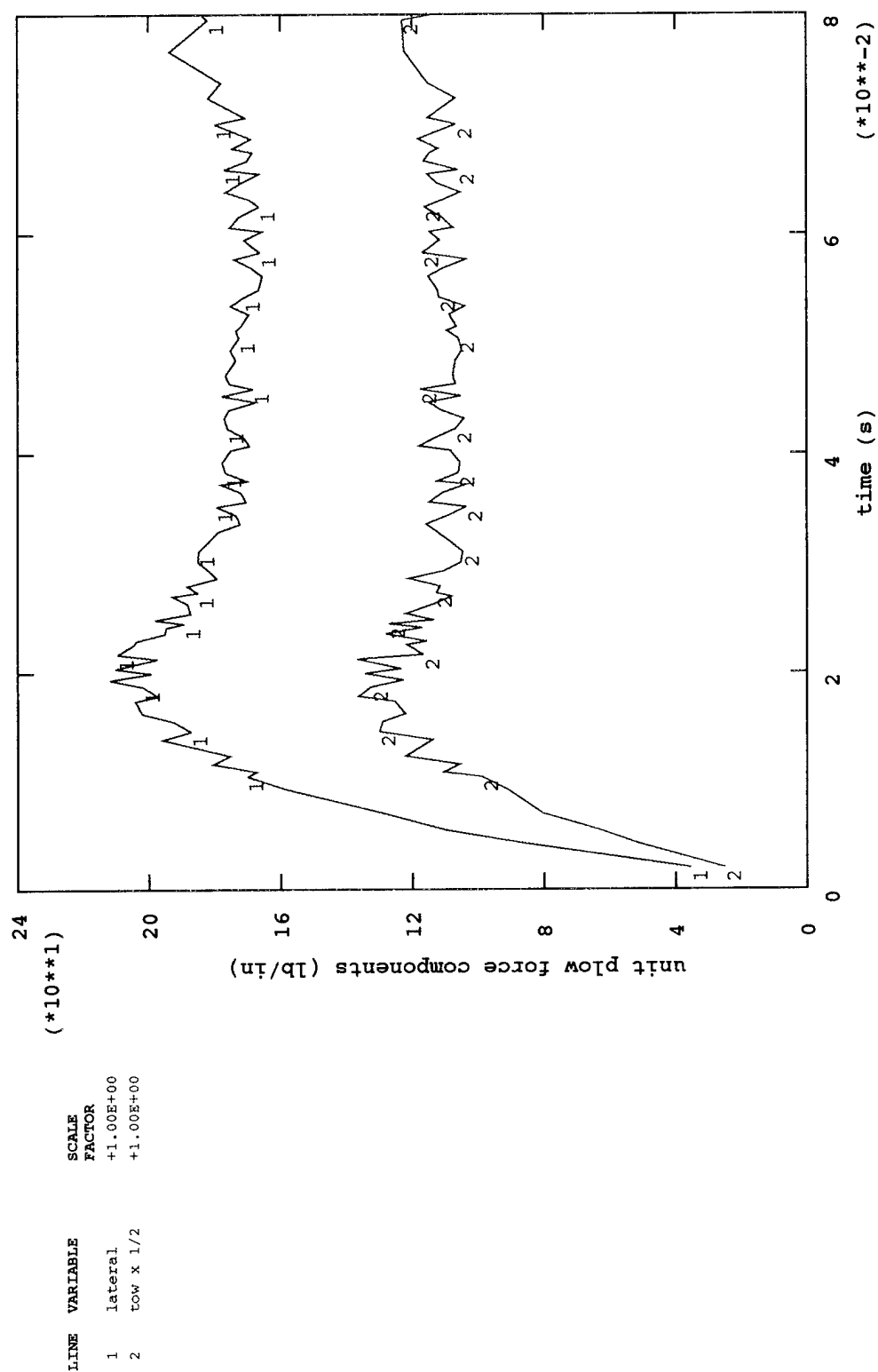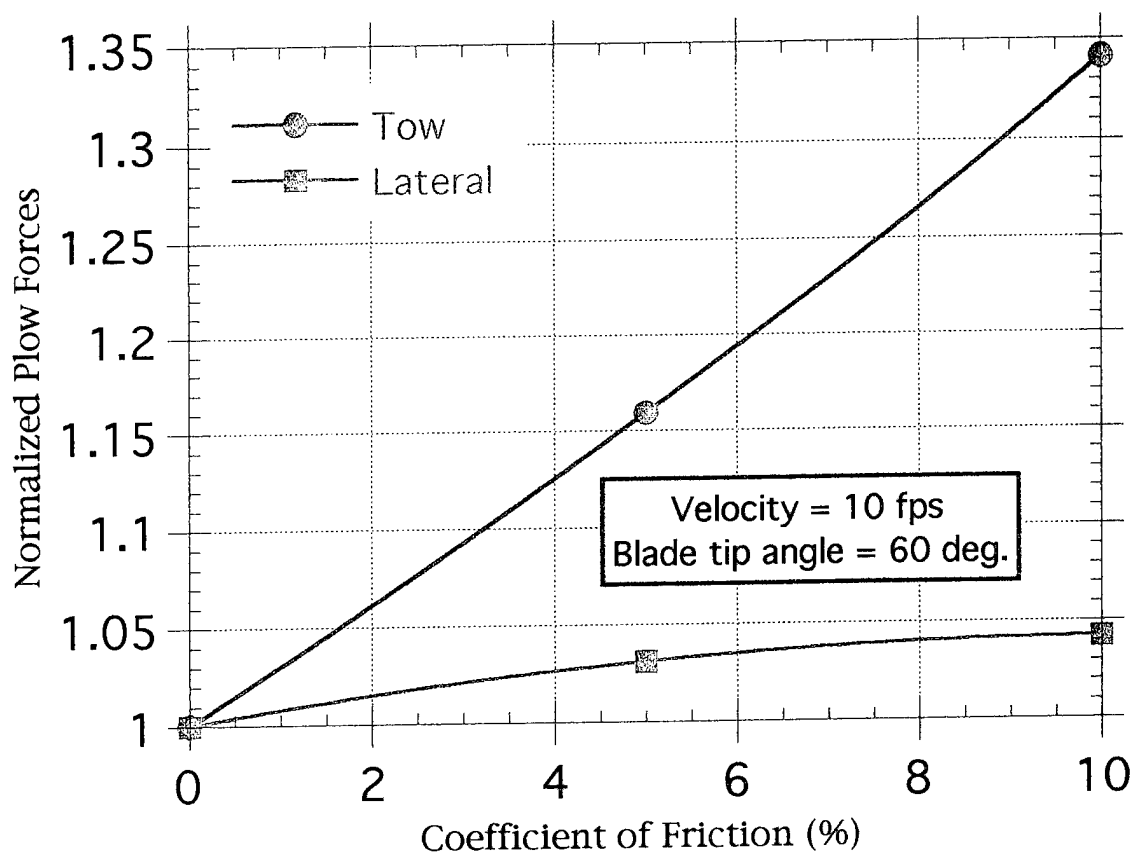The corresponding steady-state lateral contact forces on the tip of the blade vary along the interface as shown in Figure 5-11, i.e., they vary nearly linearly from zero at the tip to a maximum at the shoulder of the blade, as they did for the baseline case (Figure 5-3). The maximum value of the lateral contact force for 10 percent friction is 11.5 percent greater than for the case of no friction.

5.2.2 Behavior of Principal Stresses in the Soil. The two steady-state principal stress components for the case of 5 and 10 percent friction are plotted in Figures 5-12a and b, and 5-12c and d, respectively. Contours of their spatial distribution focus on the shoulder of the plow blade. When compared to the baseline case (Figure 5-4) it is seen that the effect of friction is to decrease the minimum principal stress and increase the maximum principal stress. For example, with the standard blade moving at 10 fps, adding 10 percent friction decreases the lowest minimum stress by 28 percent, and increases the highest maximum stress by 22 percent. The two extreme principal stresses, normalized on their average for the baseline case (-735 psi), are graphed against the coefficient of friction in Figure 5-13. Half the difference in the two extreme curves shown approximates the maximum shear stress near the plow tip. So the maximum shear stress increases dramatically with increasing friction. Indeed, by adding 10 percent friction in the plow/soil interaction model the maximum shear stress increases by a factor of 3.0. Thus, a rougher blade surface develops substantially more shear stress in the soil.

5.2.3 Pore Pressure Behavior. Histories of volumetric expansion of the soil in the path of the plow for the cases of 5 and 10 percent friction are shown in Figures 5-14a and b, respectively. Only a small increase, due to blade friction, is noted in comparison to the baseline case (Figure 5-6). By contrast, it will be shown in the shape parameter study discussed below, that a dull blade tip causes a substantial increase in volumetric expansion of the dilatant soil.

Pore pressure histories and contours of pore pressure distribution for the cases of 5 and 10 percent friction are shown in Figures 5-15a and b, and Figures 5-15c and d, respectively. Correspondingly, when compared to the baseline case (Figure 5-7), there is no noticeable difference due to blade friction. Only on very close inspection of the minimum steady-state values in the pore pressure history data, can a very slight effect be seen. This is shown in Figure 5-16, where minimum pore pressures, normalized by the corresponding value for the baseline case, are graphed against the coefficient of friction. Adding 10 percent friction lowers the minimum pore pressure by only 4 percent. This is consistent with the small effect noted in volumetric expansion.

5.3 Effect of Plow Tip Shape on Performance and Soil Response

The effectiveness of the blade in cutting through soil is important, and is related to the profile or shape of the blade tip. The shape of the blade tip has an influence on the towing force of blades as indicated with the single-step finite element model discussed earlier (Figure 2.2d). Further, the shape of the blade tip may be altered due to wear on blades used continuously in the field, causing a change in their performance. For example, it has been observed that the shoulder of the blade tip wears, so that lower sections of the blade entry are visibly sharper, although the very tip of the lower blade itself is somewhat more dulled. This parameter study helps to understand the corresponding consequence of continued blade usage.

115
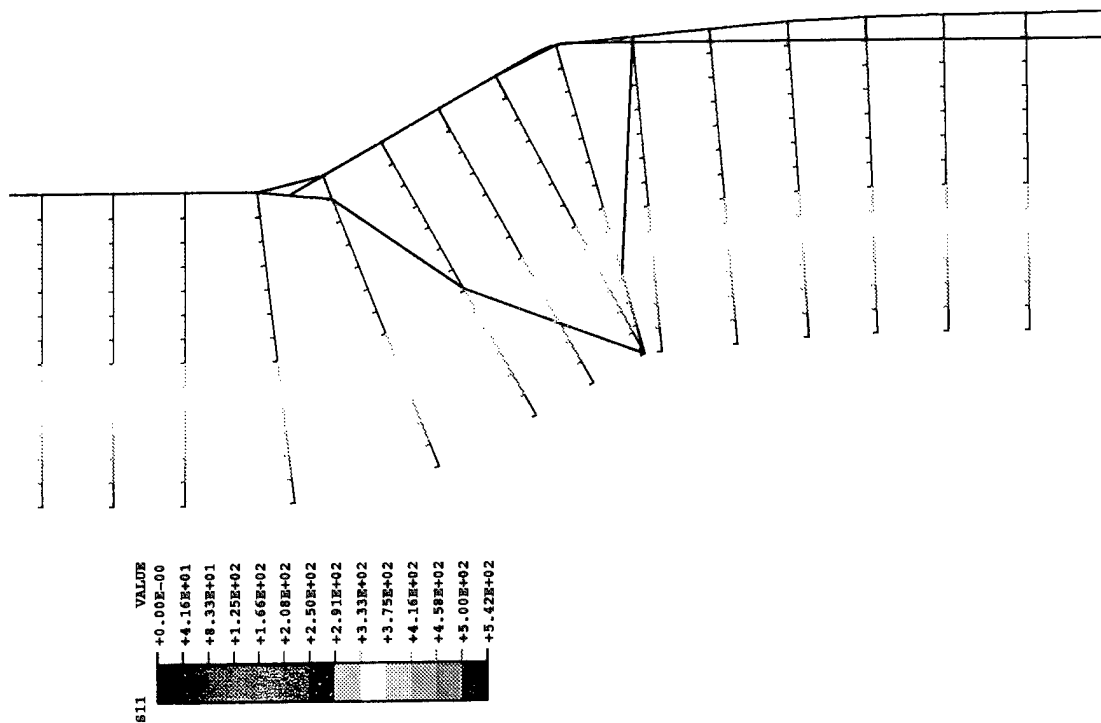
(a) Five percent friction.

Figure 5-11. Distribution of lateral interface contact stress on plow at 10 fps steady-state plow velocity with friction.
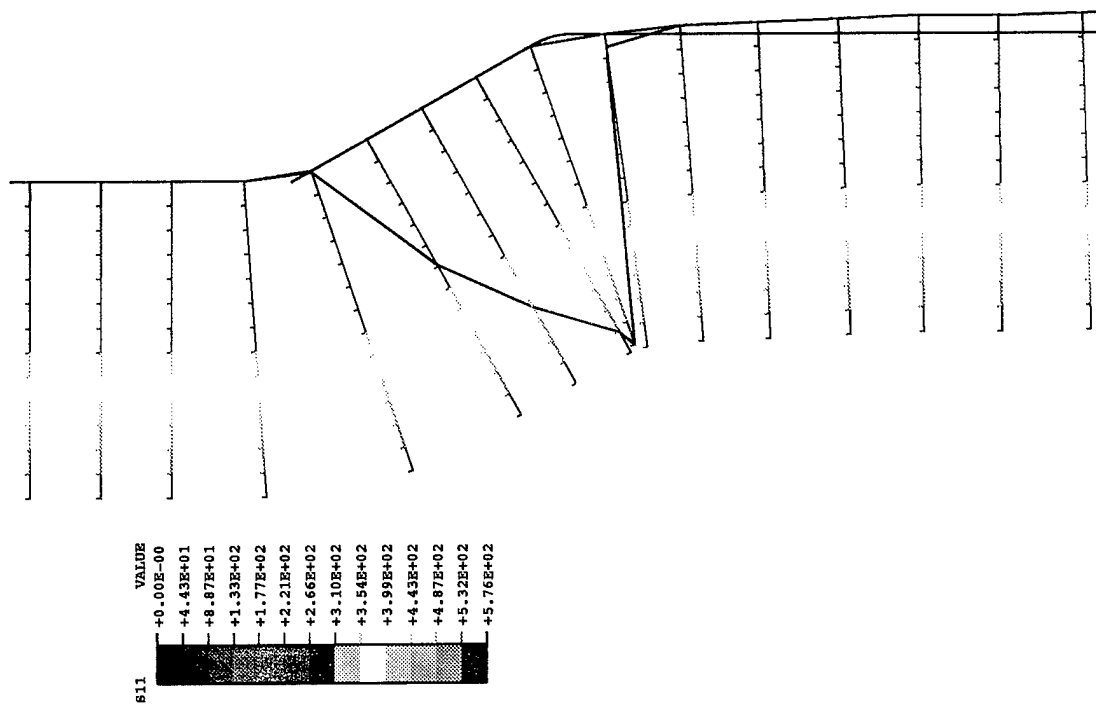
(b) Ten percent friction.

Figure 5-11 Continued.
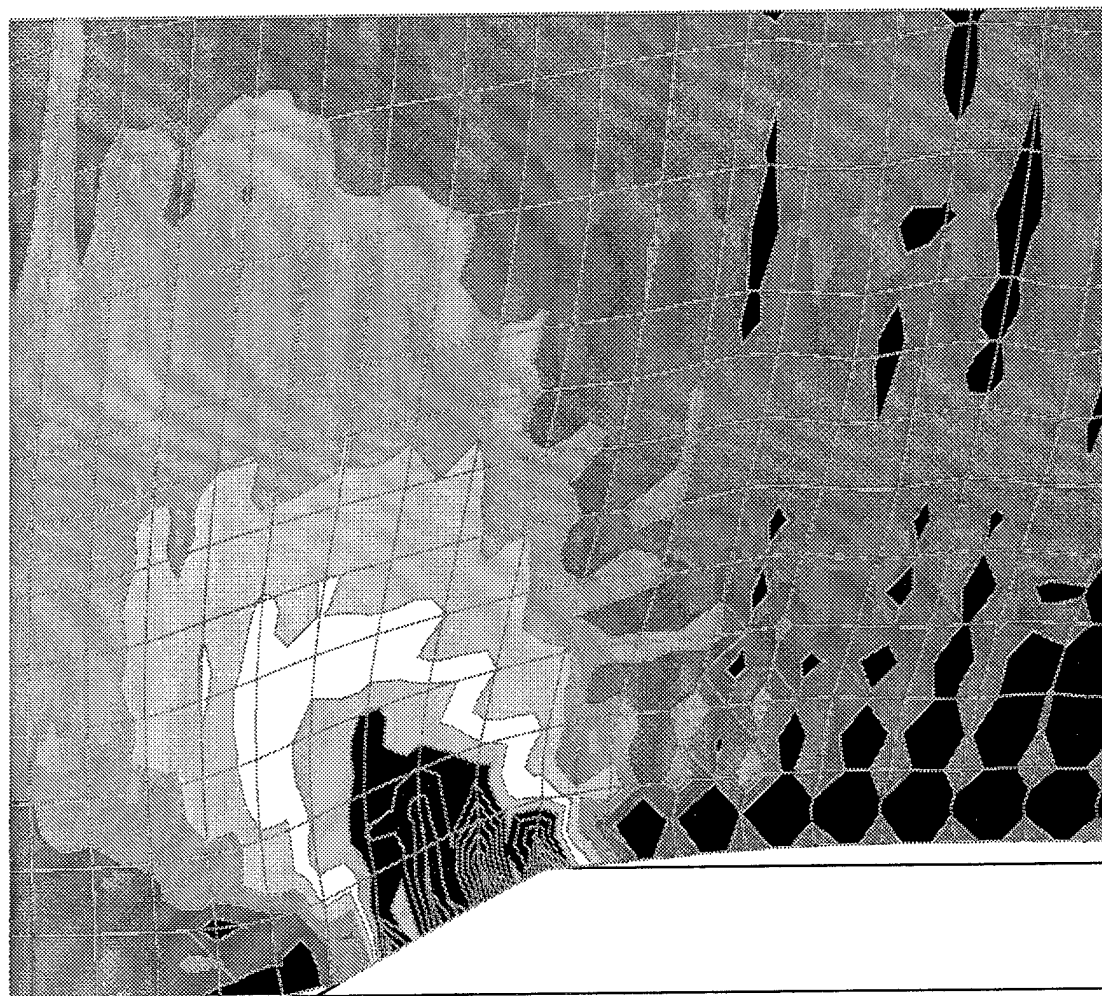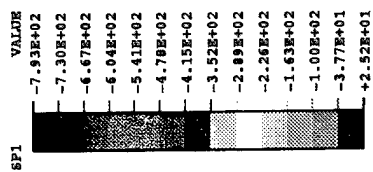
(a) Minimum principal stress SP1 distribution near plow tip with 5 percent friction.

Figure 5-12. Principal stress components in soil at 10 fps steady-state plow velocity with blade friction.

SP1   VALUE
-7.93E+02
-7.30E+02
-6.67E+02
-6.04E+02
-5.41E+02
-4.78E+02
-4.15E+02
-3.52E+02
-2.89E+02
-2.26E+02
-1.63E+02
-1.00E+02
-3.77E+01
+2.52E+01

118

SP3	VALUE
	-4.80E+02
	-4.36E+02
	-3.92E+02
	-3.49E+02
	-3.05E+02
	-2.61E+02
	-2.18E+02
	-1.74E+02
	-1.30E+02
	-8.72E+01
	-4.36E+01
	+2.61E-03
	+4.36E+01
	+8.72E+01
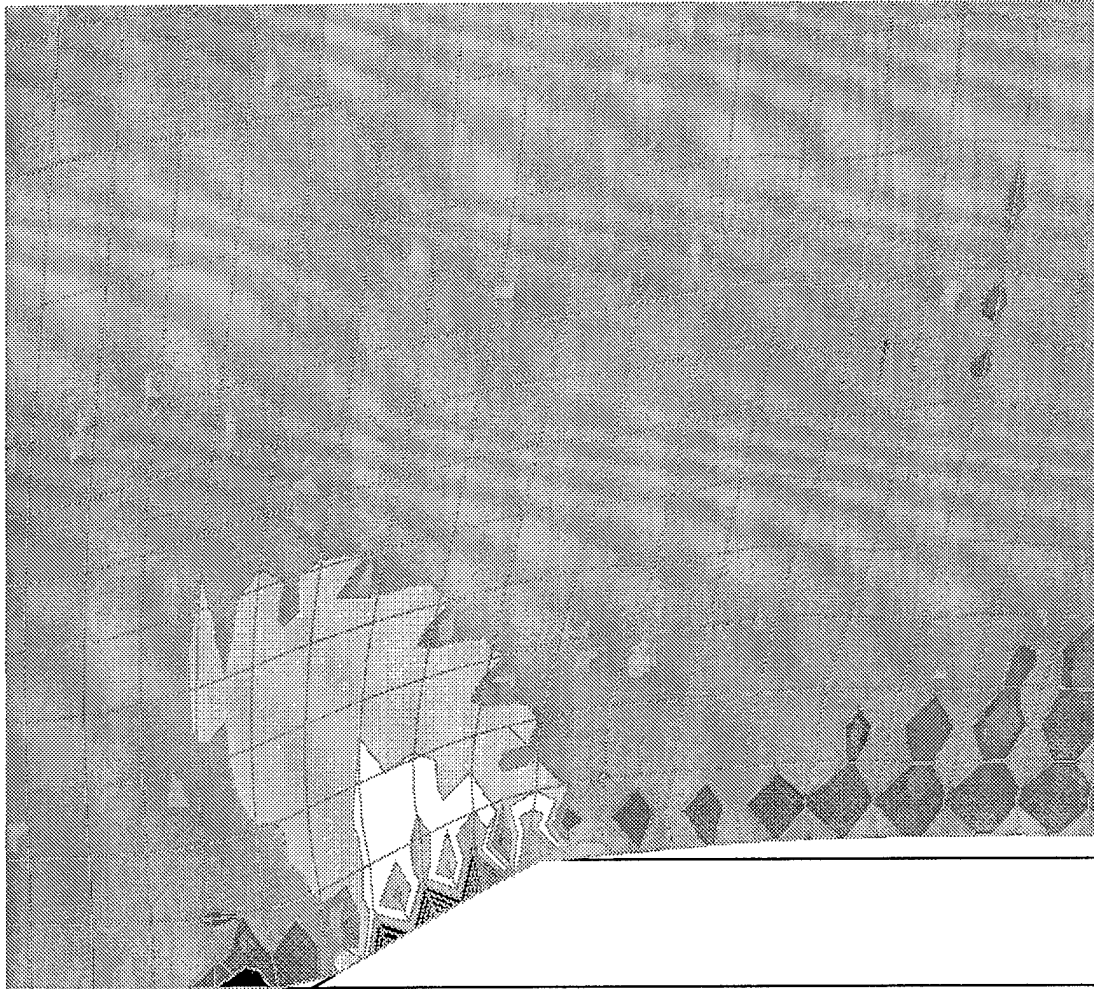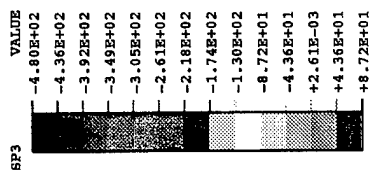
(b) Maximum principal stress SP3 distribution near plow tip with 5 percent friction.

Figure 5-12 Continued.
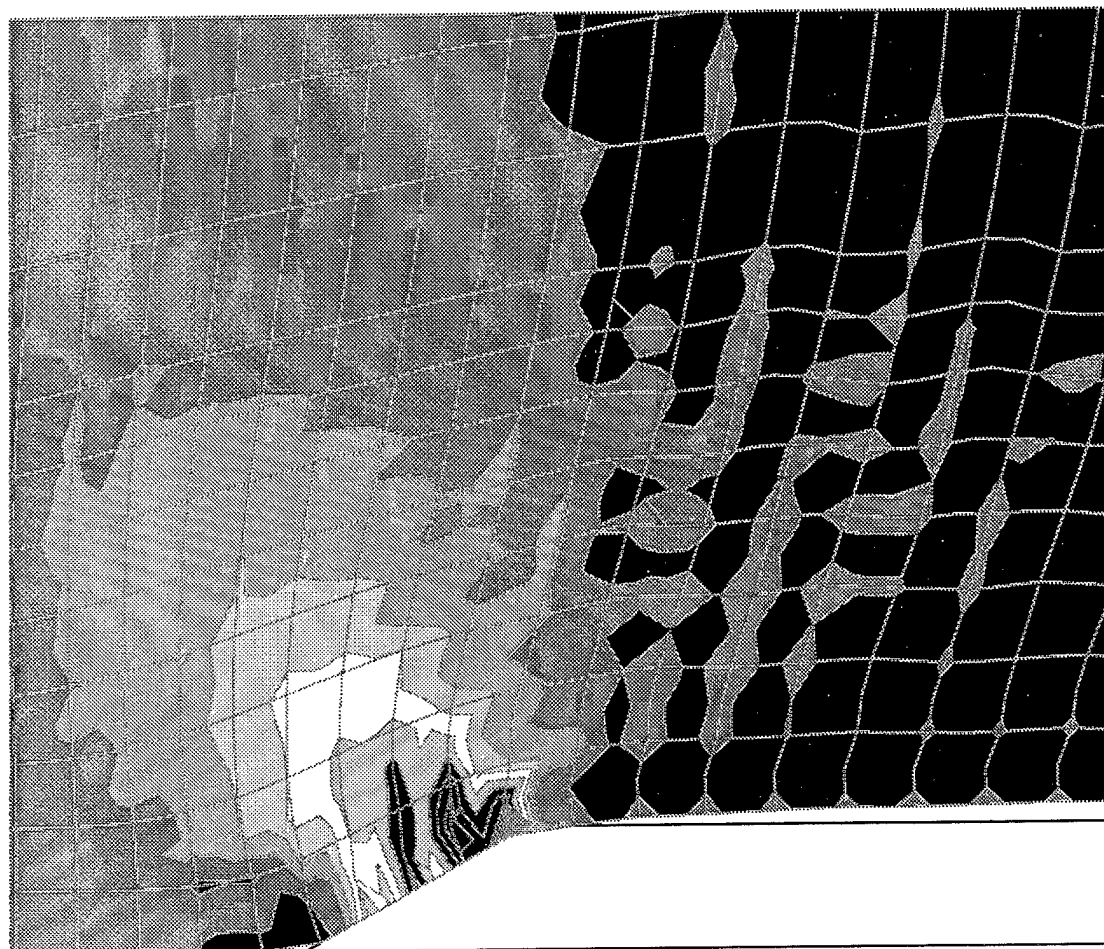
(c) Minimum principal stress SP1 distribution near plow tip with 10 percent friction.

Figure 5-12 Continued.
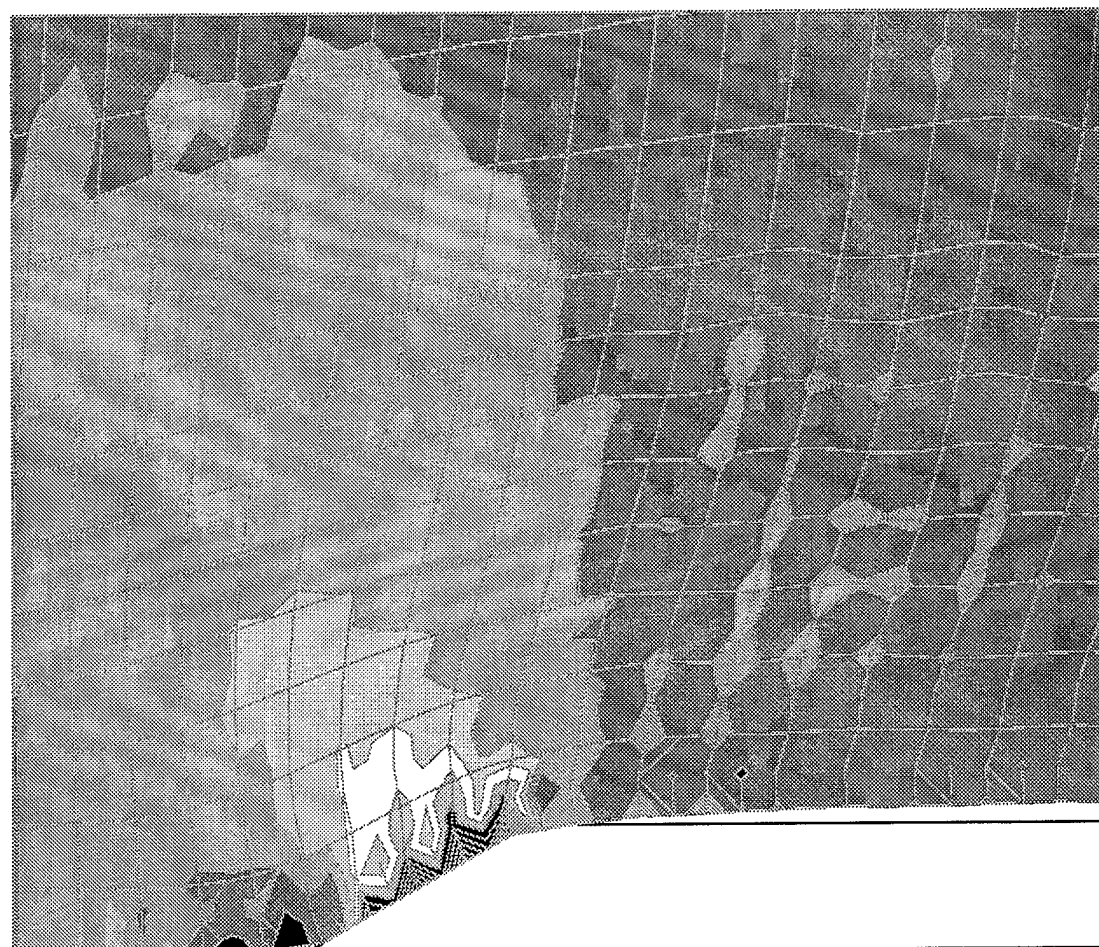
(d) Maximum principal stress SP3 distribution near plow tip with 10 percent friction.

Figure 5-12 Continued.
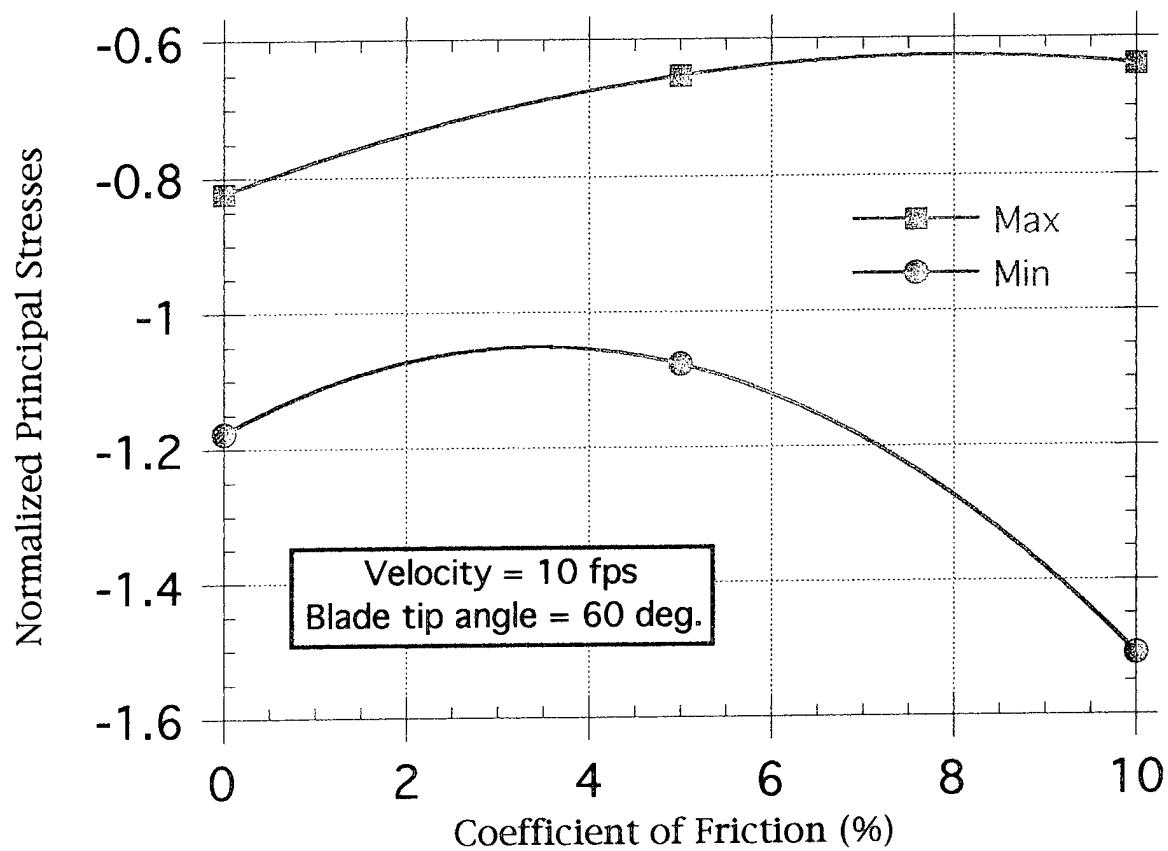
Figure 5-13. Effect of blade friction on principal stresses in soil.
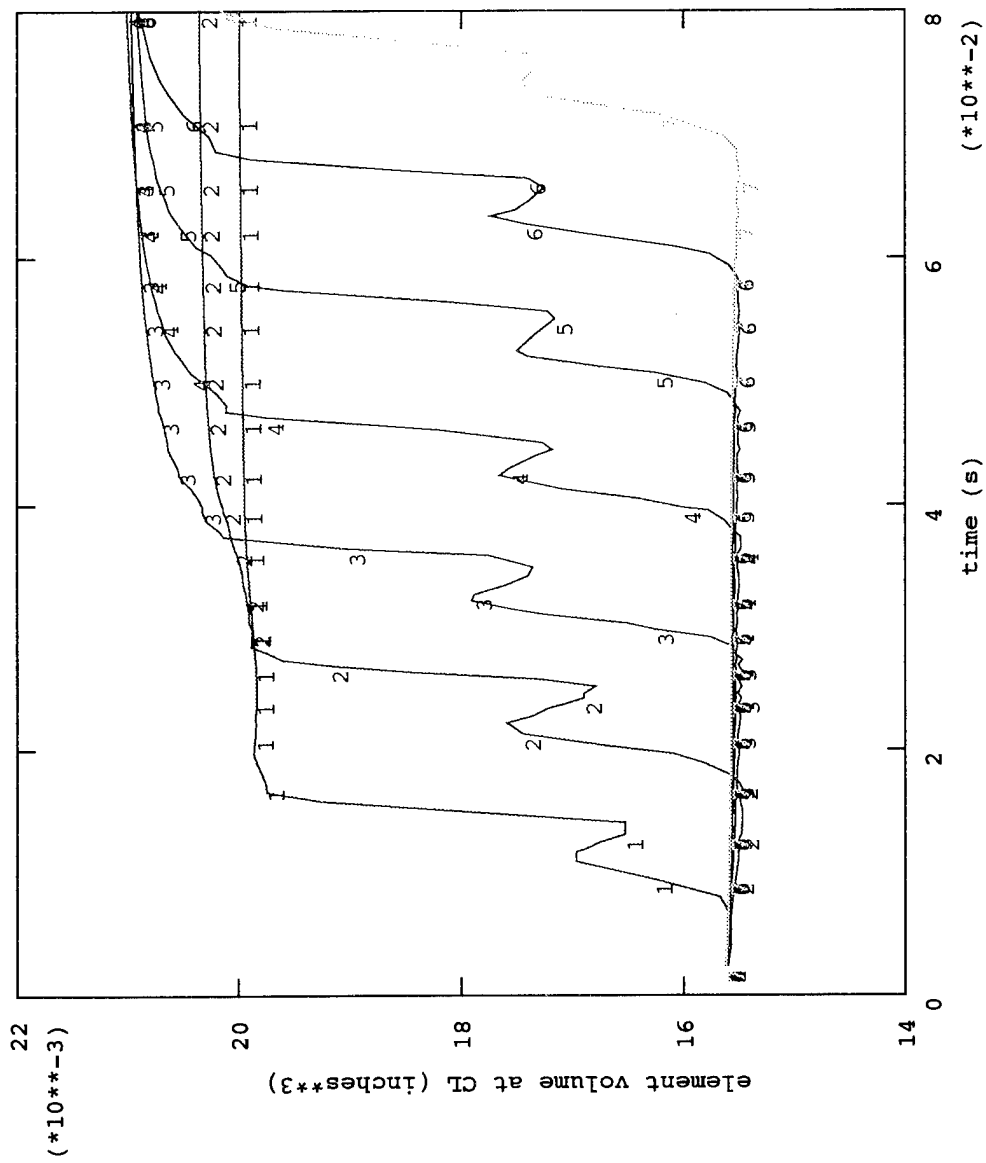
(a) Five percent friction.

Figure 5-14. Element volume change histories at 10 fps steady-state plow velocity with blade friction.
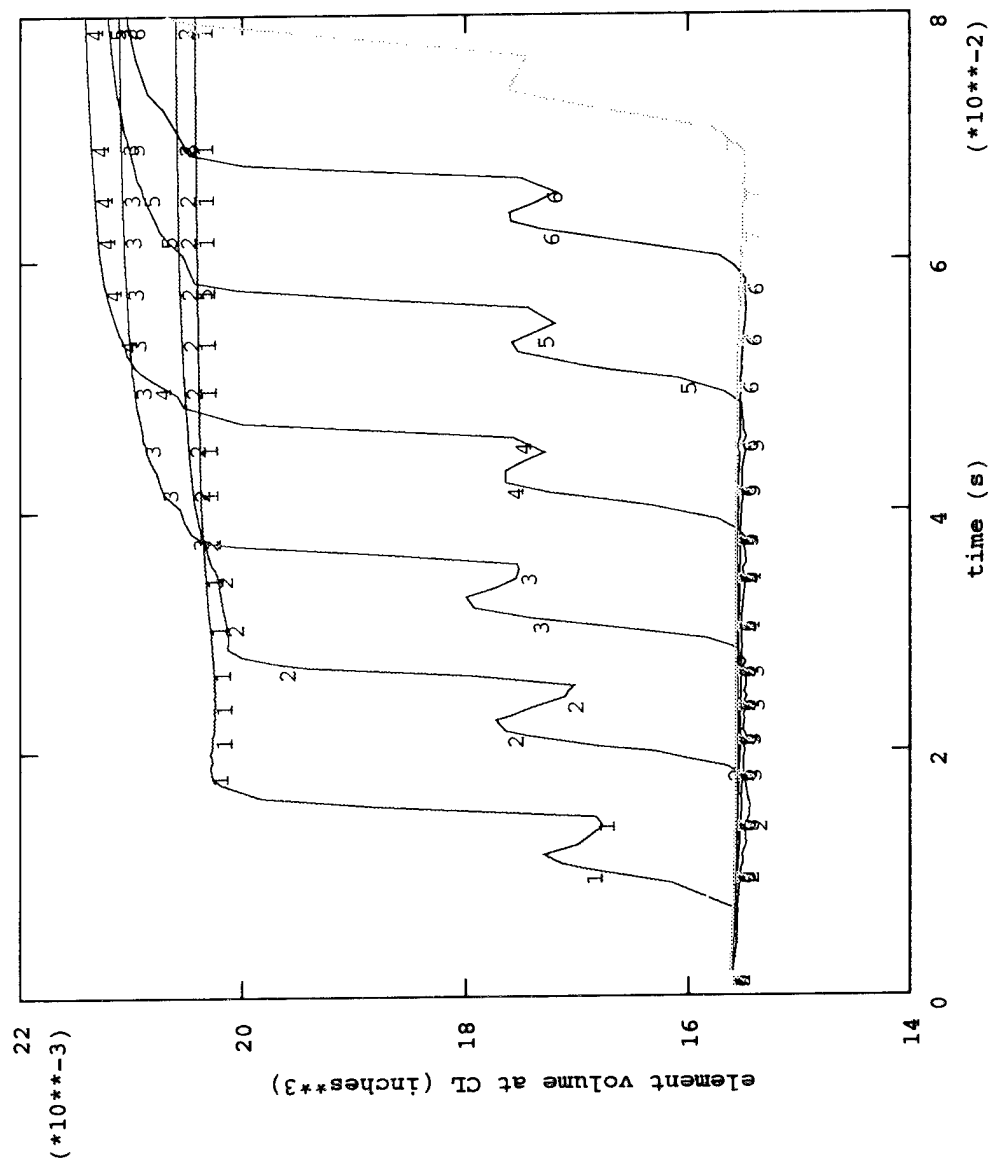
(b) Ten percent friction.

Figure 5-14 Continued.
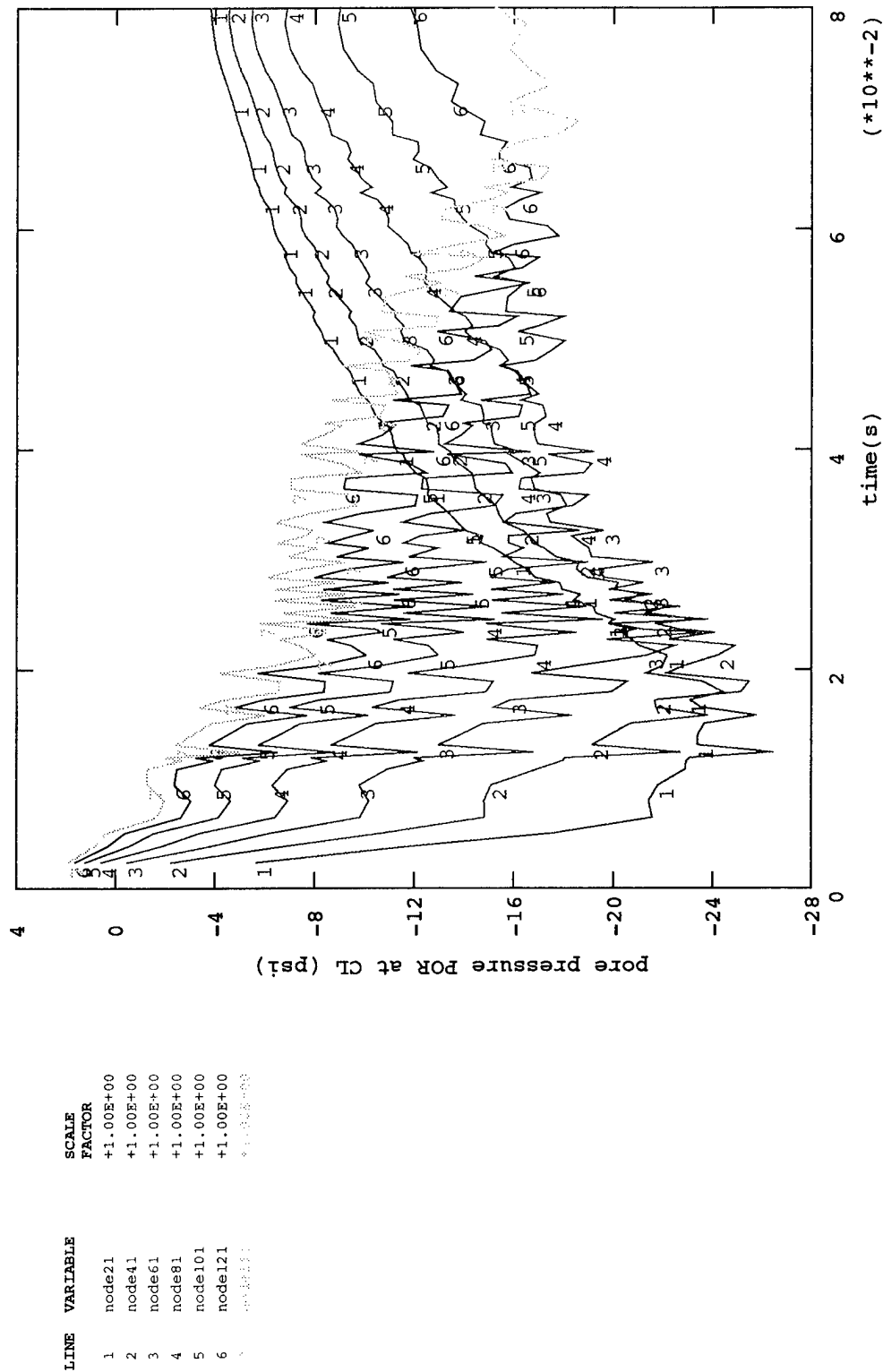
(a) Pore pressure histories at sampled response points along path of plow with 5 percent friction.

Figure 5-15. Pore pressure in soil at 10 fps steady-state plow velocity with blade friction.
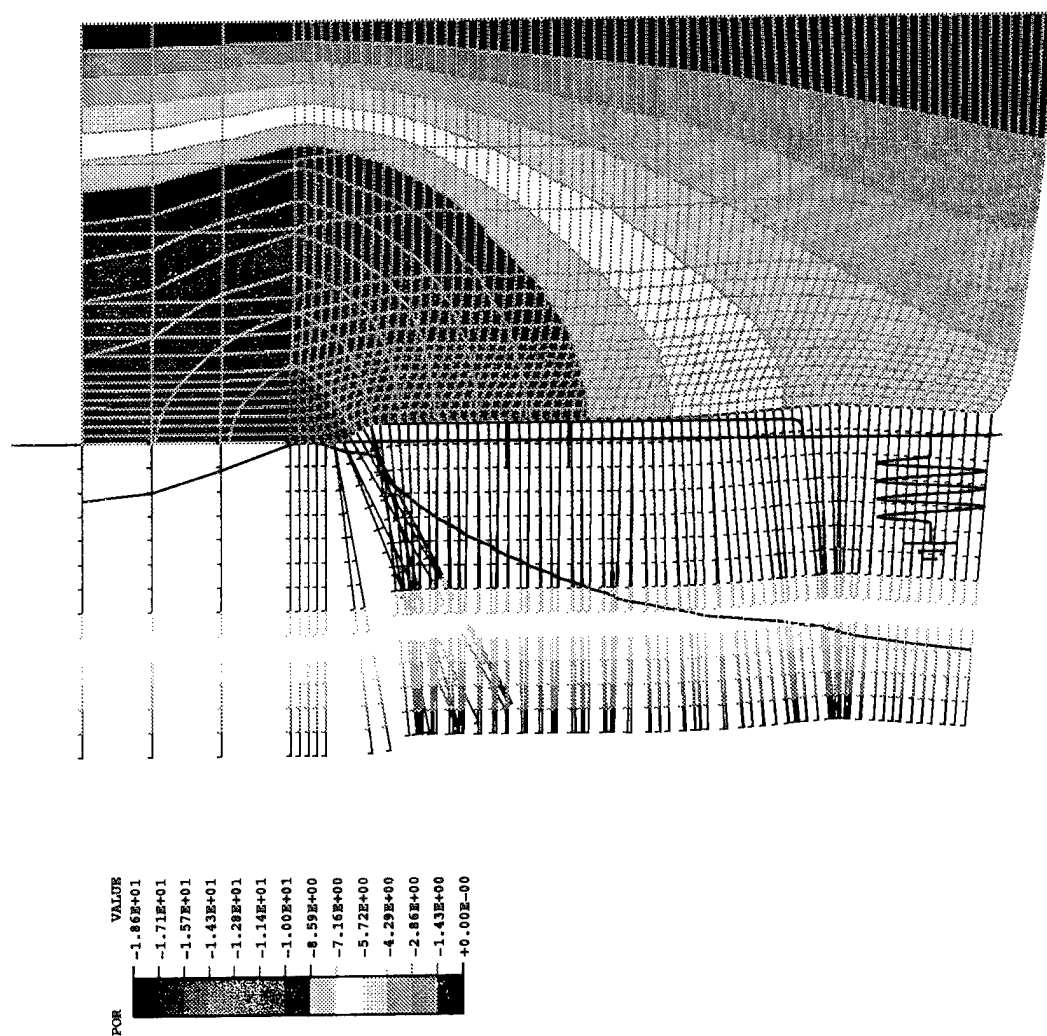
(b) Pore pressure distribution in soil surrounding plow with 5 percent friction.

Figure 5-15 Continued.
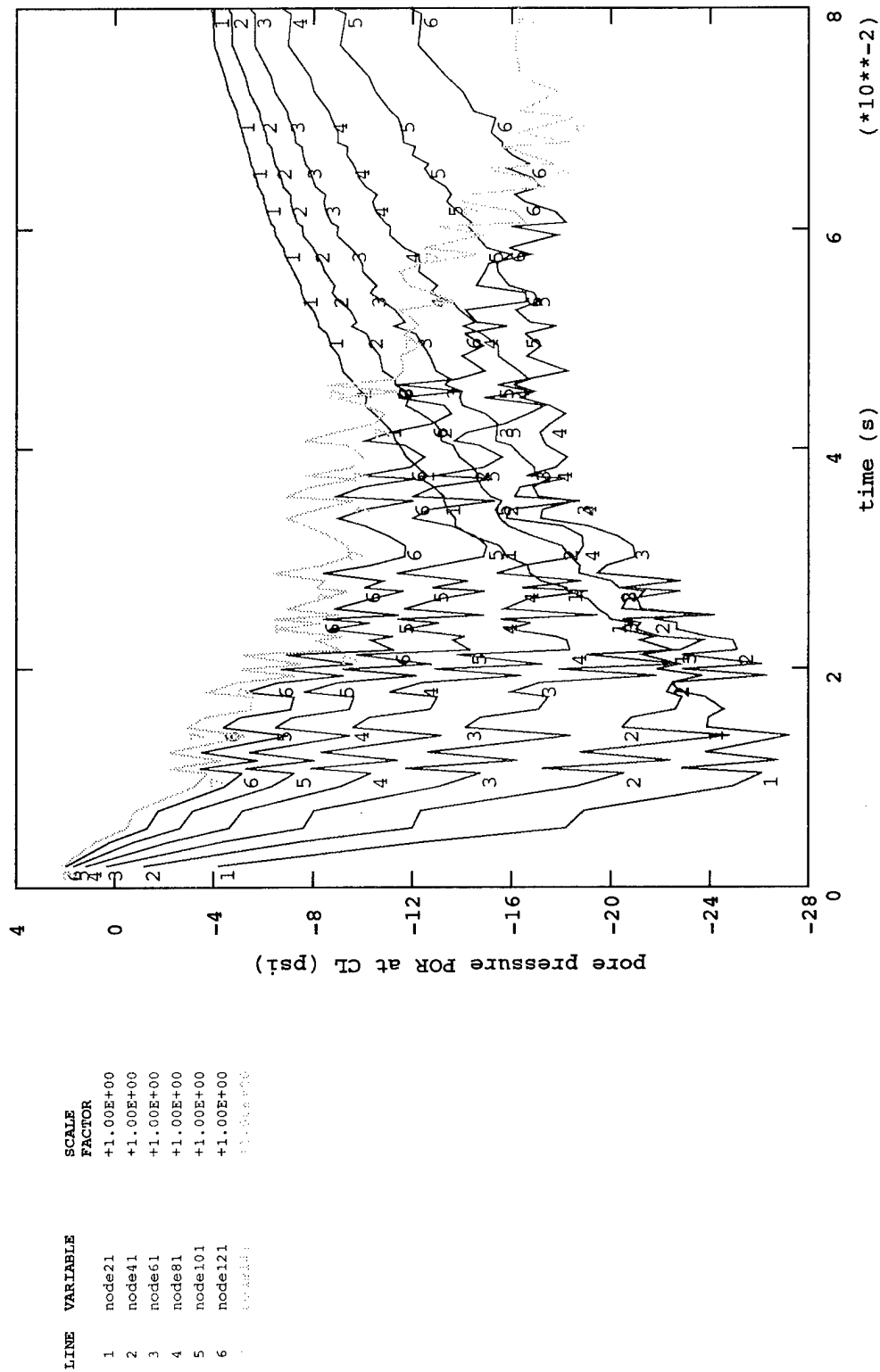
(c) Pore pressure histories at sampled response points along path of plow with 10 percent friction.

Figure 5-15 Continued.
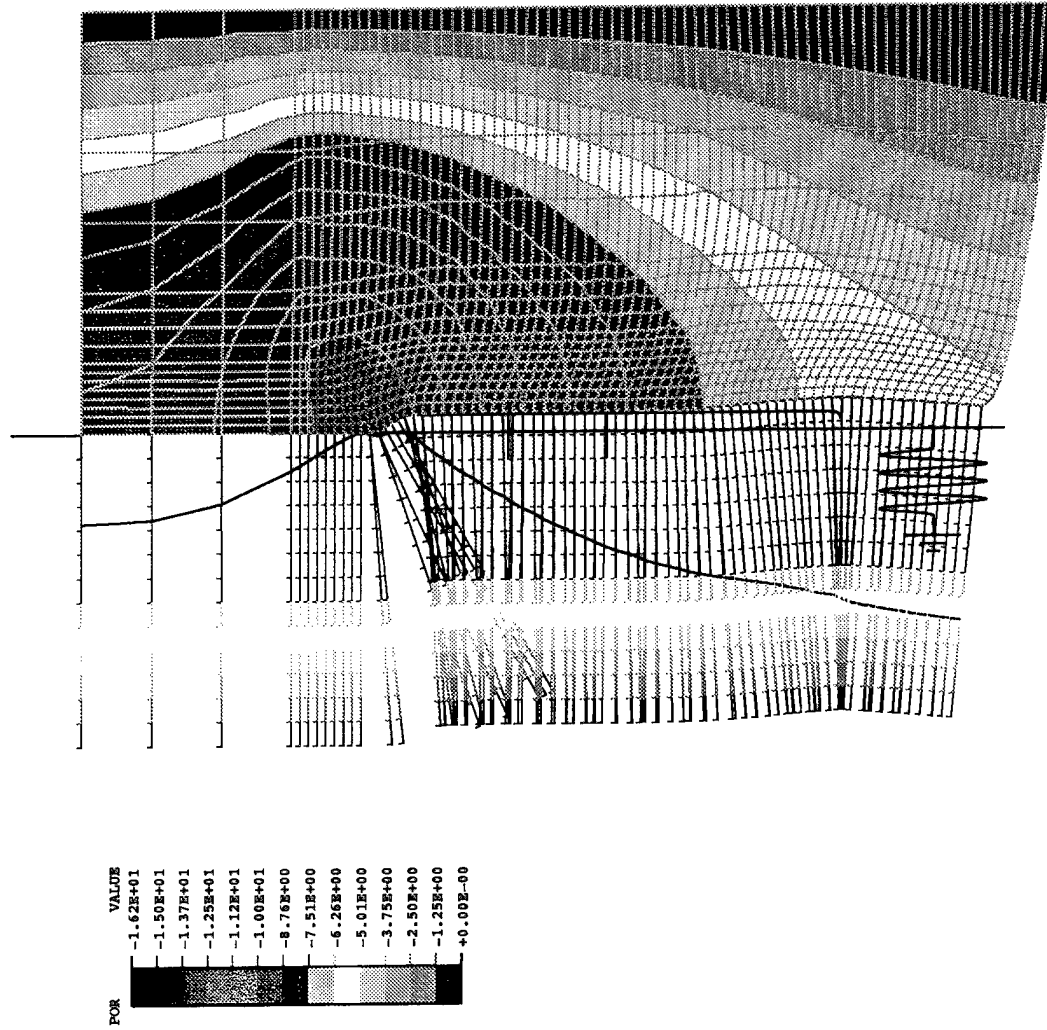
(d) Pore pressure distribution in soil surrounding plow with 10 percent friction.

Figure 5-15 Continued.

128
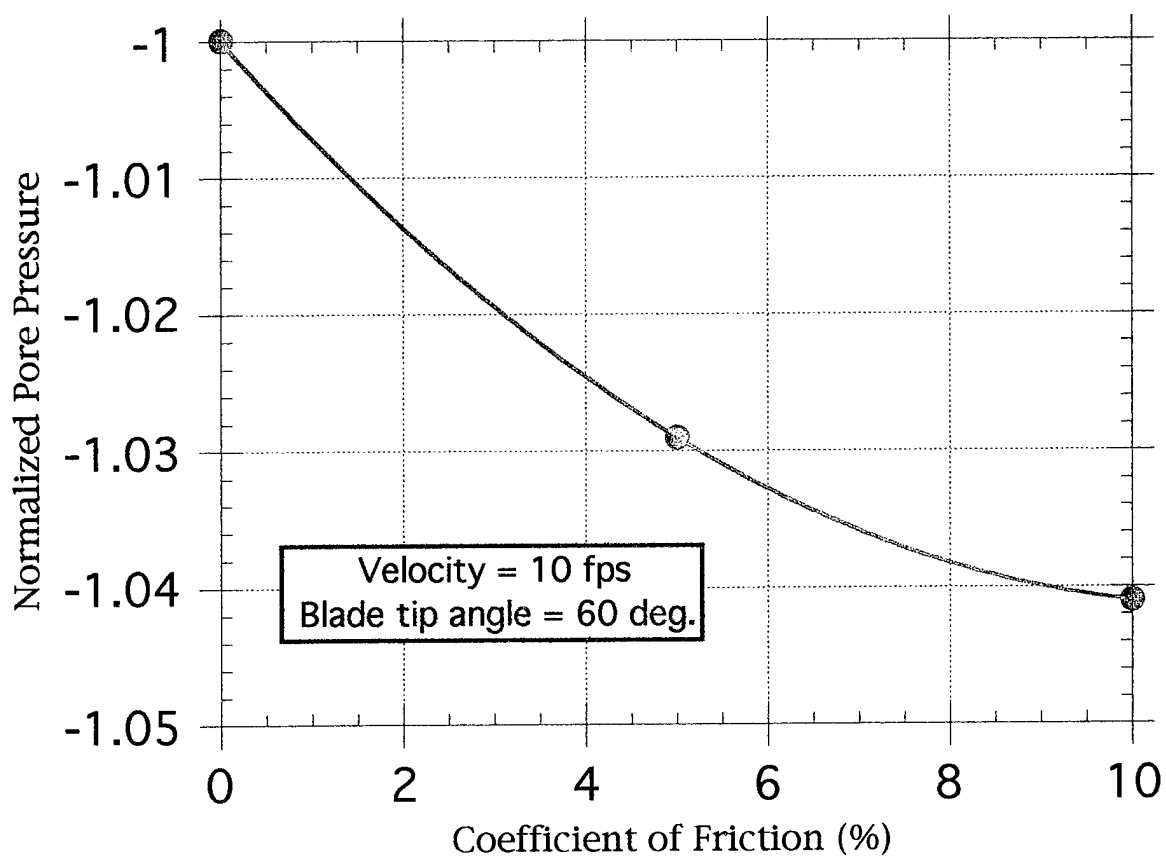
Figure 5-16. Effect of blade friction on minimum pore pressure.

In the parameter study the effect of the geometry of the blade tip is studied by exercising the plow/soil interaction model for three cases; a sharp tip, a conventional or standard tip, and a dull tip, defined by included tip angles of 30, 60, and 90 degrees, respectively. The standard frictionless blade with the 60 degree included tip angle (Figure 1-1b), moving at 10 fps is the baseline case.

5.3.1 Plow Forces. Unit plow force histories for sharp and dull frictionless blades moving at 10 fps are shown in Figure 5-17. Steady-state plow forces are clearly very different from those for the baseline case (Figure 5-1), where the tow and lateral force components were in fact nearly equal. The tow force for the sharp blade, shown in Figure 5-17a, is significantly lower, while the lateral force is only somewhat lower than in the baseline case. The lateral force is about twice the tow force for the sharp blade case. The tow force for the dull blade, shown in Figure 5-17b, is significantly higher, while the lateral force is only somewhat higher than the baseline case. The lateral force is substantially less than the tow force for the dull blade case.

These data are summarized in Figure 5-18, where the tow and lateral forces, normalized on their (nearly equal) baseline values, are graphed against the blade tip included angle. The lateral force component is insensitive but the tow force component is very sensitive to blade tip angle. For the sharp blade, the tow force is reduced to approximately 45 percent of that for the standard blade. For the dull blade, the tow force is increased to approximately 70 percent of that for the standard blade. The blade tip included angle has a substantial influence on towing force while affecting the lateral force very little.

The distribution of lateral contact forces along the plow/soil sliding interface for the two-blade configurations is shown in Figure 5-19. As expected, contact forces, i.e., forces per unit length along the contact surface, vary nearly linearly from zero at the tip to a maximum at the shoulder of the blade. While the maximum contact forces for the two-blade configurations shown and for the baseline case (Figure 5-3) differ substantially, the areas beneath all three distributions, i.e., the total lateral contact forces, differ only modestly. Assuming a linear distribution, the areas under the three contact force distributions shown all agree within 7 percent with the steady-state lateral plow forces obtained from force history data. This is consistent with the above finding that the lateral component of the plow force is insensitive to blade tip angle (Figure 5-18). However, because the maximum lateral contact force increases substantially with blade tip angle (Figure 5-19), sharper blade tips would not sustain as much shoulder wear as duller blade tips.

5.3.2 Behavior of Principal Stresses in the Soil. Principal stress distributions in the soil for the sharp and dull blades are shown in Figure 5-20. In the neighborhood of the plow tip these effective stresses are compressive, and they are focused on the shoulder of the tip of the blade. As expected, sharper blades induce less stress in the soil than duller blades. These stresses, compared with those for the standard blade (Figure 5-4), shows that the minimum principal stress increases (becomes less compressive) by 48 percent for the sharp blade, and decreases (becomes more compressive) 64 percent for the dull blade. The variation of minimum principal stress is nearly linear with blade tip angle. The maximum principal stress increases 60 percent for the sharp blade, but only decreases 8 percent for the dull blade. The variation of maximum principal stress saturates, i.e., approaches a horizontal asymptote. This variation can be seen in Figure 5-21 where the two principal stress components are normalized on the average principal stress for the

130

standard blade (-735 psi), and graphed against blade tip angle. Saturation of maximum principal stress beyond an angle of 60 degrees causes a large increase in maximum shear stress (difference between curves) for the dull blade. This is compared with a modest 23 percent decrease in maximum shear stress for the sharp blade. At the same velocity, the dull blade tip would be far more effective in overcoming the shear strength of the soil and producing a trench but at the cost of a higher tow force (Figure 5-18).

5.3.3 Pore Pressure Behavior.

The shape of the blade tip has a pronounced effect on volumetric expansion of the dilatant soil along the path of the plow as shown in Figure 5-22. Comparing the residual volumetric expansions for the sharp and dull blades in Figures 5-22a and b, respectively, with the residual volumetric expansion for the baseline case (Figure 5-6), shows noticeably less expansion occurring with the sharp blade and noticeably more expansion occurring for the dull blade. Thus, while friction may have had a small influence, blade tip shape has a significant influence on residual volumetric expansion of soil in the path of the plow.

Correspondingly, the pore pressure histories and pore pressure contours would be expected to vary significantly with the shape of the blade, and these data are shown in Figure 5-23. The significant pore pressure is the minimum steady-state value shown in the history data, and also shown as a pressure trough engulfing the blade tip in the contour data (history data are somewhat more accurate). The variation of minimum pore pressure with blade tip angle is shown in Figure 5-24 where pressures have been normalized on the minimum value for the baseline case (-17 psi). Thus a 30 degree blade tip angle will increase the minimum pore pressure by approximately 30 percent, and a 90 degree blade tip angle will decrease the minimum pore pressure approximately 18 percent.

131
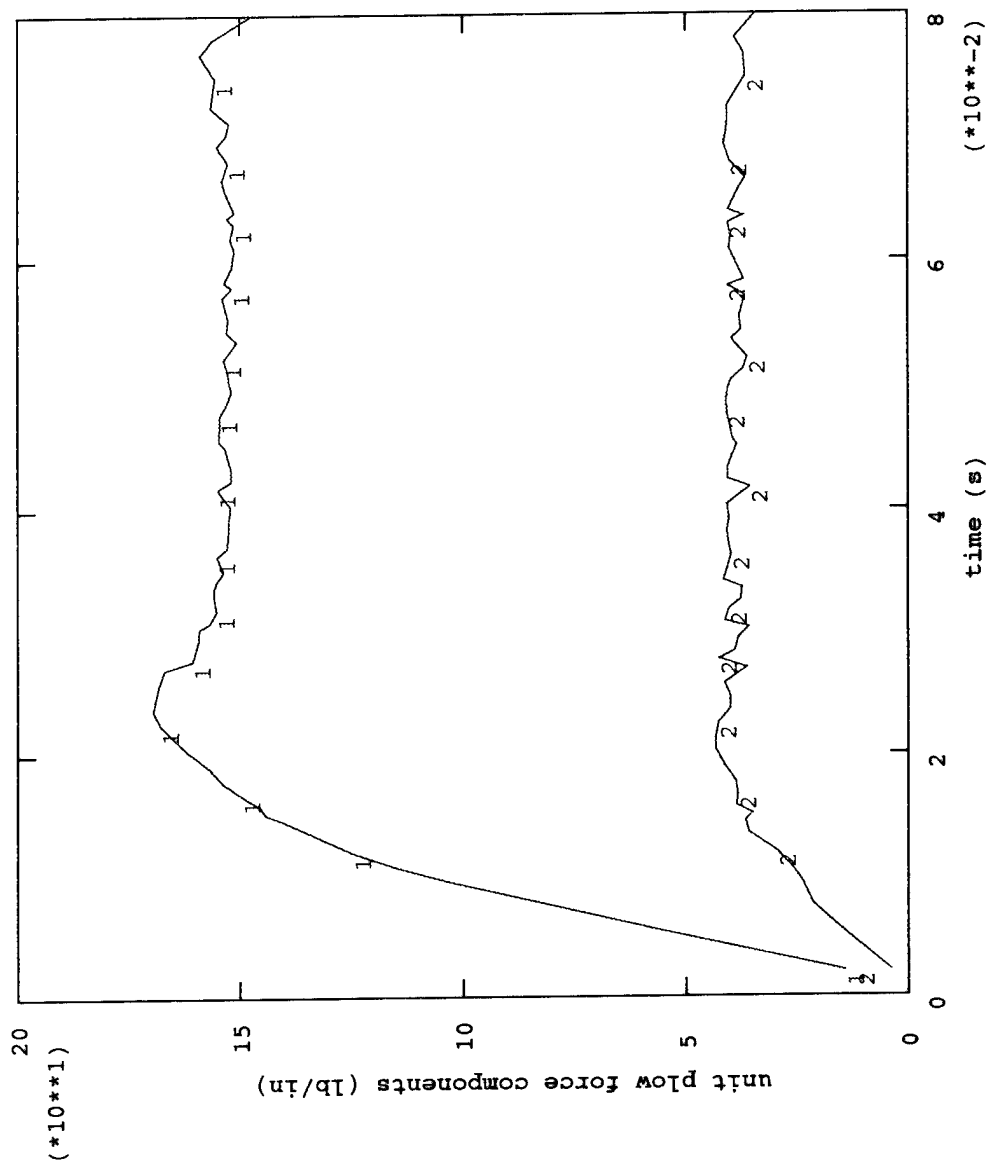
(a) Lateral and tow (half) force components per unit depth of blade with sharp tip.

Figure 5-17. Unit plow force histories at 10 fps steady state plow velocity with sharp and dull blades.
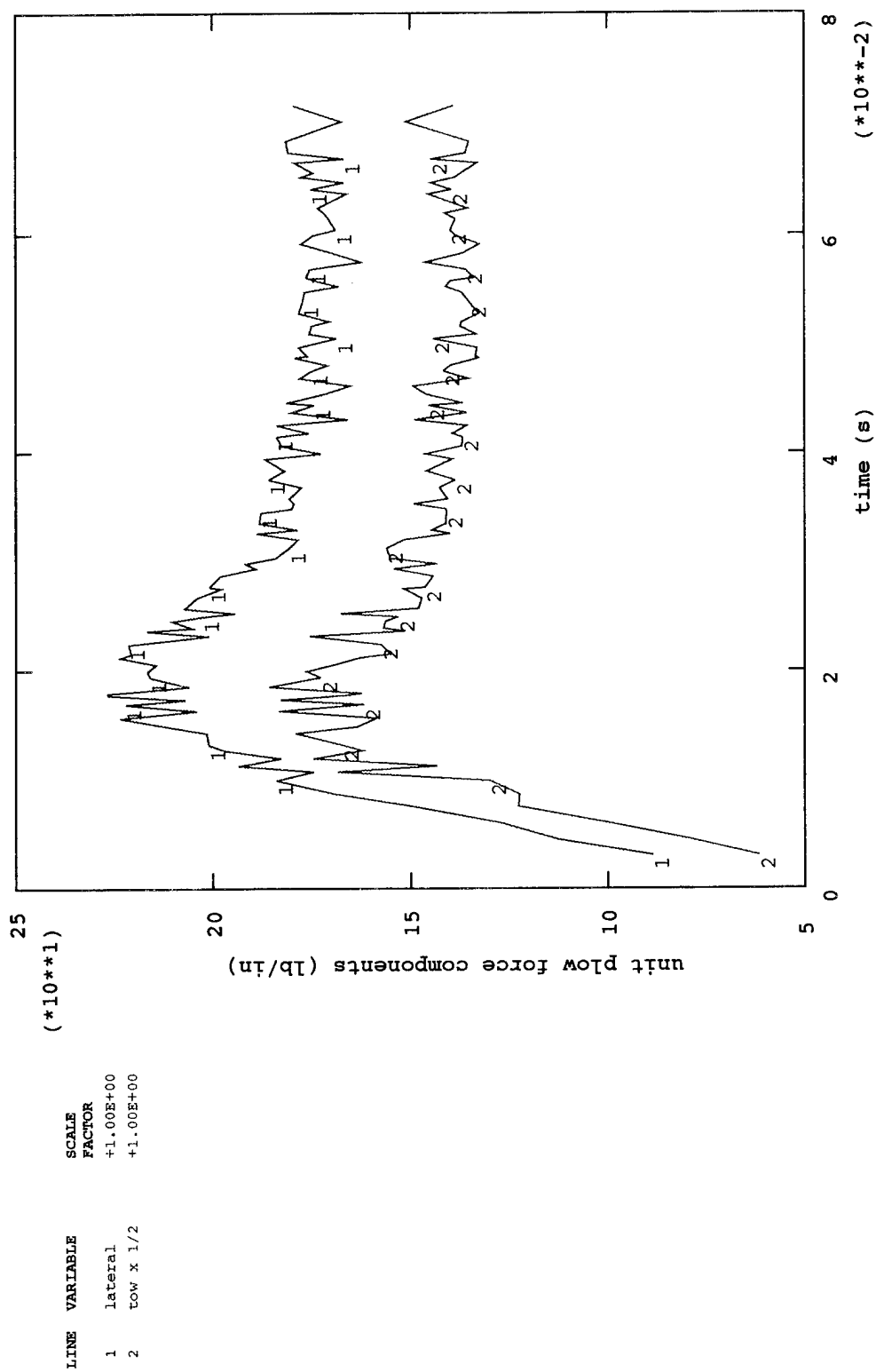
(b) Lateral and tow (half) force components per unit depth of blade with dull tip.

Figure 5-17 Continued.

133
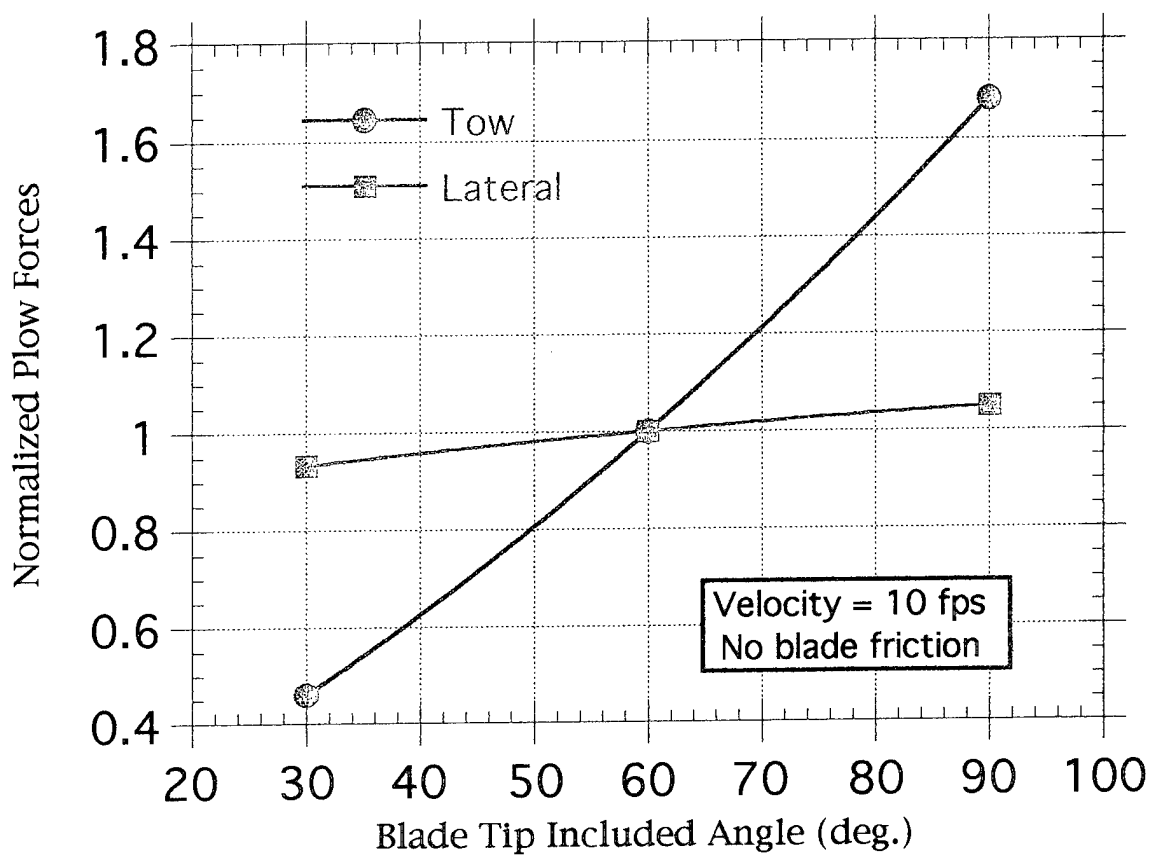
Figure 5-18. Effect of blade tip angle on steady-state plow forces.
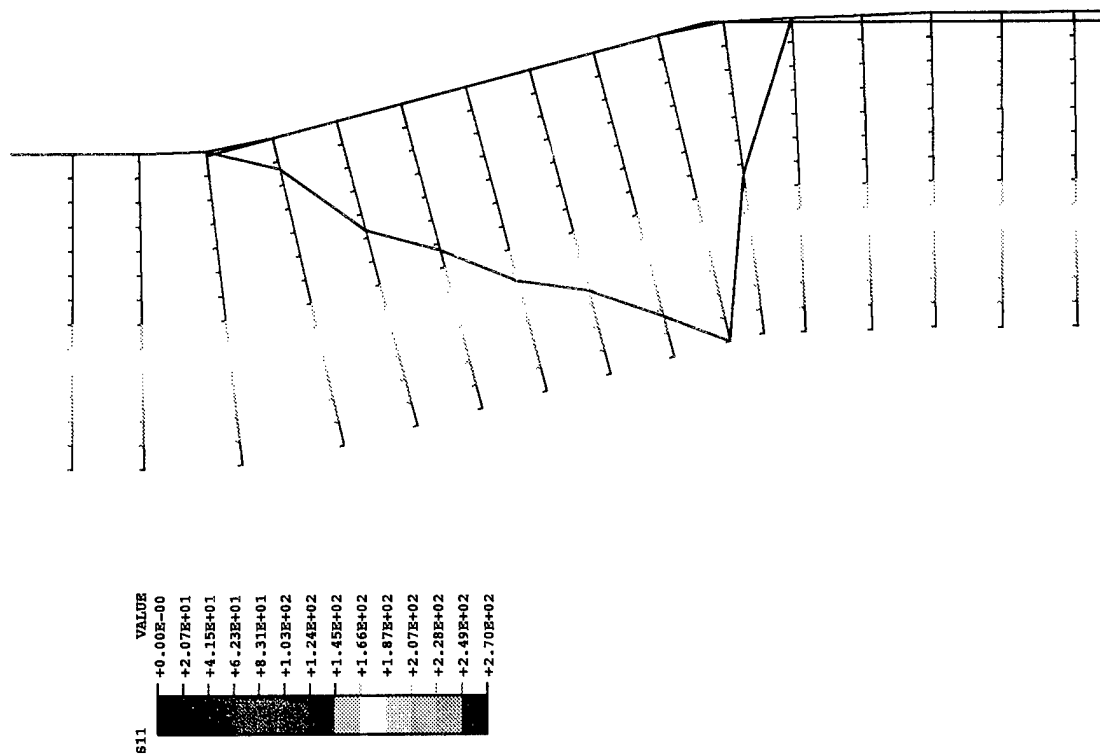
(a) Sharp blade.

Figure 5-19. Distribution of lateral interface contact forces on plow at 10 fps steady-state plow velocity with sharp and dull blades.
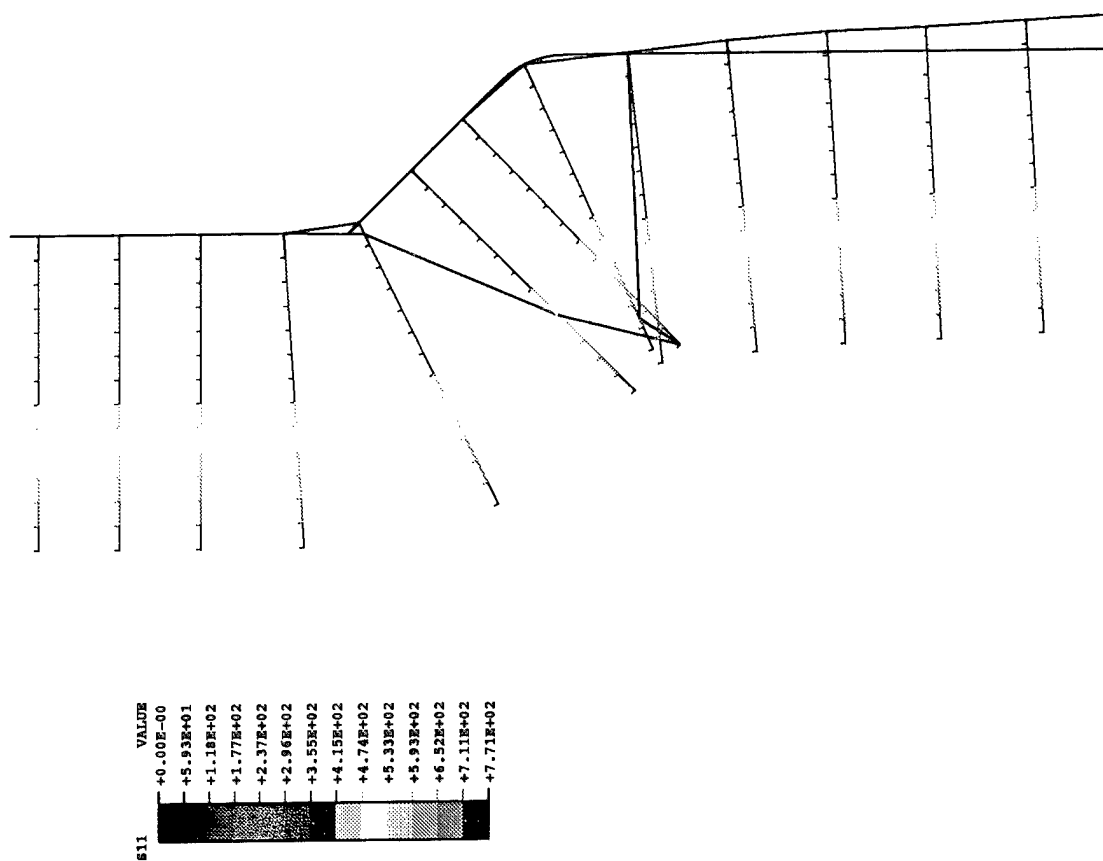
(b) Dull blade.

Figure 5-19 Continued.

136

SP1   VALUE
       -4.47E+02
       -4.12E+02
       -3.76E+02
       -3.41E+02
       -3.06E+02
       -2.71E+02
       -2.35E+02
       -2.00E+02
       -1.65E+02
       -1.30E+02
       -9.49E+01
       -5.96E+01
       -2.44E+01
       +1.08E+01
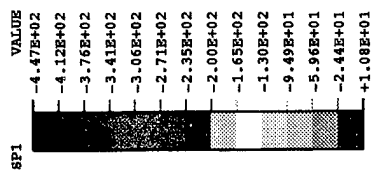
(a) Minimum principal stress SP1 distribution near sharp tip.

Figure 5-20. Principal stress components in soil at 10 fps steady-state plow velocity with sharp and dull blades.

137
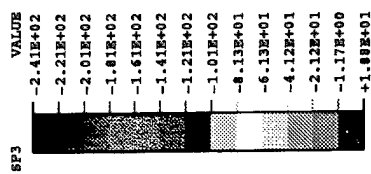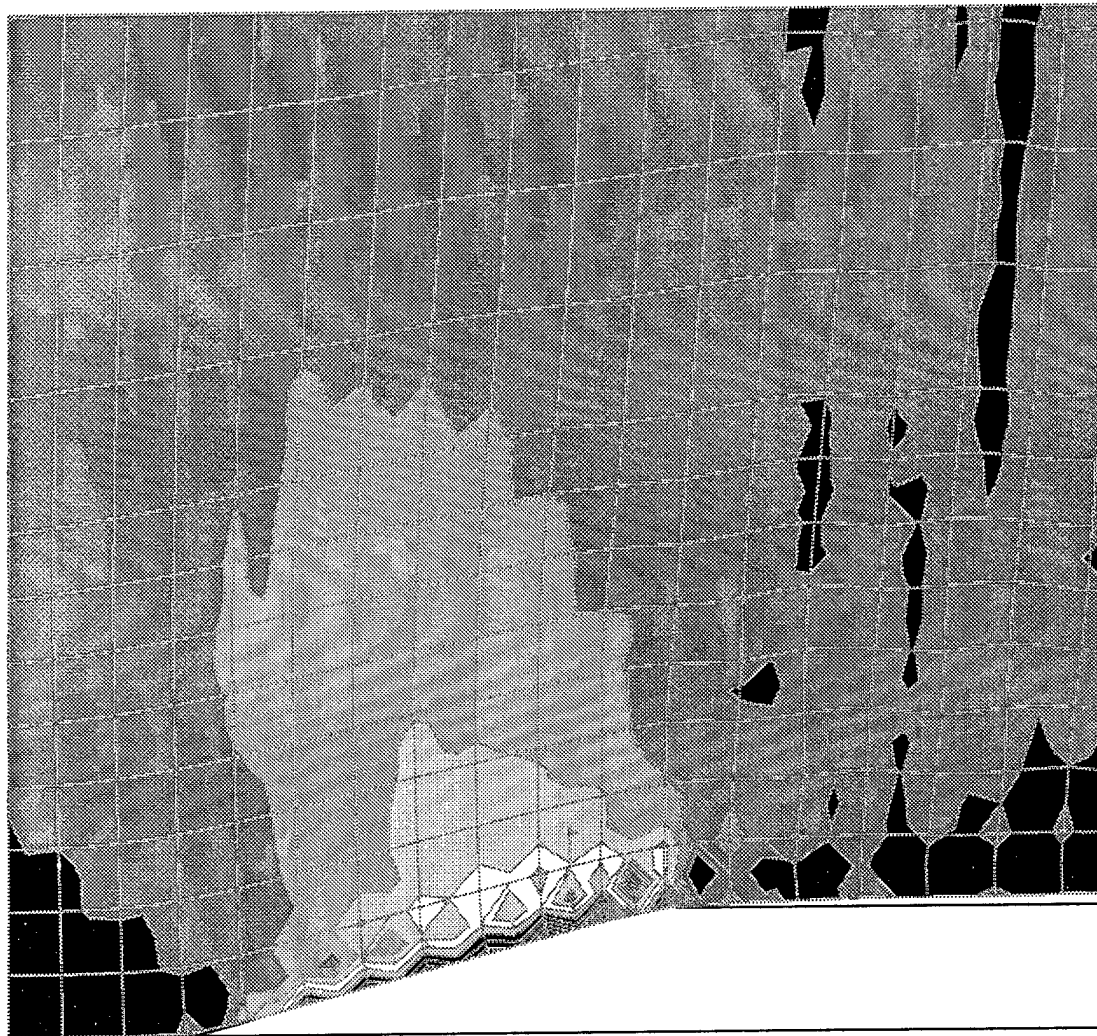
(b) Maximum principal stress SP3 distribution near sharp tip.

Figure 5-20 Continued.
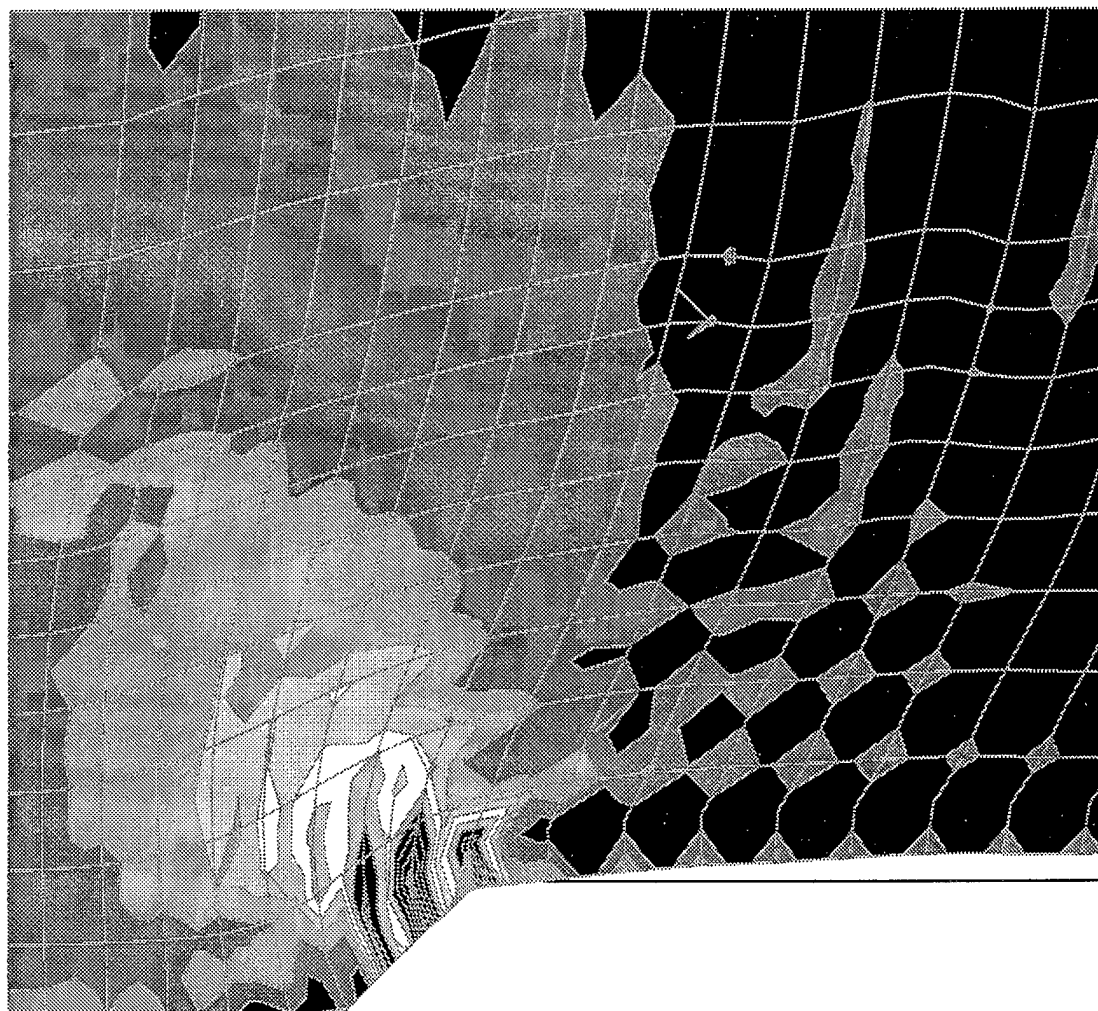
(c) Minimum principal stress SP1 distribution near dull tip.

Figure 5-20 Continued.
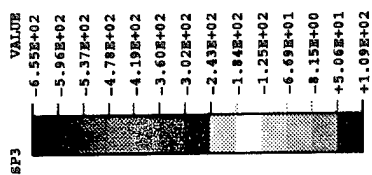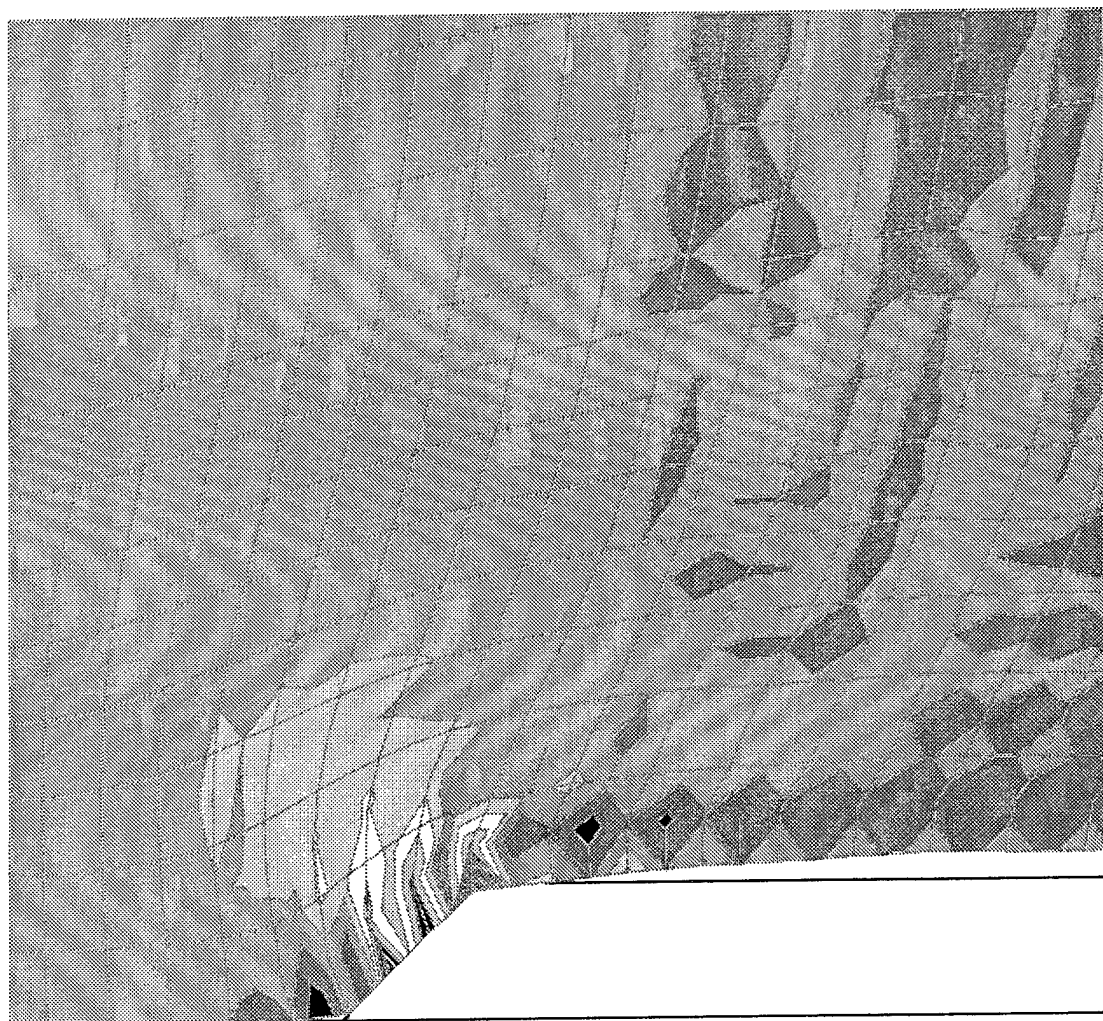
(d) Maximum principal stress SP3 distribution near dull tip.

Figure 5-20 Continued.
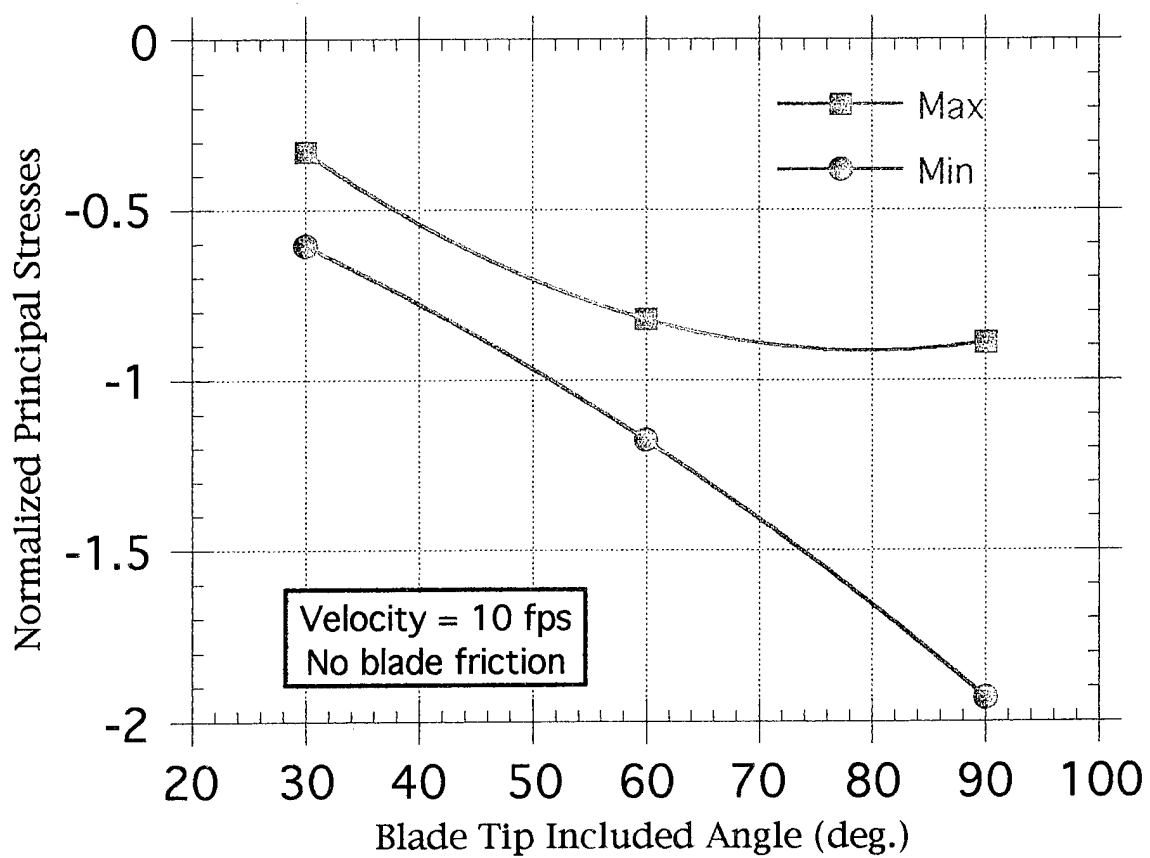
Figure 5-21. Effect of blade tip angle on principal stresses in soil.
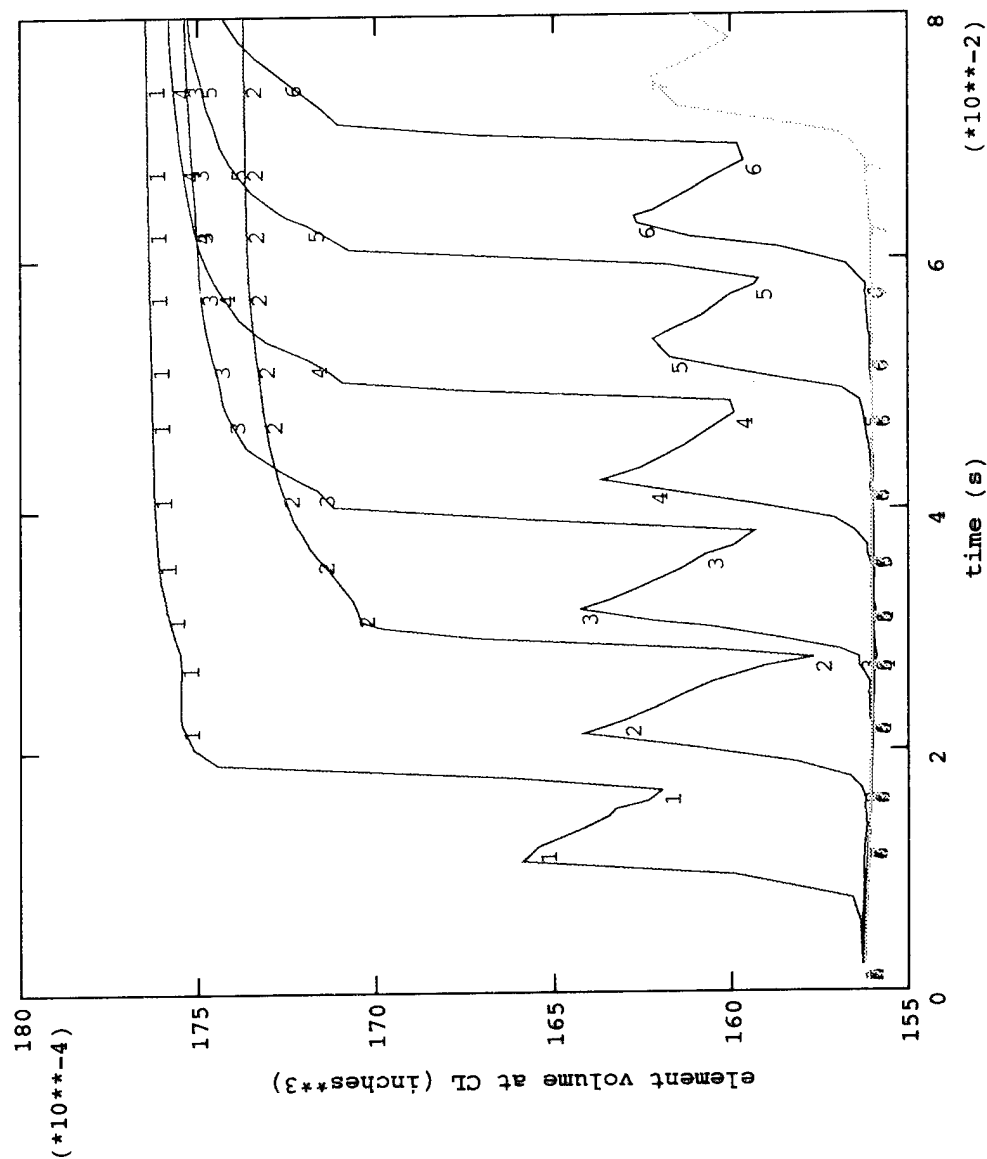
(a) Sharp blade.

Figure 5-22. Element volume change histories at 10 fps steady-state plow velocity with sharp and dull blades.

142
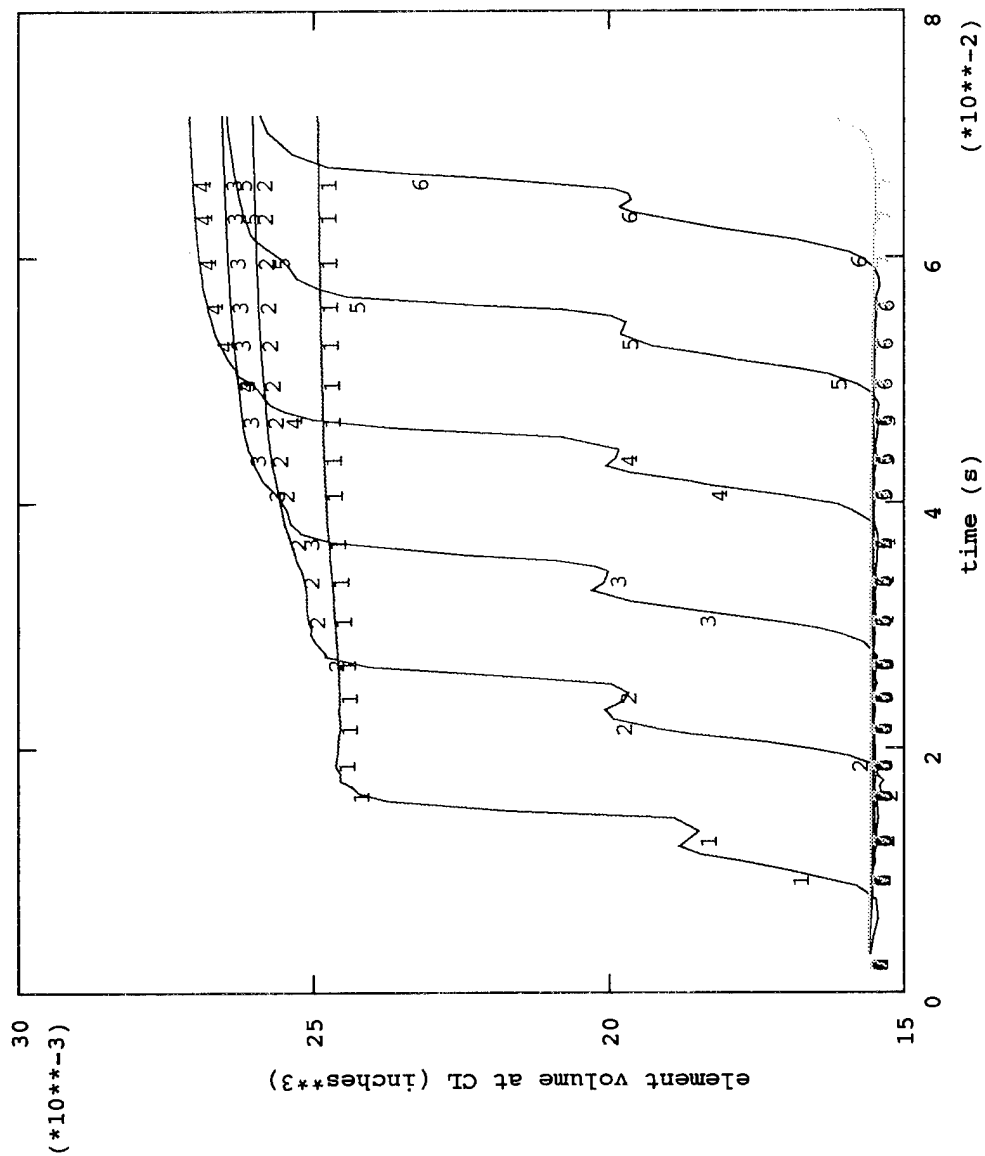
(b) Dull blade.

Figure 5-22 Continued.
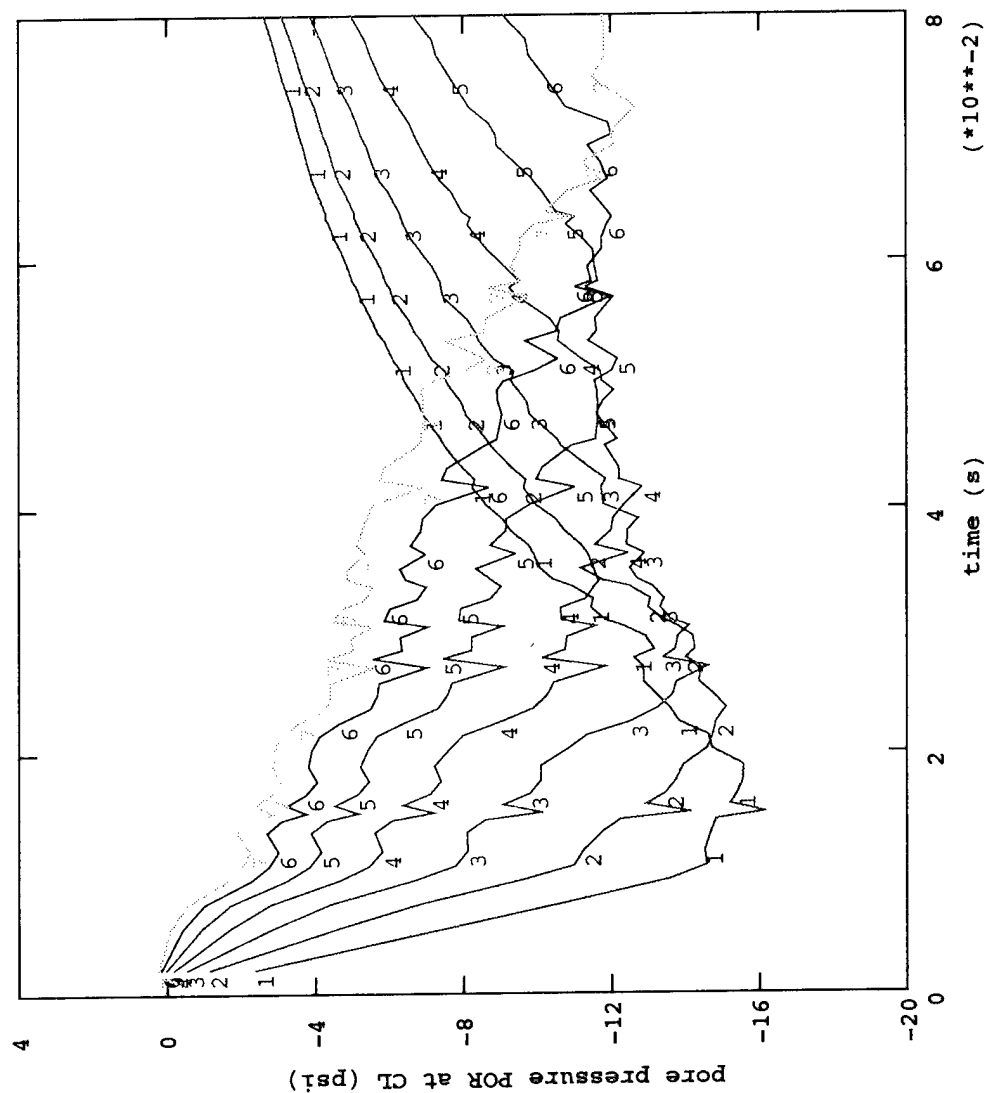
143

(a) Pore pressure histories at sampled response points along path of plow with sharp blade.

Figure 5-23. Pore pressure in soil at 10 fps steady-state plow velocity with sharp and dull blades.
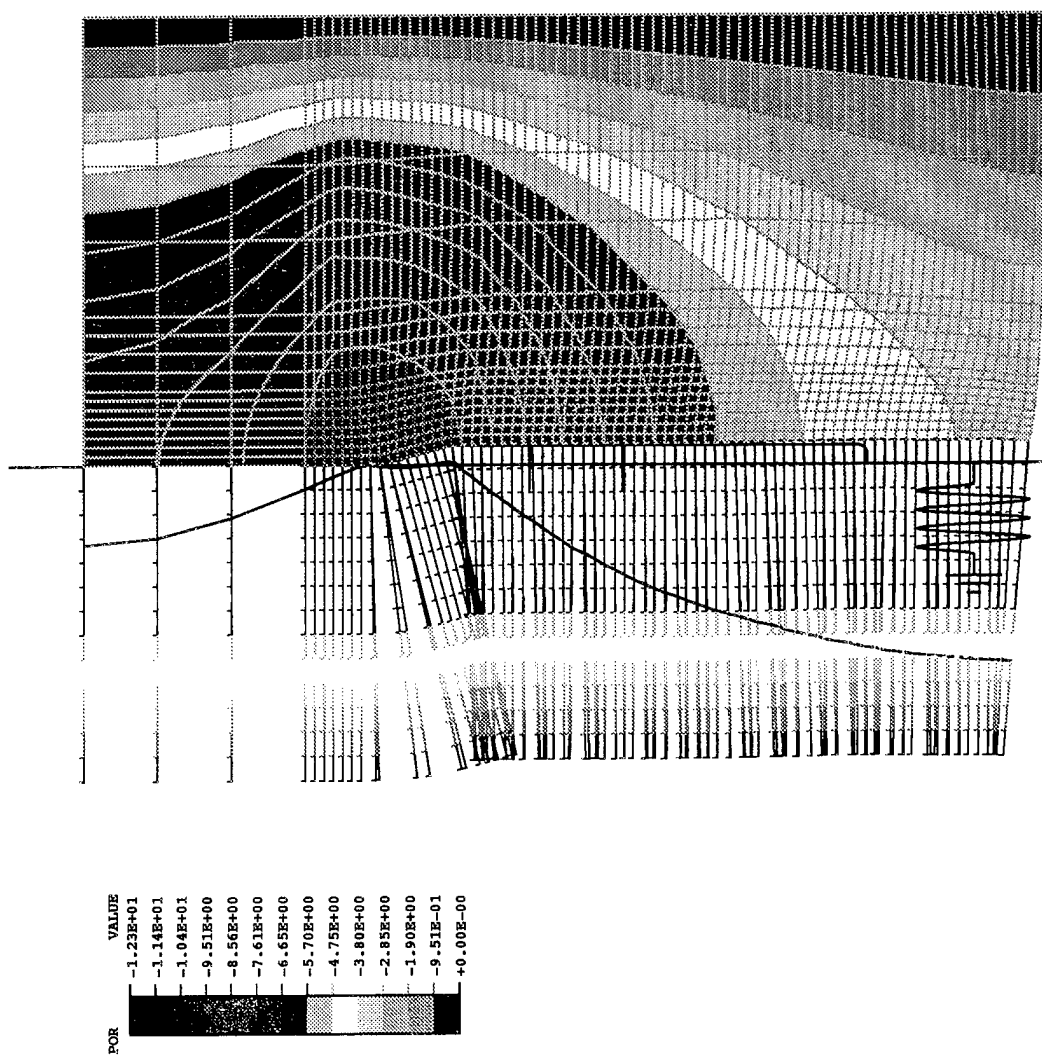
(b) Pore pressure distribution in soil surrounding plow with sharp blade.

Figure 5-23 Continued.
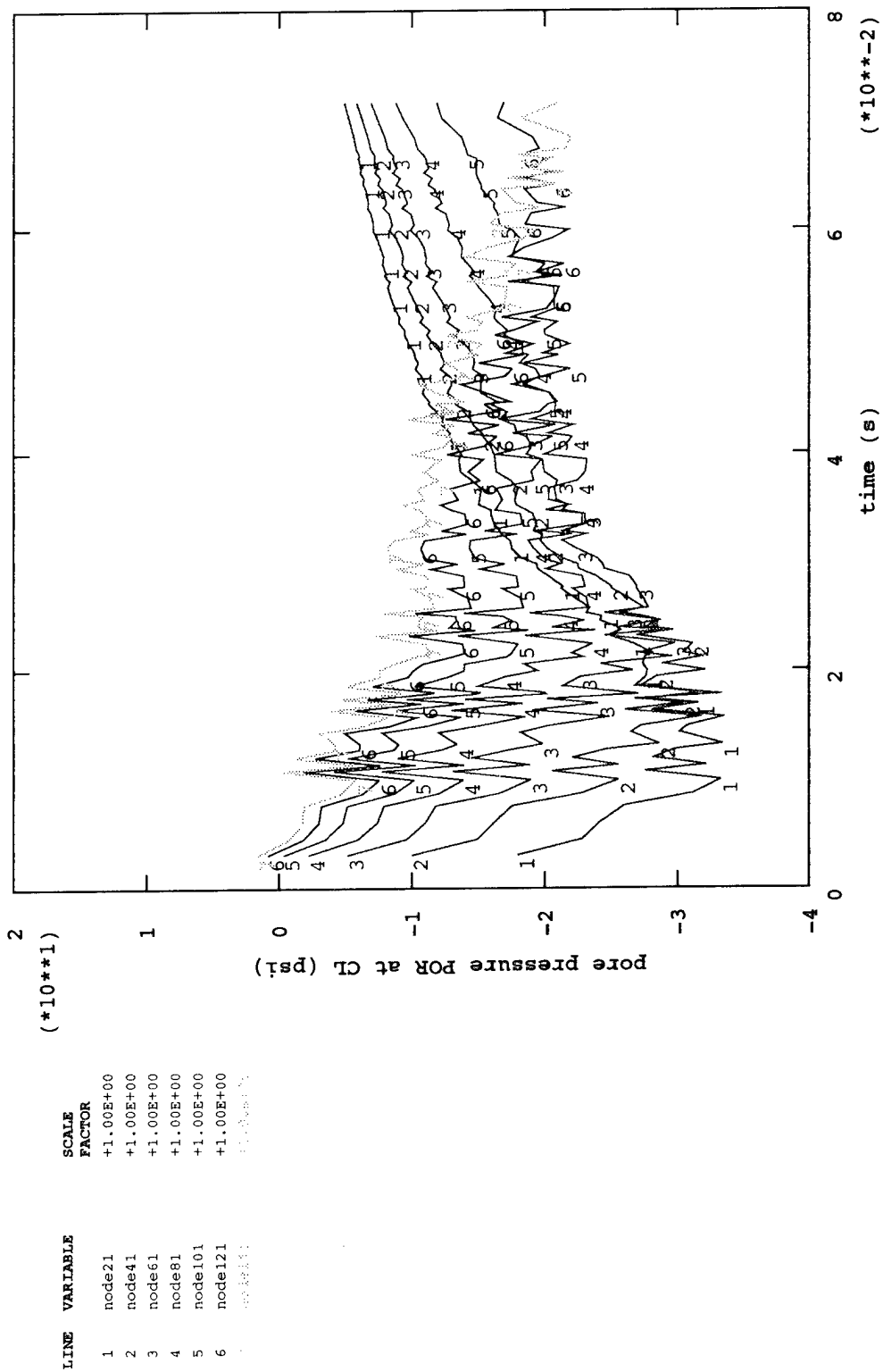
(c) Pore pressure histories at sampled response points along path of plow with dull blade.

Figure 5-23 Continued.

146
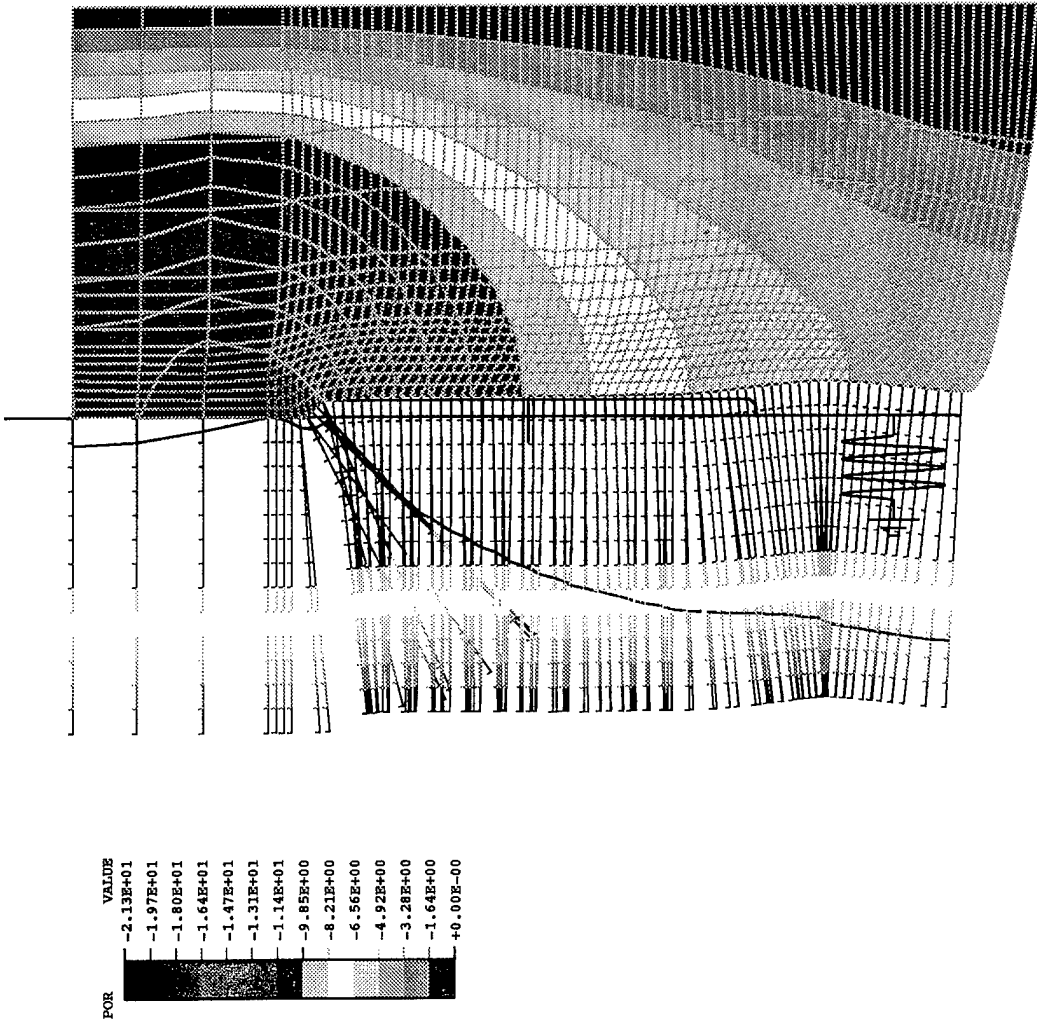
(d) Pore pressure distribution in soil surrounding plow with dull tip.

Figure 5-23 Continued.
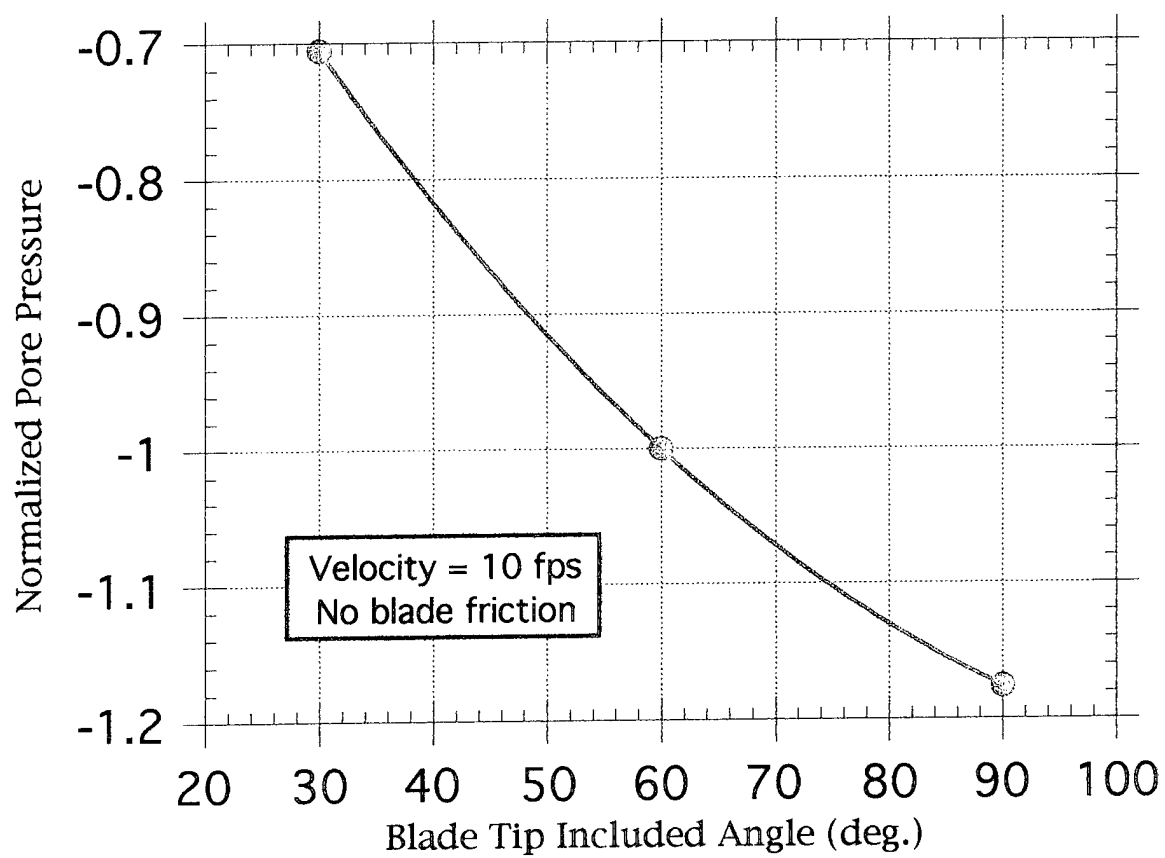
Figure 5-24. Effect of blade tip angle on minimum pore pressure.

6.0 SUMMARY AND CONCLUSIONS

The development of a rational numerical model for the interaction of a thin blade plow with seafloor sand during steady-state trenching in support of cable burial operations was addressed. Earlier attempts to explain differences between measured tow forces in the field and predicted tow forces based on conventional theories were unsuccessful. More recent laboratory experiments at NFESC have overcome difficulties in preparation of sands that replicate 100 percent saturation conditions in seafloor soil, and have successfully measured tow forces on scale models of thin blade plows moving with constant velocity. The data showed that the relationship between tow force and velocity was linear below a critical velocity, beyond which it leveled off to a constant tow force. Development of numerical models was also authorized to investigate the mechanics of plow/soil interaction, to compute plow forces, to provide a rational analysis tool for analyzing the effects of alternative seafloor soils and plow design parameters, and to assess the state-of-the-art in commercial finite element technology relative to these objectives.

Numerical modeling of plow/soil interaction is a complex problem irrespective of whether state-of-the-art commercial finite element technology or existing advanced special purpose software is employed in the solution. The fundamental problem is to model the coupled governing field equations for saturated soil in the presence of a rigid body having sliding interfaces while it is penetrating seafloor soil. The field equations are those for equilibrium of an elasto-plastic porous medium, coupled to those for pore water flow within the medium. Effective stress analysis is required, friction on sliding interfaces must be provided for, and the stress state in the soil is such that the analysis ideally should be carried out in three dimensions.

The state of commercial software coerces a multistep transient solution approach for the steady-state plow/soil interaction problem, which is an expensive approach from a computational point of view. Further, special handling techniques are necessary to the development of the model when employing commercial software. In this case, these techniques are mainly due to the imposed usage of a high order finite element formulation to supporting effective stress analysis. Data management is impacted by large, generated files due to midside node points. Moreover, when used adjacent to a sliding interface, a well-known anomaly involving high-order element nodal reaction forces, requires the addition of constrained displacement fields on element faces which are in contact with the plow. The resulting model approach is feasible but technically constrained. In the event of numerical difficulty, which is often encountered in nonlinear analysis computation, there are few options to the proposed approach for plow/soil interaction modeling when using commercial finite element technology.

A summary of two alternative modeling approaches for plow/soil interaction also developed in the course of this project was provided. The first approach was a semi-empirical model calibrated with NFESC laboratory test data, and it produced three-dimensional results in very good agreement with the experimental data base. The other approach was a new and simpler rational numerical model approach that promises to avoid the substantial computational cost of multistep transient analysis for simulating steady-state plow/soil interaction. It was successfully demonstrated using a two-dimensional nonlinear plane strain plow/soil interaction model with a simplified viscoelastic material model for soil. Steady-state behavior of plow/soil interaction was captured in a single computational finite element solution step. This alternative to multistep models requires further development including implementation of an elasto-plastic effective stress soil model and a three-dimensional finite element analysis framework. This is feasible

149

using special purpose software developed jointly at the University of California at Davis and at NFESC under ONR sponsorship. The software features dynamic effective stress analysis with modern soil constitutive laws, low-order finite element formulations for soil, and a modular architecture for producing and testing alternative algorithms and achieving numerical solutions for a broad range of structural/geotechnical problems.

The technical approach to plow/soil interaction modeling (the primary focus of this study), considered a two-dimensional multistep plow/soil interaction model demonstration. This model featured a geometrically nonlinear plane strain formulation, and a Drucker-Prager plasticity model for soil behavior. Preliminary studies, which employed simple constitutive models for soil, were initially encouraging, demonstrating that a rigid plow blade penetrating into soil at constant velocity could be simulated successfully. Simultaneously in a parallel development, preliminary calibration of a Drucker-Prager constitutive soil model demonstrated that experimental triaxial test data for seafloor soil relating effective stress to soil deformation could be reasonably replicated.

However, replacing the simplified soil material models with a calibrated Drucker-Prager effective stress soil model to achieve a satisfactory plow/soil interaction model was not straightforward. Several technical difficulties remained and had to be surmounted to achieve a reasonable working model of plow/soil interaction. These technical difficulties included appropriate modeling of soil tearing or failure at the tip of the plow blade, allowance for overly constrained drainage path lengths for the porous medium in a two-dimensional model, and unavoidable numerical experimentation with solution control parameters to achieve stable solutions and acceptable compute times.

The behavior of the two-dimensional plow/soil interaction model was initially analyzed for a nominal plow velocity, a standard blade configuration, and a frictionless plow/soil interface condition. Selected results from the analysis pertaining to both the mechanics of plow/soil interaction and the veracity of the model included the following observations:

1. Displacement of soil surrounding the plow under steady-state conditions revealed that only the tip of the plow blade is in contact with the soil. Further, a permanent groove or wake is formed behind the plow tip which is in qualitative agreement with experimental observation of the groove produced by the physical model in the laboratory apparatus. The model strictly predicts that this space is void of soil including its pore water. However, pore water under reduced pressure may reasonably be assumed to occupy the groove or wake.

2. The steady-state tow force acting on a physical model of a thin blade plow moving in a given soil was reliably measured in the laboratory, but cannot be computed by the plow/soil interaction model due to its two-dimensional nature. However, unit plow forces were predicted which were useful to the understanding of plow/soil interaction, and which complemented information available from the laboratory apparatus. For example, the model provided information on the lateral or side force acting on the plow which cannot be measured by the laboratory apparatus.

3. Predicted strain response in the soil revealed how the trench is formed from residual or plastic strain, and showed that the soil has undergone permanent volumetric

150

expansion, as should be anticipated for a dilatant seafloor soil subjected to shear stress. Predicted effective stress response in the soil showed a concentration of stress acting at the shoulder of the plow tip which reveals why steel blades, after continuous usage, have an observed distinct pattern of wear on the shoulder of the plow tip. Moreover, the computed stress response showed that the plow tip must overcome soil which has been made stronger by the shearing action of the tip itself, just ahead of the plow, and provided an explanation of why high tow forces observed in earlier field operations were not predicted.

4. In comparison to strain and effective stress, both of which exhibited high gradients, the pore pressure gradient response was very diffuse. This tended to make it more difficult to simulate the pore pressure response in plow/soil interaction due to the presence of finite, artificial boundaries in the model. However, the predicted pore pressure response in the region of interest surrounding the plow tip, was nonetheless reasonable and qualitatively consistent with measurements made with the laboratory apparatus.

Also, a subsequent parameter study with the two-dimensional plow/soil interaction model demonstrated the potential engineering utility of a future rational three-dimensional model. The effects of plow velocity, interface friction, and shape of the plow tip were investigated. The results are presented in the following:

1. Unit tow force predicted by the model was a linear function of plow velocity, in agreement with the linear relationship between tow force and velocity measured with the laboratory apparatus. However, any further direct comparison of the data is misleading because the unit tow force predicted by the two-dimensional model and (total) tow force measured in the laboratory are different quantities. Further, critical velocity, as observed experimentally, was noted in the range of velocities studied with the model. This was most likely due to two reasons: (a) the model contained no provision for cavitation of the pore fluid and (b) a proper failure condition for soil at the plow tip has as yet to be incorporated into the constitutive model. In the neighborhood of the plow tip, resisting principal stresses in the soil did increase toward an apparent bound, while maximum shear stress decreased, as the steady-state plow velocity increased. The decrease in pore pressure near the plow tip was linear with plow velocity. The decrease was without an apparent bound in the absence of a cavitation pressure cutoff in the model.

2. Unit tow force varied linearly with the coefficient of friction between the plow blade and soil. For example, 10 percent friction increased the tow force by nearly 35 percent over the frictionless case, while the lateral force increased only very modestly. Further, 10 percent friction caused the maximum shear stress in the soil near the plow tip to increase dramatically by a factor of 3.

3. The shape of pointed, plow blade tip profiles is clearly an important engineering design parameter. However, it is also an important operational parameter since,

151

during usage in the field, wear may be anticipated which will cause its shape to change with corresponding effects on performance and efficiency. In the absence of friction, the shape parameter study found that the unit plow tow force changed dramatically with blade shape, while the unit plow lateral force was nearly independent of blade shape. The unit tow force increased somewhat faster than linearly with the size of the included angle of the tip. For example, it was halved by halving the standard 60-degree angle of the plow tip, while it increased 75 percent for a 50 percent increase, corresponding to a dull blade tip (90-degree angle). Further, because the maximum lateral contact force was much reduced for the sharp blade, a sharper blade entry would potentially sustain much less shoulder wear on the tip. However, the dull blade produced larger shear stress and larger negative pore pressure in the soil. At the same towing velocity, it would be potentially more effective in soil trenching albeit at the expense of higher tow forces.

Ultimately, a three-dimensional numerical plow/soil interaction model would be necessary to accurately predict the response of a plow moving with steady-state velocity through the seafloor. In spite of the high technical risk in the development of such a model, the two-dimensional model presented in this study adequately demonstrates that it would complement the existing knowledge base supporting cable burial operations. Often, useful scientific and engineering information cannot be as easily obtained by alternative methods especially when the behavior and response of the plow depends critically on either site-specific information or on particular design details of plow blades.

7.0 RECOMMENDATIONS

Future cable burial technology requirements for numerical simulation of plow/soil interaction should be addressed by focusing on the development of three-dimensional finite element solutions. If both transient and steady-state solutions are required, then continued application of commercial finite element technology and multistep solution approaches together with super computer resources would be needed. On the other hand, if only steady-state solutions are required, then the recommended approach is to complete the development of the proposed single-step finite element solution approach, which is more computationally efficient.

The single-step finite element approach is more likely to result in an effective engineering analysis and design tool because it would require only workstation or personal computer resources. Development of supporting special-purpose software is also recommended to enhance that goal. Moreover, this approach would provide for application of classical critical state soil models and modern advanced soil constitutive models, such as the bounding surface plasticity model which was developed by the Navy and which is generally unavailable with commercial software.

It is also recommended that additional experiments be conducted to determine the failure mechanism of soil at the tip of the plow. This mechanism has not been given sufficient attention, though it is important to the material modeling process irrespective of the numerical modeling approach. This is especially important to establishment of the upper bound in plow resistance which governs actual plow design. Also, further experiments specifically designed for validating models of plow/soil interaction are recommended.

Completion of the single-step finite element solution approach for steady-state plow/soil interaction problems requires the following recommended steps be taken:

1. Perform additional experiments with the laboratory apparatus, along with further instrumentation, to define failure modes of soil at the tip of rigid penetrators, and to provide additional validation data for plow/soil interaction models.

2. Develop failure models from these experiments and implement them into the single-step finite element model.

3. Replace the existing simplified viscoelastic soil model with the bounding surface plasticity soil model in the single-step finite element software. A critical state soil model has in fact already been implemented for undrained conditions in this manner.

4. Extend the solution framework of the single-step finite element software from two dimensions to three dimensions.

5. Perform related numerical studies to verify implementation of algorithms, and validate the single-step finite element model using experimental data from the laboratory apparatus.

A related requirement for simulating two-dimensional axisymmetric penetration response of penetrometers in saturated sand is similar to the requirement addressed in this study for simulating plow/soil interaction. Moreover, a two-dimensional axisymmetric formulation of the penetrometer problem is both natural and reasonable. A typical impact velocity of a penetrometer is 50 fps, sufficiently low that the problem is amenable to a transient solution with an implicit finite element program. This has been the approach used in the present study of steady-state plow/soil interaction at velocities from 1 to 13 fps. An explicit finite element solution could also be recommended for the transient penetrometer problem, but cannot also be easily recommended for the steady-state problem.

Therefore, both problems are amenable to dynamic solutions by implicit finite element programs, both involve seafloor soil, and both require modeling of frictional interfaces using slide lines. Consequently, much of the expertise gained in the study of plow/soil interaction modeling is immediately applicable to numerical modeling of penetrometers. A general numerical modeling methodology can be designed to address both problems using two- and three-dimensional, transient and steady-state, nonlinear dynamic finite element technology.

A computer-based design and analysis tool supporting future requirements in cable burial technology and related seafloor geotechnical operations is recommended. This recommendation will have to be considered and proposed in more detail, but sufficient engineering resources (i.e., experimental, theoretical, and numerical modeling expertise) are in place to realize this product within a reasonable time frame and for a reasonable research and development investment.

8.0 REFERENCES

Abbo, A. J. and S.W. Sloan (1993). "A smooth hyperbolic approximation to the Mohr-Coulomb yield criterion," Research Report No. 087.06.1993, Department of Civil Engineering and Surveying, The University of Newcastle, New South Wales, Australia, 1993.

Armero, F. (1995). "Recent advances in the analysis and numerical simulation of strain localization in inelastic solids," Proceedings of COMPLAS 4, Barcelona, April 1995.

Arulanandan, K. and R. F. Scott , Eds., (1993). "Verification of numerical procedures for the analysis of soil liquefaction problems," Vol. 1, Experimental results and numerical predictions, Proceedings of the international conference on the verification of numerical procedures for the analysis of soil liquefaction problems, U. C. Davis, 17-20 October 1993.

Azarkhin, A. and O. Richmond (1989). "A generalization of the upper bound method with particular reference to the problem of a ploughing indenter," ASME, J. of Applied Mechanics, 10/Vol.56, March, 1989.

Baligh, M. M. (1985). "Strain path method," ASCE, J. of Geotechnical Engineering, Vol. 111, No. 9, September, 1985.

Booker, J. R., et al. (1989). "Some recent applications of numerical methods to geotechnical analysis," Research Rpt. No. 598, School of Civil and Mining Engineering, The University of Sidney, Australia, May 1989.

Cable, S. B., H. Carlisle, B. Skyers, and R. Taylor (1993). "Hydrostatic pressure effects on thin blade plow resistance in dense, saturated, cohesionless soil," TM No. 42-93-06, NCEL, Port Hueneme, June 1993.

Chi, L. and R. L. Kushwaha (1990). "A Non-Linear 3-D Finite Element Analysis of Soil Failure with Tillage Tools," J. of Terramechanics, Vol. 27, No. 4. pp. 343-366, 1990.

Dafalias, Y.F. and L.R. Herrmann (1986). "Bounding surface plasticity-part ii: application to isotropic cohesive soils", Journal of Engineering Mechanics, ASCE, Vol. 112, No. 12, pp. 1263-1291, Dec. 1986.

Dagan, G. and M. P. Tulin (1969). "A study of the steady flow of a rigid-plastic clay beneath a driven wheel", Journal of Terramechanics, Vol. 6, No. 2, Pergamon Press, 1969.

Drescher, A. and E. Detournay (1993). "Limit load in translational failure mechanisms for associative and non-associative materials," Geotechnique, 43, No. 3, 443-456, 1993.

Fiegel, G. L., and B. L. Kutter (1992). "The mechanism of liquefaction in layered soils," CR 92.009, NCEL, 560 Center Drive, Port Hueneme, CA 93043-5003, August 1992.

Gibson, R. E., J. K. L. Schiffman and S. L. Pu (1967). "Plain strain and axially symmetric consolidation of a clay layer of limited thickness," University of Illinois (Chicago Circle), MATE Report 64-7, 1967.

Girard, J., and R. Taylor (1994). "Blade geometry and soil permeability effects on thin blade plow resistance in dense, saturated, cohesionless soils - phase II report," TM-2026-OCN, Naval Facilities Engineering Service Center, Port Hueneme, CA 93043-4328, 1994.

Herrmann, H. (1992). "Literature review of soil-tool interaction results and analytical models for thin-bladed seafloor cable plows," TM No. 42-92-06, NCEL, 560 Center Drive, Port Hueneme, CA 93043-5003, September 1992.

Herrmann, L. R. and J. Mello (1994). "Investigation of an alternative finite element procedure: a one-step, steady-state analysis," CR 95.001-SHR, Naval Facilities Engineering Service Center, Port Hueneme, CA 93043-4328, December 1994.

Herrmann, L.R., et al. (1987). "Numerical implementation of plasticity model for cohesive soils", Journal of Engineering Mechanics, ASCE, Vol. 113, No. 4, pp. 500-519, April 1987.

Hibbit, Karlsson, and Sorensen, Inc. (1993). ABAQUS/Standard user's manual, Volumes I and II, 1080 Main Street, Pawtucket, RI 02860-4847, 1993.

Hoge, L. and T. A. Shugar (1992). "Three-dimensional finite element modeling of confinement stress for projectiles embedded in rock - a preliminary study," Technical Note 6727TN, Naval Civil Engineering Laboratory, Port Hueneme, CA 93043, September 1992.

Holland, T.J. (1996), Ph.D. dissertation, Dept. of Civil Engineering, U.C. Davis, 1996.

Kutter, B. L. and T. Voss (1994). "Analysis of data on plow resistance in dense, saturated cohesionless soil," CR 95.004-SHR, Naval Facilities Engineering Service Center, Port Hueneme, CA 93043-4328, February 1995.

Kutter, B. L., Y. R. Chen, and C.-K. Shen (1994). "Triaxial and torsional shear test results for sand," CR 94.003-SHR, NFESC, 560 Center Drive, Port Hueneme, CA 93043-5003, June 1994.

Shen, C. K. and X. S. Li (1991), "Pore pressure response during 1986 Lotung earthquake," proceedings, advances in geotechnical and earthquake engineering and soil dynamics, St. Louis, Mar 11-15, 1991.

Shen, C. K., Z. L. Wang and L.R. Herrmann (1986). "Final report on ocean wave induced effective stresses in an elastoplastic seafloor," Department of Civil Engineering, University of California, Davis, November, 1986.

Simo, J. C. and G. Meschke (1993). "A new class of algorithms for classical plasticity extended to finite strains - application to geomaterials," Computational Mechanics, 11, 253-278, 1993.

Simo, J. C. , J. Oliver and F. Armero (1993). "An analysis of strong discontinuities induced by softening solutions in rate independent solids," Journal of Computational Mechanics, 12, 277-296, (1993).

Simo, J. C. (1994). "A new methodology for the numerical simulation of strain softening in inelastic solids," CR 95.002, Naval Facilities Engineering Service Center, Port Hueneme, CA 93043-4328, December 1994.

True, D. G. (1994). Personal Communication, NFESC, 22 November 1994.

van Os, A. G. and W. van Leussen (1987). "Basic research on cutting forces in saturated sand," Journal of Geotechnical Engineering, Vol. 113, No. 12, December 1987.

Wang, Y. Dafalias and C.-K. Shen (1990), "Bounding surface hypoplasticity model for sand," Journal of Engineering Mechanics, ASCE, May 1990.

Whirley, R. G. and J. O. Hallquist (1991). "DYNA3D, A nonlinear, explicit, three-dimensional finite element code for solid and structural mechanics-user manual," UCRL-MA-107254, Lawrence Livermore National Laboratory, May 1991.

Wu, T.-H. (1967). "Soil mechanics," Allyn and Bacon, Inc. Boston, 1967.

Zienkiewicz, O. C. and R. L. Taylor (1989). "The finite element method," Fourth Edition, Vol. 1, Ch.2, McGraw-Hill, London, 1989.

9.0 ACKNOWLEDGMENT

Appendix A

DISCUSSION OF SOME TECHNICAL ISSUES AND PROJECT CONSTRAINTS

The impact of limited project funding and a compressed project schedule for determining the capability of commercial finite element technology, as represented by the ABAQUS program, to model plow/soil interaction is discussed. The discussion is organized into six sections: (1) Material Type and Soil Behavior, (2) Material Model, (3) Finite Element Model, (4) Parameter Study, (5) U. C. Davis Studies, and (6) Contingency Model Study. A summary of these issues and their effect on evaluation of numerical modeling with ABAQUS is provided.

1.1 Material Type and Soil Behavior

The plow is required to traverse medium and fine seafloor sands under the following conditions: 100 percent saturation, high density, drained, partially drained, and undrained conditions. Emphasis will be given to 100 percent saturated medium sand under partially drained conditions.

Required soil behavior necessitates a two-phase, effective stress soil model approach prior to cavitation, and possibly a three-phase system approach if cavitation occurs. The material is subjected to both deviatoric and dilatation stresses, as well as pore pressure changes.

Cavitation cannot be directly addressed in this study because ABAQUS does not provide for it. Thus, the analysis remains limited to a two-phase, highly dense soil, with 100 percent saturation conditions. Flow conditions are discussed below in connection with the material model. Sands are frictional materials. Therefore, a nonassociative plasticity model will be addressed. Associative models will not be studied.

1.2 Material Model

An assessment of commercial capability could be incomplete if some applicable capabilities are excluded from the study. In the case of ABAQUS, three soil models for sands are available: (1) Modified Drucker-Prager Model, (2) Modified Cap Model and (3) Modified Cam-Clay Model.

The Modified Cap Model includes three failure surfaces, a compaction/dilation limitation surface to model volume change, a curved Drucker-Prager surface so that the direction of material loading is permitted to vary, and a transition surface between the latter two surfaces which allows for modeling material softening. Most of the calibration effort is related to the Drucker-Prager shear surface. Little more effort is needed beyond that required to calibrate the Modified Drucker-Prager Model. Though study of the Modified Cap Model would be useful, it is also true that available material calibration data is limited. The Modified Cam-Clay Model includes an elliptical failure surface (in the meridian plane). It also includes a dependence on the third stress invariant. However, this model is believed to do essentially the same things as the cap model and its inclusion in the study would be somewhat duplicative.

Only one applicable material model, the Modified Drucker-Prager will be addressed. The numerical model will be limited to the extended Drucker-Prager plasticity model for the soil skeleton, along with the pore water pressure variable formulation. In the drained condition, the

model is employed solely, without pore water pressure variables. In the other two conditions, the material model is employed along with the pore water pressure variables. The partially drained condition can be handled naturally through specification of the boundary value problem in which pore water pressure is modified by whatever dissipation mechanisms are present. The undrained condition is specified by an arbitrarily low permeability coefficient. In this regard there is limited impact due to time constraints in the event of technical problems involving some of these conditions. For example, the undrained condition may be dropped from the task if numerical problems involving oscillation in pore water pressures arise.

Only a nonassociative flow rule will be considered because of the material's frictional nature. The computations are more lengthy with a nonassociative flow rule because the resulting equations of equilibrium are nonsymmetric. An associative flow rule would in effect discount volume change in the soil which is otherwise believed to be important in the present problem.

1.3 Finite Element Model

It is believed that a three-dimensional stress state prevails in the vicinity of the plow which cannot be captured by a two-dimensional model without potentially far reaching assumptions on the applicability of the results. It is also not clear that friction on the plow may be safely neglected. Friction should be retained in the study. Yet, it is known that this complicates the modeling process. Further, large deformations clearly exist in the neighborhood of the plow. Also, inertia forces due to soil particle accelerations are potentially an issue, for if they are significant they can affect pore pressure, effective stress and resistance force on the plow.

A two-dimensional plane strain plow/soil interaction model is not easily defended. ABAQUS does not support plane stress formulations for soil consolidation problems. A three-dimensional model simply cannot be considered beyond some initial concepts due to time and funding constraints. Therefore, emphasis is given to a two-dimensional plane strain finite element model of plow/soil interaction.

An attempt will be made to retain friction in the study though numerical difficulty is a distinct possibility when it is included. In ABAQUS there are finite element families for addressing node-to-node and surface-to-surface interaction under small or finite sliding assumptions with or without friction. Emphasis will be given to a frictionless plow/soil interaction model.

Large deformations will be included in conjunction with the Drucker-Prager plasticity model, so no scope changes are anticipated in this respect. However, an inconsistency may exist due to specification of large deformations in conjunction with a material model based upon small strain measures. It is believed that this approach is nonetheless worthwhile, for the alternative is to limit the analysis to small deformations which is incorrect to first order.

Quasi-static transient consolidation analysis will be pursued. Dynamic consolidation analysis cannot be evaluated since inertia forces are neglected in ABAQUS for coupled effective stress/porous media flow problems.

1.4 Parameter Study

There are many parameters to be considered in seeking to establish adequacy of the model and to learn from the model. Limited resources coupled with very large run times and

heavy post-processing and data analysis burdens will allow only so many parameters to evaluated. An attempt will be made to include limited parameter studies on the effects of plow resistance from steady-state velocity, friction, blade sharpness, and permeability.

1.5 U. C. Davis Studies

Two studies were commissioned early in the numerical model project at the University of California at Davis. The main task of these studies was to provide discussions of the relevant soil mechanics for plow/soil interaction and numerical modeling issues to guide the present development of a numerical model. If the numerical model project schedule were to have been accelerated, the main purpose of these studies would have been thwarted. However, the project could not be accelerated as results were not forthcoming early enough. Nonetheless, these two studies were eventually published (Kutter and Voss, 1995 and Herrmann and Mello, 1994) and provided useful guidance as initially planned.

1.6 Contingency Model Study

Given the importance of the problem to the Navy and the early uncertainties in modeling success, contingency modeling plans were to be made and conducted somewhat in parallel with primary numerical modeling effort. However, project constraints largely eliminated real progress on these contingencies. Further, success of the model remains a subjective issue in the absence of specific criteria. Generally, it has meant the ability of the model to replicate measured response from the laboratory apparatus.

If the two-dimensional plow/soil interaction model fails to agree with experimental observation and measurement and a three-dimensional model is deemed necessary as a result, then the course of action would be to complete the originally proposed study which called for construction of a three-dimensional model and substantial usage of super computer resources. If the two-dimensional model fails for other reasons, then the option would be to consider possibly two other courses of action depending on the difficulty. First, if the material models in ABAQUS do not suffice, then a modern material model can be implemented in ABAQUS so that other important modeling resources of ABAQUS may still be exploited. If the contact algorithms and the provisions for large sliding interfaces, etc., contained in ABAQUS proved inadequate, then an approach using Geneseos, an in-house nonlinear finite element program, can be considered in place of commercial technology.

Three noncommercial finite element technology alternatives to the main numerical model approach (featuring commercial technology), were considered as contingency model studies:

1. Application of ABAQUS with the U. C. Davis bounding surface plasticity soil model replacing the Drucker-Prager plasticity soil model. Quasi-static transient consolidation analysis could then be resumed.

2. Application and further development of Geneseos, which has the bounding surface plasticity soil model, but which requires large deformation and suitable interface modeling capabilities. Fully dynamic transient soil consolidation analysis could then be pursued.

A-3

3. Application of U.C. Davis' steady-state finite element analysis formulation of the plow problem (Herrmann and Mello, 1994). Fully dynamic steady-state consolidation analysis could then be pursued.

The current numerical model study incorporates the Drucker-Prager model to represent the response of the soil. If this model is deemed inadequate, the CAP plasticity model must also be considered to fully evaluate the current approach of using commercial technology. If both of these soil models prove inadequate and if the U.C. Davis bounding surface plasticity can potentially overcome their deficiencies, then it could be implemented with ABAQUS via a UMAT procedure (a user-written subroutine for incorporating user supplied material laws). Such a procedure has in the past been written for an earlier version of the bounding surface plasticity soil model.

The current quasi-static transient consolidation analysis approach neglects inertia effects. If these effects are determined to be significant, ABAQUS would have to be abandoned for it has no dynamic soil consolidation capability. An alternative course of action would be additional development of Geneseos to support the present problem. It has the bounding surface plasticity soil model, corresponding low order two-dimensional soil elements and either quasi-static or fully dynamic consolidation analysis capability. The three main development tasks for this approach would: (1) add a slide-line interface capability, (2) add large deformation capability, and (3) update existing three-dimensional elements to soil elements by providing for pore pressures.

All of the numerical model approaches considered to this point occur in the time domain. Accordingly, the plow must enter the soil and be towed through a transient phase until steady-state forces are established. An alternative steady-state finite element approach is under development and could be pursued if: (1) the time domain approaches fail to converge on a solution, or (2) the time domain approaches converge but are computationally prohibitive and prevent parameter studies in support of engineering design to be conducted.

This approach also requires substantial software development, but it also provides the greatest potential return. If successful, a nonlinear steady-state analysis of the plow traversing the soil could be as inexpensive as one time step in a nonlinear dynamic transient analysis. Thus parameter studies to examine the effects of numerical and physical variables would be supported.

Appendix B

STATEMENT OF WORK FOR U. C. DAVIS STUDIES

1.0 INTRODUCTION AND BACKGROUND

1.1 The Naval Civil Engineering Laboratory (NCEL) within L40 has been tasked to investigate high performance, lightweight burial plows suitable for burial of small diameter cables in specific seafloor soils. In conjunction with this, L51 has been tasked to develop a numerical model of the plow/soil interaction process, the goal of which is to calculate the soil resisting force on the blade of the plow during towing at a constant velocity (0 to 10 knots range).

1.2 The plow/soil interaction process is physically complicated and requires geotechnical clarification. A soil mechanics study is required which will include a discussion and description of the relevant physics involved including the identification of parameters and their potential effects, a discussion of the relevance of existing bounding surface soil models for clay and sand materials, a discussion and description of the requirements for a valid numerical model of plow/soil interaction, and a discussion of the potential for using existing computer programs for the numerical model.

2.0 SCOPE

2.1 The contractor shall provide all labor and materials required to prepare a discussion on the relevant physics of plow/soil interaction, necessary modifications to NCEL/UCD bounding surface soil models, requirements for numerical modeling, and potential for using commercial or available computational mechanics software (ABAQUS, DYNA3D, Geneseos, DYSAC, etc.).

2.2 The key element of the numerical model is the constitutive model used for describing the stress-strain behavior of the seafloor soil. Since NCEL is tasked to develop this model, the proposed study must be conducted within the framework of NCEL's soil models. These models have been developed in conjunction with Professor Kutter and his colleagues at UCD. (Refer to the recently completed contract N47408-89-C-1058, Validation of a Proposed Rational Material Model Characterization of Granular Soils.) Their data requirements, performance capabilities, and required modifications shall be considered while forming recommendations for the numerical modeling task at NCEL.

3.0 GOVERNMENT FURNISHED INFORMATION

3.1 **Plow/Soil Interaction Data**. The government will provide plow/soil interaction experimental data and relevant technical literature as guidance to the contractor for preparing his study.

4.0 TECHNICAL TASKS

4.1 The study shall include a discussion and description of the relevant physics and soil mechanics behavior involved in the plow/soil interaction process. The study shall include the identification of key parameters and a discussion of their importance. Parameters and variables such as soil type, particle size, permeability, relative density, pore pressure, cavitation and shear strength shall be included. This task shall form the main part of the study.

4.2 The study shall be conducted within the framework of the NCEL/UCD bounding surface plasticity soil model for clay and the bounding surface hypoplasticity soil model for sand. The data requirements, performance capabilities and any required modifications for these models shall be considered for support of a plow/soil numerical modeling task at NCEL. Soil constitutive model recommendations shall be given.

4.3 The study shall include a discussion and description of the requirements for a valid finite element numerical model of plow/soil interaction. In addition to the requirements of the constitutive model, other finite element modeling considerations shall be considered such as transient loading, steady-state loading, boundary conditions, slide lines, small and large deformations, etc. Approaches other than finite element modeling may also be included in a review of alternative approaches to plow/soil interaction. Finite element modeling recommendations shall be provided.

4.4 The study shall include an evaluation of the potential for using commercial and available general purpose finite element computer programs such as ABAQUS and DYNA3D, and available research/developing programs such as Geneseos (NCEL) and DYSAC (UCD) for modeling the plow/soil interaction problem. Computer program recommendations shall be given.

5.0 DELIVERABLES

5.1 Technical Report on Plow/Soil Interaction and Related Numerical Modeling Issues. A final technical report on the relevant soil mechanics issues involved with plow/soil interaction shall be prepared. The study shall also include recommendations on constitutive models, numerical modeling, and finite element computer programs. The report shall include an abstract of the findings.

5.2 Six (6) copies of the camera-ready final technical report shall be provided.

6.0 SCHEDULE

6.1 The final technical report shall be delivered within eight (8) months of the start of the contract.

Appendix C

ANNOTATED INPUT DATA FILE FOR PLOW/SOIL INTERACTION MODEL

A description of a typical input data file is provided for documentation of the plow/soil interaction model and in the event that future simulations are required. In the following input file listing, any command preceded by ** is ignored by ABAQUS, i.e., "commented out." The annotations provided are italicized and enclosed in parentheses following each command. Otherwise the command lines or "cards" are exactly as they appear in a typical input data file.

*HEADING, UNSYMM	*(specifies an unsymmetrical equation solver algorithm due to flow rule)*
PLOW/SOIL INTERACTION: 1/2-inch pointed blade at 5 fps, 2-D plane strain model, CPE8P elements, interface friction coeff.=0.1, Drucker-Prager soil w/o hardening/softening, yield=14 psi compression, with nonassociative flow coupled pore pressure/effective stress analysis, reduced fluid bulk modulus to compensate for no cavitation model.	*(this heading is printed on output)*
*NODE	*(key node points and their coordinates in inches that define a rectangular mesh)*
1,0.0,0.0	*(node 1 is the origin of x-y-z global axes which is placed at the start end of mesh)*
145,0.0,9.0	*(145 nodes, including midpoint nodes, to span first 9 inches along positive y-axis)*
151,0.0,12.0	*(coarser layout of 6 nodes from 9 -12 inches, to stop end of the mesh)*
3201,1.0,0.0	*(specifies a duplication of the above node pattern across to the x=1 line)*
3345,1.0,9.0	*(repeat of the second card of the list for nodes along the x=1 line of nodes)*
3351,1.0,12.0	*(repeat of the third card, along the x=1 line of nodes)*
4801,2.0,0.0	*(specifies a coarser mesh between x=1 and x=2 inches)*
4945,2.0,9.0	*(repeat of the second card for the x=2 line of nodes)*
4951,2.0,12.0	*(repeat of the third card, for x=2 line of nodes)*
5601,4.0,0.0	*(specifies an even coarser mesh between x=2 and x=4 inches)*
5745,4.0,9.0	*(repeat of the second card for the x=4 line of nodes)*
5751,4.0,12.0	*(repeat of the third card for the x=4 line of nodes)*

```
6001,6.0,0.0                          (the lower right corner of the mesh at x=6 inches)
6145,6.0,9.0                          (repeat of the second card for the x=6 line of nodes)
6151,6.0,12.0                         (repeat of the third card to the stop end of the mesh)
*NODE,NSET=PLOWNODE                   (a key node; the reaction force at this node is the tow
                                      force)

10001,0.0,-3.25                       (defines the plow node at the centroid of the rigid body
                                      plow)

*NODE,NSET=SYMMREST                   (gives name to a node on the rigid surface along the
                                      centerline)

10002,0.0,6.0                         (defines a node at the center of the 12-inch rigid surface
                                      along the centerline)

*NGEN                                 (generates the nodes between nodes 1 and 145,
                                      incrementing by 1)

1,145,1
*NGEN                                 (generates the nodes between 145 and 151, incrementing
                                      by 1)

145,151,1
*NSET,GENERATE,NSET=CL                (names the set of nodes 1 - 151 on the centerline, CL)
1,151,1
*NGEN                                 (generates the nodes between 3201 and 3345,
                                      incrementing by 1)

3201,3345,1
*NGEN                                 (generates the nodes between 3345 and 3351,
                                      incrementing by 1)

3345,3351,1
*NSET,GENERATE,NSET=T1                (names the set of nodes 3201 - 3351, T1)
3201,3351,1
*NGEN                                 (generates the nodes between 4801 and 4945)
4801,4945,1
*NGEN                                 (generates the nodes between 4945 and 4951)
4945,4951,1
*NSET,GENERATE,NSET=T2                (names the set of nodes 4801 and 4951, T2)
4801,4951,1
*NGEN                                 (generates the nodes between 5601 and 5745)
5601,5745,1
*NGEN                                 (generates the nodes between 5745 and 5751)
5745,5751,1
*NSET,GENERATE,NSET=T3                (names the set of nodes 5601 and 5751, T3)
5601,5751,1
*NGEN                                 (generates the nodes between 6001 and 6145)
6001,6145,1
*NGEN                                 (generates the nodes between 6145 and 6151)
6145,6151,1
*NSET,GENERATE,NSET=EDGE              (names the set of nodes 6001 and 6151, EDGE)
6001,6151,1
```

`*NFILL,NSET=E1`	*(names the set of nodes between sets CL and T1, E1)*
`CL,T1,16,200`	
`*NFILL,NSET=E2`	*(names the set of nodes between sets T1 and T2, E2)*
`T1,T2,8,200`	
`*NFILL,NSET=E3`	*(names the set of nodes between sets T2 and T3, E3)*
`T2,T3,4,200`	
`*NFILL,NSET=E4`	*(names the set of nodes between sets T3 and EDGE, E4)*
`T3,EDGE,2,200`	
`*NSET,GENERATE,NSET=ALL`	*(names the set of all nodes, ALL)*
`1,6151,1`	
`*NSET,GENERATE,NSET=START`	*(names the set of nodes along the start end, START)*
`1,6001,200`	
`*NSET,GENERATE,NSET=STOP`	*(names the set of nodes along the stop end, STOP)*
`151,6151,200`	
`*ELEMENT,TYPE=CPE8P`	*(specifies an eight-node plane strain /pore pressure element)*
`1,1,401,403,3,201,402,203,2`	*(defines the connectivity or node pattern for element #1)*
`*ELGEN,ELSET=SOIL`	*(generates elements 1 to 75 along y-axis, and names this set SOIL*
`1,75,2,1,15,400,100`	
`**ELSET,ELSET=ECL,GENERATE`	*(names centerline elements 1 - 75, set ECL)*
`**1,75,1`	
`*ELSET,ELSET=STOP,GEN`	*(names element set 75 -1475 along the stop end, STOP)*
`75,1475,100`	
`*ELSET,ELSET=RIGHT,GEN`	*(names set of elements 1401 - 1475, RIGHT)*
`1401,1475,1`	
`*SOLID`	*(assigns mat'l property set DP1 to elset SOIL)*
`SECTION,ELSET=SOIL,MATERIAL=DP1`	
`*MATERIAL,NAME= DP1`	*(begin the definition of a material named DP1)*
`*ELASTIC`	*(specify elastic properties)*
`6000.0,0.3`	*(modulus of elasticity = 6,000 psi; Poisson ratio = 0.3)*
`*DRUCKER PRAGER`	*(specify extended Drucker Prager plasticity model w/nonassociative flow)*
`46.2,1.,21.5`	*(friction angle or strength = 46.2 deg.; angle of dilation = 21.5 deg.)*
`*YIELD,TYPE=COMPRESSION`	*(specifies deviatoric yield behavior in compression for DP mat'l)*
`**0.1,0.0`	*(table of values for deviatoric stress and corresponding axial plastic strain,*
`**14.0,0.005`	*i.e., 14 psi @ 0.005 plastic strain, etc.; data obtained from triaxial test data;*
`**21.0,0.01`	*calibration includes strain hardening and softening behavior;*
`**25.0,0.015`	*ABAQUS could not handle this data due to DP singularity condition in tension;*

**27.0,0.021	*strain hardening/softening was discarded , only residual stress behavior retained;*
**15.0,0.14	*residual stress apparent in triaxial data)*
14.,0.0	*(elastic perfectly plastic behavior specified, residual stress =14 psi for all strain)*
*PERMEABILITY	*(specifies soil permeability coefficient as a function of void ratio)*
0.011,0.5	*(table of values gives coefficient and void ratio)*
0.015,0.563	*(for example, k = 0.015 and e = 0.563)*
0.019,0.6	*(this is measured data idealized by following relationship:*

$$k = 0.087\ e^3 , \text{ with units of in/s for k)}$$

0.030,0.7	
0.044,0.8	
0.063,0.9	
0.087,1.0	
*POROUS BULK MODULI	*(specifies a finite bulk modulus for soil phases)*
0.0,305000.0	*(0.0 implies infinite value for solid phase ; bulk modulus = 305,000 psi for fluid)*
*INITIAL CONDITIONS,TYPE=RATIO	*(specifies initial void ratio)*
ALL,0.563	*(node points in NSET ALL are assigned an initial value of 0.563)*
*INITIAL CONDITIONS,TYPE=PORE PRESSURE	*(specifies initial pore pressure)*
ALL,0.0	*(node points in NSET ALL are assigned an initial value of 0.0 psi)*
*ELEMENT,TYPE=IRS21	*(planar rigid surface element for use with first order elements)*
10001,1,3,10001	*(ele # 10001; node 1; node 3, rigid body reference node 10001)*
*ELGEN,ELSET=TUNNEL	*(generates a set of 75 ele's beginning with ele #10001)*
10001,75,2,1	*(master ele # 10001; no. of ele's; node increment; element increment)*
*INTERFACE,ELSET=TUNNEL	*(defines ele's in set TUNNEL to be contact elements)*
1.0	*(dummy mechanical property for contact element set)*
*FRICTION,TAUMAX=1000	*(Coulomb friction model with upper bound shear stress =1000psi)*
0.1	*(coefficient of friction between rigid plow and soil)*
*RIGID SURFACE,ELSET=TUNNEL,TYPE=SEGMENTS,SMOOTH=0.125	*(the ele set TUNNEL*
START,-0.0025,0.0044337567	*is to be used in conjunction with blade rigid surface defined with*
LINE,0.25,-0.44337567	*tip at origin, 60 deg. bevel and 0.25 inch half thickness)*
LINE,0.25,-6.56	*(blade length is 6.25 inches)*

LINE,0.0,-6.56	*(rigid surface specification closes on centerline)*
*ELEMENT,TYPE=IRS21	*(planar rigid surface element for use with first order elements)*
10101,3,5,10002	*(ele # 10101; node 3; node 5, rigid body reference node 10002)*
*NSET,NSET=FIRST,GENERATE	*(set of bottom corner nodes along centerline is called FIRST)*
1,149,2	*(node 1; 149 such nodes; node increment for generating set is 2)*
*NSET,NSET=LAST,GENERATE	*(set of top corner nodes along centerline is called LAST)*
3,151,2	*(node 3; 151 such nodes; node increment for generating set is 2)*
*NSET,NSET=MID,GENERATE	*(set of midside nodes along centerline is called MID)*
2,150,2	*(node 2; 150 such nodes; node increment for generating set is 2)*
*MPC	*(specifies multi-point constraint for sets MID, FIRST, LAST)*
LINEAR,MID,FIRST,LAST	*(midside nodes interpolate displ's linearly between corner nodes)*
*ELGEN,ELSET=SYMMREST	*(generates a set of 74 ele's beginning with ele # 10101 which is tied to ele # 2)*
10101,74,2,1	*(master ele # 10101; no. of ele's; node increment; element increment)*
*ELSET,ELSET=START,GEN	*(defines 14 elements along starting edge of soil region)*
1,1401,100	*(ele #1; ele#1401, ele increment = 100)*
*INTERFACE,ELSET=SYMMREST	*(defines ele's in SYMMREST to be contact elements)*
1.0	*(dummy mechanical property for contact element set)*
**SURFACE CONTACT,SOFTENED	*(change from hard to soft contact for numerical reasons)*
**0.0625,5000	*(contact begins when gap < 0.0625"; contact pressure=5000psi @ zero gap)*
*BOND SURFACE	*(specify contact surface is initially bonded and may debond)*
*RIGID SURFACE,ELSET=SYMMREST,TYPE=SEGMENTS	*(defines rigid surface with which*
START,0.0,13.0	*elements in SYMMREST are to interact; this surface is coincident with*
LINE,0.0,-1.0	*center line, extending from -1.0 to 13.0 inches)*
*NSET, NSET=CRACKREF	*(names node 1 a set of nodes called CRACKREF)*
1	*(a crack will grow ahead of the plow tip, beginning at node 1)*
*BOUNDARY	*(specifies boundary conditions on various sets of node points)*
STOP,2	*(restrains y-displacement at nodes along stop end)*
EDGE,1	*(restrains x-displacement at nodes along long edge of soil*

PLOWNODE,1

(region)
(restrains rigid body displacement of plow in the x-direction, z-direction, and about

PLOWNODE,3,6
SYMMREST,1,6

the x-, y- and z-axes)
(completely restrains rigid body displacement of centerline plow guide)

*RESTART,WRITE,FREQ=50

(save and reuse data and analysis results every 50 increments)

*STEP,NLGEOM,INC=1000

(begin history section; large displ. analysis;1000 increments allowed)

 PLOW ENTERING SOIL AT 5 FPS
*SOILS ,CONSOLIDATION,UTOL=100
0.0002,0.16,1.E-6,0.01

(step title)
(effective stress analysis for fluid-filled porous media; transient consolidation analysis; max pore pressure change in any incr. is 100 psi; initial time incr.; duration of analysis; min and max incr. sizes)

*BOUNDARY,TYPE=VELOCITY
PLOWNODE,2,2,60.
*BOUNDARY
EDGE,8,8,0.
*CONTROLS,PARAMETERS=FIELD,FIEL
D=DISPLACEMENT
0.01,0.5

(prescribe constant velocity boundary condition for plownode; in y-direction; 60 in/s)
(prescribe zero pore pressure boundary condition for edge nodes)
(relax convergence criteria on

displacement field equilibrium; defaults are: residual=0.005; solution correction=0.01)

*PRINT,CONTACT=YES

(request report on contact states in the message output file)

*DEBOND,ELSET=SYMMREST
0.0,1.0,0.00067,0.0

(specify debond and crack length vs. time curves)
(liner decay in debond force with time, vanishing after 0.00067 s)

*CRACK
GROWTH,NSET=CRACKREF,TIME
TOLERANCE=0.00067
0.0,0.0,1.0,60.1
*NODE
FILE,NSET=PLOWNODE,FREQ=10
U,RF

(crack length increases

linearly to 60.1 inches in 1 s, beginning at node crackref)
(define results file output data for PLOWNODE)

(displacement and reaction forces printed every 10 increments)

*NODE FILE,NSET=CLPOR,FREQ=10
POR
*EL
FILE,ELSET=CLSTR,POSITION=CENTRO
IDAL,FREQ=10
S,E,SINV,PE

(defines results file output data for node set CLPOR)
(pore pressure printed every 10 increments)
(define results file output data for

ele set CLSTR; stress and strain components; stress invariants; plastic strains;
and element volumes)

EVOL
*MONITOR,NODE=10001,DOF=2

(monitor plow node y-displacement status file)

```
*EL PRINT,F=0              (define data file print requests for element variables;
                           suppress output)
*NODE PRINT,F=0            (define data file print requests for nodal variables;
                           suppress output)
*END STEP                  (end of step and analysis)
```